INVESTIGATING THE ROLE OF THE MYB-BUB1 AXIS IN ADENOID CYSTIC CARCINOMA

A thesis submitted for the degree of

Doctor of Philosophy

by

Ylenia Cicirò

May 2023

Division of Biosciences
College of Health, Medicine and Life Sciences
Brunel University London

To Laura and to all patients facing rare cancers

Declaration

The data presented in this thesis is the result of my own work, unless otherwise stated, and have not been submitted for other degrees.

Ylenia Cicirò

Acknowledgements

I could not have undertaken this journey without the generous support from the Oracle Cancer Trust charity, who financed this research.

I would like to express my deepest gratitude to my supervisor, Prof Arturo Sala, for his support throughout this PhD project, for his insightful feedback, and for providing me with opportunities to improve as scientist and researcher.

This endeavour would not have been possible without our collaborators: Prof Göran Stenman and his group, especially Dr Mattias K. Andersson and Dr Paloma Tejera Nevado, from the Sahlgrenska Center for Cancer Research, University of Gothenburg, for providing the ACCX11 culture, as well as their knowledge and expertise, and allowing me to perform experiments in their laboratories and facilities; Adenoid Cystic Carcinoma Research Foundation (ACCRF) and its joint research work together with the Kiyatec company for the experiment on ACC 3D culture, and with the XenoSTART organisation for the *in vivo* studies; Prof Rossano Lattanzio and Prof Gianluca Sala (G. D'Annunzio Chieti-Pescara University) for the immunohistochemistry data.

I would like to extend my sincere thanks to Dr Denise Ragusa from Brunel University London, for the bioinformatics work and for introducing me to the *in silico* analysis, investing her time to guide me through the data analysis process. I would like to recognise her invaluable patience and feedback, providing me with support for the completion of this thesis.

I would like to thank Dr Cristina Pina (Brunel University London), who generously provided expertise and advice for the ChIP-seq experiment and analysis.

I am grateful to Prof Paola Vagnarelli and her group, Dorothee, Flo, Kostas, and Marta, for their support and advice during every stage of this PhD study. In particular, I would like to acknowledge Dorothee for her help in proof-reading this thesis.

I would also like to acknowledge Dr Jeffrey Pido (Brunel University London) from my research group for his support.

Lastly, I would be remiss in not mentioning my family, my boyfriend, and my closest friends for their unwavering support and belief in me.

Abstract

Adenoid cystic carcinoma (ACC) is a malignancy originating in salivary glands. Although more frequent in the head and neck region, ACC can also arise from exocrine glands in other body locations, such as breast, respiratory tract, and genitourinary system. ACC is slow growing but relentless, and poorly responding to chemotherapy or other therapeutic interventions, explaining the high frequency of recurrence, propensity to metastasise, and poor prognosis. Overexpression of the *MYB* transcription factor and oncoprotein is a hallmark of ACC; however, the inherent difficulty of pharmacological inhibition of transcription factors and the critical role of *MYB* in normal haematopoiesis have stalled the progression of direct targeting strategies. Another difficulty in ACC research is the lack of reliable, easy-to-use cellular models.

In this PhD study, we have developed a new model of ACC by expressing a switchable *MYB* transgene in non-tumourigenic MCF10A breast epithelial cells. Upon *MYB* expression, the model recapitulated transcriptional features of ACC patient-derived gene expression profiles, affirming clinical relevance. Analysis of *MYB*-regulated genes at the global level identified the mitotic checkpoint kinase BUB1 as a potential therapeutic target. We found that *BUB1* is directly regulated by MYB at the promoter level and co-expressed with *MYB* in ACC tumours. Pharmacological inhibition of BUB1 caused suppression of proliferation and apoptosis of primary ACC cells and impaired the growth of *MYB*-overexpressing, but not *MYB*-negative, MCF10A cells, indicating that the oncogene could be used as a biomarker of drug response in glandular tumours. Overall, these results suggest that newly designed ACC models could become valuable and versatile tools for research providing a cost-effective, reproducible alternative to patient-derived cell lines or xenotransplants. The MYB-BUB1 axis unveiled in this study using the novel cellular model of ACC has the potential to increase therapeutic opportunities for cancer patients.

Publications

Cicirò, Y. and Sala, A., 2021. MYB oncoproteins: Emerging players and potential therapeutic targets in human cancer. *Oncogenesis*, 10(2), p.19.

Cicirò, Y., Ragusa, D., Andersson, M.K., Nevado, P.T., Sala, G., Lattanzio, R., Stenman G and Sala, A., 2023. BUB1 as novel potential MYB-downstream therapeutic target in adenoid cystic carcinoma. *In preparation*.

Cicirò Y., Ragusa D., Sala A., 2023. Clinical relevance of BUB1 in cancers: therapeutic implications. *In preparation*.

Table of contents

Abbreviations

5-FU	5-Fluorouracile
ABBA	Cyclin A, BUBR1, BUB1, Acm1p
ABL	Acute Basophilic Leukaemia
AC	Acetylation
ACC	Adenoid Cystic Carcinoma
ADC	Apparent Diffusion Coefficient
ADCC	Adrenocortical Carcinoma
AJCC	American Joint Committee on Cancer
AML	Acute Myeloid Leukaemia
APC/C	Anaphase-Promoting Complex
aRT	Adjuvant Radiotherapy
ASCO	American Society of Clinical Oncology
ATALL	T-cell Leukaemia/Lymphoma
BLCA	Bladder Urothelioma Carcinoma
BRCA	Breast Invasive Cancer
C-terminal	Carboxy-terminal
CAP	Cyclophosphamide-Adriamycin-Platinum
CD	Cluster of Differentiation
CD1	Conserved Domain 1
CDK	Cyclin-Dependent Kinase
cDNA	complementary DNA
CESC	Cervical squamous cell carcinoma and Endocervical adenocarcinoma
ChIP	Chromatin Immunoprecipitation
ChIP-seq	Chromatin Immunoprecipitation Sequencing
CHOL	Choloangiocarcinoma
Chr	Chromosome
CI	Confidential Interval
CIN	Chromosome Instability
CIRT	Carbon Ion Radiotherapy
CLP/ELP	Common Lymphoid Progenitor/Early Lymphoid Progenitor
CMP	Common Myeloid Progenitor
COAD	Colon Adenocarcinoma
CPC	Chromosome Passenger Complex

CR	Complete Response
CRC	Colorectal Cancer
CSC	Cancer Stem Cells
CT	Computerised Tomography
CTRL	Control
DBD	DNA-binding domain
der(6)	Derivative 6
der(9)	Derivative 9
DFS	Disease-Free Survival
DLBC	Lymphoid Neoplasm Diffuse Large B-cell Lymphoma
DMSO	Dimethyl Sulfoxide
DNA	Deoxyribonucleic Acid
DOX	Doxycycline
DWI	Diffusion-Weighted Imaging
EMT	Epithelial-Mesenchymal Transition
EORTC	European Organisation for Research and Treatment of Cancer
ER+/-	Estrogen Receptor Positive/Negative
ES	Enrichment Score
ESCA	Esophageal Carcinoma
EV	Empty Vector
FBS	Foetal Bovine Serum
FDR	False Discovery Rate
FISH	Fluorescence In-Situ Hybridisation
FITC	Fluorescein
FNAC	Fine-Needle Aspiration Cytology
FPKM	Fragments Per Kilobase of transcript per Million mapped reads
FPN	Fusion Negative Tumour
FPT	Fusion Positive Tumour
GBM	Glioblastoma multiforme
gDNA	genomic DNA
GDV	Genome Data Viewer
GEO	Gene Expression Omnibus
GFP	Green Fluorescent Protein
GLEBS	Gle2-Binding Sequence
GMP	Granulocyte-Macrophage Progenitor
GSEA	Gene Set Enrichment Analysis

GTEx	Genotype-Tissue Expression
HE	Haematoxylin-Eosin
HNSC	Head and Neck Squamous Cell carcinoma
HSC	Haematopoietic Stem Cells
HTH	Helix-Turn-Helix
IHCC	Immunohistochemistry
INCENP	Inner Centromere Protein
IP	Immunoprecipitation
KEN	Lysine-Glutamate-Asparagine
KICH	Kidney Chromophobe
KIRC	Kidney Renal Clear cell carcinoma
KIRP	Kidney Renal Papillary cell carcinoma
LARII	Luciferase Assay Buffer II
LB	Lysogeny Broth
LGG	Lower Grade Glioma
LIHC	Liver Hepatocellular Carcinoma
LMPP	Lymphoid-Primed Multipotent Progenitor
LUAD	Lung Adenocarcinoma
LUSC	Lung Squamous Cell carcinoma
MACS	Model-based Analysis of ChIP-Seq
MAD	Mitotic Arrest-Deficient
MBS	MYB-Binding Site
MCC	Mitotic Checkpoint Complex
MCTS	Multicellular Tumour Spheroid
Meg	Megakaryocyte
MESO	Mesothelioma
miRNA	micro-RNA
MM	MCF10A Model
MNase	Micrococcal Nuclease
MRI	Magnetic Resonance Imaging
mRNA	messenger-Ribonucleic Acid
Mut	Mutated
MVAS	Mosaic Variegated Aneuploidy Syndrome
N-terminal	Amino-terminal
NCBI	National Center for Biotechnology Information
NCCN	National Comprehensive Cancer Network

NCDB	National Cancer Database
NCI	National Cancer Institute
NES	Normalised Enrichment Score
NFN	Normal Fusion Negative
NFP	Normal Fusion Positive
NOD-scid	Nonobese Diabetic/Severe Combined Immunodeficiency
NRD	Negative Regulatory Domain
NS	Not Significant
NSCLC	Non-Small Cell Lung Cancer
NSG	Normal Salivary Gland
NT	Not Treated
NTC	Non-Template Control
OR	Objective Response
OS	Overall Survival
OV	Ovarian serous cystadenocarcinoma
P	Phosphorylation
P ADJ	P Adjusted
PAAD	Pancreatic Adenocarcinoma
PBS	Phosphate Buffer Saline
PCPG	Pheochromocytoma and Paraganglioma
PCR	Polymerase Chain Reaction
PD	Progression Disease
PDX	Patient-Derived Xenograft
PET	Positron Emission Tomography
PFS	Progression-Free Survival
PIC	Proteinase Inhibitor Cocktail
PLB	Passive Lysis Buffer
PORT	Postoperative Radiotherapy
PR	Partial Response
PRAD	Prostate Adenocarcinoma
QS	Quantity Sufficient
R	Pearson correlation coefficient
R/M	Recurrent/Metastatic
R1LM	BUBR1 Localisation Motif
READ	Rectum Adenocarcinoma
RECIST	Response Evaluation Criteria in Solid Tumors

RFS	Recurrence-Free Survival
RLU	Relative Light Unit
RNA	Ribonucleic Acid
RNA-seq	RNA Sequencing
RT	Radiotherapy
RT-qPCR	Real Time-quantitative Polymerase Chain Reaction
S/T	Serine/Threonine
SAC	Spindle Assembly Checkpoint
SARC	Sarcoma
SD	Stable Disease
SEER	Surveillance, Epidemiology, and End Results
shRNA	short hairpin RNA
siRNA	small-interfering RNA
SKCM	Skin Cutaneous Melanoma
SLiM	Short Linear Motif
STAD	Stomach Adenocarcinoma
SUMO	Sumoylation
T-ALL	T-cell Acute Lymphoblastic Leukaemia
TAD	Transcription Activation Domain
TAE	Tris-Acetate-EDTA
TBS	Tris-Buffered Saline
TBST	Tris-Buffered Saline Tween20
TCGA	Cancer Genome Atlas
TGCT	Testicular Germ Cell Tumors
TF	Transcription Factor
TFBS	Transcription Factor Binding Site
THCA	Thyroid Carcinoma
THYM	Thymoma
TMA	Tissue Microarray
Tmax	Time to Maximum contrast enhancement
TMB	Tumour Mutation Burden
TMZ	Temozolomide
TNM	Tumour-lymph Node-Metastasis
TPR	Tetratricopeptide Repeat
TSS	Transcription Start Site
UCEC	Uterine Corpus Endometrial Carcinoma

UCS	Uterine Carcinosarcoma
UICC	Union for International Cancer Control
US	Ultrasound
UTR	Untranslated Region
UVM	Uveal Melanoma
WES	Whole Exome Sequencing
WHO	World Health Organization
WT	Wilt-Type
ΔΔCt	Delta Delta Ct

List of figures

List of tables

Chapter I

Introduction to adenoid cystic carcinoma

1.1 Adenoid cystic carcinoma: an indolent but aggressive tumour

First described by Robin and Laboulbene (Robin Charles & Joseph A. Laboulbene, 1853) and later referred to as “cylindroma”, a term coined by Billroth in 1859, adenoid cystic carcinoma (ACC) is a rare head and neck malignancy that mainly affects salivary glands (Billroth, 1859; Fordice *et al*., 1999). It can also arise in any site with a secretory gland component, including ceruminous and lacrimal glands, exocrine glands, breasts, uterine cervix, oesophagus, lungs, and prostate (**Figure 1. 1**) (Dodd & Slevin, 2006; Kokemueller *et al*., 2004). The sites of origin in the head and neck region are the tongue, paranasal sinuses, palate, nasopharynx, larynx, lacrimal glands, and the external auditory canal (Cantù, 2021a; Khan *et al*., 2001; Spiro *et al*., 1974). Although this type of cancer typically arises within the salivary glands, it may also affect other tissues with glandular characteristics outside the head and neck region, such as in the tracheobronchial tree, oesophagus, breast, lungs, prostate, uterine cervix, Bartholin’s glands, and skin (Cantù, 2021a). The biological behaviour of the disease is still poorly understood. Due to the relative scarcity of cases, the knowledge gap in understanding underlying disease mechanisms has resulted in fewer evidence-based therapies compared to other cancers, highlighting a clinical need for improved treatment strategies (Chae *et al*., 2015).

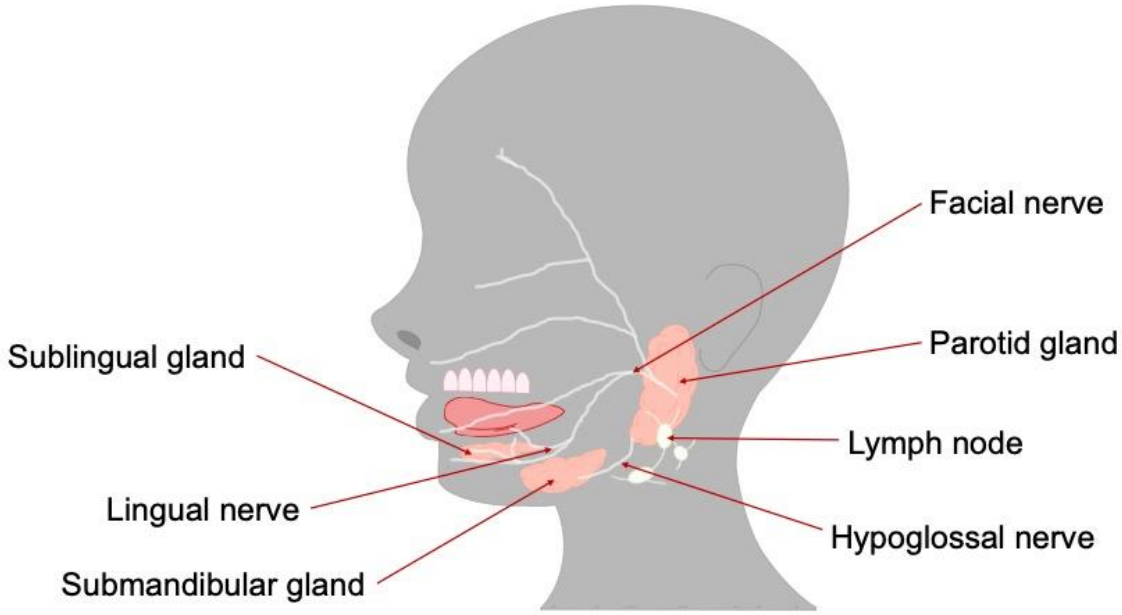

Figure 1. 1 | Schematic representation of the main sites of ACC of the head and neck. ACC affects exocrine glands. The main major salivary glands are shown under the lining of the tongue (sublingual), below the jaw (submandibular), and inside the cheeks (parotid). In humans there are around 800-1000 minor salivary glands located throughout the oral cavity within the mucosa of the buccal, labial, and also palate tissues. *Original illustration*.

1.1.1 Epidemiology of ACC

ACC accounts for 1% of the head and neck cancers and 20% of the salivary gland malignancies in adults (Fordice *et al*., 1999; Kokemueller *et al*., 2004; Spiro *et al*., 1974). Due to its rarity, comprehensive epidemiological studies on ACC, especially by anatomical site, are lacking. The latest overall incidence ratio has been estimated at 0.35 per 100 000, with incidence being directly proportional to increasing age (Boyle *et al*., 2020). In fact, the median age of diagnosis ranges between 50 and 70 years (Boyle *et al*., 2020; Ellington *et al*., 2012). Despite affecting patients prevalently in the fifth and sixth decades of life, ACC may

appear virtually at any age (Chummun *et al*., 2001; Li, N., Xu, Zhao, El-Naggar, & Sturgis, 2012), with a slight predominance in woman than men with a ratio of around 60:40 (Jaso & Malhotra, 2011). Mu and colleagues (2021) investigated a cohort of 1285 patients initially diagnosed with ACC from the Surveillance, Epidemiology and End Results (SEER) database of the National Cancer Institute (NCI) (Mu *et al*., 2021). Patients who received a diagnosis of ACC between 2010 and 2015 were included in the study and patient's details were extracted, including age, ethnicity, gender, and site of the cancer; results are reported in **Figure 1. 2** (Mu *et al*., 2021).

Limited data has been collected on the contribution of ethnicity, geographical distribution, exposure, or other environmental or epidemiologic factors to the disease development, mainly due to the scarcity of registry studies. Comparing the latest reviews on the topic, geographic distribution of ACC is similar between USA and Europe, while there is a notable difference when compared to Chinese data especially for oral cavity (30% *vs* 7.5%), major salivary glands (46% *vs* 22%), nasal cavity and paranasal sinuses (10% *vs* 30%), and lung and bronchus (4% *vs* 24%) (Ciccolallo *et al*., 2009; Li, N. *et al*., 2012; Mu *et al*., 2021). There are no identifiable lifestyle or environmental risk factors for ACC, and smoking is not known to raise the incidence, although it can be involved in oral cancers in general (Coca-Pelaz *et al*., 2015; Zvrko & Golubović, 2009).

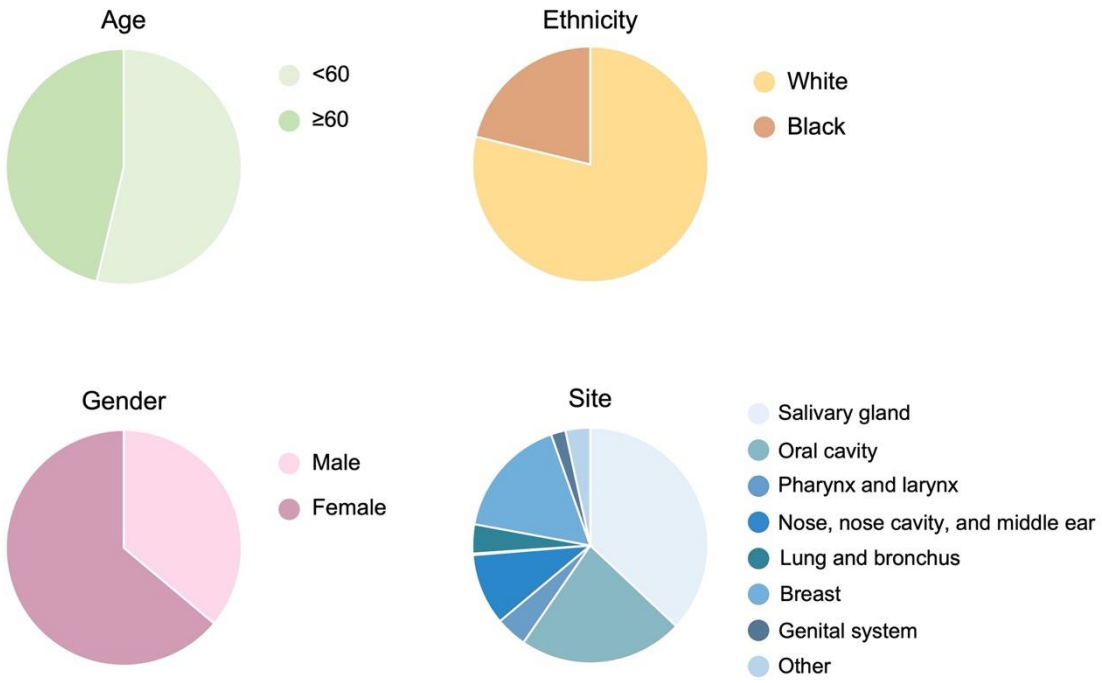

Figure 1. 2 | Baseline characteristics of all patients in the SEER dataset. Details of a cohort of 1285 patients diagnosed with ACC between 2010 and 2015. Data were extracted from the SEER database and are shown as number of patients (%). *Original illustration.*

Due to the slow progression and indolent nature of ACC, clinical heterogeneity exists among patients. Survival rates have been reported to be 70-90% for 5 years but decline steadily for subsequent years of survival (Ellington *et al*., 2012; Lloyd *et al*., 2011). While for ACC affecting major salivary glands and lung, the rate has been reported to be 71%, and 39%, respectively, the most striking feature of ACC of the breast is the positive long-term prognosis, with a 10-year survival rate accounting for 90-100% (Ciccolallo *et al*., 2009; Marchio *et al*., 2010; Molina *et al*., 2007).

To date, only a handful of multivariate analyses have investigated the prognostic value of different clinico-pathologic factors in ACC (Amit *et al*., 2015; Amit *et al*., 2015; Bjørndal *et al*., 2015; Ganly *et al*., 2015; Jones *et al*., 1997; Oplatek *et al*., 2010; van Weert *et al*., 2015; Xu *et al*., 2017; Zhang *et al*, 2013).

Among the factors influencing the survival rate in ACC of the salivary glands, the site of the primary tumour appeared to be an important player (Huang *et al*., 1997). By analysing over one hundred samples of ACC, Huang and colleagues (1997) reported a poor prognosis for ACC cases occurring in submandibular glands, maxillary antrum, and tongue, with the worse prognosis reported for submandibular glands (Huang, Minxian *et al*., 1997). These results confirmed previous data (Spiro *et al*., 1979), and could be explained by assuming that variable tumour locations and extensive invasion of nerves, bones, and muscles, hardly secure a radical cure (Spiro *et al*., 1979). Moreover, the ACC cases with the worse prognosis (i.e. submandibular) were also poorly differentiated, characteristic generally associated with poor prognosis in cancer patients.

The common and consistent independent adverse predictors repeatedly identified in these studies were tumour staging and positive surgical margins (meaning that tumour cells can be still identified at the edge of the removed tissue) (Amit *et al*., 2015; Amit *et al*., 2015; Bjørndal *et al*., 2015; Ganly *et al*., 2015; Huang, Minxian *et al*., 1997; Jones *et al*., 1997; Oplatek *et al*., 2010; van Weert *et al*., 2015; Xu *et al*., 2017; Zhang, Chun-Ye *et al*., 2013). Using multivariate analysis, Xu *et al.* (2017) confirmed ACC tumour stage and the presence of solid histology as adverse prognostic factors for recurrence-free survival (RFS) (Xu *et al*., 2017). Moreover, they also identified other adverse predictors of survival, including large tumour size, solid growth pattern, increased mitoses, high grade transformation, vascular invasion, nuclear atypia, and open chromatin (Xu *et al*., 2017). Radiotherapy has been reported to not improve survival rate, but to be effective in improving the locoregional control rate (Bjørndal *et al*., 2015).

Survival analysis of clinical and pathological risk factors for local–regional recurrence or distant metastasis indicate that tumour grade (advanced *vs* early-stage), histological grade (undifferentiated *vs* differentiated), and adjuvant radiotherapy (aRT) have prognostic impact on disease-free survival (DFS), with advanced stage and high grade independently associated with reduced DFS (Romani *et al*., 2023).

1.1.2 Clinical presentation and diagnostic evaluation

Signs and symptoms

Generally, ACC is characterised by a protracted indolent course; however, it has an aggressive long-term behaviour, with invasive perineural infiltration and high propensity for local recurrence and distant metastases resulting in eventual death (Dodd & Slevin, 2006; Spiro *et al*., 1974). For these reasons, ACC has been described as “one of the most biologically destructive and unpredictable tumours of the head and neck” (Conley & Dingman, 1974). The most common symptom is the presence of a slowly growing mass, followed by pain and facial nerve dysfunction due to propensity for perineural invasion (Vander Poorten *et al*., 1999). A study on 61 ACC of the salivary glands reported that 98% of patients presented a mass, 48% experienced pain, 30% had ulceration, and one patient had facial nerve paralysis (Nascimento *et al*., 1986). The fraction of time in which the symptoms were present varied from 1 month to 4 years (Nascimento *et al*., 1986).

The symptomatology is heavily dependent on the anatomical site of disease. For example, it has been shown that ACC facial nerve palsy may occur when the mass is located in the parotid gland in the major salivary glands (Coca-Pelaz *et al*., 2015; Vander Poorten *et al*., 1999). The classical presentation of a palate minor salivary gland tumour is that of a painless submucosal swelling, although it is also possible to observe ulceration or even oro-antral fistula (Poorten *et al*., 2014). When located in the larynx, dyspnoea could be the first presenting symptom; and in the nose or paranasal sinuses the main symptoms are nasal obstruction, deep facial pain, epistaxis, and eye problems (Biswas *et al*., 2014; Husain *et al*., 2013).

The ACC of the breast is localised (i.e. only restricted to the site of origin) in 96% of the cases, with rare cases of metastatic spread, whereas only 57% of ACC of the salivary glands is localised, with the remaining tumours showing high rate of perineural invasion and distant metastases (Ciccolallo *et al*., 2009; Ghabach *et al*., 2010; Marchio *et al*., 2010).

Diagnostic workup

The following reports explore the recommended modalities of preoperative evaluation for patients with ACC according to literature review and the American Society of Clinical Oncology (ASCO) published in 2021.

Diagnostic examination of a suspected minor salivary gland tumour is essential to discriminate the likelihood of malignancy and determine the exact anatomic location, local extent, and lymph node involvement for management considerations (Poorten *et al*., 2014).

Preoperatively, fine-needle aspiration cytology (FNAC) or core-needle biopsy can be used for tissue biopsy and ancillary tests (immunohistochemical or molecular studies) to assess for the presence of malignancy, avoiding unnecessary resection (ASCO Head and Neck Guidelines, 2021). These techniques allow to distinguish between benign and malignant specimen with an estimated sensitivity of 80% and a specificity of 97% (although across studies, this varied as widely as 57%-86% and 87%-100% for sensitivity and specificity, respectively), but fails to further classify the sample into subtypes or in providing tumour grading (Poorten *et al*., 2014; Schmidt, Hunt *et al*., 2011; Schmidt, Hall, & Layfield, 2011; Schmidt, Hall, Wilson *et al*., 2011). Therefore, incisional biopsy can be used to obtain a more accurate and complete representative specimen for diagnosis and provide histological information (Poorten *et al*., 2014).

Although pathology is the definitive diagnostic modality, imaging offers additional details for a diagnosis and correct surgical planning. Tumour characteristics including extension, nature, borders, and infiltration are delineated by computerised tomography (CT) scan, magnetic resonance imaging (MRI), and positron emission tomography (PET) (Poorten *et al*., 2014; Thoeny, 2007).

CT approaches can include ionizing radiation and using iodinated contrast agents (Burke *et al*., 2011). It is the first-choice examination for identification of erosion of the bones that may occur adjacent to the temporal bone, detection of pulmonary nodules, and presence of distant metastasis preoperatively and during the follow-up (ASCO Head and Neck Guidelines, 2021; Eggesbø, 2012; Fang *et al*., 2022; Ju *et al*., 2019).

MRI has a better soft tissue contrast and spatial resolution, making it the preferred option for depicting skull base involvement and perineural invasion (Lee, YYP *et al*., 2008). Some reports suggested that Tmax (time to maximum contrast enhancement) in contrast enhanced MRI can be helpful to distinguish malignant and non-malignant minor salivary gland tumours (Matsuzaki, Yanagi *et al*., 2012; Matsuzaki, Hara *et al*., 2012).

Diffusion-weighted imaging (DWI) with apparent diffusion coefficient (ADC) can be used to identify benign and malignant sinus tumours and classify ACC and non-ACC nasal masses with a maximum accuracy of 82% and a sensitivity of 100% (Gencturk *et al*., 2019; Wang, Feng *et al*., 2017).

PET (with or without CT) does not provide the spatial resolution for anatomical detail, useful for a better preoperative evaluation, but it can be used for exclusion of metastatic disease, more accurate prediction of nodal and distant metastatic disease in high-grade tumours, and identification of recurrent and metastatic disease, although false positives may alter the results (Kim, Min-Joo *et al*., 2013; Lee, Hwan *et al*., 2019; Roh *et al*., 2007).

Another imaging technique is the ultrasound (US), and it is mainly used to describe superficial lesions, especially those located in the parotid and submandibular glands (Fang *et al*., 2022).

1.1.3 Classification of ACC

Diagnostic classification of ACC is performed by histopathological analysis of tumour specimen. The histopathological examination also aids in differential diagnosis of other tumours such as squamous and basaloid carcinomas (Ferlito *et al*., 1997; Shaikh *et al*., 2014; Tsang *et al*., 1991). ACC encompasses a diverse histopathological spectrum which has resulted in controversies around standardised classification systems (van Weert *et al*., 2015). ACC presents itself mainly in non-luminal, basaloid cells with a limited amount of cytoplasm, or less often in luminal cuboidal cells with a duct-like phenotype, highlighting its origin from

the intercalated duct region of the glandular structures (Chen, J. *et al*., 1988; Coca-Pelaz *et al*., 2015). ACC histologically appears as a mixed tumour, consisting of tubular, cribriform and/or solid growth patterns (**Figure 1. 3**) (van Weert *et al*., 2015). The most prevalent histology is cribriform, in which cells present different sizes and shapes, surrounded by punch-out spaces (pseudolumina or pseudocystis), with a stroma containing hyaline material and/or myxoid glycosaminoglycans, and tumour cell nests surrounding the lumina (Cheng *et al*., 1992; Coca-Pelaz *et al*., 2015). Tubular architecture of ACC, typical mixed with the cribriform one, presents gland-like groups of luminal cells with a central lumen; conversely, solid ACC tumours grow in sheets without lumen formation (**Figure 1. 3**) (Cheng *et al*., 1992; Coca-Pelaz *et al*., 2015; Moskaluk, 2013).

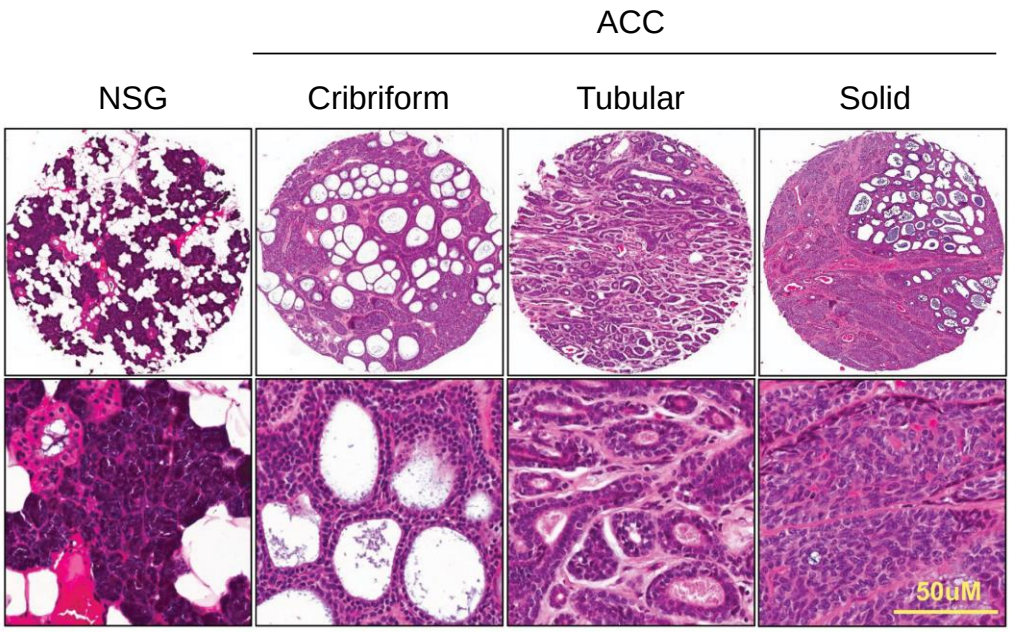

Figure 1. 3 | Haematoxylin and eosin staining of ACC. Normal salivary gland (NSG) and adenoid cystic carcinoma (ACC) tissues stained with haematoxylin and eosin (HE). The different morphology is indicated above the pictures. Scale bars= 50 µm. Adapted from Wang, Yu-Fan et al., 2014.

Currently, two classification systems are employed: Perzin/Szanto and Spiro, which also correlate with prognostic outlooks, according to the percentage of solid tumour component (Perzin *et al*., 1978; Spiro *et al*., 1974; Szanto *et al*., 1984). To predict a worse prognosis of the cancer, the cut-off values based on the solid component are >30% and >50% in the Perzin/Szanto and Spiro systems, respectively (Perzin *et al*., 1978; Spiro *et al*., 1974; Szanto *et al*., 1984). Similar to the cut-off set by Szanto, the current World Health Organization (WHO) for salivary gland tumours averts that ACC cases with a solid component accounting for more than one third of the tumour may lead to a worse clinical outcome (El-Naggar, 2017).

Another grading system has been proposed by van Weert and colleagues (2015), in which they distinguished presence or absence of solid compartment, independently from the amount

(van Weert *et al*., 2015). Recently, Morita *et al.* (2021) proposed a novel criterion (the minAmax) for pathological classification of ACC tumour grade, in which the maximum oval fitting the solid tumour nest of was estimated, and the length of the minor axis of the oval (minAmax) was measured (Morita *et al*., 2021).

Nevertheless, the clinical utility of histopathology has been debated, also due to the lack of diversified treatment regimens (in detail in paragraph 1.1.5) (van Weert *et al*., 2015).

A list of other proposed grading systems can be found in **Table 1. 1**.

Table 1. 1 | Criteria of histopathological grading for ACC.

SYSTEM	DESCRIPTION			STUDY
	Grade I	**Grade II**	**Grade III**	
Perzin/Szanto	Mostly tubular, no solid	Mostly cribriform, solid component < 30%	Solid component > 30%	(Perzin *et al.*, 1978; Szanto *et al.*, 1984)
Spiro	Mostly tubular or cribriform, occasionally solid	Mixed with substantial solid (>50%)	Only solid component	(Spiro *et al.*, 1974)
	S-	**S+**		
van Weert	Solid component absent	Solid component present		(van Weert *et al.*, 2015)
	Low-grade	**High-grade**		
MinAmax	MinAmax ≤ 0.20 mm	MinAmax > 0.20 mm		(Morita *et al.*, 2021)

1.1.4 TNM classification

Being a solid tumour, ACC is also classified according to the TNM classification system. Published by the Union for International Cancer Control (UICC) and the American Joint Committee on Cancer (AJCC), the TNM Classification of malignant tumours is the global recognised standard for classifying cancers (TNM Classification of Malignant Tumours, UICC; update 2023). The TNM gives a description of tumour site and size (T), regional lymph node involvement (N), and distant metastatic spread (M), providing information about the severity of an individual's cancer and helping in designing an appropriate plan for treatment (TNM Classification of Malignant Tumours, UICC, update 2023).

The T classifier ranges from a value of 1 to a value of 4 according to the size of the tumour; N goes from 1 to 3 according to the number of lymph nodes involved (one or more than one) and the size of the primary tumour; M describes the spread of the cancer to other sites of the body. Moreover, a value of "0" is used when no evidence is found, i.e. T0 means no presence of tumour, N0 stands for no presence of cancer in lymph node region, and M0 no metastatic spread to other sites. When a tumour cannot be evaluated, the nomenclature includes an "X" (TX, NX, MX) (Adenoid Cystic Carcinoma: Stages, Cancer.Net; Conquer Cancer, the ASCO foundation, 2021).

Combinations of T, N, and M scores determine the staging of the cancers. The earliest-stage salivary gland cancer is stage 0 (carcinoma *in situ*), and stages range from I to IV, according to the severity of the condition. Additional details are reported in **Table 1. 2**.

Table 1. 2 | Staging classification of ACC. TX, main tumour cannot be assessed due to lack of information; T0, no evidence of a primary tumour; NX, regional lymph nodes cannot be assessed due to lack of information. Adapted from AJCC, Cancer Staging Manual.

STAGE	TNM	DESCRIPTION
0	**Tis** **N0** **M0**	The cancer is confined to the cells lining the salivary duct (Tis). It has not spread to nearby lymph nodes (N0) or distant sites (M0). This stage is also known as carcinoma **i**n **s**itu (Tis).
I	**T1** **N0** **M0**	The cancer is 2 cm (about ¾ inch) or smaller. It's not growing into nearby tissues (T1). It has not spread to nearby lymph nodes (N0) or to distant sites (M0).
II	**T2** **N0** **M0**	The cancer is larger than 2 cm but no larger than 4 cm (about 1½ inch). It's not growing into nearby tissues (T2). It has not spread to nearby lymph nodes (N0) or to distant sites (M0).
III	**T3** **N0** **M0**	The cancer is larger than 4 cm and/or is growing into nearby soft tissues (T3). It has not spread to nearby lymph nodes (N0) or to distant sites (M0).
		OR
	T0, T1, T2, T3	The cancer is any size and might have grown into nearby soft tissues (T0-T3) **AND** has spread to 1 lymph node on the same side of the head or neck as the primary tumour.

	N1 **M0**	The cancer has not grown outside the lymph node and the lymph node is no larger than 3 cm (about 1¼ inch) (N1). It has not spread to distant sites (M0).
IVA	**T4a** **N0 or N1** **M0**	The cancer is any size and is growing into nearby structures such as the jawbone, skin, ear canal, and/or facial nerve. This is known as **moderately advanced disease** (T4a) **AND**: • It has not spread to nearby lymph nodes (N0) **OR** • It has spread to 1 lymph node on the same side of the head or neck as the primary tumour but has not grown outside of the lymph node and the lymph node is no larger than 3 cm (about 1¼ inch) (N1). It has not spread to distant sites (M0).
		OR
	T0, T1, T2, T3 or T4a **N2** **M0**	The cancer is any size and might have grown into nearby soft tissues or structures such as the jawbone, skin, ear canal, and/or facial nerve (T0-T4a) **AND** any of the following: • It has spread to 1 lymph node on the same side as the primary tumour but has not grown outside of the lymph node and the lymph node is larger than 3 cm but not larger than 6 cm (about 2½ inches) (N2a) **OR** • It has spread to 1 lymph node that is 3 cm or smaller and the cancer has grown outside of the lymph node (N2a) **OR** • It has spread to more than 1 lymph node on the same side as the primary tumour, but it has not grown outside of any of the lymph nodes and none of the lymph nodes are larger than 6 cm (N2b) **OR** • It has spread to 1 or more lymph nodes, either on the opposite side of the primary tumour or on both sides of the neck but has not grown outside any of the lymph nodes and none are larger than 6 cm (N2c). It has not spread to distant organs (M0).

IVB	**Any T** **N3** **M0**	The cancer is any size and might have grown into nearby soft tissues or structures (Any T) **AND** any of the following: • it has spread to a lymph node that is larger than 6 cm but has not grown outside of the lymph node (N3a) **OR** • it has spread to a lymph node that is larger than 3 cm and has clearly grown outside the lymph node (N3b) **OR** • it has spread to more than one lymph node on the same side, the opposite side, or both sides of the primary cancer with growth outside of the lymph node(s) (N3b) **OR** • it has spread to a lymph node on the opposite side of the primary cancer that is 3 cm or smaller and has grown outside of the lymph node (N3b). It has not spread to distant organs (M0).
		OR
	T4b **Any N** **M0**	The cancer is any size and is growing into nearby structures such as the base of the skull or other bones nearby, or it surrounds the carotid artery. This is known as **very advanced disease** (T4b). It might or might not have spread to nearby lymph nodes (any N). It has not spread to distant organs (M0).
IVC	**Any T** **Any N** **M1**	The cancer is any size and may have grown into nearby soft tissues or structures (Any T) AND it might or might not have spread to nearby lymph nodes (Any N). It has spread to distant sites such as the lungs (M1).

1.1.5 Available treatments for ACC

Surgery

The first line of treatment for ACC patients in the absence of distant metastases is surgical resection, with some precautions depending on the location of the tumour. When in presence of a T4b disease or cervical lymph node metastases invading the carotid artery, the tumour is considered unresectable (Fushimi *et al*., 2018).

Regardless of the site, R1 resection (close margins of resection within 1 mm) is preferred over the radical resection (R0, negative margins and complete removal of tumour residues) when R0 is too risky or potentially lethal, and its often accompanied by aRT to obtain a promising prognosis for patients (Millar *et al*., 2004; Naylor *et al*., 2008; Ning *et al*., 2019; Woida & Ribeiro-Silva, 2007). However, the ASCO guideline for management of salivary gland malignancy reports that “the extent of adequate free margin is not well-established because of the absence of prospective randomized trials, the different anatomical sites that these tumors involve, and the diverse histologic types” (ASCO Head and Neck Guidelines, 2021).

The National Comprehensive Cancer Network (NCCN) Guidelines 2019 (Head and Neck Cancers, NCCN, 2019) set guidelines for optimal surgical practices for head and neck surgery. In particular, surgeons encounter challenging conditions due to the complex branching of the facial nerve within the parotids and its functional and aesthetic importance, which also require consideration around the issue of perineural invasion that may determine the resection of the nerve. In these cancers, surgeons aim for complete excision, avoiding the removal of additional parotid tissue containing adjacent at-risk lymph nodes because of the low rate of metastasis (removal of adjacent lymph nodes is a treatment reserved for advanced (T3-T4) parotid cancers only) (Xiao *et al*., 2016). The proximity to the facial nerve leads to a close surgical margin of less than 5 mm; however, early-stage low and intermediate grade parotid cancers demonstrated a 100% locoregional control at a mean follow-up of 74 months in 15 patients with T1-2 N0 cancer treated with surgery alone, even presenting a resulting surgical

margin of 2 mm (Zenga *et al*., 2019). These results were also confirmed in another series of 18 patients with early stage acinic cell carcinomas of the parotid gland without adverse features, where only one patient experienced recurrence with a median follow-up of 64 months (Zenga *et al*., 2018). In another report of 32 not advanced parotid gland malignancy a 5-year DFS of 90.6% was observed (Stodulski *et al*., 2017).

The hypoglossal nerve is almost always preserved during resection of ACC affecting the submandibular gland because of its deep location; however, the lingual nerve is often approached by the tumour together with the involvement of the adjacent lymph nodes (Cantù, 2021b). Thus, for this location of the cancer, the preferred surgical procedure is complete resection of nodular and glandular content of the submandibular compartment (Batsakis, 1979). For paranasal sinuses, the best treatment is surgery followed by postoperative radiotherapy (PORT); however, advanced stage tumours complicate the possibility of a clean resection, with around 60% of the cases presenting positive margins after the treatment (Cantu *et al*., 2010; Miller, E. D. *et al*., 2017).

For ACC of the oropharynx at the base of the tongue, less invasive resection methods such as transoral robotic resection are possible but limited by the size of the tumours. Mandibulotomy may be required for larger tumours (Cantù, 2021b). For ACC of the larynx, the most common procedure is total laryngectomy (Cantù, 2021b). In general, regardless of the location of the primary ACC, the most common treatment is conservative total surgical resection, advocated also by the United Kingdom National Multidisciplinary Guidelines for parotid glands, whereas partial parotidectomy is preferred for small, low-grade superficial T1 or T2 low-grade malignant tumours (Sood *et al*., 2016).

However, postsurgical residual disease and positive margins are associated with poor prognosis, whilst negative or clean margins (with no residual tumoural tissue) are associated to improved overall survival (OS) (Gillespie *et al*., 2012; Ishida *et al*., 2020; Morse *et al*., 2019).

Radiotherapy

Salivary gland malignancies are historically known to be radioresistant (Cerda *et al*., 2014). PORT is commonly used for ACC patients and essential for ACC treatment, independently on the margin status of the tumour, and "a dose of at least 60 Gy is indicated for patients with T3-4 tumours, incomplete or close resection, bone invasion, perineural invasion, and pN(+)", reporting a significantly improved 10-year local control in patients treated with PORT compared to surgery alone (Terhaard *et al*., 2005). This promising result was confirmed by analysis of available registries. Mahmood and colleague (2011) analysed a population of more than 2000 patients with high-grade (poorly differentiated or undifferentiated) and/or locally advanced malignant major salivary gland tumours (T3/4 or N+) extrapolated from the SEER (Mahmood *et al*., 2011). They found significantly improved survival with aRT among ACC patients with both high-grade and locally advanced disease (Mahmood *et al*., 2011). A comparable efficacy of PORT treatment was suggested after the analysis of more than 4000 salivary gland ACC samples collected from the National Cancer Database (NCDB) (Safdieh *et al*., 2017). Moreover, it has been shown that aRT improves the survival rate also in patients with early-stage disease (Lee, Anna *et al*., 2017). Although the promising and significant difference in outcome in patients that underwent surgery alone or in combination with aRT, some studies reported a not significant effect in patients' survival rate (Ellington *et al*., 2012; Lloyd *et al*., 2011).

Particle therapies, including neutron, proton, and carbon ion therapies, have been investigated in ACC. It has been demonstrated that the 5-year local control rate is 24-57% and the OS is 26.5-87% (Bhattasali *et al*., 2016).

At the end of the 80's, Catterall & Errington (1987) published for the first time the positive results achieved by using fast neutron radiotherapy rather conventional X-ray radiation therapy (RT) for head and neck ACC treatment, reporting a local control and 5-year survival rates of 72% and 50%, respectively (Catterall & Errington, 1987). Following studies on ACCs reported a remarkable difference in locoregional control in neutron therapy compared to the

conventional radiotherapy (56% *vs* 17%) or electron radiation (75% *vs* 32%) (Huber *et al*., 2001; Lindsley *et al*., 1996). However, in patients treated with neutron therapy, no benefit in survival rate were detected compared to surgery alone (Balamucki *et al*., 2012; Choi *et al*., 2013; Shen *et al*., 2012). Moreover, neutron radiotherapy has been reported to have a higher risk of late side effects, thus the NCCN guidelines for head and neck tumours no longer recommends neutron therapy for salivary gland neoplasms (Head and Neck Cancers, NCCN, 2019).

Two other types of heavy particle are proton beam radiotherapy and carbon ion radiotherapy (CIRT). The former has shown to be effective in achieving a good local control and less side effects compared to the neutron therapy; the latter is the most recent type of radiotherapy investigated, and it has been demonstrated its efficacy in cancers where photon beams therapy is not effective, including inoperable salivary gland tumours (Okada, T. *et al*., 2010; Vischioni *et al*., 2020). CIRT can be a new option to evaluate for the treatment of ACC patients, in the attempt to overcome ACC radioresistance properties. Unfortunately, only a few centres in the world perform CIRT, mainly due to its high costs and the need of peculiar shielding thick enough to prevent the leakage of radiation (Cantu *et al*., 2010).

Chemotherapy

ACC tumours do not benefit from systemic chemotherapy; thus, no recommendation by NCCN about standard chemotherapy is accepted for ACC treatment (Head and Neck Cancers, NCCN, 2019). Nevertheless, over the years various studies attempted to investigate single-agent cytotoxic drugs or combinatorial chemotherapy in patients with ACC tumours; however, the response rates for chemotherapeutic drugs quoted in the literature are variable and inconsistent (Dodd & Slevin, 2006). The objective tumour response to cisplatin in metastatic tumours, for example, remains unclear, with studies suggesting a favourable subjective

response and objective tumour regression in 7 patients out of 10, alongside with studies reporting no significant response in ACC metastatic tumours treated with cisplatin (Dick Haan *et al*., 1992; Licitra, Lisa *et al*., 1991; Schramm *et al*., 1981). According to a review published by Laurie and colleagues (2011), 141 patients were analysed across different clinical trials using single-agents mitoxantrone, cisplatin, epirubicin, vinorelbine, paclitaxel, and gemcitabine; major responses were sporadically observed (18 patients out of 141), stable disease (SD) was reported in 64 of 111 patients, and paclitaxel and gemcitabine yielded nil response rate (Airoldi *et al*., 2001; Gilbert *et al*., 2006; Mattox *et al*., 1990; Schramm *et al*., 1981; Van Herpen *et al*., 2008; Vermorken *et al*., 1993; Verweij *et al*., 1996). Although combinatorial chemotherapy with cisplatin may show a higher objective response rate than single-agent chemotherapy, the toxicity derived from the combination is the limiting factor in using multiple chemotherapeutic agents concomitantly (Fang *et al*., 2022).

Cytotoxic drug responses were also analysed in four ACC trials: cisplatin, doxorubicin, and cyclophosphamide-adriamycin-platinum (CAP) were the most common administrated regimens and major objective responses were noted in 9 of 36 patients (Belani *et al*., 1988; Creagan *et al*., 1988; Dreyfuss *et al*., 1987; Licitra, L. *et al*., 1996). Use of anthracycline in combination with cisplatin was also suggested as potential therapeutic strategy cells (Laurie *et al*., 2011).

Currently, chemotherapy is mainly used as palliative treatment effective in a small portion of metastatic and recurrent ACC patients where surgery and/or radiotherapy are not reasonable options (Laurie *et al*., 2011; Fang *et al*., 2022; de Sousa *et al*., 2022). However, chemotherapy alone is not sufficient to increase patients' survival rate, and combination with other types of therapeutics could be a path to explore for those patients with inoperable or incurable tumours.

Target-specific therapy

Due to the rarity of ACC, there are no disease-specific agents designed for its treatment; in spite of that, different pharmacological agents targeting MYB-regulated proteins, including tyrosine kinases, have been used in phase I and phase II clinical trials, and some of them will be discussed in this paragraph.

It has been found that 65% to 100% of ACCs overexpress *KIT* (CD117), suggesting that the KIT inhibitors imatinib and dasatinib could represent possible therapeutic targets (Chae *et al*., 2015; Holst *et al*., 1999; Penner *et al*., 2002). Although these drugs administered as single treatments did not show an objective response in a phase II trial, combinatorial treatment with cisplatin improved the response (Hotte *et al*., 2005; Ochel *et al*., 2005; Pfeffer *et al*., 2007; Wong *et al*., 2013).

Other therapies investigated in ACC include cetuximab, gefitinib, and lapatinib, three widely used drugs that target the tyrosine kinase EGFR, in view of its positivity in ACC (74-91%) (Agulnik *et al*., 2007; Dahse *et al*., 2009; Hitre *et al*., 2013; Jakob *et al*., 2015; Locati, Laura D. *et al*., 2009; Macarenco *et al*., 2008; Vered *et al*., 2002). Monotherapy with gefitinib or lapatinib did not show any positive effect, although SD was reached in 68% (13/18) of the cases with gefitinib and in 79% (15/19) of the cases treated with lapatinib (Agulnik *et al*., 2007; Jakob *et al*., 2015). Compared with the gefitinib and lapatinib studies, the monoclonal antibody cetuximab showed contrasting results in different studies. In a phase II trial, the drug did not show better results, with no overall response, and 87% of cases (20/23) with SD (Locati, L. D. *et al*., 2009).

The pathways involved in ACC pathogenesis are not fully elucidated, thus investigating drugs with a broader spectrum of targets can be a reasonable alternative. In fact, multikinase inhibitors, including dovitinib, axitinib, sunitinib, lenvatinib, sorafenib, and regorafenib have been considered for ACC disease; common targets for these medications are VEGFRs, FGFRs, and PDGFRs (Chau *et al*., 2012; Dillon *et al*., 2013; Ho, Alan Loh, Sherman, Fury, Baxi, Haque, Sima, Antonescu, Katabi, & Pfister, 2014; Thomson *et al*., 2015). Therapeutic

strategies involving these molecules were inefficient in achieving an objective response (OR); however, partial response (PR) was observed in 10.5%, 9%, and 10.5% of patients treated with dovitinib, axitinib, or sorafenib, respectively (Chau *et al*., 2012; Dillon *et al*., 2013; Ho, Alan Loh *et al*., 2014; Thomson *et al*., 2015).

Other targets have been investigated; a collection of clinical trials is highlighted in **Table 1. 3**Table 1. 3. Results have been reported according to the categories of the Response Evaluation Criteria in Solid Tumors (RECIST) from European Organisation for Research and Treatment of Cancer (EORTC) and NCI (RECIST 1.1, EORTC and NCI, 2000).

Table 1. 3 | Clinical trials investigating molecular targets studied in ACC. Abbreviations: N, number of patients. RECIST categories: CR, complete response; PR, partial response; SD, stable disease; PD, progressive disease. PFD, progression-free survival (median, in month); OS, overall survival (median, in month). HDAC, histone deacetylase; Number (%); NS, not specified; (*) mean, not median.

TARGET	PHASE	AGENT	N	CR	PR	SD	PD	PFS	OS	STUDY
NOTCH1	I	Brontictuzumab	NS	0 (0)	2 (NS)	3 (NS)	-	9.9	-	Ferrarotto *et al*.; 2018
PRMT5	I	GSK3326595	14	-	3 (21)	-	-	-	-	Siu *et al*.; 2019
ATRA	II	Tretinoin	16	0 (0)	0 (0)	11 (69)	5 (28)	3.7	-	Hanna *et al*.; 2021
	II	Cetuximab	23	0 (0)	0 (0)	20 (87)	3 (13)	-	-	Locati *et al*.; 2009
EGFR	II	Gefitinib	19	0 (0)	0 (0)	16 (84)	2 (11)	4.3	25.9	Jakob *et al*.; 2015
	II	Lapatinib	19	0 (0)	0 (0)	15 (79)	9 (53)	3.5	NR	Agulnik *et al*.; 2007
FGFR	II	Dovitinib	34	0 (0)	2 (6)	22 (65)	1 (3)	8.2	20.6	Dillon *et al*.; 2017

TARGET	PHASE	AGENT	N	CR	PR	SD	PD	PFS	OS	STUDY
HDAC	II	Lenvatinib (VEGFR, KIT, PDGFR)	26	0 (0)	3 (12)	20 (77)	3 (12)	9.1	27	Locati *et al*.; 2020
	II	Lenvatinib (VEGFR, KIT, PDGFR)	32	0 (0)	5 (16)	24 (75)	1(3)	17.5	-	Tchekmedyian *et al*.; 2019
	II	Vorinostat	30	0 (0)	2 (7)	27 (90)	1 (4)	10	11.5	Goncalves *et al*.; 2017
KIT	II	Imatinib	10	0 (0)	0 (0)	2 (20)	5 (50)	6 *	-	Pfeffer *et al*.; 2007
	II	Imatinib	15	0 (0)	1 (7)	2 (13)	6 (40)	2.5	7.5	Hotte *et al*.; 2005
	II	Imatinib+ Cisplatin	28	0 (0)	3 (11)	19 (68)	4 (14)	15	35	Ghosal *et al*.; 2011
	II	Dasatinib	40	0 (0)	1 (3)	20 (50)	12 (30)	4.8	14.5	Wong *et al*.; 2016
	II	Sunitinib	13	0 (0)	0 (0)	11(85)	2 (15)	7.2	18.7	Chau *et al*.; 2012
PD-1	II	Nivolumab	45	0 (0)	4 (9)	26 (57)	-	4.9	-	Fayette *et al*.; 2019
	II	Pembrolizumab +/−radiation therapy	10	0 (0)	0 (0)	5 (50)	2 (50)	4.5	NR	Mahmood *et al*.; 2021
		Pembrolizumab	9	0 (0)	0 (0)	7 (78)	2 (22)	6.6	27.2	
VEGF	II	Pazopanib (VEGFR, KIT, PDGFR)	46	0 (0)	1 (2)	35 (76)	10 (22)	5.9	16.6	Guigay *et al*.; 2016
	II	Sorafenib (VEGFR, KIT, PDGFR)	19	0 (0)	2 (11)	13 (68)	4 (21)	11.3	19.6	Thomson *et al*.; 2015

1.1.6 Molecular biology of ACC

MYB aberrations

A defining molecular characteristic of ACC is the t(6;9)(q22–23;p23–24) chromosomal translocation, which involves *MYB*, located at chromosomal band 6q23, and *NFIB* transcription factor, located at chromosomal band 9p22–23 (**Figure 1. 4 A**) (Nordkvist *et al*., 1994; Persson *et al*., 2009). The prevalence of t(6;9) in ACC patients varies, with estimates ranging between 60-80% of salivary ACC cases (Brill *et al*., 2011; Persson *et al*., 2009; Stenman *et al*., 2010; Warner *et al*., 2018). Persson and colleagues (2009) investigated the cytology of 11 ACC samples from salivary glands and breast, finding that 100% of them harboured the t(6;9) translocation and showing that *MYB-NFIB* fusion is a recurrent event (Persson *et al*., 2009). Notably, the *MYB-NFIB* fusion transcript has been shown to be specific for ACC cancers regardless of the site of origin, being detected in ACC of salivary gland and breast, lacrimal gland, lung, vulva, and skin (North *et al*., 2015; Roden *et al*., 2015; von Holstein *et al*., 2013; West *et al*., 2011; Xing *et al*., 2017).

The t(6:9) is a balanced translocation producing two derivative chromosomes, der(6) and der(9) **Figure 1. 4 A**). The translocation breakpoints have been mapped using fluorescence *in situ* hybridisation (FISH), recurrently occurring at 6q22–23 leaving the coding exons of *MYB* mostly intact or with small truncations at the 3' end of the gene, and at 9p23-24 encompassing the 3' portion of *NFIB* (Geurts *et al*., 1998). The exchange of genetic material produces a *MYB-NFIB* fusion product on the der(6), which is transcribed into a chimaeric mRNA (Persson *et al*., 2009). Although rarer, a reciprocal *NFIB-MYB* fusion product has also been detected by RT-PCR, indicating that this rearrangement also exists (Persson *et al*., 2009).

*The MYB-NFIB fusion consists of the N-terminal part of MYB, including the DNA-binding domain (DBD) and transcription activation domain (TAD) linked to the C-terminal end of NFIB (**Figure 1. 4***

Figure 1. *4* B) (Persson *et al*., 2009). A functional protein translated from the fusion transcript has been described (Persson *et al*., 2009).

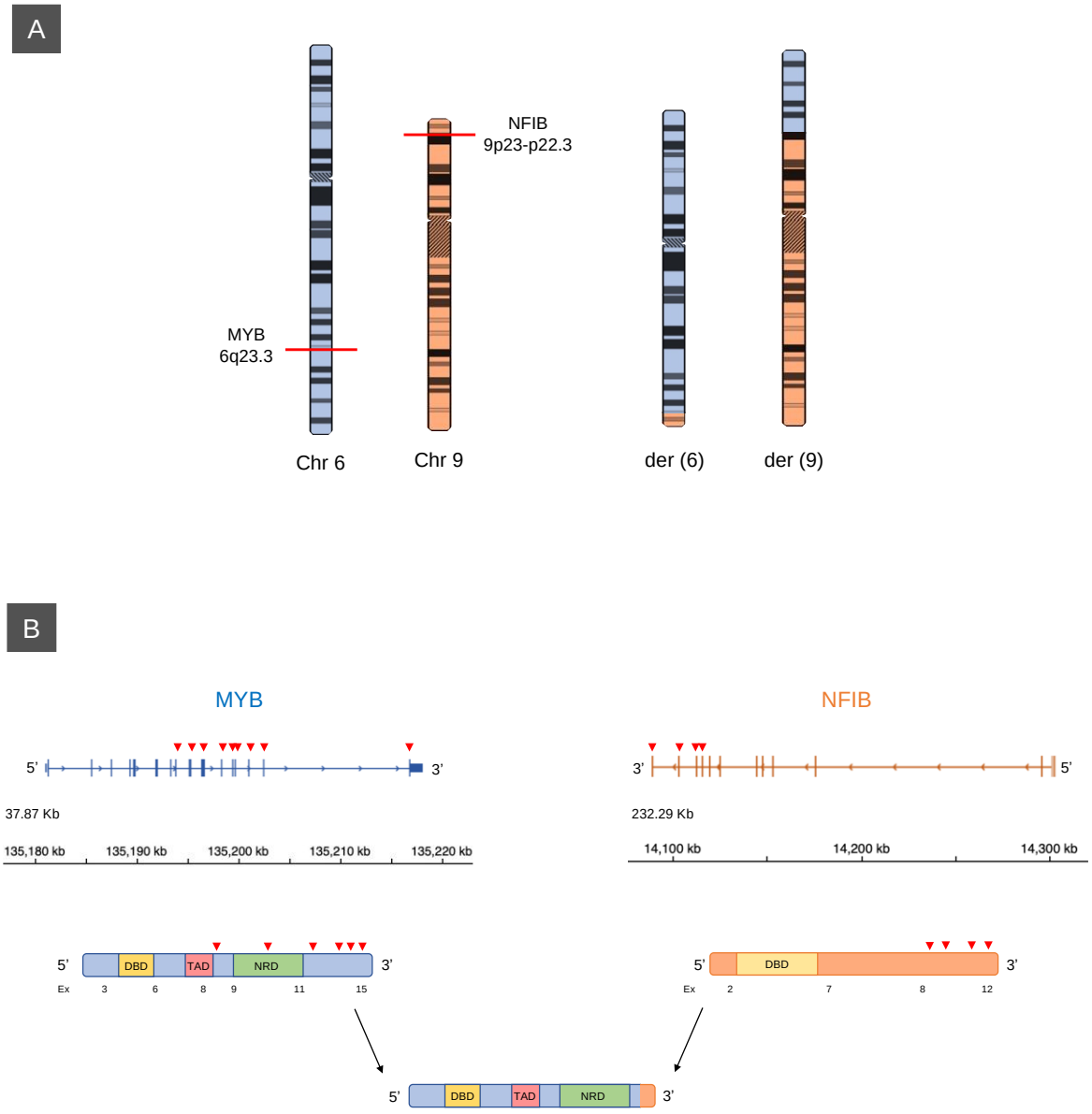

Figure 1. 4 | Schematic representation of *MYB-NFIB* fusion in ACC. (**A**) Ideogram showing chromosome 6 (Chr 6) and chromosome 9 (Chr 9) and their derivative after the fusion. The red lines indicate the sites of the breakpoints in proximity of *MYB* and *NFIB.* (**B**) *MYB* and *NFIB* transcripts; *MYB* (showed in blue) (ENSG00000118513) is composed of 15 or 16 exons depending on the variant considered, more than 40 different transcripts have been associated to this gene (https://www.ensembl.org). *NIFB* (showed in orange) consists of 11-12 exons (ENSG00000147862). Breakpoints reported in the literature are highlighted by the red arrows. The *MYB-NFIB* fusion transcript is shown at the bottom of the panel; red triangles indicate the approximate location of the breakpoints and the protein domains involved. Ex, exon; DBD, DNA binding domain; TAD, transactivation domain; NRD, negative regulatory domain. *Original illustration, source: NCBI, genome data viewer GDV.*

The most common *MYB-NFIB* chimaeric transcripts involves *MYB* exon 14 joined with *NFIB* at exon 9 and was found in 7 cases out of 11 analysed; altogether 24 different translocation variants were identified as consequence of alternative splicing and variable breakpoints in both *MYB* and *NFIB* (Persson *et al.,* 2009). Following studies have in fact reported additional fusion rearrangements involving different exons of both genes (Chahal *et al.*, 2018; McIntyre *et al.*, 2019; Mitani *et al.*, 2011; Togashi *et al.*, 2018). A collection of 80 t(6;9) translocations extracted from 6 studies is reported in

Table 1. 4 **Table 1. 4** and shows the multiple variable breakpoints between exons in *MYB* and *NFIB* (Chahal *et al*., 2018; McIntyre *et al.*, 2019; Mitani *et al.*, 2011; Panaccione *et al.*, 2017; Persson *et al.*, 2009; Togashi *et al.*, 2018). Taken together, these observations provide information on the breakpoints, suggesting that they can occur in *MYB* between exon 8 and 15, and in *NFIB* between exon 8 and 12, or in the *MYB* untranslated region (UTR). Moreover, it has been reported that in a subset of ACCs, *MYB* is replaced by the closely related *MYB-like1* (*MYBL1*) gene linked to *NFIB*, or other fusion partners, resulting in gene rearrangements likely to have the comparable oncogenic properties as the more common *MYB-NFIB* fusions (Brayer *et al.*, 2016; Mitani *et al.*, 2011). Despite the trend observed and the exons involved in the translocation, independent research reported the same breakpoint sequence CCCCTTGCAG in both exon 14 and 15 (McIntyre *et al.*, 2019; Mitani *et al.*, 2011; Persson *et al.*, 2009; Wagner *et al.*, 2022). Overall, more than 70% of ACCs rearrangements implicates *MYB* or *MYBL1*, with the former being present in around 60% of the cases, and the latter in approximatively 35% of *MYB-NFIB* negative ACCs (Fujii *et al.*, 2017; Mitani *et al.*, 2016).

Table 1. 4 | Breakpoint sites of t(6;9) reported in six studies. Colour-scale is used according to the total number of samples analysed for the specific breakpoint.

Breakpoint exonic sites of t(6;9)	Persson *et al*, 2009	Mitani *et al*, 2011	Panaccione *et al*, 2017	Togashi *et al*, 2017	Chahal *et al*, 2018	McIntyre *et al*, 2019	Total
MYB 8 – NFIB 8	2						2
MYB 8 – NFIB 9	1				3		4
MYB 8 – NFIB 11		1					1
MYB 8 – NFIB 12		5		1			6
MYB 9 – NFIB 11		1		2			3
MYB 9 – NFIB 12		1		2			3
MYB 11 – NFIB 12		3					3
MYB 12–NFIB 8	1						1
MYB 12–NFIB 9	1		1		1		3
MYB 12 – NFIB 11		1					1
MYB 12 – NFIB 12				1			1
MYB 13 – NFIB 9		1					1
MYB 13 – NFIB 11		1					1
MYB 13 – NFIB 12		4					4
MYB 14–NFIB 8	12						12
MYB 14–NFIB 9	7		3				10
MYB 14 – NFIB 11				1			1
MYB 14 – NFIB 12		1		4			5
MYB 14 – NFIB 3'UTR				3			3
MYB 15 – NFIB 11		2				3	5
MYB 15 – NFIB 12		3				5	8
MYB 16 – NFIB 12		1				1	2

Although the percentage of ACC samples presenting t(6;9) translocation (i.e. fusion-positive ACC) vary through the existing body of literature, there is still an ongoing debate about the biological consequences these fusions have on the establishment and progression of the disease. The exact mechanism of action of the MYB-NFIB fusion remains to be elucidated due to the lack of knowledge regarding whether MYB activation is the result of truncations in the MYB gene, or if the translocated region of NFIB plays a salient role (Wagner et al., 2022). As schematised in ***Figure 1. 4 B*** *and already discussed before, breakpoints occur in different exons (8 to 16) of MYB, giving raise to different transcripts, for example including or excluding totally or partially the sequence containing the negative regulatory domain (NRD) (****Figure 1. 4*** **Figure 1. *4* B**).

Different studies suggest that, regardless of the chimaeric transcripts and breakpoints, the outcome of the t(6;9) is an increase in mRNA level of *MYB* and overexpression of its encoded protein product (Gao *et* al., 2014; Persson *et al*., 2009; Rettig *et al*., 2016). Therefore, to understand the consequence of the translocation, it is crucial to understand the consequences of *MYB* reactivation.

It has been reported that the segment of MYB corresponding to amino acids 358- 452 located in the NRD domain might play a role in protein turnover (Corradini *et al*., 2005). Compared to the full length MYB, hematopoietic cells with the protein presenting deletions of the amino acids at positions 389-418 of MYB showed increase protein stability, proposing that the lack of this regulatory portion may enhance the activity of MYB in ACC (Corradini *et al*., 2005). It has been suggested that the 5 amino acids SWYLG encoded by exon 9 of *NFIB* are critical for the proper function of the transcription factor, however their contribution to ACC pathogenesis is expected to be limited (Geurts *et al*., 1998; Gründer *et al*., 2003). However, the functional role of NFIB within the translocation remains to be fully elucidated. One of the hypotheses related to the mechanism of *MYB* activation lies in the disruption of the negative regulatory feedback of *MYB* as consequence of the deletion of microRNA (miRNA) binding sites located in the MYB 3' UTR, especially miR-150 (Gao, R. *et al*., 2014; Persson *et al*.,

2009). Analysis of miRNA in ACC was performed by Gao and colleagues (2014) from a large collection of salivary gland tumours (Gao, R. *et al*., 2014). They investigated a miRNA signature and found that in both fusion-positive and negative cases, miR-150 was downregulated in tumour samples compared to the matched adjacent normal tissue, suggesting a regulatory role of miR-150 independent on the fusion status (Gao, R. *et al*., 2014). Moreover, they generated cell lines of normal salivary gland expressing *MYB* full-length, *MYB* with impaired 3' UTR, as well as truncated *MYB*, and *MYB-NFIB* fusion gene (Gao, R. *et al*., 2014). Interestingly, they found a significant prolonged MYB protein half-life only in those cells expressing the fusion construct, suggesting that the NFIB segment could stabilise MYB (Gao, R. *et al*., 2014). It has been recently reported that the loss of the 3' UTR of *MYB* and flanking sequences was significantly associated with shorter 5-year and 10-year OS in ACC patients, as well as with patients' tumour grading, indicating the possible presence of genes or sequences in 6q23.3-qter with tumour suppressive functions, contributing to poor prognosis and short OS in ACC (Persson *et al*., 2022). Drier and colleagues (2016) used Chromosome Conformation Capture analysis to map the chromatin landscape and examined the translocated genomic loci (Drier *et al*., 2016). They found that *MYB* overexpression in ACC following chromosome rearrangement can be triggered by super-enhancers located in the *NFIB* portion that translocate in proximity of the *MYB* promoter, thus activating its transcription (Drier *et al*., 2016). Overexpression of *MYB* does not seem to be specifically dependent on *NFIB* but can be also detected in cells harbouring rearrangements with other partner genes, such as *TGFBR3* and *RAD51B* (Drier *et al*., 2016). A more recent study on ACC suggests that MYB is activated by engagement of an alternative *MYB* promoter, the transcription start site 2 (TSS2), located upstream of exon 2, leading to a N-terminal truncated form of the protein (Frerich *et al*., 2019). The truncation qualitatively alters the specificity of MYB binding to DNA, activating alternative downstream pathways, including gene sets implicated in neuronal cell migration, resulting in poor outcome in a subgroup of ACC patients (Frerich *et al*., 2019). Dysregulation of *MYB* can also lead to overactivation of downstream target genes involved in critical pro-tumourigenic pathways with genes involved in apoptosis (*API5*, *BCL2*, *BIRC3*,

HSPA8, *SET*), cell-cycle control (i.e. *CCNB1*, *CDC2*, *MAD1L1*, *AURKA*), and cell growth and angiogenesis (*CD53*, *FGF2*, *MYC*, *VEGFA*, *IGF1R*, *MET*) (Drier *et al*., 2016; Persson *et al*., 2009).

Human cancers usually evolve through a multistage carcinogenesis process that is driven by the progressive accumulation of gene mutations and epigenetic abnormalities over the time (Greenman *et al*., 2007; Weinstein *et al*., 1997). Although MYB transcriptional regulatory activity is a key component of ACC tumourigenicity, potential involvement of secondary genetic mechanisms is still poorly understood (Moskaluk, 2013). Aside from *MYB* alterations, whole exome sequencing (WES) analysis identified an overall low mutational burden, with mutations including *PIK3CA*, *ATM*, *CDKN2A*, *SF3B1*, *SUFU*, *TSC1*, *CYLD*, *FGFR*, and *NOTCH* (Stephens *et al*., 2013). The role of MYB as driver of ACC is also strengthened by studies reporting ACC cases exhibiting upregulation of known direct targets of MYB, including genes belonging to the apoptotic pathway (*API5*, *BCL2*, *BIRC3*, *HSPA8*, *SET*), cell growth, angiogenesis (*CD53*, *FGF2*, *KIT*, *MYC*, *VEGFA*), cell cycle control (*CCNB1*, *CDC2*, *MAD1L1*), and cell adhesion (*CD34*) (Persson *et al*., 2009). Other studies reported mutations in genes belonging to several DNA-related pathways, such as chromatin-remodelling, histone acetyltransferase/deacetylase, and DNA damage response (Stransky *et al*., 2011).

Strong experimental evidence demonstrating that *MYB* alone can transform normal human epithelial cells is lacking. In our laboratory, in collaboration with the Stenman's group, we observed increased proliferation rates of human glandular epithelial cells transduced with *MYB* or *MYB-NFIB* fusion (Andersson *et al*., 2020). Treatment of the transduced cells with a MYB inhibitor Naphthol AS phosphate significantly reduced the relative proliferation of the cells (Uttarkar *et al*., 2015), suggesting a *MYB*-dependent effect. However, despite acquiring a partially transformed phenotype *in vitro*, *MYB*-expressing epithelial cells were unable to grow as xenografts when transplanted into immunocompromised mice (Andersson *et al*., 2020). Nevertheless, the low mutational burden seen in patients supports the hypothesis that *MYB* overexpression is the main, common oncogenic event (Miller, L. E. *et al*., 2022).

In addition to MYB, vertebrates also express A-MYB (MYBL1), encoded by the *MYBL1* gene located on chromosome 8q, which presents a nearly identical DNA binding domain and a similar overall structure (George & Ness, 2014). *MYBL1* has been firstly proposed to be an oncogene in glioma (Ramkissoon *et al*., 2013). Interestingly, the tumours with *MYB* or *MYBL1* fusions did not display unique gene expression signatures; instead, the truncated *MYB* and *MYBL1* gene products appear to be equally oncogenic and interchangeable in ACC cancers (Brayer *et al*., 2016). Although not as common as *MYB*, overexpression of *MYBL1* has been detected in 16% of ACC cases, which brings the percentage of tumours with activation of either *MYB* or *MYBL1* to 93% of cases (Persson *et al*., 2022). Therefore, it seems likely that the development of ACC tumours requires the rearrangement of *MYB* or *MYBL1* oncogenes.

Additional gene alterations/mutations found in ACC

Comparative genomic hybridisation analysis unveiled additional cytogenetic abnormalities in ACC, including DNA copy number losses at chromosome 12q12–q13 and 1p32–36, and gains at chromosome 22q12–q13, 8, 16p, 17q, (El-Rifai *et al*., 2001; Freier *et al*., 2005; Rao *et al*., 2008; Toida *et al*., 2001). Vékony and colleagues (2007) showed that 40% of ACC cases presented overexpression of *PDGFB* (located on 22q13) (Vékony *et al*., 2007). Moreover, additional gained regions were found on chromosome 9q, 11q, and 19q where fibroblast growth factors and their receptors are located, suggesting that their dysregulation may have a role in ACC development (Liu, J. *et al*., 2012; Vékony *et al*., 2007).

Using microarray analysis, two independent studies uncovered that ACCs undergoing high grade transformation (dedifferentiation) express genes associated with early development, such as *SOX4*, *TFAP2*, *NGFI-A*, *TGFB3*, as well as genes belonging to the Wnt/β-catenin pathway, and genes involved in morphogenesis (Frierson Jr *et al*., 2002; Patel *et al*., 2006). A

key role was also proposed for *KIT* (CD117) encoding a receptor tyrosine kinase involved in promoting cell growth, differentiation, and haematopoiesis (Funasaka *et al*., 1992; Huang, Eric *et al*., 1990; Nocka *et al*., 1989).

More than 90% of ACCs express *KIT* transcript and protein, but not non-neoplastic salivary gland tissue, suggesting that the receptor has no role in normal salivary gland function (Freier *et al*., 2005; Holst *et al*., 1999). *KIT*-positive tumours have been described, including malignancy of the gastrointestinal tract and seminoma, in which gain-of-function mutations results in overexpression of the protein (Izquierdo *et al*., 1995; Sarlomo-Rikala *et al*., 1998). Although the reason for the abundant KIT expression in ACC remains unclear, KIT has been proposed to promote cell migration, perineural invasion, local recurrence, and distant metastasis (Pérez-Losada *et al*., 2002; Tang, Y. *et al*., 2010). If in gastrointestinal stromal tumours displaying mutations in *KIT*, treatment with KIT inhibitors has been demonstrated to be effective; however, ACC tumours with upregulated *KIT* seem to be resistant to the treatment, suggesting that *KIT* does not play a critical role in ACC, despite its overexpression (Heinrich *et al*., 2003; Holst *et al*., 1999; Hotte *et al*., 2005).

Recent studies integrating proteomics, genomics, and clinical data from Ferrarotto and colleagues (2021) have defined and characterised distinct molecular ACC subtypes: ACC-I and ACC-II (Ferrarotto *et al*., 2021). The cluster I presented a strong upregulation of *MYC* and its target genes and enrichment in *NOTCH*-activating mutations, as well as the mutation of their negative regulator (*SPEN*); cluster II presented overexpression of *TP63* and receptor tyrosine kinases (RTKs) such as AXL, MET, and EGFR, and a better clinical course compared to the ACC-I subtype (**Figure 1. 5**) (Ferrarotto *et al*., 2021). The NOTCH family consists of four transmembrane protein receptors (NOTCH1-4) that are activated by five ligands: DLL1,3,4, JAG1 and JAG2 which induce cell proliferation, survival, migration, stem cells renewal, and metastasis (Feeney *et al*., 2022; Kopan & Ilagan, 2009).

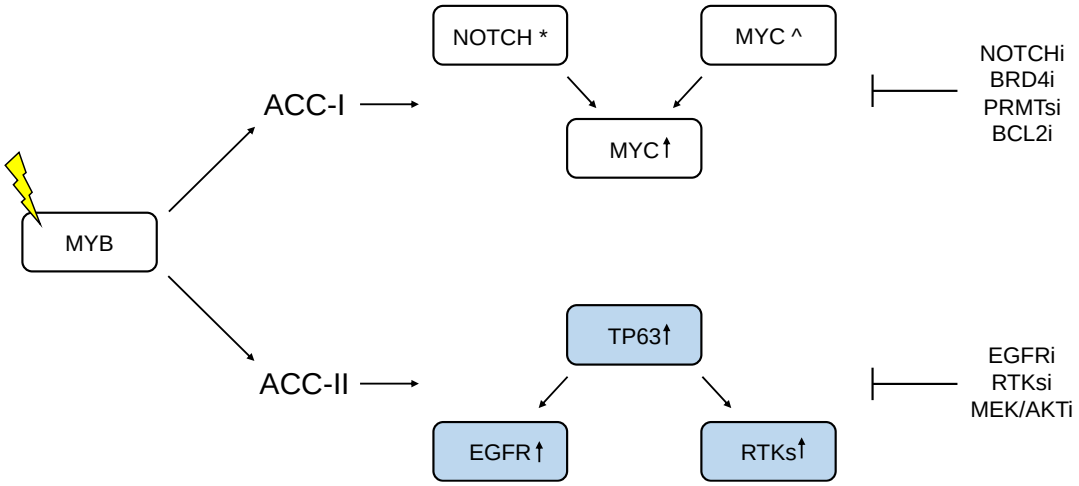

Figure 1. 5 | Schematic representation of ACC subtypes (ACC-I and ACC-II). According to Ferrarotto and colleagues (2021), ACCs can be classified and stratified based on their molecular alterations: *MYC*-overexpressing ACCs falls in the ACC-I subtype, while ACC-II subtype presents *TP63* overexpression. As simplified in the figure, the two different classes show unique molecular profiles, hence, targeted therapies can be directed towards one or the other cluster, accordingly. (*) mutation; (^) amplification; (↑) overexpression of the genes. Adapted from Ferrarotto *et al*., 2021.

Although cribriform and tubular histology were found in cluster II ACCs, the subtype I showed an enrichment in solid component (Ferrarotto *et al*., 2021). As already discussed, solid pattern in ACC is associated with a more aggressive cancer, likely increasing propensity to metastasise. Interestingly, *NOTCH* mutations have been solely associated to a metastatic ACC profile, and therefore, association of the *NOTCH* cascade to a poorer prognosis was uncovered (Ferrarotto *et al*., 2017; Ferrarotto *et al*., 2021). *NOTCH* has been associated with a rapidly progressive disease and reduction in OS in the recurrent/metastatic (R/M) ACC setting (Feeney *et al*., 2022). Dysregulation in *MYC* and *TP63* signalling could also expose potential therapeutic vulnerabilities specific for each subtype (**Figure 1. 5**) (Ferrarotto *et al*., 2021). Interestingly, *MYC*, a master oncogene aberrantly expressed in 70% of human cancers

(Madden *et al*., 2021), is also a well-known MYB target (Fujii *et al*., 2017), providing the opportunity to pharmacologically repress targets of both oncoproteins, including BRD4, PRMTs, and BCL2. *BCL2,* a key regulator of cell death and MYB target (Mitra *et al*., 2016), is upregulated in ACC-I, together with the activated form of *NOTCH1* (*NICD1*) (Ferrarotto *et al*., 2021). Preclinical studies on inhibitors of BCL2 and GSI have shown synergetic effects in other solid tumours, including non-small cell lung cancer (NSCLC), myeloma, and breast cancer (Li, M. *et al*., 2010; Sakakibara-Konishi *et al*., 2017; Séveno *et al*., 2012), suggesting that this could be an effective new therapeutic combination for ACC-I group.

In ACC-II, overexpression of *TP63* has been proposed as the driver of RTKs, including EGFR, MET, and AXL, which was also suggested in other studies (Carroll *et al*., 2006; Dang *et al*., 2015; Ferrarotto *et al*., 2021). Multi-kinase inhibitors, such as cabozantinib, an inhibitor of AXL, MET, and VEGFR, are therefore being studied in a clinical trial (NCT03729297). Moreover, AXL and MET are mediators of cancer resistance to EGFR inhibitors (Giles *et al*., 2013; Taniguchi *et al*., 2019; Zhang, Zhenfeng *et al*., 2012); therefore, a double targeting therapy approach using a combination of cabozantinib and EGFR inhibitors, such as erlotinib, may be a good strategy in ACC-II tumours.

Finally, epigenetic dysregulation could also play an important role in ACC as 35 to 50% of cases have mutations in genes involved in histone modification and chromatin remodelling, including *KDM6A*, *ARID1A*, *KMT2C* (previously *MLL3*), and *CREBBP* (Almeida *et al*., 2017; de Sousa *et al*., 2022; Ho, Allen S. *et al*., 2019).

1.2 MYB (c-MYB)

1.2.1 MYB protein structure

MYB is a transcription factor belonging to the MYB family, highly conserved across species (Cicirò & Sala, 2021). In humans, *MYB*, *MYBL1*, and *MYBL2* genes (encoding for the corresponding transcription factors, also known as C-MYB, A-MYB, and B-MYB, respectively) are similar in structure, although their expression is often non-overlapping and they interact with specific co-factors, suggesting that different MYB members have distinct roles (Gewirtz & Calabretta, 1988; Nomura *et al*., 1988; O'Rourke & Ness, 2008; Ramsay, Robert G. & Gonda, 2008).

MYB orchestrates a variety of cellular processes through regulation of gene expression by direct interaction with target gene sequences. MYB plays an essential role in haematopoiesis by regulating cell proliferation and differentiation, as well as in the cell cycle (Mucenski *et al*., 1991; Nakata *et al*., 2007; Pilkinton *et al*., 2007).

MYB is a 75 kDa protein comprising 640 amino acids. It contains three main domains: the DNA binding domain (DBD), the transactivating domain (TAD), the negative regulatory domain (NRD) (**Figure 1. 6**) (Aziz, Natasha *et al*., 1995; Cicirò & Sala, 2021; Ogata *et al*., 1992; Sakura *et al*., 1989). Different isoforms of MYB have been found in normal and cancer cells and named according to their molecular weight (Dudek, H. & Reddy, 1989; Shen-Ong, 1987). The dominant human isoform is the p72 (72 kDa, 640 aa), but alternative splicing can also result in an additional exon between exon 9 and exon 10 (the 9B, originally named 9A), generating an alternative isoform of 89 kDa (O'Rourke & Ness, 2008; Shen-Ong, 1987). Functionally, different isoforms are thought to differ in their transactivation activity (Wang, Xunde *et al*., 2018; Woo *et al*., 1998).

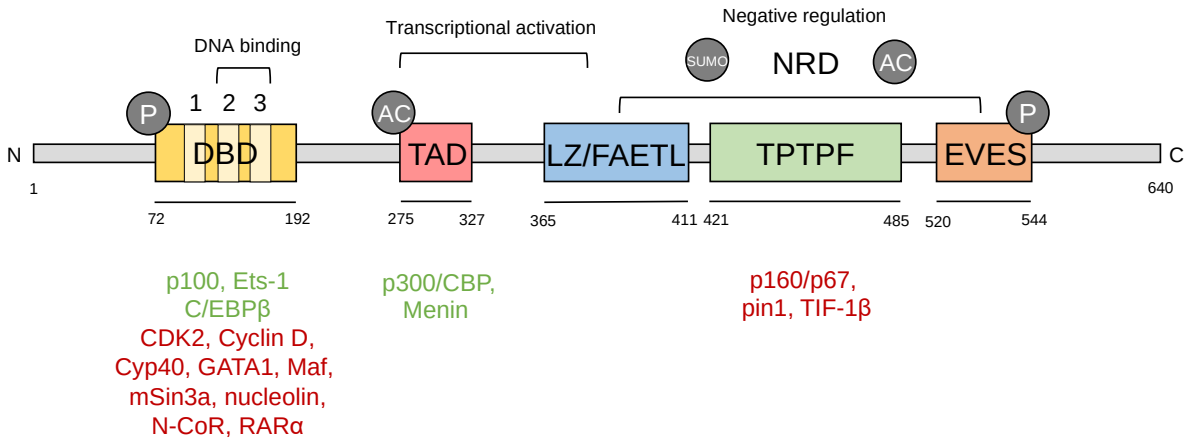

Figure 1. 6 | Schematic representation of MYB protein structure. MYB protein consists of 640 residues. The DNA-binding domain (DBD) is comprised of three repeats (R1, R2, and R3). The transactivation domain (TAD) is the interaction site for p300/CBP MYB co-activator and is required for transcriptional activity. The negative regulatory domain (NRD) extends from the LZ/FAETL motif to the EVES peptide sequence, involved in intramolecular and intermolecular protein–protein interactions. Post-translational modification affecting the structure are phosphorylation (P), acetylation (AC), and sumoylation (SUMO). For each domain, the N-terminal starting residue and the C-terminal one is displayed. The main functions associated with different domains are highlighted. MYB co-activators and co-repressors are listened in green and red, respectively. *Original illustration*.

The DBD is a conserved helix-turn-helix (HTH) domain containing three tryptophan repeats segments (R1, R2, and R3) that are involved in DNA binding (Ogata *et al*., 1992). The first portion of the DBD is dispensable for DNA binding, although it facilitates DNA interactions, while the final part is crucial for the DNA interaction with co-factors (Ogata *et al*., 1992). It has also been suggested that the DBD may be involved in nuclear localisation; MYB proteins lacking either the first two tryptophan repeats, or the TAD remain inside the nucleus, but the protein partially migrates outside the nuclear region after depletion of the whole DBD,

suggesting that the nuclear localisation sequence of MYB might be located in the N-terminal region (Sakura *et al*., 1989).

The TAD functions in transcriptional transactivation of target genes. The TAD is acidic and contains a well-characterised short linear motif (SLiM) in the form of an LxxLL motif, which is involved in the interaction with co-activators such as CREB-binding protein (CBP) and p300 through their KIX domain (Kasper *et al*., 2002; Oelgeschläger, M., Janknecht, Krieg, Schreek, & Lüscher, 1996; Parker *et al*., 1999).

NRD motifs are often found in transcription factors as regulatory domains repressing the recruitment of gene expression machinery and the activity of the TAD (Marceau *et al*., 2019). In MYB, the NRD accommodates multiple highly conserved S/TP sequences and Cdk consensus sites (Wijeratne *et al*., 2022). Its regulatory mechanisms remain unknown, however it is believed to act as a regulator of its own activity, as deletions of the NRD result in increased transactivation of MYB (Dubendorff *et al*., 1992; Gonda *et al*., 1989).

MYB is able to transactivate gene expression by recognising and binding the (T/C)AACNG sequence (**Figure 1. 7**), known as the canonical MYB binding site (MBS), and activates transcription via interactions with co-activators, particularly CREB-binding protein (CBP) (Biedenkapp *et al*., 1988; Dai *et al*., 1996). It has been reported that MYB activation relies on the TAD, which functions by recruiting the main co-activators CBP and p300, independently of DNA binding (Dai *et al*., 1996; Foos *et al*., 1993; Kanei-Ishii *et al*., 1994; Oelgeschläger, M. *et al*., 1996). MYB can either cooperate or compete with other transcription factors, such as members of the CAAT enhancer binding protein (CEBP) family, the ETS family, and GATA1, which are known regulators of haematopoiesis (Bartůněk *et al*., 2003; Mink *et al*., 1996; OelgeschlaÈger *et al*., 2001; Oelgeschläger *et al.*, 1996; Shapiro, 1995; Takahashi, Tomomi *et al*., 2000; Wang, D. M. *et al*., 2007). MYB has also been shown to act as a repressor of transcription of specific genes (Zhao *et al*., 2011). Post-translational modifications, such as phosphorylation, acetylation, ubiquitination, and sumoylation, affect the ability of MYB to interact with other factors, modifying its transcriptional activity (Aziz, N. *et al*., 1993; Bies &

Wolff, 1997; Bies *et al*., 2002; Cures *et al*., 2001; Lüscher *et al*., 1990; Ramsay, Robert G. *et al*., 1995; Sano & Ishii, 2001; Sramko *et al*., 2006; Tomita *et al*., 2000).

A list of the main interactions with co-activators and co-repressors is shown in **Figure 1.**.

A [	425	292	0	1478	1519	0	1	8	401	422	]
C [	422	428	1513	3	2	1527	60	3	482	528	]
G [	300	397	5	39	0	0	68	1516	147	225	]
T [	380	410	9	7	6	0	1398	0	497	352	]

Figure 1. 7 | MYB motif logo. In humans, the MBSs are characterised by the sequence shown on the upper part of the figure. MYB motifs are coherent with the average length of the characters for eukaryotic transcription factor binding site (TFBS), between 5 and 20. The bottom part shows a matrix with frequencies of each base. The figure was downloaded from JASPAR dataset; matrix ID MA0100.3.

1.2.2 MYB in normal cellular physiology

MYB regulates the process of blood formation by modulating proliferation and differentiation of haematopoietic stem cells (HSCs). Haematopoiesis relies on the activity of HSCs, which are able to differentiate into specialised blood cells, as well as dividing to form an identical HSC through self-renewal. Within the haematopoietic hierarchy, which follows an

arrangement with progressively mature cell types of two fundamental lineages of myeloid and lymphoid cells

Figure 1. *8* (**Figure 1. 8**), MYB has been described as a regulator of multiple functions, including HSCs self-renewal, myeloid progenitor development, erythropoiesis, B cell differentiation, and T cell development (Bender *et al*., 2004; Lieu & Reddy, 2009; Lipsick, J. S. & Baluda, 1986; Mucenski *et al*., 1991; Sheiness & Gardinier, 1984; Thomas *et al*., 2005; Thompson & Ramsay, 1995; Vegiopoulos *et al*., 2006). Myb-null mouse models indicate that MYB is important for adult, but not embryonal, erythropoiesis (Mucenski *et al*., 1991). A conditional *MYB* knockout in adult haematopoietic stem cells revealed that the transcription factor is essential for self-renewal, and, in its absence, there is accelerated differentiation (Lieu & Reddy, 2009). In agreement with these observations, the expression of *MYB* is high in haematopoietic progenitor cells and is downregulated during differentiation (Gonda & Metcalf, 1984; Westin *et al*., 1982). In fact, early studies already suggested a role for MYB in stem cell proliferation and differentiation (Gewirtz & Calabretta, 1988; Mucenski *et al*., 1991; Sandberg *et al*., 2005). Regulation of stemness by MYB has also been demonstrated in different tissues, including neurons, vascular smooth muscle cells, and stem cells of the intestinal crypts (Lieu & Reddy, 2009; Malaterre *et al*., 2007; Ramsay, Robert G., 2005; Sandberg *et al*., 2005; Shikatani *et al*., 2016).

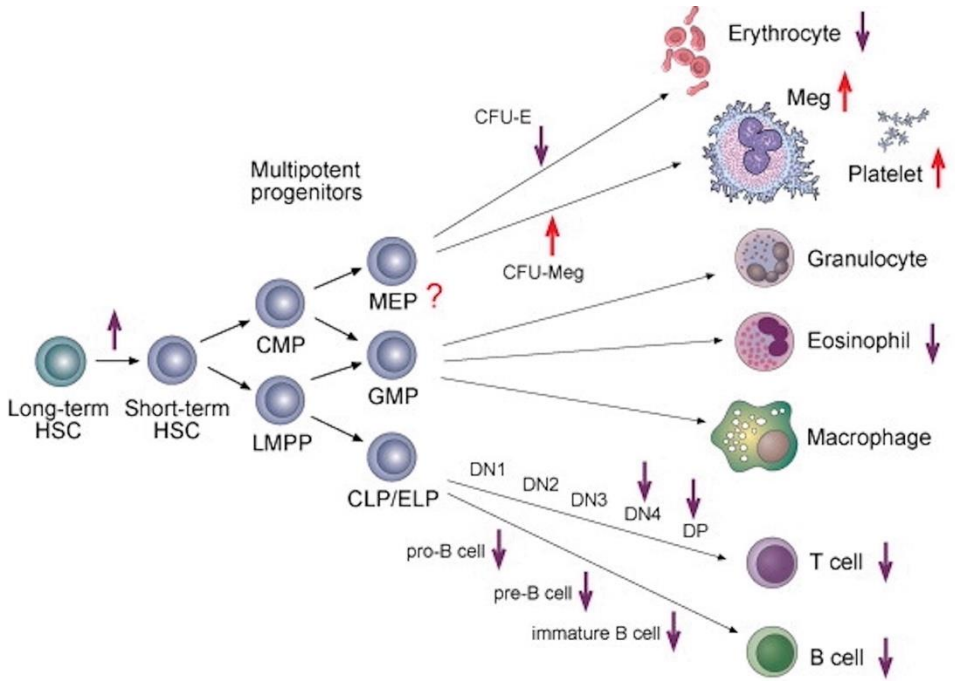

Figure 1. 8 | Diagram of haematopoiesis showing the defects observed in mouse models harbouring *Myb* deficiency. (↓) decrease in the frequency of the cell type/maturation stage in the absence of Myb. (↑) increase in the frequency of the cell population after the loss of Myb. Abbreviations: LMPP, lymphoid-primed multipotent progenitor; CMP, common myeloid progenitor; GMP, granulocyte–macrophage progenitor; CLP/ELP, common lymphoid progenitor/early lymphoid progenitor; Meg, megakaryocyte. Figure adapted from Greig *et al*., 2008.

1.2.3 Role of deregulated *MYB* expression in human cancers

Dysregulation of *MYB* has been described in both haematopoietic and solid malignancies (Clappier *et al*., 2007; Li *et al*., 2016; Okada *et al*., 1990; Quelen *et al*., 2011; Thompson *et al*., 1997; Torelli *et al*., 1987). In fact, the oncogenic version of vertebrate *MYB*, i.e. the viral oncogene *v-myb*, was firstly identified as the transforming gene of E26 and AMV retroviruses resulting in leukaemias in birds (Lipsick, Joseph S. & Wang, 1999; Roussel *et al*., 1979). In cancer, alterations of *MYB* have been described in the form of dysregulated expression (up-

or downregulation), structural chromosomal abnormalities, genomic amplifications, and mutations (Ho *et al*., 2013).

MYB is a known translocation partner in several haematological cancers. The first recurrent genomic rearrangements of the *MYB* locus were evidenced in acute T cell leukaemia, where *MYB* and *TCRB are fused* in the t(6;7)(q23;q34) translocation (Clappier *et al*., 2007). In the Atlas of Genetics and Cytogenetics in Oncology and Haematology, 15 different translocations involving *MYB* and a second partner gene have been reported, of which 9 are in haematological neoplasms (MYB, 4602, Atlas of Genetics and Cytogenetics in Oncology and Haematology, 2009). Some examples of translocations involving the *MYB* locus are the t(X;6)(p11;q23) resulting in the *MYB-GATA1* fusion gene found in acute basophilic leukaemia (ABL); *MYB-MNX1* (6;7)(q23;q36) in an acute myeloid leukaemia (AML) cell line GDM-1; t(6;6)(q23;q24) involving *MYB*/*PLAGL1* in T acute lymphoblastic leukaemia (T-ALL); t(6;6)(q23;q25) with *MYB* and *ESR1* in angiocentric glioma; t(6;11)(q23;q21) *MYB/MAML2* in low-grade gliomas where was also identified the t(5;6)(q31;q23) linking *MYB* and *PCDHGA1* (Bandopadhayay *et al*., 2016; Nagel *et al*., 2005; Pinto *et al*., 2016; Quelen *et al*., 2011; Quintana *et al*., 2011).

MYB duplication may be leukaemogenic in T cell acute lymphoblastic leukaemia (T-ALL) (Lahortiga *et al*., 2007). Oncogenic *TAL1* is aberrantly expressed in T-ALL as a consequence of somatic mutations in its regulatory sequences which create new MYB-binding sites and a super-enhancer (Mansour *et al*., 2014). Lahortiga *et al.* (2007) detected *MYB* duplication (and consequential overexpression) in a small fraction of T-ALL patients (8.4%) and in five different cell lines (Lahortiga *et al*., 2007).

MYB is altered in acute basophilic leukaemia (ABL), where its locus is fused to *GATA1* as a consequence of the t(X;6)(p11;q23) translocation that results in a decrease or loss of *GATA1* expression (Quelen *et al*., 2011). It has been reported that transgenic expression of the fusion in a *GATA1*-deficient murine model led to myelodysplasia and leukaemia development (Belloni *et al*., 2011). Acute myeloid leukaemia (AML) is often characterised by recurrent mutations or

gene fusions involving the gene *MLL*; such translocations have been associated with aggressive leukaemia (Estey, 2018; Meyer *et al*., 2006). *MYB* is a key downstream effector of *MLL* fusions, promoting it as a possible target for therapies in *MLL*-driven leukaemias (Hess *et al*., 2006). The small molecule inhibitor celastrol (Uttarkar *et al*., 2016) acts by targeting the KIX domain of p300, disrupting its interaction with MYB and inhibiting MYB-dependent transcriptional activation, which caused inhibition of AML cells growth *in vitro* and *in vivo* (Uttarkar *et al*., 2016).

The KIX domain is also the target of Naphthol AS-E phosphate, a compound shown to be effective in inhibiting the expression of the *MYB* gene itself, as well as a variety of its targets, resulting in myeloid differentiation and leukaemic cell apoptosis (Uttarkar *et al*., 2016).

Recently, a novel therapeutic peptide was developed, called MYBMIM, designed to interact with the KIX domain of the CBP protein, mimicking the interaction of the naïve MYB:CBP/p300 complex (Ramaswamy *et al*., 2018). MYBMIM causes the dissociation of the MYB:CBP/p300 complex in AML, its displacement from oncogenic enhancers enriched for MBSs, and downregulation of the expression of genes associated with *MYB*, including the oncogenes *MYC* and *BCL2* (Ramaswamy *et al*., 2018). NOD-scid mice engrafted with primary patient-derived *MLL*-rearranged leukaemia cells and treated with the peptide did not demonstrate any growth advantage and extended survival (Ramaswamy *et al*., 2018).

Taken together, these approaches elucidate the dependence of leukaemias on *MYB* and their susceptibility to aberrant *MYB*, paving the way for its therapeutic blockade.

Paediatric low-grade gliomas encompass a heterogeneous set of brain tumours. The *MYB-QKI* fusion disrupts both *MYB* and *QKI*, resulting in hemizygous deletion of 3' *MYB* and 5' *QKI*, and has been identified as a recurrent aberration in angiocentric gliomas (Bandopadhayay *et al*., 2016). Three different mechanisms of oncogenic activation downstream of the translocation have been identified: activation of *MYB via* translocation of a super-enhancer located in the 3' UTR of *QKI* upstream of the *MYB* promoter; enhanced expression of the *MYB* allele through a positive feedback loop consequent to transcriptional activation by the MYB-QKI fusion protein;

rearrangement of *QKI* locus leading to haploinsufficiency and loss of its tumour-suppressing activity (Ichimura *et al*., 2006; Mulholland *et al*., 2006; Yang, G. *et al*., 2010).

MYB is overexpressed in colorectal (CRC) cancers with a frequency of 80% and its upregulation has been associated with poor prognosis (Ramsay, R. G. *et al*., 1992; Williams *et al*., 2008). *MYB* overexpression is caused by attenuation of transcriptional pausing in the intron 1 regulatory sequence (Hugo *et al*., 2006). An interesting therapeutic approach for *MYB*-positive CRC cancers is the MYPHISMO study protocol. This is the first-in-human phase I clinical trial of a combined treatment using the TetMYB vaccine and an Anti-PD1 antibody (BGB-A317) in patients with advanced CRC or ACC (Pham *et al*., 2019). The MYPHISMO study is based on promising pre-clinical data of vaccine-induced tumour clearance and establishment of anti-tumour memory (Pham *et al*., 2019; Williams, B. B. *et al*., 2008). To date, the study is still ongoing and therefore no results are publicly available yet.

Breast cancer is a heterogeneous neoplasia, and the clinical outcome is determined by its molecular profile (Goldhirsch *et al*., 2013; Vuong *et al*., 2014). Over 70% of breast cancers are oestrogen receptor-positive (ER+) and almost invariably also *MYB* positive (Yang, R. *et al*., 2019). *MYB* expression levels increase in an oestrogen-dependent way, suggesting a strong correlation between *MYB* and ER, also corroborated by the fact that proliferation of ER+, but not oestrogen receptor-negative (ER-), breast cells is inhibited following *MYB*-knockdown (Drabsch *et al*., 2007; Quintana *et al*., 2011).

Mitra and colleagues (2016) demonstrated that ER+ breast cancer cell lines, including MCF-7, were much more sensitive (> 10 times) to killing by inhibitors of CDK9 (CDKi) than ER-/MYB-cells (Mitra *et al*., 2016). Cyclin-dependent kinases (CDKs) are proteins essential to a wide range of cellular functions, crucial for cell division and transcription, therefore treatment of breast cancer cells with the CDK9i also impaired cell proliferation and cell cycle progression, inducing arrest at both the G1/S and G2/M cell cycle phases (Mitra *et al*., 2016). Moreover, expression

of relevant *MYB* target genes including *BCL2* and *CCNB1* was suppressed by the pharmacological inhibition of CDK9; ectopic *MYB* expression restored their expression levels and cell survival, suggesting that CDKi may be effective in ER+ breast cancer by targeting MYB transcription (Mitra *et al*., 2016).

Dismally, breast cancer often results in acquired resistance to targeted therapies (Brufsky & Dickler, 2018). One of the proposed mechanisms that leads to treatment resistance is the activation of epithelial–mesenchymal transition (EMT), that can be targeted with microRNAs, specifically the miR-200 family (Korpal *et al*., 2008; Park, Sun-Mi *et al*., 2008; Ward *et al*., 2013). ER+ tamoxifen-resistant breast cancer cells treated with miR-200b/c showed reduced levels of *MYB* expression (Gao, Y. *et al*., 2019). The EMT markers *vimentin*, *ZEB1*, and *ZEB2* were also downregulated. The authors observed that naïve breast cancer cells expressed lower levels of *MYB*, compared to the drug-resistant cells, and were more sensitive to tamoxifen, suggesting the involvement of *MYB* in the EMT process (Gao, Y. *et al*., 2019).

MYB downstream targets

MYB is considered undruggable due to the difficulty in targeting inherently disordered proteins such as transcription factors, and also because its depletion may be deleterious to the organismal homeostasis (Bushweller, 2019). Despite these caveats, pharmacological therapies aiming at interfering with the oncogenic activity of *MYB* (or its downstream targets) are under investigation. A list of preclinical and clinical cancer studies is reported in **Table 1. 5.**

Table 1. 5 | Selection of preclinical therapeutic strategies adopted to target MYB or MYB-regulated genes. BC, breast cancer.

TREATMENT	TARGET	CANCER	STUDY
AT7519, BE-09-LN53	CDKs	ER + BC	(Mitra *et al*., 2016)
ATRA	MYB	ACC	(Mandelbaum *et al*., 2018)
Celastrol	MYB-C/EBPβ-p300	AML	(Uttarkar *et al*., 2016)
Mebendazol	MYB	AML	(Walf-Vorderwülbecke *et al*., 2018)
miR-200b/c	EMT markers	ER + BC	(Gao, Y. *et al*., 2019)
Monensin A	MYB	AML, ACC	(Yusenko *et al*., 2020)
MYBMIM	MYB:CBP/p300	AML	(Ramaswamy *et al*., 2018)
Naphthol AS-E phosphate	MYB-C/KIX(p300)	Leukaemia	(Uttarkar *et al*., 2015)
Plumbagin	MYB/p300	AML	(Uttarkar *et al*., 2016)
VX-970	ATR	ACC	(Andersson *et al*., 2020)
Linsitinib	IGFR	ACC	(Andersson *et al*., 2017)

The diverse range of cellular processes orchestrated by MYB are dictated by regulation of target genes which could be potentially exploited for pharmacological targeting of *MYB*-expressing tumours. Over the years, many putative targets have been identified, but a comprehensive validated collection is still lacking, with different studies producing non-overlapping results (Bianchi *et al*., 2010; Quintana *et al*., 2011; Zhao *et al*., 2011). *MYB*-regulated genes are involved mainly in cell cycle progression and control of programmed cell death, but also in cytoskeletal and microtubule functions (Suzuki & Forrest, 2009). Of note,

some of the *MYB* target genes encode for protein kinases (De Dominici *et al*., 2018; Ferrao *et al*., 1997; Ku *et al*., 1993). Interestingly, many *MYB* target genes are involved in transcriptional regulation, which has led to the hypothesis of MYB as master regulator of transcriptional programmes or as part of a wider transcription factor network of regulators (Lorenzo *et al*., 2011). A selection of MYB-related genes can be found as **Supplementary Table 1**.

In a study recently published by our research team, we have identified the DNA damage-activated kinase ATR as a MYB downstream target in ACC. *ATR* expression was high in *MYB*-expressing ACCs and pharmacological inhibition of ATR inhibited ACC growth *in vitro* and *in vivo* (Andersson *et al*., 2020). In the same study, a cluster of *MYB* or *MYB-NFIB* downstream genes were identified, mostly involved in the regulation of DNA repair, cell cycle, cell division and apoptosis, including the gene encoding the kinase BUB1, whose role in ACC has been the subject of this PhD project.

1.3 BUB1

1.3.1 BUB1 protein

Budding uninhibited by benzimidazole 1 (BUB1) was found to be upregulated *MYB*-transformed MCF10A and in ACC samples compared to normal salivary glands (Andersson *et al*., 2020).

BUB1 is a highly conserved serine/threonine protein kinase involved in the mitotic checkpoint (Kim, Taekyung & Gartner, 2021) (**Figure 1. 9**). Different stages of the cell cycle are tightly regulated by gateway control mechanisms known as checkpoints (**Figure 1. 10**) (Le Breton *et al*., 2005). Cell cycle checkpoints act to prevent the progression to the next stage of the cell cycle if cell size, DNA replication or integrity, and chromosome attachment are abnormal (Barnum & O'Connell, 2014).

TPR: 1-150
GLEBS: 240-280
R1LM: 266-310
CD1: 458-476
ABBA: 527-532
KEN: 535-537, 625-627
Kinase extension: 724-783
Kinase: 784-1085

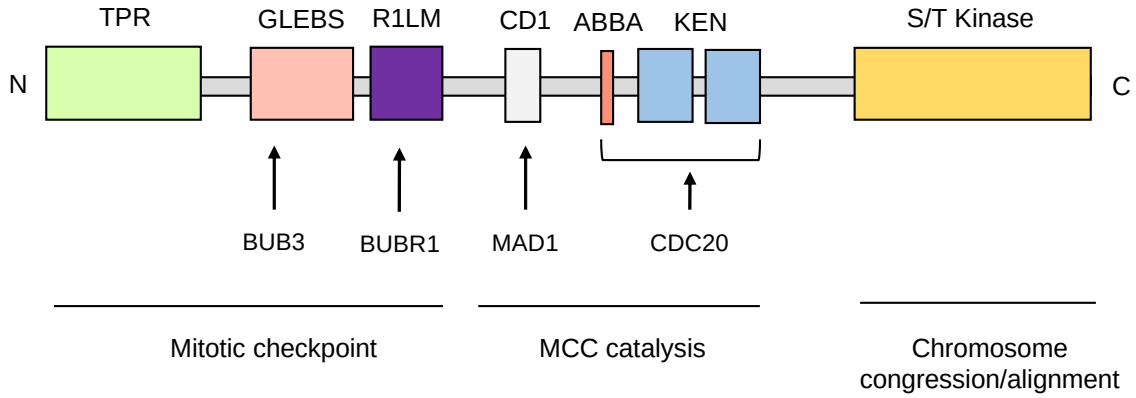

Figure 1. 9 | Schematic representation of the different domains of BUB1 protein. Domains are indicated on the top of the protein. Arrows show the sites for localisation and/or binding of the interacting proteins. TPR= tetratricopeptide repeat; GLEBS= Gle2-binding-sequence; R1LM= BUBR1 localisation motif; CD1= conserved domain 1; ABBA= cyclin A, BUBR1, BUB1, and Acm1p; KEN= lysine-glutamate-asparagine; S/T= serine/threonine; MCC= mitotic checkpoint complex. *Original illustration.*

The main function of BUB1 is to organise the spindle assembly checkpoint (SAC) during mitosis, monitoring chromosome segregation and stable attachment of the spindle-microtubule polymers to large proteinaceous structures at the centromere of multiple chromosomes (kinetochores) (**Figure 1. 10**) (Barnum & O'Connell, 2014; Zhang, Yuqing *et al*., 2022). The SAC is a safeguard mechanism to inhibit anaphase onset until the mitotic spindle is correctly positioned; it is activated if there is a failure in kinetochores attachment (Pesenti *et al*., 2016). The SAC is composed of different proteins, such as BUB1, BUB3, MAD1, MAD2, and MAD3 (BUBR1 in higher eukaryotes), AURKB, and CDC20 (Hoyt *et al*.,

1991; Li, R. & Murray, 1991; Zhang, Yuqing *et al*., 2022). BUB1 recruits several proteins to support chromosome alignment, and its knockout in mouse models results in embryonic lethality, suggesting it is necessary for faithful mitosis (Perera *et al*., 2007; Tilston *et al*., 2009; Zhang, Yuqing *et al*., 2022). Indeed, treatment of HeLa cells with siRNAs against BUB1 results in severe defective SAC signalling and chromosome alignment and, as a consequence, cells proceeded to anaphase with unaligned chromosomes (Chen, Q. *et al*., 2021; Zhang, Gang *et al*., 2017).

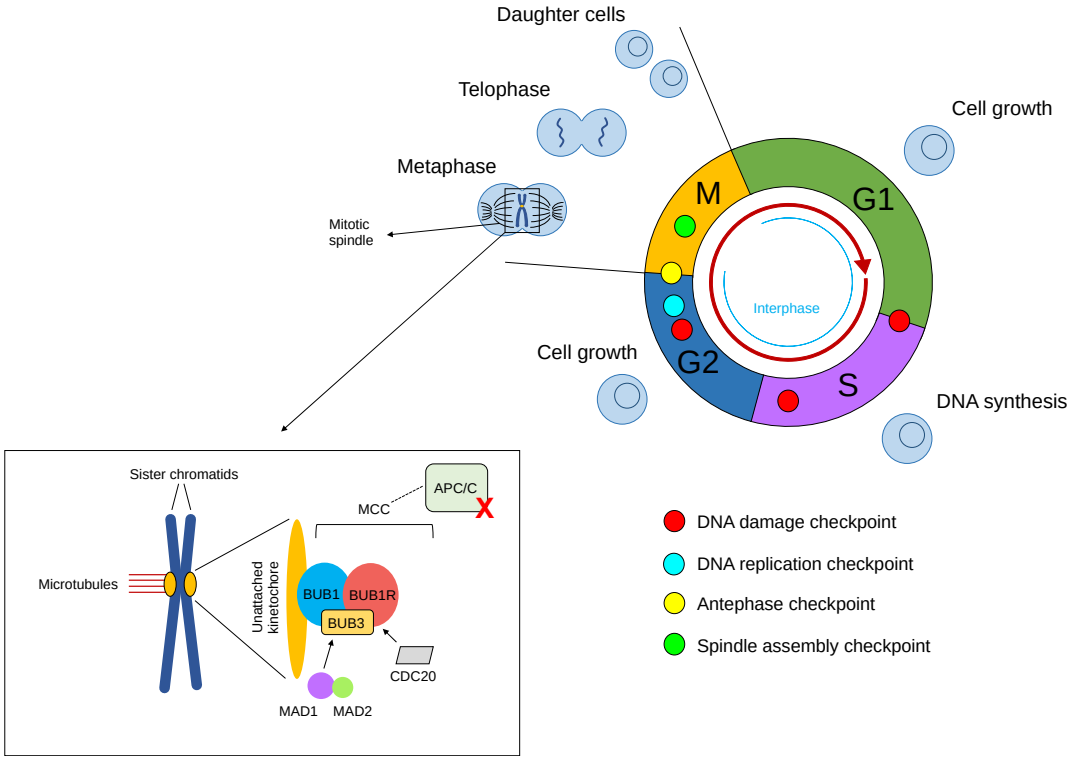

Figure 1. 10 | Schematic representation of cell cycle phases and proteins assembled at the kinetochore. Cell cycle includes interphase (G1, S, and G2), and mitosis (M). Mitosis includes prophase, metaphase, anaphase, and telophase to obtain two identical daughter cells. In case of unattached kinetochores at the mitotic spindle, the spindle assembly checkpoint (SAC) is activated, and the mitotic checkpoint complex (MCC) proteins are recruited (box at the bottom left). By sequestering Cdc20, the MCC keeps the APC/C inactive (red X), maintaining sister-chromatid cohesion and determining the cell cycle arrested until all kinetochores have properly aligned and segregation can proceed correctly. *Original illustration.*

BUB1 protein consists of 1085 residues (D'Arcy *et al*., 2010; Kang *et al*., 2008) and the N-terminal region is the most conserved in both BUB1 and BUBR1 and their homologues, and it was shown to be essential for the SAC; indeed, murine embryonic fibroblasts with mutant forms of the N-terminal region caused chromosome instability (Schliekelman *et al*., 2009). The crystal structure of this region revealed a triple-tandem arrangement of the tetratricopeptide repeat (TPR) motif essential for kinetochore localisation (Bolanos-Garcia *et al*., 2009; Leontiou *et al*., 2019). The BUB3-interacting motif (also known as Gle2-binding-sequence, GLEBS) enhances the recruitment of BUB3, while BUBR1 localises on the BUBR1 localisation motif (R1LM) (Bolanos-Garcia *et al*., 2009; Elowe & Bolanos-Garcia, 2022). BUB1 conserved domain 1 (CD1) SLiM recruits MAD1 (Elowe & Bolanos-Garcia, 2022). CDC20 binding is mediated by two KEN boxes and the ABBA (cyclin A, BUBR1, BUB1, and Acm1p) domain, that ensure CDC20 phosphorylation providing a catalytic mechanism for the anaphase-promoting complex (APC/C) inhibition (Tang, Z. *et al*., 2004). Finally, the kinase domain at the carboxyl-terminus of the protein is involved in protein phosphorylation and dephosphorylation required for SAC signalling (Zich & Hardwick, 2010).

1.3.2 *BUB1* involvement in human cancers and salivary gland neoplasms

Alterations in BUB1 including deletions, point mutations, and expression changes, have been observed in several malignancies (Cahill *et al*., 1998; Hernando *et al*., 2001; Klebig *et al*., 2009; Ohshima *et al*., 2000; Ru *et al*., 2002; Shichiri *et al*., 2002; Wang *et al*., 2015). In general, cancers are characterised by uncontrolled proliferation and aneuploidy (Sherr, 1996). However, the mechanism by which BUB1 promotes tumourigenesis it is not yet clarified.

Mouse models carrying *Bub1* mutations exhibit increased chromosome segregation errors and aneuploidy (Ricke *et al*., 2011; Ricke *et al*., 2012). However, other studies on breast

cancer cell lines reported that most *BUB1* mutations do not cause functional protein changes, suggesting that mutations might not be the leading cause of chromosomal instability in this cancer (Yuan *et al*., 2006).

In fact, genomic instability can occur in different ways. It has been reported that mutations in checkpoint genes are rare, nonetheless a weakened SAC is a common feature in cancers, and likely cooperates with additional genetic changes to facilitate cancer initiation (Kops *et al*., 2005). Moreover, SAC proteins can also be affected by epigenetic changes (Kops *et al*., 2005; Shichiri *et al*., 2002). Conversely, it has been demonstrated that cancer can be promoted also when SAC components are upregulated, suggesting that any perturbation of checkpoint proteins might be decisive for cells' fate (Grabsch *et al*., 2003; Shigeishi *et al*., 2001; Yuan *et al*., 2006). The causative connection between spindle defects, genomic abnormalities, and oncogenesis has been recently investigated. For instance, it has been reported that the breast-cancer-associated gene 1 (*BRCA1*) maintains genomic stability through interplay with the tumour suppressor gene *p53* and modulating spindle checkpoint genes, including *MAD2*, *BUB1*, and *BUBR1* (Wang, Rui-Hong *et al*., 2004). Another BRCA family member, *BRCA2*, is involved in DNA repair and acts as a tumour suppressor but, paradoxically, its truncated version provokes cell growth arrest, which is overridden by mutations in *BUB1*, enforcing the hypothesis of spindle checkpoint implication in carcinogenesis (Lee, Hyunsook *et al*., 1999). Although the mechanisms of action are not fully understood and still controversial, different studies correlate *BUB1* expression (and limitedly *BUB1* mutations) with poor prognosis in several cancers, including breast cancer, glioma, prostate cancer, and salivary gland tumour (Bie *et al*., 2011; Finetti *et al*., 2008; Glinsky *et al*., 2005; Nakagawa *et al*., 2008; Shigeishi *et al*., 2006).

BUB1 expression has been linked to abnormal cell proliferation in salivary gland malignancies (Shigeishi *et al*., 2006). *BUB1* expression was higher in malignant salivary gland tumours compared to the benign type and the normal submandibular gland tissue, suggesting that overall *BUB1* can be associated with proliferative activity of glandular malignancies (Shigeishi

et al., 2006). mRNA levels of *BUB1* tightly correlated with PCNA protein in 3 submandibular glands and 15 salivary gland tumours, and with Ki-67 labelling index, which has been reported as prognostic marker of various salivary gland carcinomas (Hellquist *et al*., 1997; Nordgård *et al*., 1997; Shigeishi *et al*., 2006). Moreover, *BUB1* expression levels weakly correlated with the clinical stage, and patients with larger tumours and/or lymph node metastases showed higher *BUB1* mRNA expression (Shigeishi *et al*., 2006).

One of the pioneer studies on checkpoint involvement in cancer comes from Cahill and colleagues (1998) who showed how chromosome instability (CIN) and aneuploidy are consistently associated with the mutational inactivation of *BUB1* in CRC (Cahill *et al*., 1998). They discovered that cells with CIN transfected with *BUB1* mutants prematurely exit mitosis even in presence of microtubule mis-segregation, bypassing the checkpoint machinery, suggesting the importance of BUB1 in the accurate supervision of the mitotic exit (Cahill *et al*., 1998). Shichiri and colleagues (2002) analysed *BUB1* mutational status and mRNA levels in 103 CRC carcinomas samples compared to the normal colonic mucosa (Shichiri *et al*., 2002). They found that *BUB1* was expressed in all the normal colonic mucosa but inactivated in 3 samples out of 103; however, mRNA levels were markedly higher in cancers compared to their normal tissues (Shichiri *et al*., 2002).

Other studies suggested that *BUB1* may be involved in germline mutations in familiar CRC (Broderick *et al*., 2017). Deleterious *BUB1* (none stop-gain, frameshift, or splice-site) variants have been associated with increased risk of developing CRC at young age, with mosaic variegated aneuploidy syndrome (MVAS) and variable dysmorphic features (de Voer *et al*., 2013; Djursby *et al*., 2020; Mur *et al*., 2018). Broderick and colleagues (2017) screened more than 2000 samples of familiar/early onset CRC or normal controls to investigate hereditary genes (Broderick *et al*., 2017). Interestingly, none of the reported variants were found during the screening, with only one likely pathogenic *BUB1* variant reported, together with four variants found in control samples (Broderick *et al*., 2017). Nevertheless, these alterations are

rarely seen in other cancers, suggesting that they are restricted to CRC (Myrie *et al*., 2000; Shigeishi *et al*., 2001; Shigeishi *et al*., 2001).

The role of *BUB1* in familiar cancer has been a topic of debate in the last years and its causal implication in CRC tumourigenesis is yet to be demonstrated.

The role of *BUB1* in breast cancers was investigated by several groups (Han *et al*., 2015; Wang, Zhanwei *et al*., 2015; Yuan *et al*., 2006). It has also been demonstrated that the breast cancer cell line MDA-MB-231 with depleted *BUB1 via* short hairpin RNAs (shRNA) lacks the ability to generate xenograft in immunocompromised mice (Han *et al*., 2015). According to this study, *BUB1*-depleted MDA-MB-231 and MCF7 breast cancer cells showed a reduced cancer stem cells (CSCs) potential, thus diminishing the pool of cells capable of self-renewal and able to boost tumour pathways and resistance to anti-cancer therapies (Han *et al*., 2015; O'Brien *et al*., 2009). CSCs confer resistance to therapies, and as consequence of the reduced CSCs population after *BUB1* depletion breast cancer cells showed an increased sensitivity to radiation compared to the control (Han *et al*., 2015). Hence, the authors suggested that BUB1, like other mitotic regulators, such as AURKA, BUBR1, and PLK1, might be used as a target for anti-CSCs therapy (Han *et al*., 2015).

Variable expression of *BUB1* was detected in 19 aneuploid breast cancer cell lines (Myrie *et al*., 2000). Interestingly, no mutations were found, although nine variations were identified, none of which, however, predicted significant changes in the protein structure, suggesting that while regulation of BUB1 protein may be crucial for cancer development, putative deleterious mutations in *BUB1* do not fully support its role in breast cancer pathogenesis (Myrie *et al*., 2000).

A study conducted by Wang *et al.* (2015) showed that increased expression of *BUB1* (as well as *MAD2L1*) is significantly associated with increased risk of recurrence and death, lower relapse-free survival and OS in breast cancer patients (Wang, Zhanwei *et al*., 2015). In *in vitro* experiments, Wang and colleagues (2015) observed that downregulation of *MAD2L1* and *BUB1* resulted in reduced cell growth, migration, and invasion of breast cancer cells (Wang,

Zhanwei *et al*., 2015). Some clues on the mechanisms of action were revealed by studies showing that suppression of *BUB1* expression leads to crucial inhibition of TGF-β-mediated cell migration and invasion, highlighting the biological relevance of *BUB1* and *MAD2L1* in breast cancer progression (Nyati *et al*., 2015; Wang, Zhanwei *et al*., 2015). Yuan and colleagues (2006) analysed a panel of 12 breast cancer cell lines and found increased mRNA transcript levels of the checkpoint genes *MAD1L1*, *MAD2L1*, *MAD2L2*, *BUB1*, *BUB1B*, *BUB3*, *CDC20*, and *TTK* in cancerous cells compared to the normal breast cell line MCF10A (Yuan *et al*., 2006).

Also in gastric carcinoma, mutational inactivation of the *BUB1* gene is not involved in the pathogenesis, but its expression levels correlate with tumour proliferating activity (Grabsch *et al*., 2003; Shigeishi *et al*., 2001; Shigeishi *et al*., 2001). The first demonstration that *BUB1* mRNA is associated with tumour growth comes from Shigeishi *et al.*'s study (2001) reporting that *BUB1* expression is strongly correlated with PCNA and Ki-67 protein levels, two common immunohistochemical markers used for evaluating cell proliferation (Bologna-Molina *et al*., 2013; Shigeishi *et al*., 2001). A few years after this discovery, Grabsch and colleagues (2003) corroborated the results by analysing a set of 43 gastric carcinomas and examined gene expression of BUB family members (*BUB1*, *BUBR1*, *BUB3*) (Grabsch *et al*., 2003). *BUBs* were found simultaneously overexpressed in 61% of the cohort analysed, with *BUB1* overexpressed in 84% of the tumours (Grabsch *et al*., 2003). In addition, the correlation between *BUB* genes and *Ki-67* was investigated, resulting in a significant strong positive correlation that suggested a proliferative-dependent overexpression of *BUB1* in gastric cancers (Grabsch *et al*., 2003).

Mitotic checkpoint defects are found in about 40% of human lung cancer cell lines (Takahashi, Takao *et al*., 1999). Accordingly, a proportion of lung cancer can be expected to present alterations in gene checkpoints. However, studies indicate that *BUB* gene family members are not frequently dysregulated in lung cancer, if present at all (Haruki *et al*., 2001). The rarity of *BUB1* mutations in this cancer was validated in multiple studies, strengthening the idea that

the gene is not a target for genetic alterations in this type of neoplasm and additional investigations may shed light on the mechanistic impact of mitotic checkpoint impairment in lung cancer (Haruki *et al*., 2001; Sato *et al*., 2000; Yamaguchi *et al*., 1999).
Bioinformatics analysis on lung adenocarcinoma identified the overexpression of *BUB1* as one of the genes potentially relevant to clinical outcomes, showing an impact on the survival of patients, and suggesting BUB1 as a potential target for therapeutic strategies in this context (Li, P. *et al*., 2022; Wang, Luyao *et al*., 2020).

Mutations of BUB1 have been described in T cell leukaemia/lymphoma (ATLL) (Ohshima *et al*., 2000). In 8 B-cell lymphoma cases, only one nonsense mutation was found, suggesting a lower mutational rate compared to ATLL (Ohshima *et al*., 2000). Moreover, chromosomal analysis showed significantly more frequent numerical and structural abnormalities in T than B cell lymphoma, suggesting that functional loss of checkpoint genes might prompt the progression of CIN (Ohshima *et al*., 2000).
By transfecting various leukaemic cell lines with vectors expressing either wild-type (WT) or mutant *BUB1*, a significant lower mitotic index was detected in cells expressing the mutant compared to the WT form (Ru *et al*., 2002). Similar results were obtained by analysing the mitotic index of leukaemia cells harbouring deletions in the *BUB1* coding sequence, rendering the protein non-functional (Ru *et al*., 2002). Indeed, in the presence of the defective forms of *BUB1*, treatment of these cells with nocodazole, a spindle-disrupting agent, did not prevent prematurely exit from mitosis and start of a new round of DNA synthesis (Ru *et al*., 2002).

BUB1 gene and protein are overexpressed in bladder cancers samples compared to matched normal controls (Jiang, N. *et al*., 2021). Following siRNA-mediated *BUB1* downregulation, more than 1500 genes were dysregulated, especially those related to *JAK-STAT* signalling (Jiang, N. *et al*., 2021). This study showed that *STAT3* transcriptional activity depended on *BUB1* expression since BUB1 directly binds and phosphorylates STAT3 at Ser727, promoting the development of bladder cancer (Jiang, N. *et al*., 2021).

Constitutive activation of the TGF-β/SMAD signalling pathway serves an important role in the development and progression of liver cancer; in fact, overexpression of TGF-β signalling enhances expression of genes involved in cell growth and its effect is mediated *via* interaction with SMAD transcription factors (Derynck & Zhang, 2003; Dituri *et al*., 2019; Wrana *et al*., 1994). Overexpression of *BUB1* promoted proliferation of liver cancer cells *in vitro*, while cell growth became inhibited after shRNA-mediated *BUB1* knockdown (Zhu *et al*., 2020). It was found that BUB1 promoted liver cancer cells proliferation by increasign the phosphorylated form of SMAD2 (Zhu *et al*., 2020).

Overall, in virtue of its role in cell cycle control and genomic stability, investigating the functions of BUB1 in cancer is gaining interest to open new potential diagnostic, prognostic and therapeutic options.

Aims

The main goal of this PhD project was to develop a new, easy to manipulate cellular model of ACC with which to study the molecular links between the MYB oncoprotein and the mitotic checkpoint kinase BUB1.

Specific aims were:

1) To generate a *MYB* switchable system based on the non-tumourigenic MCF10A breast cell line, which was validated with patient derived cells and tumours (**Chapter III**)
2) To dissect the mechanisms used by MYB to regulate *BUB1* expression, *in vitro* and *in vivo* (**Chapter IV**)
3) To investigate the therapeutic potential of inhibiting BUB1 activity in ACC models, *in vitro* and *in vivo* (**Chapter V**)

Chapter II

Materials and methods

This thesis contains experiments performed in collaboration with other research groups or Companies. **Table 2. 0** summarises their work and contributions.

Table 2.0 | Summary of the experiments and the performers

Experiment	Performer(s)	Affiliation	Location
ACCX11 establishment	Göran Stenman's group	Sahlgrenska Center for Cancer Research	Gothenburg, Sweden
ACCX11 culturing and treatment	Ylenia Cicirò	Brunel University London	London, UK
MCF10A engineering	Ylenia Cicirò	Brunel University London	London, UK
Luciferase assay	Ylenia Cicirò	Brunel University London	London, UK
Cell health assays	Ylenia Cicirò	Brunel University London	Gothenburg, Sweden/London, UK
FACS and imaging	Ylenia Cicirò	Brunel University London	London, UK
siRNA	Göran Stenman's group	Sahlgrenska Center for Cancer Research	Gothenburg, Sweden
3D spheroid	Kiyatec	Kiyatec	Greeneville, SC
In vivo	XenoSTART	XenoSTART	S. Antonio, Texas, USA
RT-qPCR	Ylenia Cicirò	Brunel University London	London, UK
ChIP	Göran Stenman's group	Sahlgrenska Center for Cancer Research	Gothenburg, Sweden
	Ylenia Cicirò	Brunel University London	London, UK
Western blot	Ylenia Cicirò	Brunel University London	London, UK
IHC	Gianluca Sala/ Rossano Lattanzio	Università di Chieti-Pescara	Chieti-Pescara, Italy
Bioinformatics	Ylenia Cicirò/Denise Ragusa	Brunel University London	London, UK

2.1 Cell lines

MCF10A, a non-tumourigenic human mammary epithelial cell line, was grown in 10 cm dishes in DMEM/F12 medium (Gibco, Paisley, UK), 5% horse serum (v/v) (Gibco), and 100 U/mL penicillin-streptomycin (PenStrep) antibiotic (Gibco), supplemented with 20 ng/mL of human epidermal growth factor (hEGF) (Invitrogen, Inchinnan, UK), 500 ng/mL hydrocortisone (MP Biomedicals, California, USA), 100 ng/mL cholera toxin (Invitrogen), 10 µg/ml insulin (Sigma-Aldrich). Cells were maintained at a density of 5 x 10^5 cells/mL with medium change every 48 hours. Cells were detached by washing them in 1X Phosphate Saline Buffer (PBS) (Gibco) followed by incubation in trypsin-EDTA (0.25%) (Gibco) for 10 minutes at 37° C. Medium was added to quench the trypsin with a ratio of 3:1, cells were then pelleted by centrifugation at 400 x g for 5 minutes and resuspended in fresh culturing medium for replating. Cells were maintained in incubation at 37° C and 5% CO_2.

Engineered MCF10A cells (MM), transduced with a *MYB*-expressing lentivirus, were cultured in the same medium used for MCF10A cells with the addition of 2 µg/mL doxycycline (DOX) (MP Biomedicals). Medium was replaced every 48 hours.

The patient-derived xenograft (PDX) human cell line ACCX11 was obtained from Prof Göran Stenman (Sahlgrenska Center for Cancer Research (SCCR), University of Gothenburg, Gothenburg, Sweden). Cells were cultured in T25 flasks as per publication (Andersson *et al*., 2017; Persson *et al*., 2009). Cells were passaged every 7 days. For replating, medium was discarded, 2 mL of trypsin-EDTA (0.25%) (Gibco) were added to wash the cells and 1 mL of trypsin-EDTA (0.25%) (Gibco) was used to detach the cells. Once detached, ACC cells were centrifuged at 300 x g for 5 minutes and plated in fresh medium.

HEK293T cells were cultured in T75 flasks in DMEM GlutaMAX (4.5 mg/mL glucose, L-glutamine) (Gibco), supplemented with 10% v/v foetal bovine serum (FBS) (Gibco), and

100 U/mL PenStrep antibiotic (Gibco). Cells were passaged every 2-3 days and maintained at 80% confluency. Passaging was performed by mechanical detachment of cells and replacement of medium.

Cells were monitored for mycoplasma using the MycoSensor Assay Kit (Agilent, Cheshire, UK).

2.2 Three-dimensional culture (3D spheroid)

Three-dimensional (3D) ACC spheroids were performed by the Adenoid Cystic Carcinoma Research Foundation (ACCRF, MA, USA) in collaboration with the biotech company Kiyatec (Greeneville, SC).

Cryopreserved PDX tissues were thawed, dissociated, and cells were plated. Spheroids were cultivated for 7 days before treating them and performing functional assays.

2.3 *In vivo* models

In vivo studies were performed by the Adenoid Cystic Carcinoma Research Foundation (ACCRF, MA, USA) in collaboration with XenoSTART (S. Antonio, Texas, USA).

ACCX11 tumour fragments were implanted into the flanks of NSG immunodeficient mice and let grow until palpable. Mice were then randomised into drug and control groups and monitored. Individual animals reaching a tumour volume as predetermined study endpoint were removed from the study. The study involved mice used as non-treatment (NT) control group, and mice treated with BAY1816032. Additional information is confidential.

2.4 Luciferase assay

Vector construction

Vectors pGL3-BUB1 WT and pGL3-BUB1 Mut were made by subcloning a portion of *BUB1* promoter region into pGL3-Basic reporter vector (Mammalian, #VGG098) from Biomatik Corporation (Kitchener, Canada) (**Figure 2. 1 A**). The wild-type sequence (BUB1 WT) was extrapolated from the National Center for Biotechnology Information (NCBI) website (https://www.ncbi.nlm.nih.gov), by selecting 500 bp upstream to the transcription start site (TSS) (codon ATG, position 110677995) (**Figure 2. 2**). The sequence was screened searching for canonical MYB binding sites (MBSs) -(T/C)AACNG- and the MBSs presents were point mutated in order to create the BUB1 Mut sequence (**Figure 2. 2**). Both BUB1 WT and BUB1 Mut were subcloned into the pGL3-Basic (lacking promoter and enhancer features) backbone vector upstream the luciferase gene by using KpnI and XhoI as restriction enzymes at 5' and 3', respectively (**Figure 2. 1 A-B**)**.** Cloning was performed by Biomatik Corporation and the vectors were delivered as 4 µg lyophilised plasmid containing the gene insert.

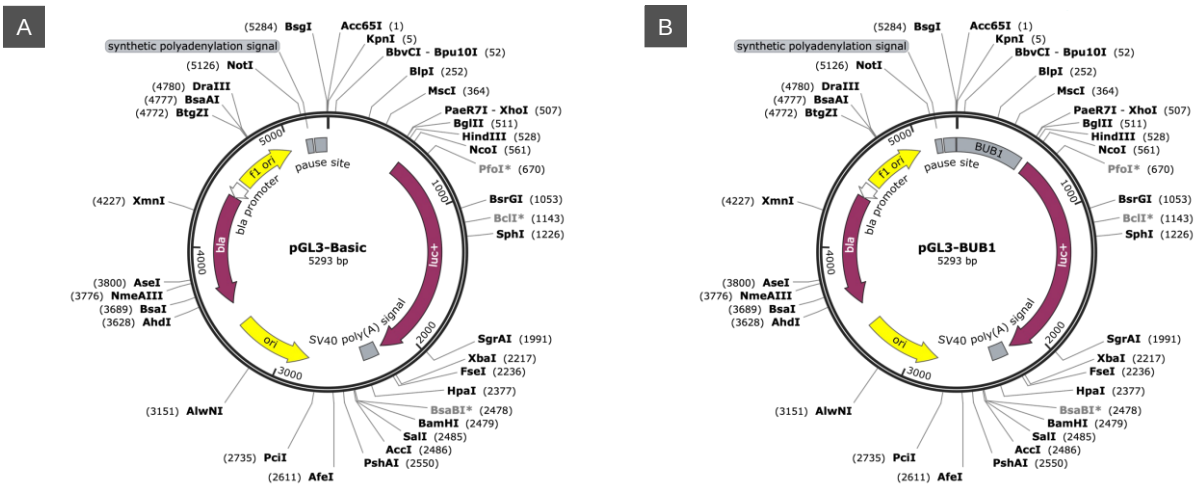

Figure 2. 1 | pGL3 vectors from Biomatik Corporation. (**A**) pGL3-basic vector is a luciferase reporter vector with a modified coding region for firefly (*Photinus pyralis*) luciferase. It lacks promoter and enhancer. (**B**) pGL3-BUB1 (WT/Mut) contains the BUB1 sequence of 512 bp (500 bp *BUB1* promoter plus 12 bp of for the restriction enzymes; see **Figure 2. 2** for more details) either wild type (WT) or mutated (Mut).

BUB1 WT

5'- ggtacc ATTTAAGCGAAGGGGAGAAGAAACGCGACTCTCAGGACCCAAGGGCTGAGGCAGGGTTTTTCTGTCTCAAAG
ACCTCCAGTTAAGACATTTTTCTCCTGCAAAGCCTTTCCTACAATGATGGCTTAATCGTGTAATTATGTAAACC
AGTCACAACCTGGATAGCTAAAACAAAAAAAACCAATTCCCTACGCCCGAGCCAAGCCTGCTCCCCCTCGCCG
TGCCGCATCCCAAACACCCCGCGCTCGCTCAGCCAACGGCCAGGTTTCGGTTCAACCGAAAACCACGGGAA
GTGGGAGGAGCTACTGGCTCAAGGGAGGGAGGTGGGACTTGACCTCCGAGCAACGGCCCCGGTGATTGGC
CAACCTTCTGCCGCCGCCACCAATGGGCAGGCGCCCTGAAACGTTCGGCGAGCCGACTGCGGCTGCGCGG
GGTATTCGAATCGGCGGCGGCTTCTAGTTTGCGGTTCAGGTTTGGCCGCTGCCGGCCAGCGTCCTCTGGCC ctcgag -3'

BUB1 Mut

5'- ggtacc ATTTAAGCGAAGGGGAGAAGAAACGCGACTCTCAGGACCCAAGGGCTGAGGCAGGGTTTTTCTGTCTCAAAG
ACCTCCCCTTAAGACATTTTTCTCCTGCAAAGCCTTTCCTACAATGATGGCTTAATCGTGTAATTATGTAAACC
AGTCACAACCTGGATAGCTAAAACAAAAAAACCAATTCCCTACGCCCGAGCCAAGCCTGCTCCCCCTCGCCG
TGCCGCATCCCAAACACCCCGCGCTCGCTCAGCCCCCGGCCAGGTTTCGGTTCCCCCGAAAACCACGGGAA
GTGGGAGGAGCTACTGGCTCAAGGGAGGGAGGTGGGACTTGACCTCCGAGCCCCGGCCCCGGTGATTGGC
CAACCTTCTGCCGCCGCCACCAATGGGCAGGCGCCCTGAAACGTTCGGCGAGCCGACTGCGGCTGCGCGG
GGTATTCGAATCGGCGGCGGCTTCTAGTTTGCGGTTCAGGTTTGGCCGCTGCCGGCCAGCGTCCTCTGGCC ctcgag -3'

Figure 2. 2 | *BUB1* promoter regions cloned. In uppercase the 500 bp upstream the TSS of *BUB1*. In lowercase the sequence of the restriction enzymes used to create sticky ends and subclone these portions into the pGL3-Basic backbone: KpnI and XhoI at the 5' and 3' end, respectively. The top section shows *BUB1* wild type (BUB1 WT) promoter region extrapolated from the NCBI repository. The bottom one shows the BUB1 Mut sequence containing point mutations (in red) to alter the canonical MBSs (T/C)AACNG highlighted in yellow. All the mutations were performed following the rule CAACG/CG converted to CCCCGG. The underlined MBS is antisense.

Plasmids expansion and purification

pGL3-BUB1 (WT/Mut) lyophilised plasmids were resuspended in pure water to a final concentration of 100 µg/mL. Bacterial transformation was performed by mixing 100 ng of plasmid DNA into 50 µL of competent cells (*E. coli*, DH5α strain) in a tube, and incubating it on ice for 30 minutes. Heat shock was carried out for 45 seconds at 42° C, followed by 3 minutes back on ice. 2 mL of liquid selective LB medium were added, and the tube was placed

in a shaking incubator at 37° C for 1h. 0.5 mL of the mix was streaked onto an LB-agar plate containing ampicillin (100 µg/mL, Merck Life Science, UK) and incubated at 37° C overnight. 12 hours later, individual colonies were picked and first grown in 3 mL liquid selective LB medium containing ampicillin (50 µg/mL, Merck) in a shaking incubator at 37° C overnight, and further expanded in 100 mL selective LB medium with addition of ampicillin (50 µg/mL, Merck). Plasmids were purified using NucleoBond Xtra Midi kit (Macherey-Nagel, Duren, Germany). Overnight cultures were pelleted by centrifugation at 4500 x g for 15 minutes, the supernatants were discarded, and the pellets resuspended in 8 mL of Resuspension Buffer containing RNAse A by pipetting up and down. 8 mL of Lysis Buffer were added to the suspensions and the tubes inverted 5 times and incubated at room temperature for 5 minutes; meanwhile the columns to filter the solutions were equilibrated with 12 mL of Equilibration Buffer. 8 mL of Neutralisation Buffer were added and mixed to the homogeneous suspensions, loaded into the columns, and allowed to drain by gravity flow. The columns were washed with 5 mL of Equilibration Buffer first and 8 mL of Wash Buffer after, allowing drainage by gravity. 5 mL of Elution Buffer were added, and the eluate was collected in clean centrifuge tubes. To precipitate the DNA, 0.7 volumes of room-temperature isopropanol were mixed to the eluate by vortexing and centrifuged at 4500 x g for 20 minutes. After discarding of the supernatant, the pellets were washed with 2 mL of 70% ethanol, centrifuged at 4500 x g for 10 minutes, and following the removal of the supernatant, let dry for 10 minutes at room temperature. The DNA was reconstituted in 100-200 µL molecular grade water and quantified by Nanodrop 2000c spectrophotometer (Thermo Fisher Scientific, Oxford, UK).

Luciferase assays

$5x10^4$ MCF10A cells were seeded per well in 24-well plates. The next day, plasmids were transfected with jetPRIME Transfection Reagent (Polyplus, Lancing, UK). jetPRIME buffer were mixed with DNA in a microcentrifuge tube, with a ratio DNA:jetPRIME reagent 1:2, and

incubated at room temperature for 10 minutes. The mix was delivered onto the wells drop-wise in a final volume of 500 µL/well and the plate incubated at 37° C and 5% CO_2 for 48 hours. pLXSN (empty vector EV and MYB) plasmids (Sala *et al*., 1995) were co-transfected with pGL3-BUB1 (WT or Mut) to a final concentration of 0.5 µg. pRenilla luciferase vector was used as internal control. The vector pGL3-Basic was used as empty vector (EV) luciferase control. All the different combinations of DNA plasmids are reported in **Table 2. 1**.

Table 2. 1 | Different combinations of DNA plasmid delivered for DNA transfection.
The volumes and concentrations shown are referred to a single well of a 24-well plate. Buffer, jetPRIME Buffer; Reagent, jetPRIME Reagent.

		DNA					
Buffer	**Reagent**	**pGL3 EV**	**pGL3-BUB1 WT**	**pGL3-BUB1 Mut**	**pLXSN-EV**	**pLXSN-MYB**	**pRenilla**
50 µL	1 µL	0.25 µg	/	/	0.25 µg	/	0.001 µg
50 µL	1 µL	0.25 µg	/	/	/	0.25 µg	0.001 µg
50 µL	1 µL	/	0.35 µg	/	0.15 µg	/	0.001 µg
50 µL	1 µL	/	0.35 µg	/	/	0.15 µg	0.001 µg
50 µL	1 µL	/	/	0.35 µg	0.15 µg	/	0.001 µg
50 µL	1 µL	/	/	0.35 µg	/	0.15 µg	0.001 µg

Luciferase activity was detected with the Dual-Luciferase Reporter Assay System (Promega, Chilworth, UK). Culture medium was removed by aspiration, cells were rinsed with 1X PBS solution (Gibco) and 100 µL of 1X Passive Lysis Buffer (PLB) were dispensed into each well. The plate was gently rocked for 20 minutes at room temperature to perform passive lysis. In round-bottom tube suitable for luminometry assay, 10 µL of cell lysate were mixed with 50 µL

of Luciferase Assay Buffer II (LARII) and firefly luciferase activity was measured using a Junior LB 9509 Portable Luminometer (Berthold Technologies, Harpenden, UK). After the first measurement, 50 µL of Stop and Glo Reagent was added, the tube gently flicked and pRenilla luciferase activity measured. To calculate Relative Light Unit (RLU), firefly counts were divided by pRenilla counts used to control transfection efficiency. The experiment was performed in triplicates.

2.5 Pharmacological treatments

A list of all the drugs used is reported in **Table 2. 2**.

Table 2. 2 | List of drugs used. DMSO, dimethyl sulfoxide.

Drug name	Working concentration	Manufacturer
BAY1816032	1-10 µM	MedChemExpress, New Jersey, USA
Gemcitabine	0.01-10 µM	Selleck Chemicals, Planegg, Germany
Paclitaxel	0.01-10 µM	Selleck Chemicals
Vinorelbine	0.01-10 µM	Selleck Chemicals
DMSO	0.2%	Fisher Scientific, Loughborough, UK
Doxycycline	2 µg/mL	MP Biomedicals

MM (EV/MYB) cells and ACCX11 cells were seeded in a 96-well plate at a density of 4 000 cells/well (for MTT and alamarBlue assays) or 8 000 cells/well (for apoptosis assay) in 100 µL of complete medium and incubated at 37° C and 5% CO_2 for 24 hours. Medium was discarded and fresh medium containing different concentrations of BAY1816032 (BUB1 inhibitor) was added. DMSO was used as vehicle control. Cells were incubated at 37° C and 5% CO_2 for 72 hours (for MTT and alamarBlue assays) or 48 hours (for apoptosis assay) covered in foil to prevent exposure to light.

2.6 Cell health assay

Proliferation assay

Proliferation of naïve or engineered MCF10 cells was quantified using the MTT assay (Cayman Chemical, Ann Arbor, US) that measures cellular metabolic activity by the conversion of 3-(4,5-dimethylthiazol-2-yl)-2,5- diphenyltetrazolium bromide (MTT) into formazan. 10 µL of MTT reagent were added to each well and mixed by shaking for 1 minute, followed by a 3-hour incubation at 37° C and 5% CO_2. To dissolve formazan crystals, 100 µL of dissolving buffer were added to each well and cells were incubated for further 12 hours. The intensity of the colourimetric reaction was quantified by absorbance at 570 nm using the CLARIOstar Plate Reader (BioTek, Winooski, US) and values were normalised to DMSO (control vehicle) treated cells.

Cell viability assay

ACCX11 cells were seeded in 96-well black pigmented plates, treated or untreated with drugs. After 72 hours, the resazurin-based alamarBlue Reagent (Thermo Fisher Scientific) was

added in an amount equal to 10% of the medium volume in the well. In living cells, resazurin is reduced to resorufin, a highly fluorescent coloured compound. Plates were covered with foil to prevent exposure to light and incubated for 4 hours at 37° C and 5% CO_2. Next, plates were left for 15 minutes at room temperature before cell viability was measured by reading fluorescence at 544 nm using a SpectraMax L Microplate Reader (Molecular devices, San Jose, USA).

Apoptosis assay

For apoptosis assays, ACCX11 cells were seeded in white-walled 96-well luminometer plates with or without the BUB1 inhibitor and incubate for 48 hours at 37° C and 5% CO_2. Caspase-Glo 3/7 Reagent (Promega) was added in a proportion 1:2 to the volume of medium in the well and gently mixed by pipetting. Plates were incubated for 1 hour at 37° C and 5% CO_2 covered in foil. Luminescence emission is proportional to Caspase activity and was measured with the SpectraMax L Microplate Reader (Molecular devices) with an excitation filter of 560 nm.

2.7 Lentiviral vector transduction

Lentiviral vectors

The inducible lentiviral vector pINDUCER21 (ORF-EG) backbone (hereby referred to as “EV”, empty vector, #46948) and pINDUCER21-MYB (#51305) were purchased from Addgene (Teddington, UK) (**Figure 2. 3**) and delivered as bacterial stabs. The viral packaging vectors pCMV(-PL) and pMD2.G (Addgene, #20783 and #12259, respectively) were used to assemble lentiviral particles and expanded following the procedure described in “Vector expansion and purification” section.

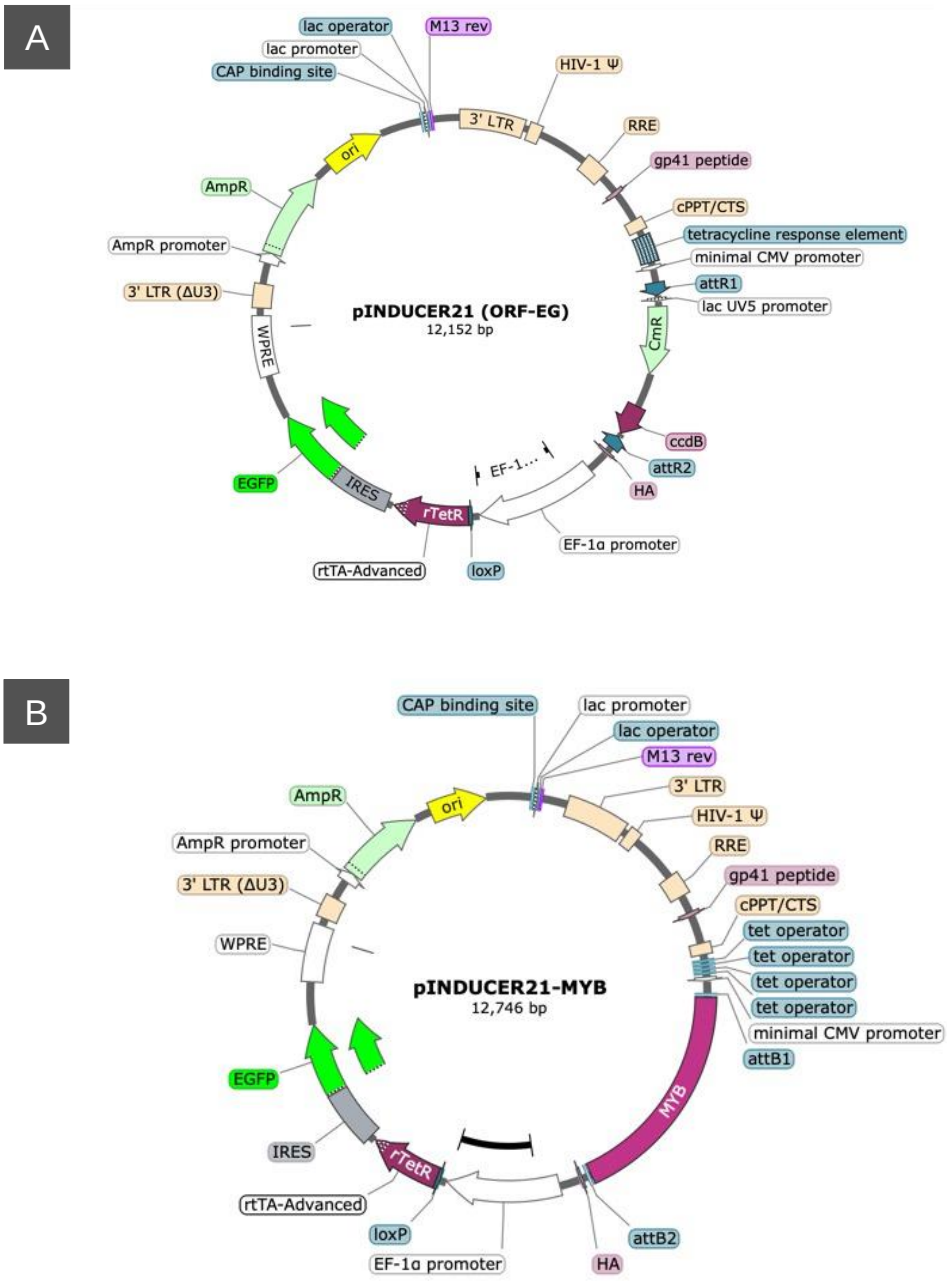

Figure 2. 3 | Inducible lentiviral gene expression vectors. (**A**) Maps of the lentiviral vectors pINDUCER21 (ORF-EG, empty backbone or empty vector EV) and (**B**) pINDUCER21 overexpressing *MYB*. Chloramphenicol cm + ccdB cassette in pINDUCER21-EV was removed in the pINDUCER21-MYB to clone into the gene of interest. Vector maps were downloaded from Addgene website and modified by using Snapgene. Both plasmids contain enhanced green fluorescent protein (EGFP) and a tetracycline-inducible expression system (Tet-On). Conditional *MYB* expression is turned on in the presence of DOX.

Vector expansion and purification

Bacterial stabs containing the vector of interest were streaked using a sterile inoculation loop onto LB-agar plates containing ampicillin (100 µg/mL, Merck) for the pINDUCER21-MYB, and in LB-agar plates containing ampicillin (100 µg/mL, Merck) and chloramphenicol (25 µg/mL, Merck) for pINDUCER21 EV. Plates were incubated at 37° C overnight and 30° C for the pINDUCER21-MYB or -EV, respectively. Colonies were picked and grown in 3 mL liquid selective LB medium in a shaking incubator at 37/30° C overnight with ampicillin (50 µg/mL, Merck) for the pINDUCER21-MYB plasmid and ampicillin (50 µg/mL, Merck) and cloramphenicol (30 µg/mL, Merck) for the EV, and further expanded in 100 mL selective LB medium mainteining the same appropriate concentrations of antibiotics. Plasmids were purified using NucleoBond Xtra Midi kit (Macherey-Nagel) as previously described.

Virus production in HEK293T cells

HEK293T cells were cultured in T175 flasks. Each flask was co-transfected with plasmids using the quantities reported in **Table 2. 3**. Plasmids were diluted in TE buffer (Thermo Fisher Scientific) and delivered *via* transfection using TurboFect Reagent (Invitrogen) mixed with Opti-MEM (Gibco).

Table 2. 3 | Plasmids used for virus production. The quantities are relative to a T175 flask. TE, Tris-EDTA buffer; Q.S. quantity sufficient.

	PLASMID	WEIGHT
TE: Q.S. to 45 µL	pCMV	2.98 µg
	pMD2.G	4.48 µg
	pINDUCER21(EV/MYB)	4.48 µg
	Opti-MEM	237 µL
	TurboFect	37 µL

After adding the plasmid mixture to each flask, cells were incubated at 37° C and 5% CO_2 for 24 hours, after which the transfection medium was replaced with fresh medium, and cells were further incubated for 48 hours. The supernatant containing viral particles was collected 72 hours post-transfection. Cells were incubated in fresh medium which was harvested 96 hours post-transfection. The supernatants were centrifuged overnight at 4° C at maximum speed. The viral pellets were resuspended in leftover medium after decanting, aliquoted in microcentrifuge tubes, and stored at -80° C until further use.

Lentiviral vector transduction

Dilutions of virus aliquots were added to a constant number of cells for transduction and the cultures were incubated for 24 hours at the standard conditions. Cells were then rinsed twice in 1X PBS (Gibco) and incubated again. Calculation of the virus titre was performed as follows:

According to the results obtained, the volume resulting in > 80% GFP-positive cells was chosen and scaled based on the number of cells. For transduction, the correct amount of virus was added to the cultured medium; Polybrene (Merk Millipore, Massachusetts, USA) was added at a final concentration of 5 µg/mL to boost transduction efficacy. Cells were incubated at 37° C and 5% CO_2 for 24 hours, washed with 1X PBS (Gibco) twice and then cultured in standard medium conditions. tubes, and stored at -80° C until further use.

Flow cytometry

48 hours post-transduction, flow cytometry was used to detect the pINDUCER21 GFP marker. Non transduced cells were used as a control. Samples were analysed on the ACEA Novocyte Flow Cytometer (Agilent). Gating strategies are indicated in **Figure 2. 4**. Cells were gated for live cells by plotting FCS-H against SSC-H; positivity to GFP marker was determined by gating the area tangent to area of the cell population in the unstained control (SSC-A against FITC-A). This gate was also applied to the sample transduced and the percentage within the gate was deemed positive.

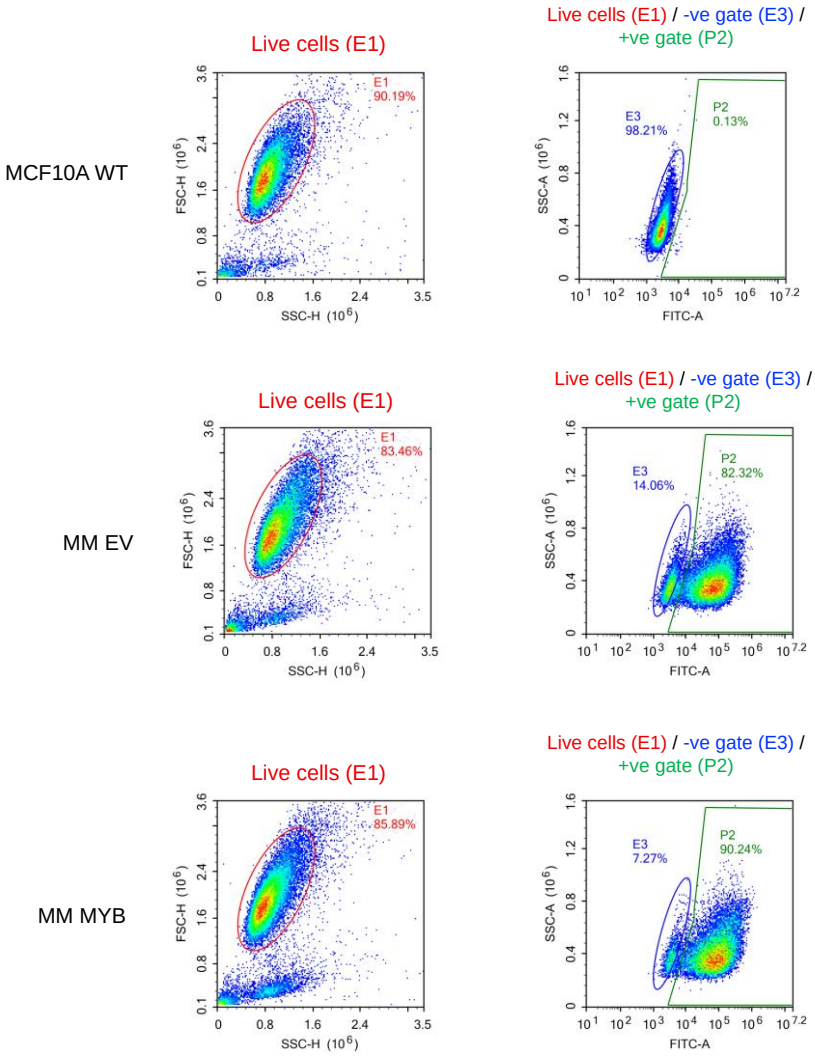

Figure 2. 4 | Gating strategies for selective live cells and GFP-positive cells. MCF10A parental cells (WT) were used as non-transduced control. Live cells were gated (E1 gate) with FSC-H against SSC-H (top left). From lived cells, negative cells area (E3) was selected by SSC-A against FITC-A to detect positive cells (P2) (top right). The same gating was applied for MCF10A cells transduced with pINDUCER21-EV vector (MM EV) or pINDUCER21-MYB vector (MM MYB). Percentage of positive cells is showed into the areas.

Imaging

Images of cell cultures of MM cells were captured using the Cytation 5 Cell Imaging Multi-Mode Reader (Biotek) plate reader using bright field and FITC channels.

2.8 siRNA

siRNA-mediated *MYB* knockdown was performed by Prof Göran Stenman's group (Sahlgrenska Center for Cancer Research (SCCR), University of Gothenburg, Gothenburg, Sweden). ACC cells were transfected with 50 nM of Stealth siRNAs for *MYB* (HSS106819, HSS106821) or control siRNAs, using the Lipofectamine RNAiMAX transfection reagent (Thermo Fisher Scientific) in antibiotic-free medium and maintained for 48 hours.

RNA was extracted and stored at -80° C.

2.9 Real-time quantitative polymerase chain reaction (RT-qPCR)

RNA extraction

Total RNA was extracted from cultured cells using the Monarch Total RNA Miniprep Kit (New England BioLabs, Hitchin, UK). For the sample disruption and homogenisation step, up to 3 x 10^6 cells were pelleted by centrifugation at 500 x g for 1 minute and resuspended in 300 µL of RNA Lysis Buffer by gentle pipetting. The resuspended sample was transferred into a DNA removal column fitted with a collection tube to eliminate genomic DNA. The tube was spun for 30 seconds at 16 000 x g, the DNA column was discarded and the flow-through, containing the RNA, was mixed with an equal volume of ≥ 95% ethanol thoroughly by pipetting, transferred into an RNA purification column fitted with a collection tube and centrifuged for 30 seconds at 16 000 x g. On-column DNase I treatment for enzymatic removal of residual DNA was performed by adding 500 µL of RNA Wash Buffer and centrifuged for 30 seconds at 16 000 x g. 5 µL DNase I was mixed with 75 µL DNase I Reaction Buffer and the mixture was pipetted directly into the column and incubated at room temperature for 15 minutes. Following 15 minutes of incubation, the column was rinsed once with RNA Priming Buffer. This was followed by two washing with RNA Wash Buffer. For the elution step, 30-50 µL of nuclease-free water was added to the centre of the column matrix and centrifuged for 30 seconds. RNA

quality and quantity was measured by Nanodrop 2000c (Thermo Fisher Scientific). The RNA samples were stored at -80° C.

cDNA synthesis

RNA was reverse-transcribed into complementary DNA (cDNA) using the High-Capacity RNA- to-cDNA Kit (Applied Biosystems, Waltham, US). The reaction was performed on ice in PCR tubes. 500 ng of RNA were converted to cDNA within a final volume of 20 µL reaction according to the

Table 2. *4* **Table 2. 4**. The reaction was incubated in a DNA Engine Dyad thermocycler (Bio-Rad, Hemel Hempstead, UK) at 37° C for 1 hour, followed by 5 minutes at 95° C to stop the reaction, and 4° C on hold.

Table 2. 4 | Reverse transcription reaction volumes. RT, reverse transcription; Q.S., quantity sufficient.

COMPONENT	VOLUME PER REACTION	
	+RT REACTION	-RT REACTION
2X RT Buffer Mix	10.0 µL	10.0 µL
20X RT Enzyme Mix	1 µL	/
RNA sample	Up to 9 µL	Up to 9 µL
Nuclease-free H_2O	Q.S. to 20 µL	Q.S. to 20 µL

RT-qPCR

Gene expression in MM cells was quantified by real-time reverse-transcriptase polymerase chain reaction (qPCR). For each target gene, three technical replicates were run in 96-well microtiter plates (MicroAmp Fast Optical 96-Well Plate, Applied Biosystems). cDNA was diluted 1:2 and 2 µL were used as template in 20 µL reaction according to the FastGene 2x IC Green Universal qPCR Mix (fluorescein) (Nippon Genetics Düren, Germany) protocol (**Table 2. 5**). K562, a leukaemia cell line, was used as positive control for *MYB* overexpression. The plate was sealed and briefly centrifuged to spin down the content and eliminate air bubbles before the run. Reactions were run on QuantStudio 7 Flex Real-Time PCR Machine (Thermo Fisher Scientific) with the cycling parameters showed in **Figure 2. 5**. Primer sequences used in this study were designed using Primer-BLAST from NCBI and they can be found in **Table 2. 6**.

Table 2. 5 | qPCR volumes per reaction used for MM cells. NTC, Non-Template Control; Q.S., quantity sufficient.

COMPONENT	VOLUME PER REACTION	
	qPCR	NTC
2X FastGene IC Green	10 µL	10 µL
Forward Primer (10 µM)	0.8 µL	0.8 µL
Reverse Primer (10 µM)	0.8 µL	0.8 µL
Template DNA	2 µL 1:2 cDNA	/
PCR-grade water	Q.S. to 20 µL	Q.S. to 20 µL

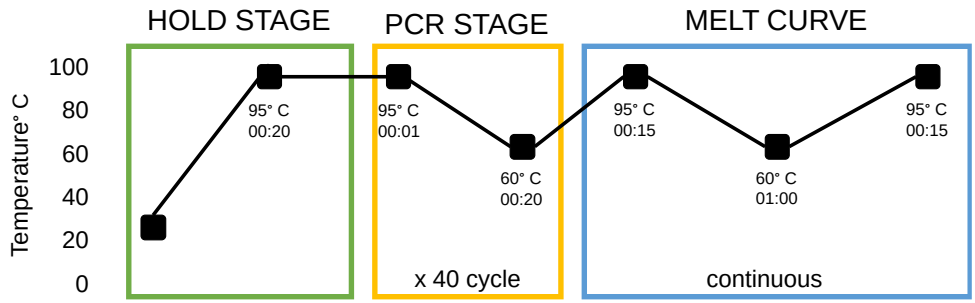

Figure 2. 5 | Parameters for qPCR amplification. Setting used for quantification of gene expression. Temperatures and timings are shown in each box corresponding to different stages. *Original illustration*.

Table 2. 6 | List of qPCR primers. Sequences are 5' – 3' direction.

GENE	FORWARD SEQUENCE	REVERSE SEQUENCE
MYB	GGGAACAGATGGGCAGAAATCG	GCTGGCTTTTGAAGACTCCTGC
BUB1	GCTCTGTCAGCAGACTTCCTTC	CAGCAGATGTGAAGTCTCCTGG
GAPDH	GTCTCCTCTGACTTCAACAGCG	ACCACCCTGTTGCTGTAGCCAA

qPCR on ACC cells was done using the AB 7500 Fast Real-Time PCR system using TaqMan Gene Expression Assays (Applied Biosystems) for *MYB* (Hs00920556_m1*) and *BUB1* (Hs01557695_m1). *UBC496* (Hs01871556_s1) was used as reference gene. For each target gene, three technical replicates were run in 96-well microtiter plates (MicroAmp Fast Optical 96-Well Plate, Applied Biosystems). Summary of the volumes needed for the reactions can be found in **Table 2. 7**.

Table 2. 7 | qPCR volumes per reaction used for ACC cells. NTC, Non-Template Control; Q.S., quantity sufficient.

COMPONENT	VOLUME PER REACTION	
	qPCR	NTC
20× TaqMan Gene Expression Assay	1 µL	1 µL
2× TaqMan Gene Expression Master Mix	10 µL	10 µL
cDNA template (1 to 100 ng)	4 µL	/
PCR-grade water	Q.S. to 20 µL	Q.S. to 20 µL

Differential gene expression was calculated using the delta delta Ct (ΔΔCt) method. *GAPDH* and *UBC* were used as endogenous reference genes for MM and ACC samples, respectively. Fold changes were calculated according to the formula:

$$\Delta \boldsymbol{Ct} = average\ Ct\ gene - average\ Ct\ endogenous$$

$$\Delta\Delta \boldsymbol{Ct} = \Delta Ct\ treated - \Delta Ct\ untreated$$

$$\boldsymbol{Fold\ change} = 2^{-\Delta\Delta Ct}$$

2.9 Chromatin immunoprecipitation (ChIP) analysis

Chromatin immunoprecipitations (ChIP) were performed with cross-linked chromatin from ACCX11 cells following the instruction of the SimpleChIP Enzymatic Chromatin IP Kit (Magnetic Beads) (Cell Signaling Technology, Massachusetts, USA).

Cell culture cross-linking and sample preparation. This step was performed by Prof Göran Stenman's group (Sahlgrenska Center for Cancer Research (SCCR), University of Gothenburg, Gothenburg, Sweden). To crosslink proteins to DNA, 540 µL of 37% formaldehyde were added to 4 X 10^6 cells (in 20 mL culturing medium) and the culture was incubated at room temperature for 10 minutes. 2 mL of glycine were added, and cells were further incubated at room temperature for 5 minutes. Medium was removed and cells washed twice with 20 mL ice-cold 1X PBS (Gibco), completely removing wash from culture dish each time. A mix of 2 mL of ice-cold 1X PBS (Gibco) and 10 µL 200X Protease Inhibitor Cocktail (PIC) was added and cells were scraped and collected into a conical tube. Cells were centrifuged at 2 000 x g for 5 minutes at 4° C. Supernatants were discarded and pellets were sent to Brunel University London for the following steps.

Nuclei Preparation and chromatin digestion. To digest the chromatin, nuclei pellets were resuspended in 1 mL ice-cold 1X Buffer A mixed with 0.50 µL of 1 M dithiothreitol (DTT) and 5 µL 200X PIC for each immunoprecipitation (IP) prep and incubated on ice for 10 minutes with frequent mixing by inverting the tube. The solution was centrifuged at 2 000 x g for 5 minutes at 4° C; supernatant was removed, and pellets were resuspended in 1 mL ice-cold 1X Buffer B and 0.50 µL of 1 M DTT. Centrifugation and removal of the supernatant was repeated, and the pellets resuspended in 100 µL of Buffer B and 5 µL of 1 M DTT. 0.5 µL Micrococcal Nuclease (MNase) were added per IP prep and tubes were placed for 20 minutes at 37° C with frequent mixing by inverting every 3 minutes to digest DNA to the length of approximately 150-900 bp. Digestion was stopped by adding 10 µL of 0.5 M EDTA and tubes were placed on ice for 2 minutes before centrifugation at 16 000 x g in a for 1 minute at 4° C. Supernatant was removed and nuclear pellets were resuspended in 100 µL of 1X ChIP Buffer 0.5 µL 200X PIC and incubated on ice for 10 minutes.

Analysis of chromatin digestion and concentration. To analyse the quality of the chromatin digestion and the concentration, an aliquot of 50 µL chromatin sample was used. 100 µL nuclease-free water, 6 µL 5 M NaCl, and 2 µL RNAse A were added and mixed by vortexing

before incubation for 30 minutes at 37° C. To each RNAse A digested sample, 2 µL of Proteinase K were added, the sample was vortexed and incubated at 65° C for 2 hours.

DNA purification using spin columns. DNA was purified using spin columns. Each sample was mixed with 750 µL of DNA Binding Buffer, vortexed, and transferred into DNA spin column in collection tube. Tube was centrifuged at 18 500 x g for 30 seconds, after which the procedure was repeated twice. 50 µL of DNA Elution Buffer were added to the centre of the column which was centrifuged at 18 500 x g for 30 seconds. 1 µL of eluted DNA was quantified by Nanodrop 2000c spectrophotometer (Thermo Fisher Scientific) and 10 µL were qauntified by agarose gel electrophoresis. 1.5% agarose gel was made dissolving agarose powder in 1X Tris-acetate- EDTA (TAE) buffer and SYBR Safe Gel Stain (Invitrogen) was added at 0.5 µL/mL. DNA was mixed with 6X loading dye (New England BioLabs) and loaded onto the gel's wells. 10 µL of the 50 bp Quick-Load Purple DNA marker (New England BioLabs) were loaded to determine DNA fragment size. Gel was run at 60 V for 45 minutes. GelDoc EZ Imager (Bio-Rad) and the integrated software ImageLab 3.0 were used for image capture. The gel showing the fragments is reported in **Figure 2. 6**.

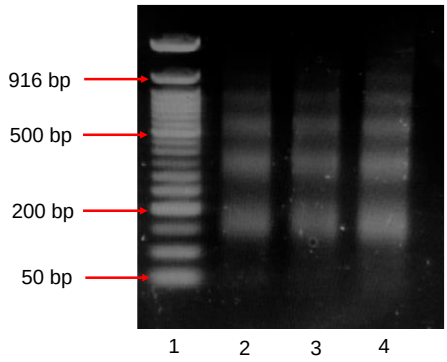

Figure 2. 6 | Enzyme-digested chromatin. Lane 1 shows the 50 bp ladder. Lane 2, 3, and 4 show ChIP prep. Purified DNA from each chromatin sample was run on a 1.5% agarose gel. Optimised chromatin digestion produced chromatin fragments ranging from 150 to 900 bp, corresponding to one to five nucleosomes in length. Red arrows indicate the corresponding size of the DNA marker.

Chromatin Immunoprecipitation. 10 µg of digested, cross-linked chromatin were used per IP and mixed in a conical tube with 400 µL of 1X ChIP Buffer and 2 µL of 200X PIC. 10 µL were removed and used as Input Sample. The following antibodies were used for immunoprecipitation: Anti-c-Myb (phospho S11) [EP769Y] (ab45150) (Abcam, Cambridge, UK) diluted 1:50; Normal Rabbit IgG #2729 (Cell Signaling Technology) diluted 1:50. IP samples were incubated overnight at 4° C with rotation. The next day, 30 µL of ChIP-Grade Protein G Magnetic Beads were added to each IP reaction and tubes were incubated for 2 hours at 4° C with rotation. Then tubes were placed in a magnetic separation rack and bead pelleted until the solution was clear; supernatant was removed, and magnetic beads pellet was washed by adding 1 mL of low salt solution 1X ChIP Buffer and tubes were incubated at 4°C for 5 min with rotation. The last steps were repeated twice for a total of three low salt washes. An additional wash was performed by adding 1 mL of high salt wash (1X ChIP Buffer and 70 µL 5M NaCl), beads were incubated at 4°C for 5 min with rotation, pelleted with the magnetic rack, and the supernatant was discarded.

Elution of chromatin from antibody/Protein G Magnetic Beads and reversal of cross-links. To elute chromatin, 150 µL of the 1X ChIP Elution Buffer were added to each IP sample for 30 minutes at 65° C with gentle vortexing at 1 200 rpm. Protein G magnetic beads were placed in the magnetic rack until the solution was clear. The chromatin supernatant was carefully transferred to a new tube. Tubes (including the input diluted into 150 µL of the 1X ChIP Elution Buffer) were reverse cross-linked by adding 6 µL 5 M NaCl and 2 µL Proteinase K, and incubated 2 hours at 65° C.

Finally, the DNA was purified by using spin column as already performed in the "*DNA purification using spin columns"* step.

ChIP sequencing

Chromatin immunoprecipitation sequencing (ChIP-seq) (including library construction) was performed by Novogene (Cambridge, UK). A minimum of 40 ng (2 ng/µL) of high-quality enriched DNA with main peak of 100-500 bp was supplied for sequencing. Libraries were constructed using Illumina Sequencing PE150 library preparation. Sequencing was performed at 20M reads per sample. ChIP-seq results were delivered as raw fastq files, with input and no-input controls of three technical replicates per sample.

2.10 Western blot

All the solution used for western blot analysis are listened below:

Laemmli buffer (2X stock concentration)

- 4% SDS
- 20% glycerol
- 10% 2-mercaptoethanol
- 0.004% bromphenol blue
- 0.125 M Tris HCl

pH was adjusted to 6.8

SDS-PAGE gel (10% SDS)

Resolving gel

- 1.25 mL ProtoGel Resolving Buffer (Tris/SDS) (Geneflow, Lichfield, UK)
- 1.63 mL 30% acrylamide (Merck)
- 2.1 mL ddH_2O
- 50 µL APS (Thermo Fisher Scientific)

- 5 µL TEMED (Fisher Scientific)

Stacking gel

- 625 µL ProtoGel Stacking Buffer (Tris/SDS)
- 375 µL 30% acrylamide
- 1.5 mL ddH_2O
- 25 µL APS
- 2.5 µL TEMED

Running Buffer (Tris-Glycine/SDS)

- 25 mM Tris base
- 190 mM glycine
- 0.1% SDS

pH was adjusted to 8.3

Transfer Buffer

- 25 mM Tris base
- 190 mM glycine
- 20% methanol
- SDS was included at a final concentration of 0.1%

pH was adjusted to 8.3

Ponceau S Staining Solution

- 25 mL glacial acetic acid
- 400 mL ddH_2O
- 0.5 g Ponceau S

Tris-buffered saline (TBS) buffer (10X)

- 24 g Tris

- 88 g NaCl
- 900 mL of water

pH was adjusted to 7.6

For 1X TBS-Tween 20 detergent (TBST)

- 100 mL of 10X TBS
- 1 mL Tween 20 detergent
- 900 mL of ddH_2O

Blocking Buffer

- 5% non-fat dried milk in TBST

Sample preparation. For western blot analysis, 10 cm dishes with cells at a confluency of 80% were used. Medium was removed, and adherent cells were rinsed with ice-cold 1X PBS (Gibco) supplemented with 1X cOmplete, EDTA-free Protease Inhibitor Cocktail (Roche, Basel, Switzerland). Direct lysis was performed by adding 1X Laemmli buffer (approximatively 60 µL/1 x 10^6 cells) to the cells and mechanically scraping the cells from the plate.

Cells were collected and transferred into a microcentrifuge tube and boiled at 95° C for about 30 minutes with frequently mixing by vortexing.

Loading and running the gel. 30 µL of protein samples were loaded onto the wells of a SDS-PAGE gel, along with the Colour Prestained Protein Standard, Broad Range molecular weight marker (New England BioLabs). The SDS-PAGE gel was run using the Wet/Tank Blotting System (Bio-Rad) in Running Buffer and run at 100 V for 1-2 hours.

Transferring the protein from the gel to the membrane. Proteins were transferred onto a nitrocellulose membrane (Bio-Rad) preparing a stack as shown in the **Figure 2. 7**. All the components of the stack were kept wet with ice-cold Transfer Buffer. Wet electrophoretic transferring was performed into the Wet/Tank Blotting System (Bio-Rad) placed on ice and filled with ice-cold Transfer Buffer. Run conditions were 300 mA for 1.5 hours. At the end of

the run, protein transfer was checked by staining the membrane with Ponceau S Staining Solution for 5 minutes at room temperature in gently shacking.

Figure 2. 7 | Prepared stack for transferring of the proteins. Schematic set up of a stack to create the "sandwich" electrophoretic transfer holding gel and membrane in the middle. Two filter papers were used each side together with a sponge. Voltage is applied between the electrodes and proteins migrate to the membrane following the current generated by the applied voltage across the electrodes. Direction of the current is shown on the left side of the scheme. *Original illustration*.

Antibody staining. To prevent non-specific binding of the antibodies, the membrane was incubated in blocking buffer for 1 hour at room temperature with gentle shaking. The blocking buffer was then discarded, and the membrane was incubated with primary antibodies in blocking buffer overnight at 4° C with gentle shaking. c-Myb Antibody (D-7): sc-74512 (Santa Cruz Biotechnology, California, USA) was used at 1: 500 dilution; GAPDH Monoclonal antibody (Proteintech, Rosemont, USA) was used at 1: 30 000 dilution. The next day, the antibodies were removed, and the membrane washed three times with TBST Buffer, 5 minutes each, with constant agitation. The membrane was then incubated for 1 hour at room

temperature with the conjugated secondary antibody (Anti-mouse IgG, HRP-linked Antibody #7076 (Cell Signaling Technology), dilution 1: 10 000) in blocking buffer. Washing steps were repeated, and the membrane was kept in TBST until analysis. Chemoluminescence was detected using the Bio-Rad ChemiDoc XRS (Bio-Rad) kit. The membrane was placed inside the machine and an appropriate amount of Immobilon Forte Western HRP substrate (Merck Millipore) was placed onto the membrane in order to be covered. Images were analysed with ImageJ software.

2.11 Immunohistochemistry (IHC)

Immunohistochemistry analysis on tissue microarrays (TMAs) was performed by Prof Gianluca Sala and Prof Rossano Lattanzio from Università di Chieti-Pescara, Italy. Samples were provided by the Adenoid Cystic Carcinoma Research Foundation (AACRF; Needham, MA, USA) team, in collaboration with the research organisation XenoSTART (S. Antonio, Texas, USA).

To detect BUB1 the primary Anti-BUB1 (clone EPR18947, ab195268, Abcam) was used. Secondary antibody was biotinylated goat anti-rabbit (Abcam).

2.12 Bioinformatics analysis

All bioinformatics methods were performed under the guidance of Dr Denise Ragusa (Brunel University London).

Datasets

Microarray datasets were downloaded from the Gene Expression Omnibus (GEO, https://www.ncbi.nlm.nih.gov/geo/) repository. The Andersson dataset (GEO accession

number GSE88804) (Andersson *et al*., 2017) reported expression data of 13 surgical samples of ACC and 7 NSG samples. The Chowbina dataset (GEO accession number GSE36820) presented microarray analysis on 3 normal samples and 11 ACC xenograft samples. The Gao dataset (GEO accession number GSE59702) (Gao, R. *et al*., 2014) contains expression profiling by array of 12 ACC with matched normal tissues. Differential expression analysis was performed using the R package *limma*.

Clinical phenotype and expression data for unmatched healthy and tumour samples were extracted from the Cancer Genome Atlas (TCGA, https://www.cancer.gov/tcga) and Genotype-Tissue Expression (GTEx, https://gtexportal.org/home). Access to information for the TCGA patients was obtained from the GDC Data Portal and processed. Only primary tumour data were used in the analysis. A list of samples available from the TCGA dataset and the correspondent normal anatomical site is reported in **Supplementary Table 2**.

RNA sequencing

RNA sequencing (including library construction and sequencing) was performed by Novogene (Cambridge, UK). A minimum of 1 µg (20 ng/µL) of high-quality total RNA was supplied for sequencing. Libraries were constructed using Illumina Sequencing PE150 library preparation with Ribozero rRNA depletion. Sequencing was performed on Novaseq 6000 platform, at 20M paired-end reads per sample. Results were delivered as raw fastq reads.

Analysis of RNA-seq and ChIP-seq data

Fastq RNA-seq raw reads were analysed with the open-source software package of the Tuxedo Suite. Tophat2 with bowtie2 were used to map paired-end reads (Kim, Daehwan *et al*., 2013; Langmead & Salzberg, 2012). The *Homo sapiens* genome build GRCh38 was used as reference. GENCODE38 (Frankish *et al*., 2019) was used as the reference human genome

annotation. Aligned reads were filtered by quality using samtools (Li, H., Handsaker, Wysoker, Fennell, Ruan, Homer, Marth, Abecasis, Durbin, & 1000 Genome Project Data Processing Subgroup, 2009) with a minimum selection threshold set at 30. Transcript assembly and quantification was achieved using HTSeq 2.0 (Putri *et al*., 2022). Differential expression between sample and control was performed by collapsing technical replicates for each condition and the use of the DESeq2 tool (Love *et al*., 2014) in R library v 1.32.0. The differential expression was expressed in the form of log2 fold change between sample and control.

ChIP-seq data in the form of fastq files were mapped to the Homo sapiens GRCh38 reference genome using bowtie2. Reads were filtered by a standard quality threshold of 30 using samtools (Li, H. *et al*., 2009). MACS was used to call peaks with a p value threshold of 0.01 by comparison with the input control (Zhang, Yong, Liu, Meyer, Eeckhoute, Johnson, Bernstein, Nusbaum, Myers, Brown, & Li, 2008). True peaks were selected when two of three replicates overlap in the same sequence. Binding motif analysis and peak visualisation was performed on Integrative Genomics Viewer (IGV).

Gene Ontology (GO) and pathway analysis

GO analysis was performed using the online tool ExpressAnalyst (www.expressanalyst.ca) and the PANTHER Biological Process (BP) and REACTOME repositories. GO and pathway terms were filtered by false discovery rate (FDR) ≤ 0.05.

Gene Set Enrichment Analysis (GSEA)

GSEA was performed on the GSEA software v 4.2.3 by inputting RNA-seq values in the values of counts generated by HTSeq 2.0 (Putri *et al*., 2022) against a custom gene signature. The

signature was constructed by common intersection of upregulated differentially expressed genes from the datasets described in section 2.6.1. Standard GSEA settings were employed: 1000 permutations, gene set, and Signal2Noise metric.

2.13 Data visualisation

Plots were constructed in Microsoft Excel for Mac v 16.71 and *ggplot2* library in R Studio v 4.2.3. Venn diagrams were generated in VennPainter (Lin *et al*., 2016). Correlations were computed and visualised using *ggplot2* (v 3.3.5) and *corr* packages in R Studio v 4.2.3.

2.14 Statistical analysis

Two tailed Student's T-test and Wilcoxon test were used to calculate statistical significance on 3 replicates. Statistical significance was deemed at a p value threshold of < 0.05. Variance in plots is shown as error bars representing standard deviation. Statistical significance is symbolised as: p value ≤ 0.05 (*), 0.001 (**), 0.0001 (***), and 0.00001 (****). Calculations were performed in R studio v 4.2.3.

Chapter III

Generation of an ACC-like cell line based on breast MCF10A cells

3.1 Introduction

The existing body of research on ACC has established that the recurrent reciprocal translocation t(6;9)(q22-23; p23-24), resulting in fusion gene partners comprising *MYB* and *NFIB,* is found in ACC of the breast, and salivary and lachrymal glands (Persson *et al*., 2009). The *MYB-NFIB* fusion gene accounts for about 30 – 86% of cases, depending on the study, and results in the activation of *MYB* by disrupting its 3′ UTR, which contains microRNA regulatory sites that negatively regulate *MYB* expression (Persson *et al*., 2009). However, *MYB* translocations that retain the 3′ UTR are still associated with high *MYB* expression, indicating the existence of additional mechanisms for *MYB* overexpression in ACC. Nevertheless, *MYB* activation can occur through copy number gain or enhancer hijacking with breakpoints located either upstream or downstream of the gene (Drier *et al*., 2016). Therefore, it was crucial to study both the functional properties of the *MYB-NFIB* fusion as well as the biology and gene expression in fusion-negative ACC.

It has already been shown that overexpression of *MYB* or *MYB-NFIB* fusion(s) have similar effects on the biology of human glandular epithelial cells after forcing their expression by transduction, resulting in analogous cellular, molecular, and transcriptional consequences (Andersson *et al*., 2020). This study, alongside with the one from Gao *et al.* (2014), underlined the possibility of focussing on *MYB* overexpression for the creation of cellular models, rather than fusion-dependent models (Gao, R. *et al*., 2014). Gao and colleagues (2014) performed global mRNA/miRNA analyses ACC samples with matched normal tissues, finding a characteristic molecular landscape for ACC that is independent of *MYB* rearrangements (Gao, R. *et al*., 2014). In fact, to identify candidate *MYB* target genes, they analysed a collection of 12 ACC tumours (6 fusion-positive and 6 fusion-negative) and their matched adjacent normal

samples, finding a similar downstream expression profile regardless of the fusion-status (Gao, R. *et al*., 2014).

Developing stable ACC cell lines has been challenging due to the limited numbers of patients and the inability to retain key ACC molecular alterations in *in vitro* cultures. Patient-derived mouse xenografts (PDXs) have been successfully established from ACC primary tumours, and it has been proven that they maintain the characteristic ACC histology and molecular features (Moskaluk *et al*., 2011). Although cells derived from ACC PDXs, as well as from biopsy specimens, have been described before, PDX models suffer from high cost and the need for tumour engraftment, which requires time and has a success rate of less than 50% (Cho *et al*., 2016). Moreover, cells derived from ACC tumour tissue can be cultured *in vitro* for a limited time only, leading to researchers having to use substitute models for morphological, cytogenetic, and functional studies. These include cell lines with *MYB* fusions (i.e. UTSW-ACC52 and UTSW-ACC112) immortalised *via* integration of viral constructs containing the *E6/E7* genes of HPV16 (Queimado *et al*., 1999), or *via h-TERT* (MDA-ACC-01) (Li, J. *et al.*, 2014). Other immortalised ACC cell lines were developed from patients' samples after surgical resection, such as the UFH2 cell line from a tumour biopsy taken from a metastatic parotid gland ACC (Jiang, Y. *et al.*, 2019), or the UM-HACC-2A line established from the minor salivary gland of a patient carrying t(6;9) *MYB-NFIB* chromosomal rearrangement (Warner *et al*., 2018). The former was validated for *MYB* expression by RNA sequencing and immunoblotting. Although these models retain ACC features, the typical t(6;9) translocation and MYB fusion characterising the primary tumour are lost over time (Li, J. *et al*., 2014; Queimado *et al*., 1999), limiting their use as models for the study of ACC. ACCX6, ACCX11, and ACCX5M1 are primary/short-term ACC cell lines derived from PDXs (Andersson *et al*., 2017; Chen, C. *et al.*, 2017). These cell lines maintain their growth and molecular characteristics only for a limited number of passages (Andersson *et al*., 2017; Chen, C. *et al*., 2017). ACCX11 was also used to perform experiments shown in this chapter. A list of ACC cell lines can be found in **Table 3. 1**.

Table 3. 1 | List of available established cell lines. List of ACC cell lines and main characteristics listed by the Adenoid Cystic Carcinoma Research Foundation (ACCRF), MA, USA. FCP = fibronectin-coated plates. OSGM = optimized salivary gland medium.

CELL LINE	CONDITION	MYB-NFIB STATUS	REFERENCE
UTSW-ACC52	Immortalized with HPV E6/E7	No	(Queimado *et al*., 1999)
UTSW-ACC112	Immortalized with HPV E6/E7	No	(Queimado *et al*., 1999)
(MDA-)ACC-01	Immortalized with hTERT	No	(Li, J. *et al*., 2014)
UM-HACC-2A	FCP and OSGM	Yes	(Warner *et al*., 2018)
UFH2	/	Yes	(Jiang, Y. *et al*., 2019)
ACC(X)11	Established from PDX	Yes	(Chen, C. *et al*., 2017)
ACC(X)6	Established from PDX	Yes	(Chen, C. *et al*., 2017)
ACCX5M1	Established from PDX	Yes	(Andersson *et al*., 2017)

Despite progresses made so far, establishment of stable ACC cell lines is still a challenge to overcome, exacerbated by the remarkable tumour heterogeneity that characterises this type of cancer, making each ACC case unique.

Since the ACC research community needs robust *in vitro* models to study ACC, in this chapter we describe the generation of a switchable *MYB*-overexpressing cell line based on lentiviral transduction of the glandular MCF10A breast cell line, to establish a new *in vitro* model of ACC that allows to capture MYB role in glandular cells. The switchable model was validated using RNA-sequencing to elucidate the transcriptional profile of the engineered cell line and establish transcriptional similarities with ACC patient signatures.

3.2 Results

3.2.1 Generation of a conditional *MYB*-expressing MCF10A cell line using a lentiviral system

MCF10A cells were transduced with a lentiviral vector (pINDUCER21-MYB) that drives expression of human *MYB* after adding DOX into the culturing medium (**Figure 2. 3 B** from **Chapter II**). As a negative control we used the empty vector (pINDUCER21-EV) (**Figure 2. 3 A** from **Chapter II**). Successful vector transduction was checked before functional experiments by detecting expression of GFP by fluorescent microscopy (**Figure 3. 1**). We established by flow cytometry analysis that the transduction efficiency was ≥ 80% in the sample population analysed (**Figure 3. 2 A**-**B**).

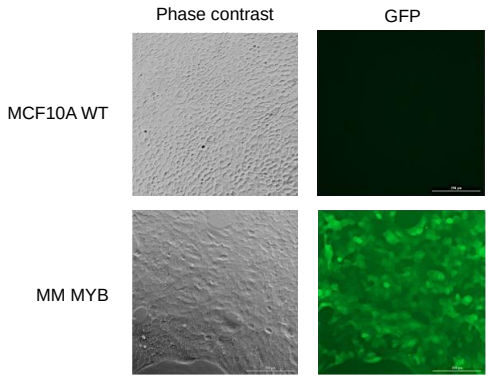

Figure 3. 1 | GFP signal captured in MCF10A cells after transduction with the pINDUCER21 lentiviral vector (MM). Phase contrast channel shows cultured cells. Transduced cells appear green (GFP-MM MYB, bottom right square) compared to the control ones (GFP-MCF10A WT, up right square). The analysis was performed with the Cytation 5 Cell Imaging reader using phase contrast and FITC channels and compared to the parental MCF10A cells (MCF10A WT). Both vectors used (pINDUCER21-MYB and pINDUCER21 empty backbone) contain the GFP coding sequence. The magnification used is 40X.

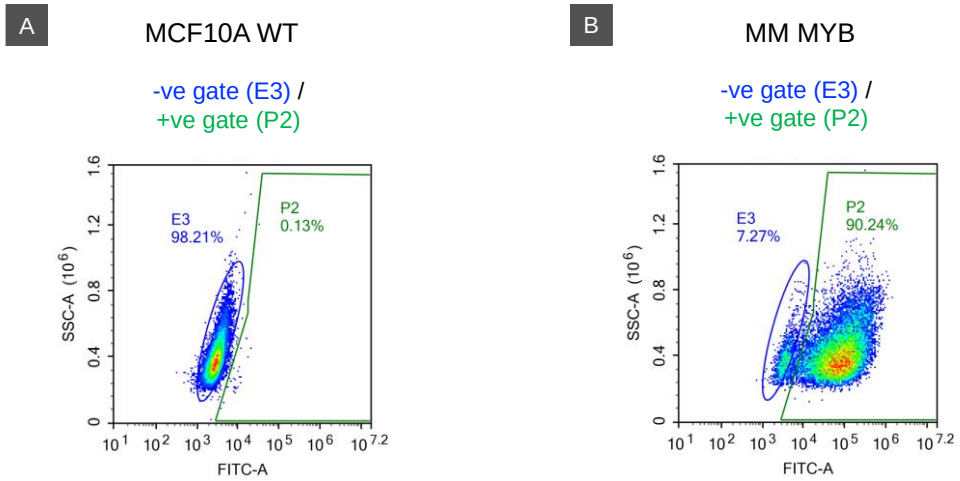

Figure 3. 2 | Flow cytometer analysis of MCF10A cells. (**A**) MCF10A parental cells (WT) were used as control to set the gate for GFP-positive cells. (**B**) MCF10A cells after transduction with pINDUCER21-MYB (MM MYB) showed a proportion of positive cells higher than 80%.

3.2.2 *MYB* expression in pINDUCER21-MYB MCF10A cells (MM cells) in the presence or absence of the inducer DOX

To determine whether MCF10A cells were able to express *MYB* in the presence of DOX, qPCR analysis was performed on MM MYB cells before and after the treatment. As shown in **Figure 3. 3 A**, addition of DOX increased *MYB* expression levels (MM MYB +DOX) compared to the MM MYB -DOX control. Moreover, immunoblotting confirmed the presence of MYB protein in MM MYB +DOX cells, but not in the absence of the inducer (**Figure 3. 3 B**).

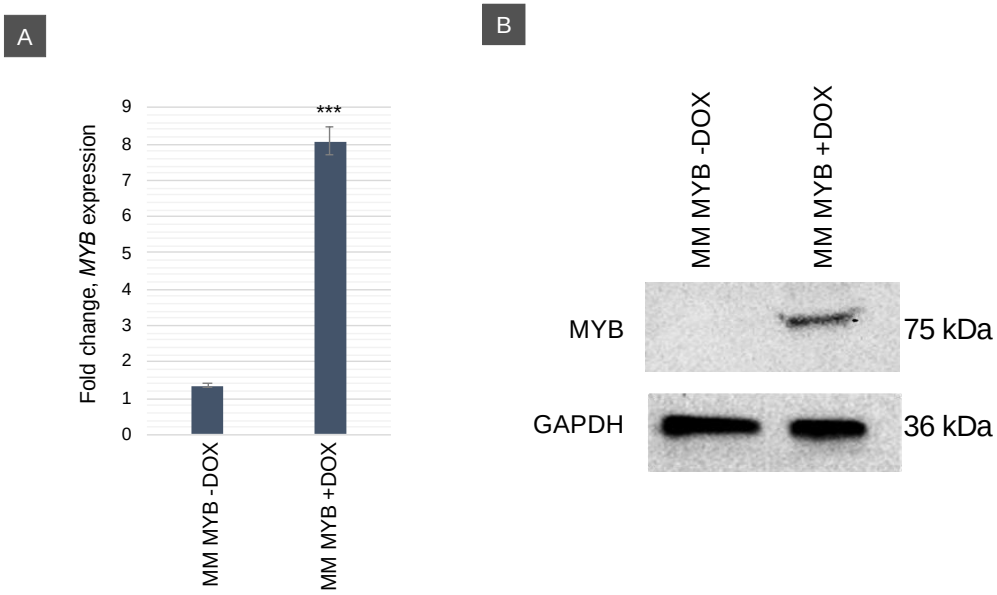

Figure 3. 3 | *MYB* expression in MM cells before and after DOX treatment.

(A) RT-qPCR analysis showed *MYB* expression values as fold change between -DOX and +DOX conditions, calculated by ΔΔCt method by normalisation to *GAPDH* gene used as housekeeping gene. (**B**) Immunoblotting analysis showing the presence of MYB protein in MM MYB +DOX cells but not in -DOX condition. GAPDH was used as internal control. p value ≤ 0.0001 (***)

3.2.3 RNA sequencing validates MM MYB cells as a faithful model of human ACC

MM MYB cells were used in RNA-seq experiments to establish gene expression profiles and compare these to those of PDX-derived ACCX11 cells. ACCX11 cells were provided by Professor Göran Stenman, Sahlgrenska Cancer Center (University of Gothenburg, Sweden), in collaboration with the Adenoid Cystic Carcinoma Research Foundation (ACCRF, MA, USA), and XenoSTART (S. Antonio, Texas, USA).

Differential expression of genes after MYB *overexpression*

RNA-seq analysis was performed on MM MYB cells with or without DOX treatment to identify differentially expressed genes caused by switching *MYB* on or off. A total of 798 differentially expressed genes were found and divided as up- or downregulated according to their fold change, with a fold change threshold $\geq \pm 1$ and an FDR cut-off of 0.05. Specifically, 335 genes were identified as upregulated and 463 as downregulated in the presence of the inducer (**Figure 3. 4 A**). Numbers of genes were further classified according to strength of the p value (**Figure 3. 4 B**). A list of the top 100 differentially expressed genes can be found in **Supplementary Table 3**. As expected, *MYB* was found to be one of the most differentially expressed genes, with a strongly significant p value of 2.86E-23. To confirm the specificity of the results, the same analysis was performed on the empty vector-infected cells (MM EV) prior and after addition of DOX. The analysis highlighted no significant changes in gene expression, confirming that differences observed in the MM-MYB cell lines were caused by *MYB* overexpression and not by the presence of DOX (**Figure 3. 4 C-D**).

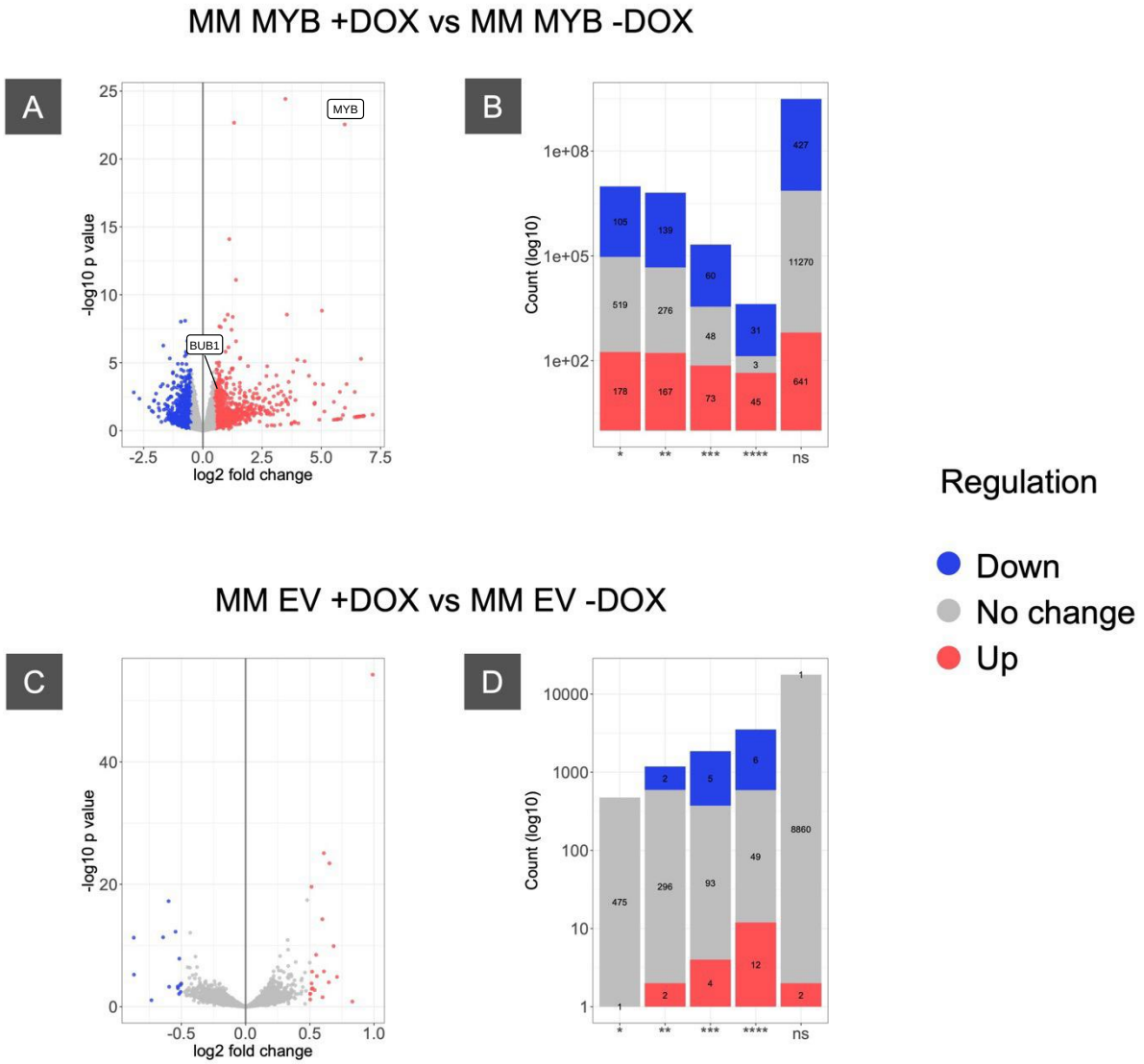

Figure 3. 4 | RNA-seq analysis of MM MYB and MM EV cells in the presence or absence of doxycycline (DOX). (**A**) Volcano plot presenting genes significantly up- (red) and down- (blue) regulated in MM MYB +DOX compared to the -DOX condition. (**B**) Number of genes up- or downregulated in MM MYB cells enumerated according to the strength of the p value. (**C**) Volcano plot presenting genes significantly up- (red) and down- (blue) regulated in MM EV +DOX compared to the -DOX condition. (**D**) Number of genes up- or downregulated in MM EV cells enumerated according to the strength of the p value. p value ≤ 0.05 (*), 0.001 (**), 0.0001 (***), and 0.00001 (****).

As expected, *MYB* expression was not detected in MM EV cells in the presence of DOX **Figure 3. 5**). To assess similarities in gene expressions between the new cellular model and true ACC cells, RNA-seq was also performed in 7 replicates of ACC (ACCX11 cell line) and 3 normal salivary gland (NSG) controls. *MYB* expression was higher in ACC samples compared to the NSG controls, with a fold difference comparable to that between MM MYB -DOX and +DOX conditions (**Figure 3. 5**).

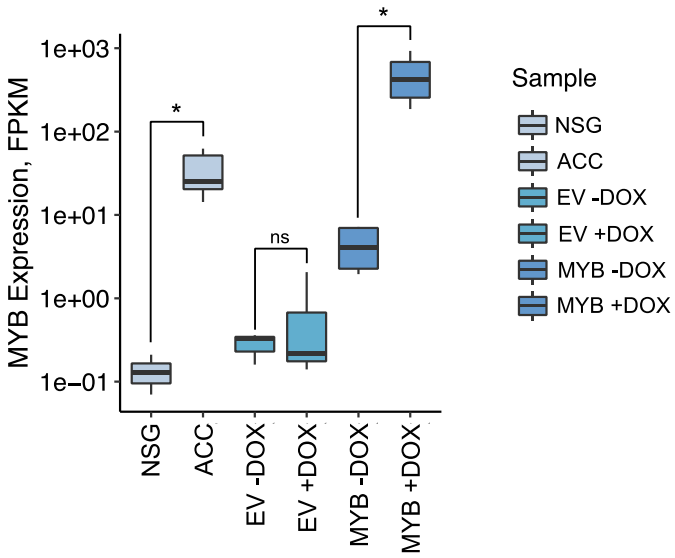

Figure 3. 5 | *MYB* expression levels in MM cell lines and ACC samples. RNA-seq was carried out to detect expression of *MYB* in ACC samples, NSG, MM EV, and MM MYB cells cultured in the presence or absence of DOX. Expression is reported as fragments per kilo base of transcript per million mapped fragments (FPKM) and t-test was used to perform the statistical analysis. p value ≤ 0.05 (*); ns, not significant.

To evaluate the biological relevance of the differentially expressed genes, we carried out gene ontology (GO) analysis. **Figure 3. 6 A** shows network analysis, using Panther:BP database, of the selected genes meeting the criteria of significance with a p value ≤ 0.05. Biological processes associated with the differentially expressed genes were extracted from the GO analysis according to the p value ≤ 0.05 and filtered by FDR ≤ 0.1 and are listed in **Figure 3. 6 B**. The main activated pathway was the cell cycle, followed by DNA replication, chromosome segregation, negative regulation of apoptotic processes, DNA repair, cell adhesion, and blood circulation (**Figure 3. 6 B** and **Table 3. 2**). To investigate in more detail the biological processes involved, the same analysis was carried out using the REACTOME repository. The results suggest that *MYB* expression is significantly associated with mitotic-related processes, including M-M/G1, G1-G1/M, M phase, and G1/S transition, as well as, prometaphase, metaphase and anaphase, together with interferon signalling and checkpoint programs (both cell-cycle and replication stress-related) (**Figure 3. 7**).

The differentially expressed genes were further divided into upregulated and downregulated, and GO analysis was performed. Biological processes matching up- and downregulated genes are reported in **Figure 3. 8**. Cell cycle was confirmed as the top activated pathway, followed by DNA replication, chromosome segregation, and DNA repair. According to the analysis, downregulated genes belonged to the negatively regulated apoptotic activity (**Figure 3. 8**).

Figure 3. 6 | Gene ontology GO analysis of differentially expressed genes in MM MYB +DOX. (**A**) Network analysis of the differentially expressed genes filtered by statistically significance p value ≤ 0.05. (**B**) Gene ontology biological processes extracted from Panther:BP database related to the genes meeting the criteria. The size of the dots indicates the percentage of genes mapped to the specific process.

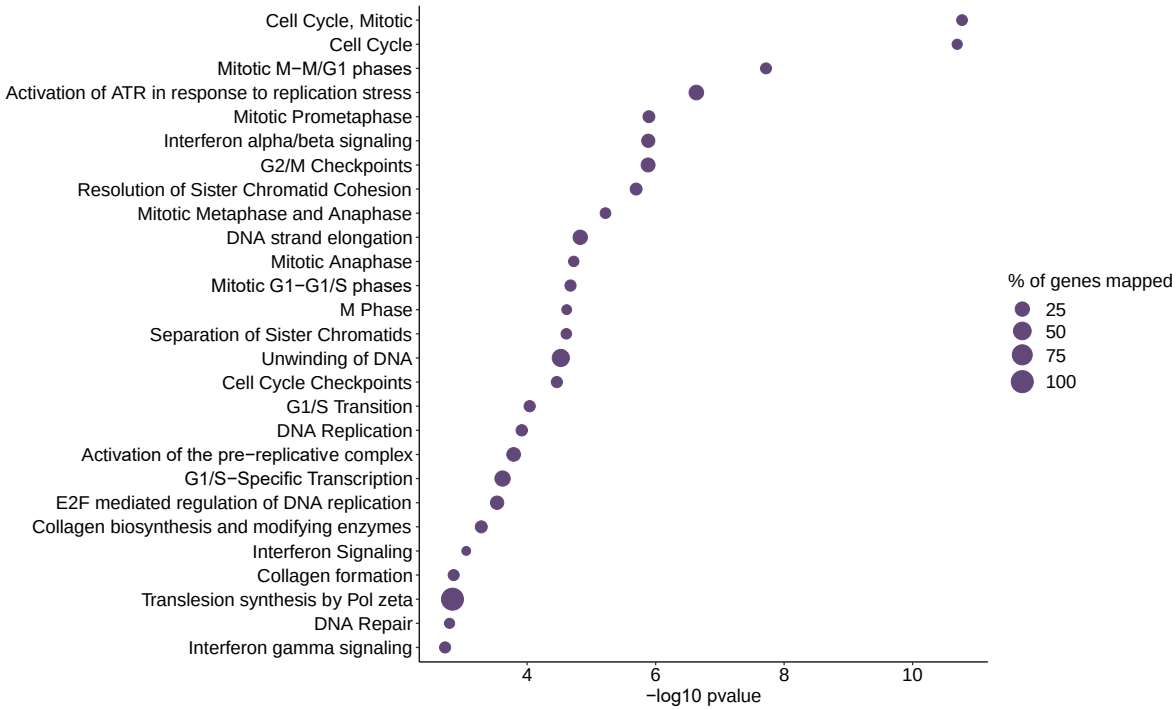

Figure 3. 7 | Gene ontology (GO) terms relating to the biological processes of differentially expressed genes in MM MYB +DOX cells. Plot bar showing the biological processes activated in MM cells after MYB activation, according to REACTOME database. Processes were filtered by p value ≤ 0.05 and adjusted by FDR ≤ 0.1. The size of the dots indicates the % of genes mapped for each biological process analysed.

Table 3. 2 | List of genes differentially expressed in MM MYB +DOX classified by biological processes according to the REACTOME database.

BIOLOGICAL PROCESS	P VALUE	TOTAL NUMBER OF GENES	GENES MAPPED
Cell cycle	5.49E-21	647	ANLN; SPDL1; MCM2; TIPIN; AURKA; BIRC5; CLSPN; CDC45; CDC7; DMC1; VRK1; E2F1; SUV39H1; CENPT; OIP5; UBE2S; NCAPG; FBXO5; GMNN; CENPA; MAD2L2; CDC20; HELLS; ZWINT; CKS2; PKMYT1; CHTF18; SGO1; RBM38; LRRCC1; CAMK1; PSRC1; CABLES1; USP44; NEK3; DSCC1; KNL1; CEP55; TICRR; NUF2; FANCD2; SASS6; MIS18A; CHAF1B; CDC25A; MAD2L1; SKA3; DDIAS; MCM7; CENPV; BUB1; CKS1B; UBE2C; MLF1; AURKB; KIF18B; SAPCD2; ERCC6L; CENPW; KIFC1; UHRF1
DNA replication	1.10E-10	155	MCM2; CLSPN; CDC45; CDC7; CHTF18; DSCC1; TICRR; CHAF1B; MCM7; POLA2; MCM10; ORC1; SAMHD1; GINS2; RFC3; GINS4; RFC4; RRM2; EXO1; GINS3; BLM
Chromosome segregation	5.78E-07	83	BIRC5; CENPT; OIP5; SGO1; KNL1; NUF2; MIS18A; SKA3; BUB1; CENPW; CEP85; ESPL1
DNA repair	1.31E-05	379	CLSPN; DMC1; MAD2L2; TICRR; FANCD2; CHAF1B; UHRF1; SAMHD1; EXO1; BLM; EYA2; NTHL1; UBE2T; RAD54L; NEIL3; RAD51AP1; OGG1; EEPD1; FAAP24; XRCC4; FANCB; XRCC2; WDHD1; FANCG
DNA recombination	3.39E-03	104	EXO1; BLM; RAD54L; RAD51AP1; XRCC4; XRCC2; XRCC2; HMGB3; HMGB2
Blood circulation	1.24E-02	38	STAT1; FLI1; CXCL10; HOXB2

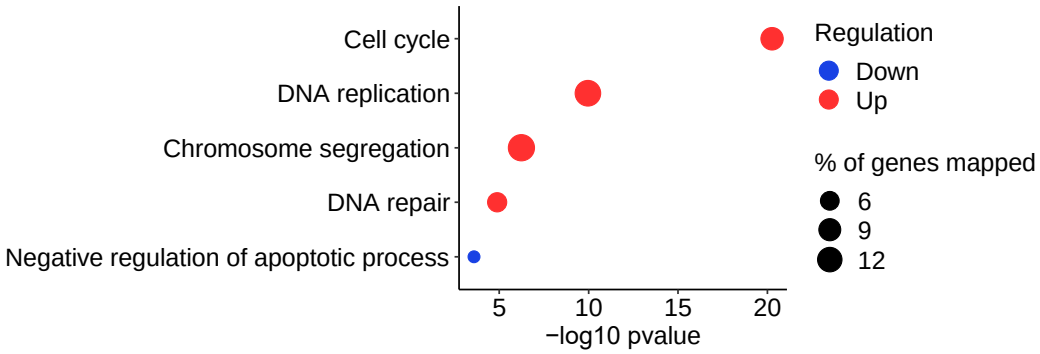

Figure 3. 8 | Gene ontology (GO) terms relating to the biological processes of up- and downregulated genes in MM MYB +DOX cells. Plot bar showing the biological processes activated in MM cells after MYB activation, according to Panther:BP database. Results were filtered by p value ≤ 0.05 and adjusted by FDR ≤ 0.1. Different colours are used to distinguish the regulation. The size of the dots indicates the % of genes mapped for each biological process.

Comparing the transcriptional landscape of MM MYB cells with that of ACC

To understand if induction of *MYB* in MM MYB cells recapitulates the gene expression patterns observed in ACC cell lines and primary tumours, a gene expression signature for ACC was constructed and compared with the RNA-seq analysis of *MYB*-overexpressing MM MYB cells. To establish an ACC gene expression signature, four publicly available datasets were analysed. Specifically, data from three ACC microarray datasets (Andersson, Chowbina, and Gao) was downloaded from the Gene Expression Omnibus (GEO) repository and combined with the RNA-seq analysis of ACC-X11 (PDX-derived) cell line (Cicirò dataset). Details of the datasets are in **Table 3. 3**.

Table 3. 3 | Details of the datasets used. H: human, X: xenograft.

DATASET	ACCESSION NUMBER	TYPE	NUMBER OF ACC SAMPLES	NUMBER OF NSG SAMPLES	REFERENCE
Andersson	GSE88804	H	13	7	(Andersson *et al*., 2020)
Chowbina	GSE36820	X	11	3	/
Cicirò	E-MTAB-12978	H	7	3	/
Gao	GSE59702	H	12	12	(Gao, R. *et al*., 2014)

Firstly, we identified genes differentially expressed in ACC tumour samples compared to NSG using the R package *limma*. Genes were filtered by fold change with a threshold $\geq \pm 1$ and an FDR cut-off of 0.05.

Figure 3. 9 shows the volcano plots of differentially expressed genes for each dataset and the number of up- or downregulated genes classified by statistical significance. The top 100 genes of each dataset are reported in **Supplementary Table 4**, **Supplementary Table 5**, **Supplementary Table 6**.

A

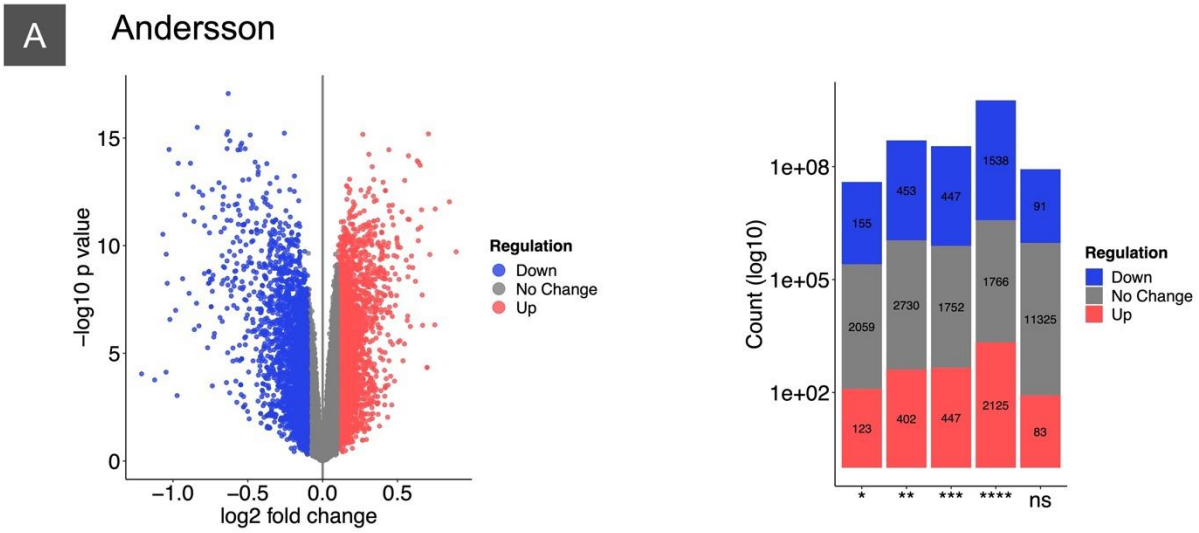
Andersson
−log10 p value
log2 fold change
Regulation
Down
No Change
Up
Count (log10)
1e+08
1e+05
1e+02
155
453
447
1538
91
2059
2730
1752
1766
11325
123
402
447
2125
83
*
**
***
****
ns

B

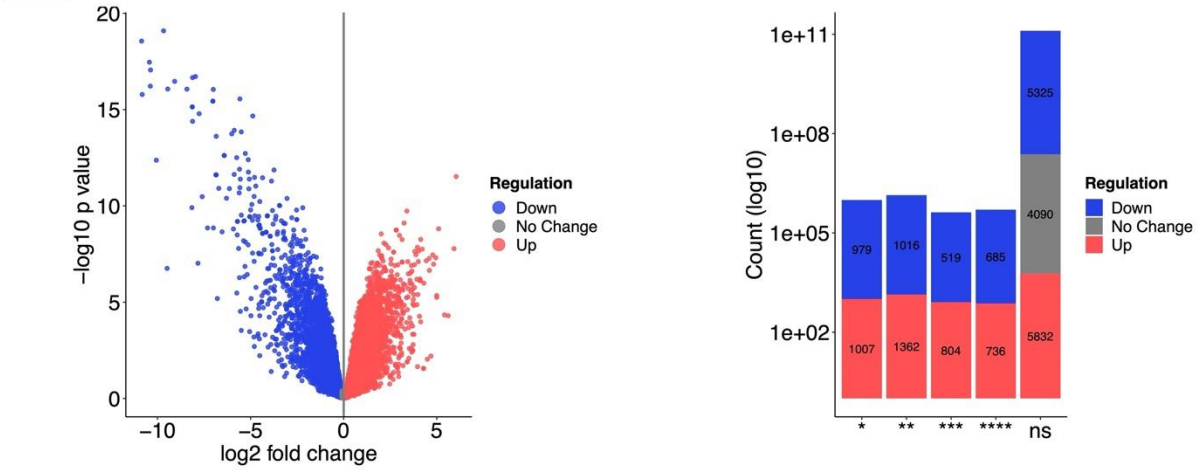
Chowbina
−log10 p value
log2 fold change
Regulation
Down
No Change
Up
Count (log10)
1e+11
1e+08
1e+05
1e+02
979
1016
519
685
5325
4090
1007
1362
804
736
5832
*
**
***
****
ns

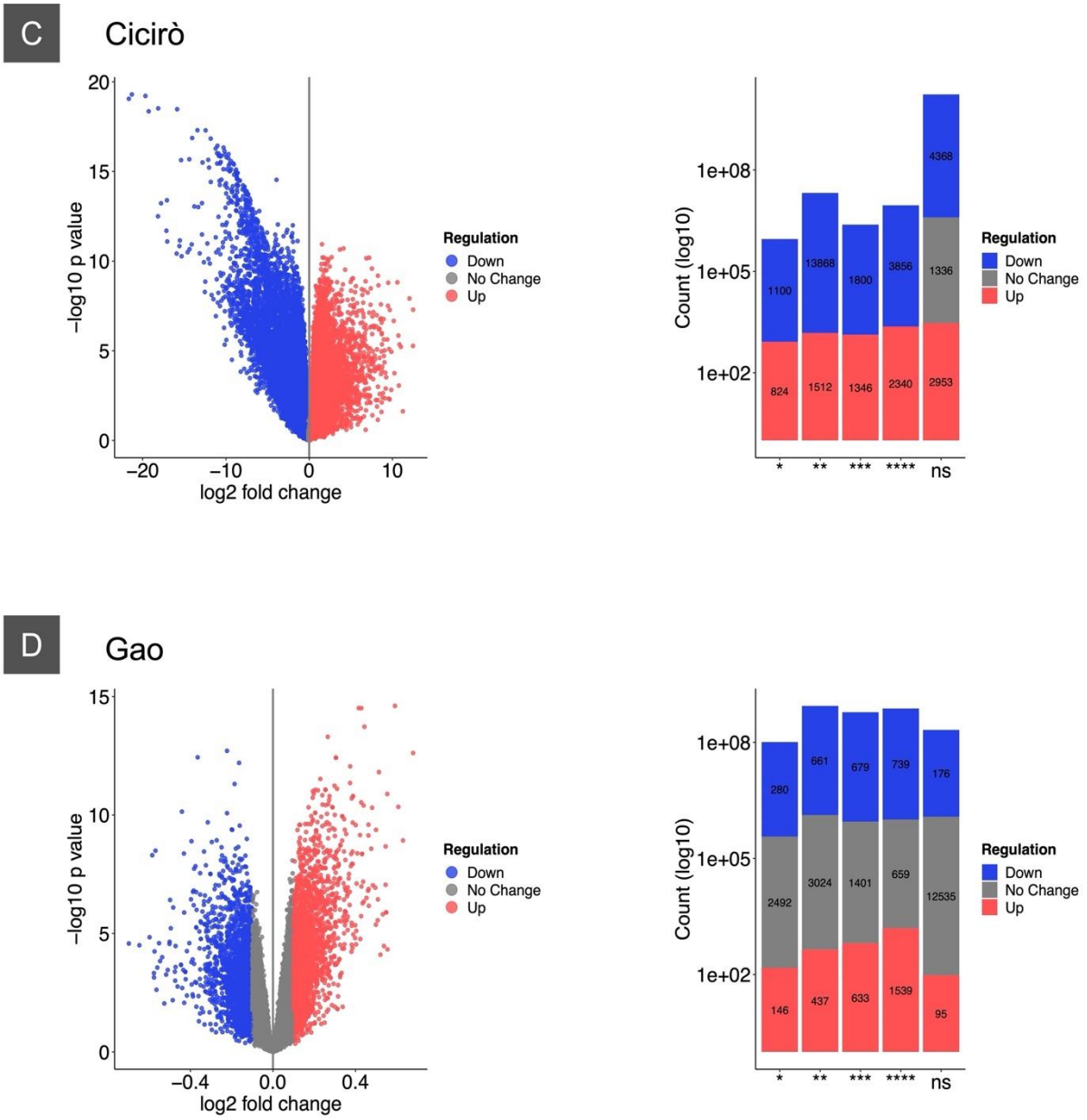

Figure 3. 9 | Differentially expressed genes in publicly available datasets. Volcano plots (left) illustrated the differentially expressed genes in (**A**) Andersson, (**B**) Chowbina, (**C**) Cicirò, and (**D**) Gao datasets. Bar plots (right) show the number of differentially expressed genes, according to p value. Colours indicate upregulation (red), downregulation (blue), or no change in expression (grey). p value ≤ 0.05 (*), 0.001 (**), 0.0001 (***), and 0.00001 (****); ns, not significant.

To confirm the biological relevance of up- and downregulated genes in ACC for each dataset, GO analysis was performed using Panther:BP database (**Figure 3. 10**). Significant GO terms were selected with a p value ≤ 0.05 and filtered by FDR ≤ 0.1. Interestingly, the top scoring pathways were related to the cell cycle and its regulation, as well as regulation of chromatin and chromosomes.

A

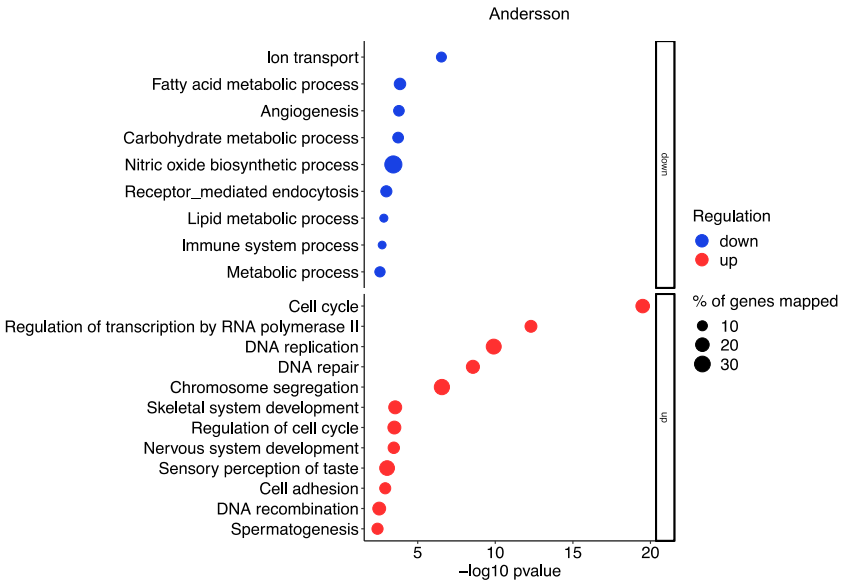
Andersson
Ion transport
Fatty acid metabolic process
Angiogenesis
Carbohydrate metabolic process
Nitric oxide biosynthetic process
Receptor_mediated endocytosis
Lipid metabolic process
Immune system process
Metabolic process
Cell cycle
Regulation of transcription by RNA polymerase II
DNA replication
DNA repair
Chromosome segregation
Skeletal system development
Regulation of cell cycle
Nervous system development
Sensory perception of taste
Cell adhesion
DNA recombination
Spermatogenesis
down
up
5
10
15
20
−log10 pvalue
Regulation
down
up
% of genes mapped
10
20
30

B

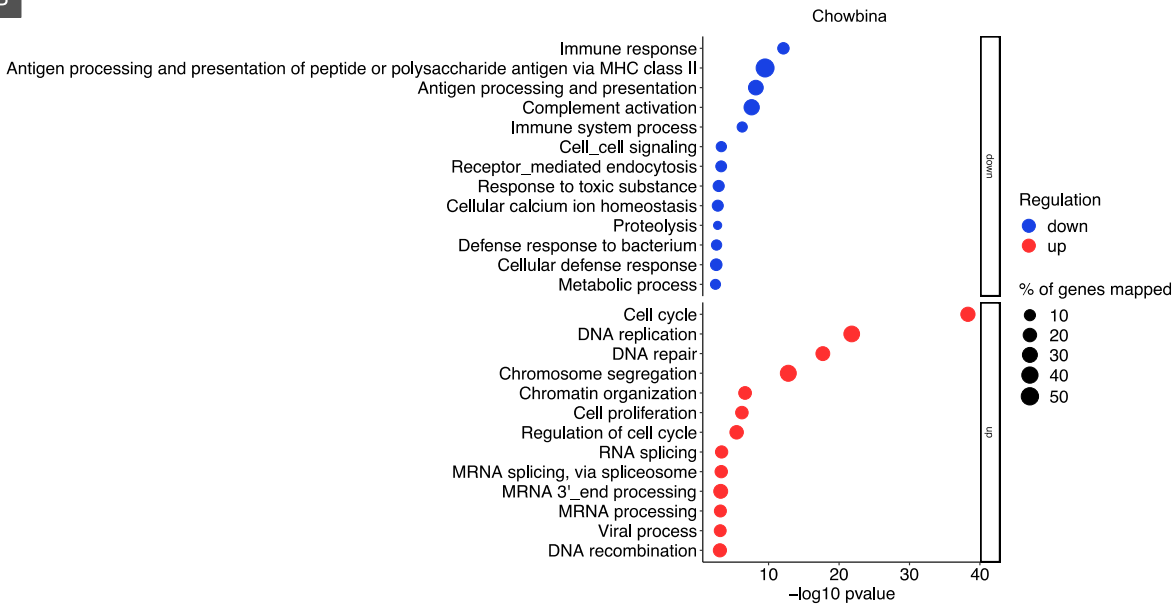
Chowbina
Immune response
Antigen processing and presentation of peptide or polysaccharide antigen via MHC class II
Antigen processing and presentation
Complement activation
Immune system process
Cell_cell signaling
Receptor_mediated endocytosis
Response to toxic substance
Cellular calcium ion homeostasis
Proteolysis
Defense response to bacterium
Cellular defense response
Metabolic process
Cell cycle
DNA replication
DNA repair
Chromosome segregation
Chromatin organization
Cell proliferation
Regulation of cell cycle
RNA splicing
MRNA splicing, via spliceosome
MRNA 3'_end processing
MRNA processing
Viral process
DNA recombination
down
up
10
20
30
40
−log10 pvalue
Regulation
down
up
% of genes mapped
10
20
30
40
50

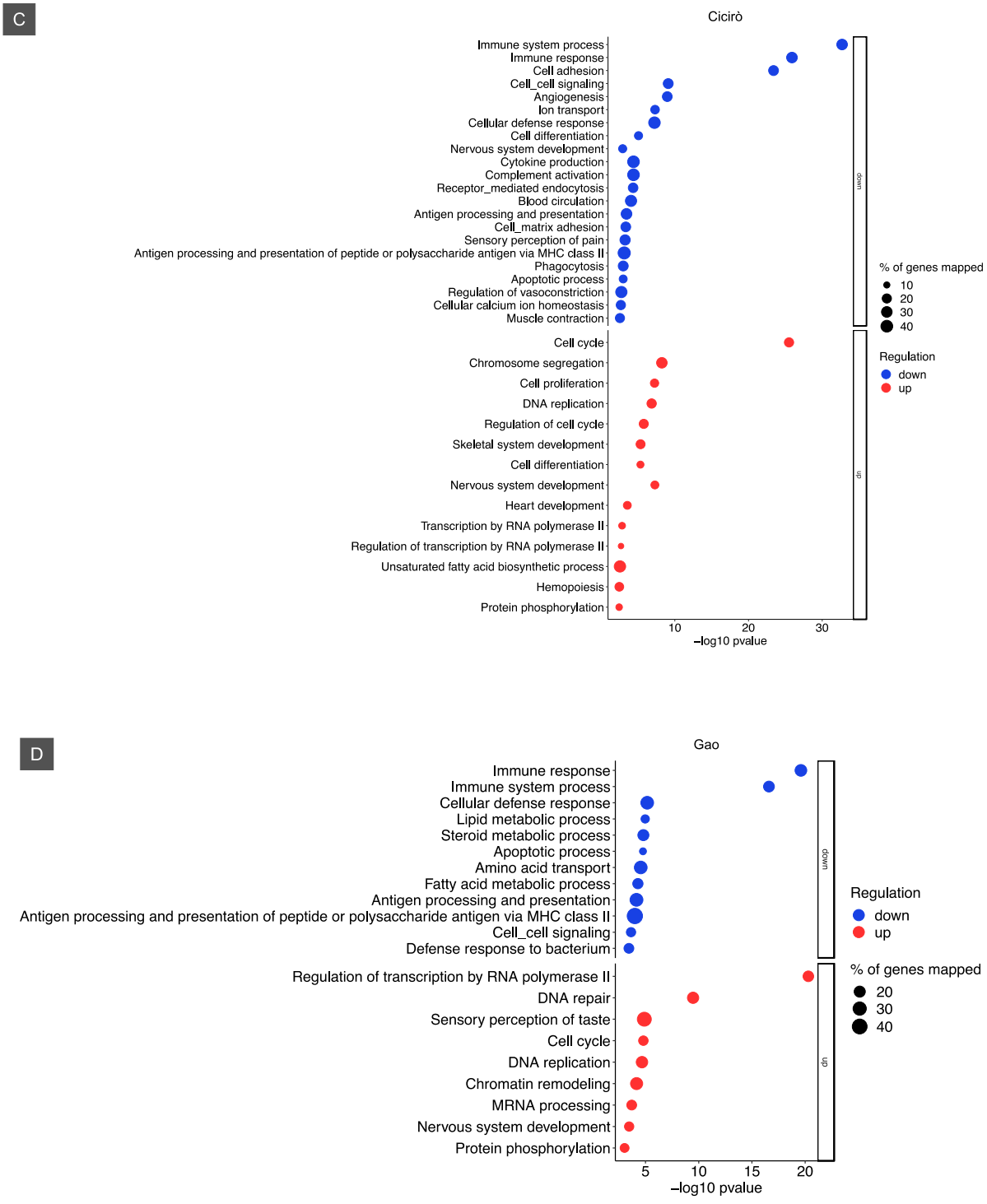

Figure 3. 10 | GO analysis of the publicly available datasets of ACC. Dot plot showing the biological processes resulted most significantly up- or downregulated in (**A**) Andersson, (**B**) Chownina, (**C**) Cicirò, and (**D**) Gao dataset. The size of the dots indicates the percentage of the genes mapped in each biological process, and up- and downregulated genes are shown in blue and red, respectively.

Next, the pathways extracted from each GO analysis were intersected using the REACTOME database. The Venn diagrams in **Figure 3. 11 A-B** illustrate the shared pathways. Positively regulated genes shared among the different datasets were related to cell cycle and DNA replication processes, whereas the only processes related to the downregulated genes was the immune system.

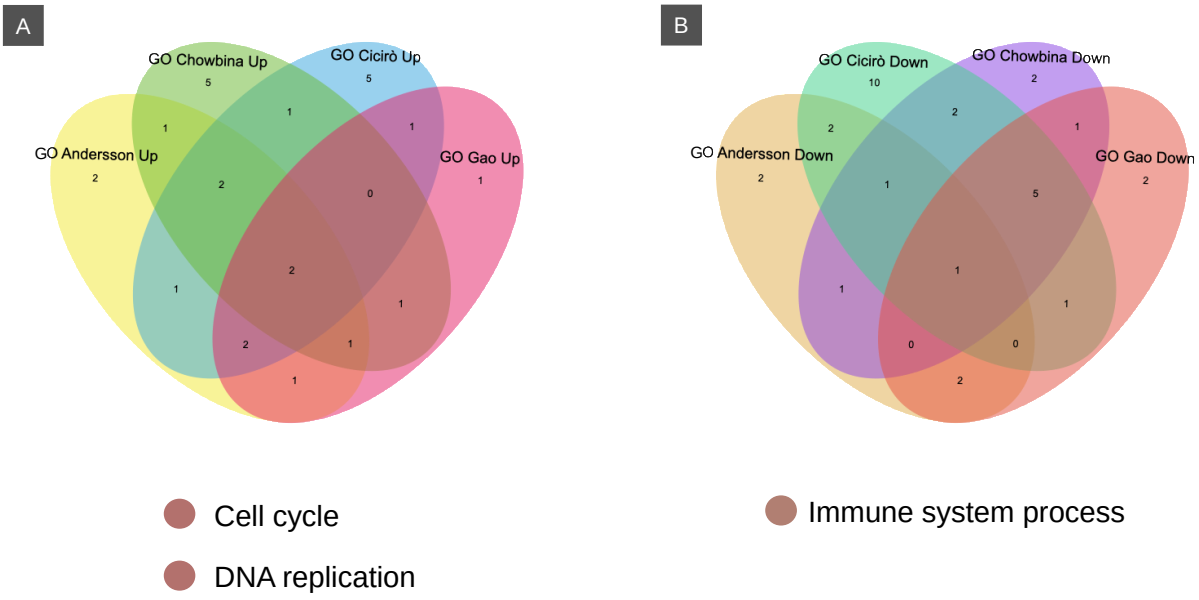

Figure 3. 11 | Biological processes common to the Andersson, Chowbina, Cicirò, and Gao datasets. Venn diagrams of shared pathways extracted from GO analysis of (**A**) upregulated or (**B**) downregulated genes.

To investigate whether *MYB* fusion-negative ACC tumours exhibit a different downstream gene expression profile compared to *MYB-NFIB* fusion-positive ACC, GSE59702 microarray from GEO Gene Expression Omnibus (GEO) database was downloaded and analysed. This set (Gao dataset) contains ACC samples classified according to their fusion status: 8 fusion positive tumours (FPT) with their matched normal tissue (NFP), 4 fusion negative tumours

(FNT) paired with their normal tissue (NFN), for a total of 24 samples. FPT and FNT tumours were compared to their matched normal samples and differentially expressed genes were identified. Genes were filtered by a fold change threshold ≥ ± 1 and an FDR cut-off of 0.05, and analysis was performed using the R package *limma*. Comparison of fusion positive and fusion negative differentially expressed genes revealed a total of 60 genes downregulated and 55 genes upregulated (**Figure 3. 12**). The vast majority of the genes (25 378 genes) showed no changes (**Figure 3. 12**).

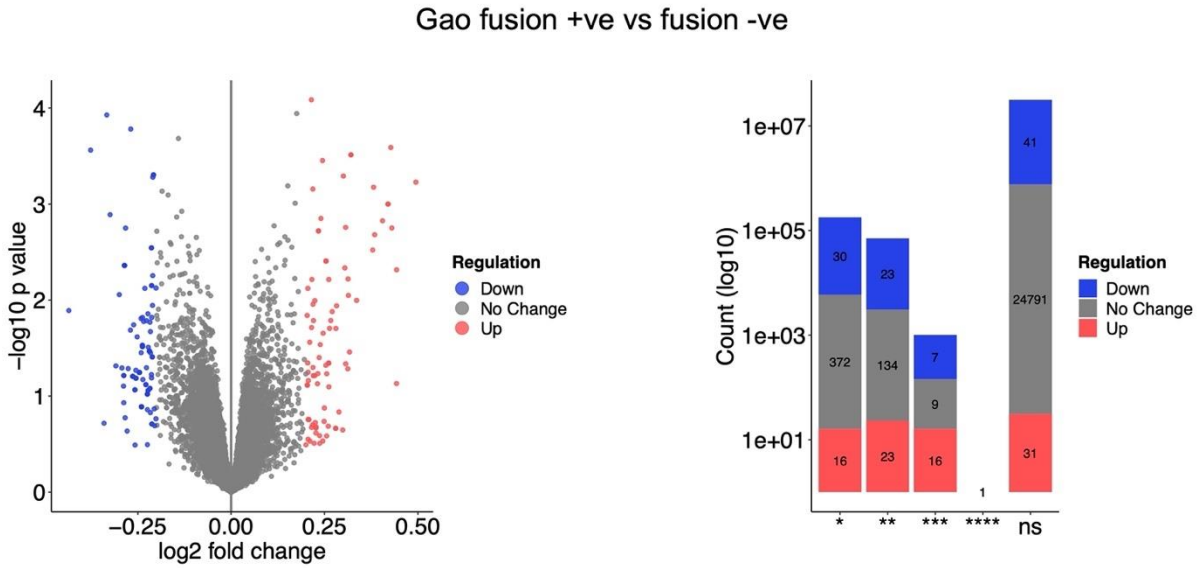

Figure 3. 12 | Comparison of differentially expressed genes in fusion positive and fusion negative ACC. Volcano plot of differentially expressed genes (left). The number of differentially expressed genes according to the p values is shown on the right. p value ≤ 0.05 (*), 0.001 (**), 0.0001 (***), and 0.00001 (****); ns, not significant.

We also carried out unsupervised hierarchical clustering of gene expression and the resulting heatmap showed high gene expression similarities between tumour samples, regardless of their fusion status, validating the hypothesis that *MYB* rearrangements or *MYB* activation

(without fusion to another gene partner) are functionally equivalent in ACC cancers (**Figure 3. 13**) as previously postulated in our laboratory (Andersson *et al*., 2020).

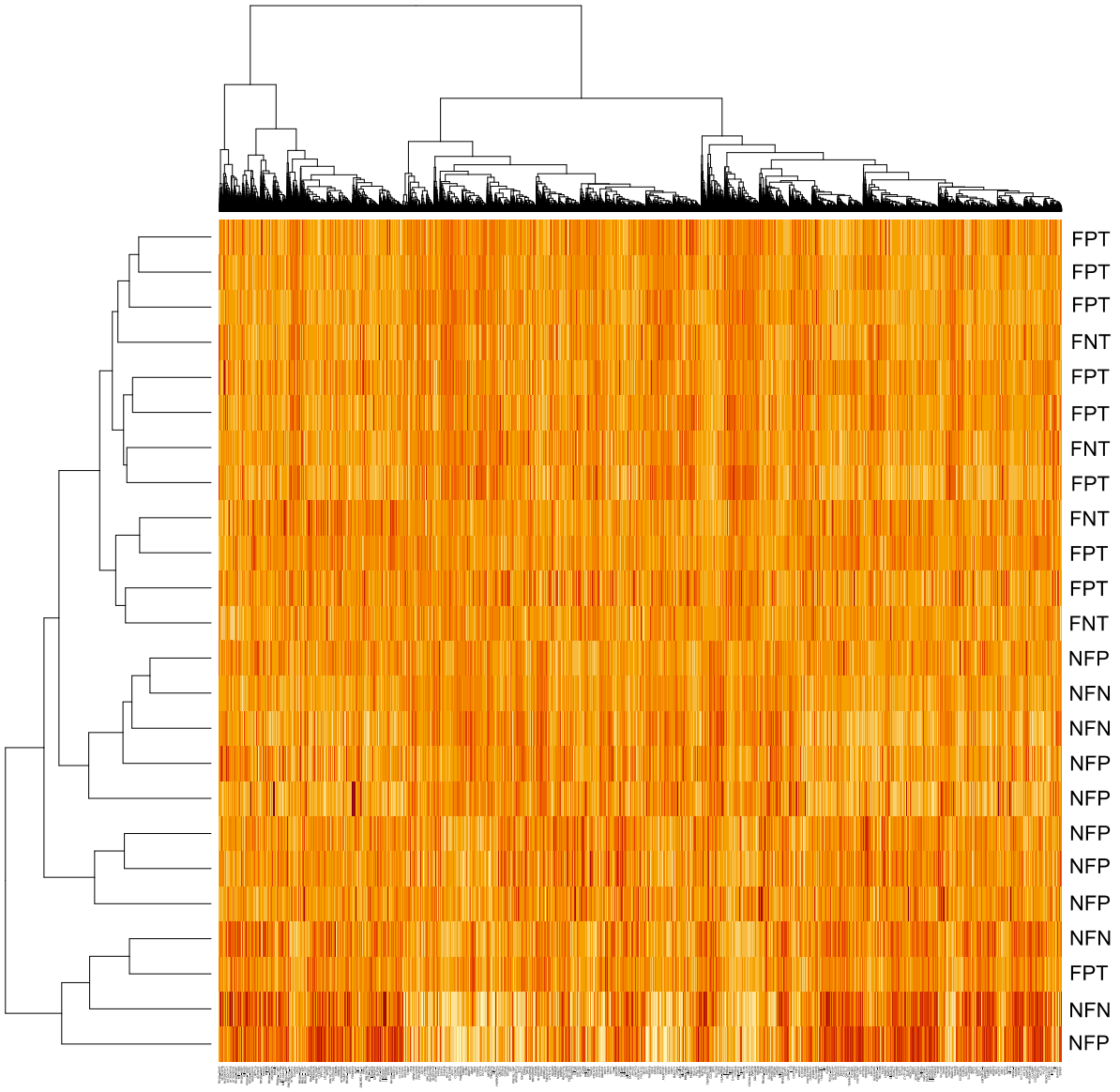

Figure 3. 13 | Comparison of ACC fusion positive and fusion negative samples. Heatmap generated from the Gao microarray dataset (GEO accession GSE59702) to assess similarities in gene expression in ACC samples with different *MYB* rearrangement status. FPT = fusion positive tumour. FNT = fusion negative tumour. NFP = match normal of a fusion positive tumour. NFN = match normal of a fusion negative tumour.

Identification of an ACC patient signature

The *singscore* method was used to normalise gene expression across datasets taking into account the theoretical minima and maxima for scores in each sample. The normalised upregulated genes were intersected and plotted in a Venn diagram (**Figure 3. 14**). The 156 upregulated genes shared between the four datasets were considered as a genuine ACC signature. The identity of each gene is listed in the **Supplementary Table 7**.

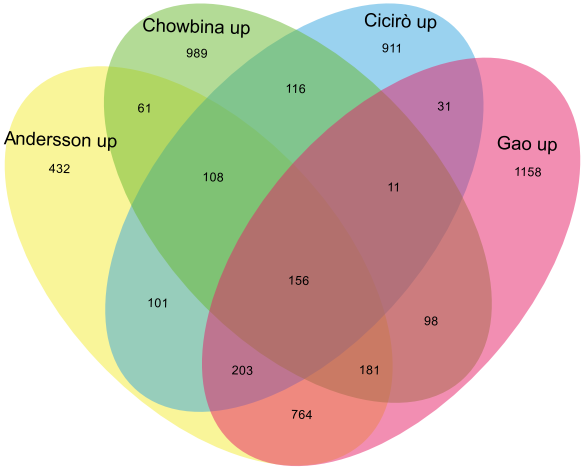

Figure 3. 14 | Gene signature of ACC-patient gene expression extrapolated from published array and RNA-seq datasets. The Venn diagram shows the upregulated genes shared in the four databases.

We performed Gene Set Enrichment Analysis (GSEA) to determine whether the *a priori* defined 156 gene set signature shows statistically significant enrichment in MCF10A cells overexpressing or not overexpressing *MYB*. The enrichment analysis of the gene signature against MM MYB ± DOX RNA-seq counts revealed a significant enrichment in MM MYB +DOX, compared with the condition -DOX, with a Normalised Enrichment Score NES of 1.55 and p value < 10E-16 (**Figure 3. 15 A**).

The top 50 core enriched genes (also known as 'leading edge') extracted from GSEA identified patient-specific genes recapitulated in the MM MYB +DOX model (**Figure 3. 15 B**). The full list is reported in **Supplementary Table 8**.

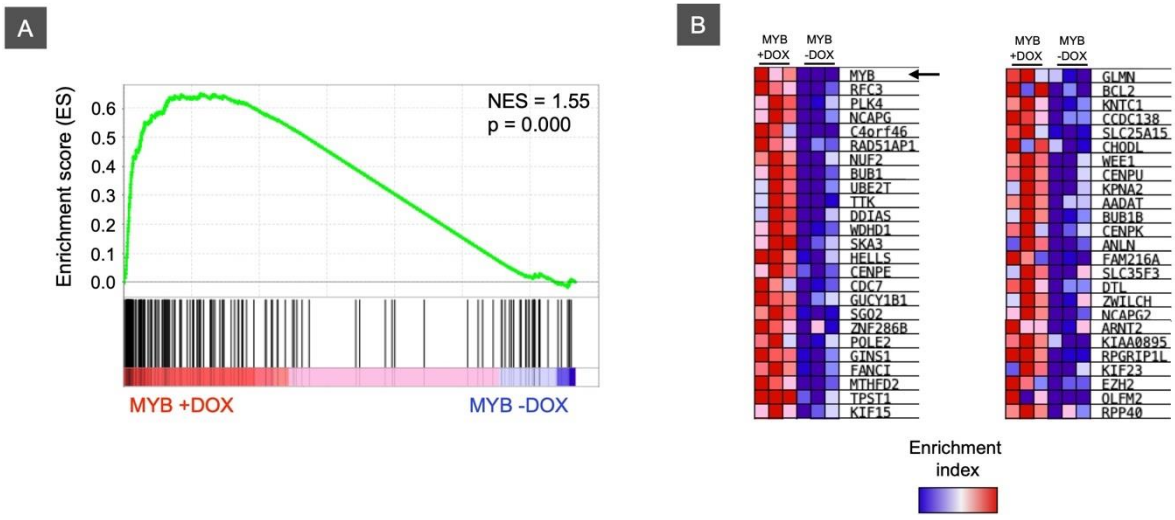

Figure 3. 15 | Comparison of MM MYB transcriptional profile with the ACC patient signature. (**A**) GSEA enrichment plots of MM MYB cell line's expression profile using the 156-signature. The enrichment score (ES) reflects the degree to which the gene-set is overrepresented at the top or bottom of the ranked list of genes. The normalised ES (NES) corrects for differences in ES between gene-sets due to differences in gene-set sizes. The horizontal coloured bar indicates the shift from positively enriched genes (red) to negatively enriched genes (blue). (**B**) Top 50 core enriched genes of MM MYB compared to the ACC signature from GSEA. The black arrow indicates MYB gene.

3.3 Discussion

The chromosome exchange resulting in the fusion of the transcription factor genes *MYB* in chromosome 6 and *NFIB* in chromosome 9 is a hallmark of ACC, which is characterised by the overexpression of *MYB* (Brill *et al*., 2011; Persson *et al*., 2009). However, abnormally high expression of wild type *MYB* can also occur through promoter/enhancer element alterations (Drier *et al*., 2016). Independently from the mechanism of activation, *MYB* overexpression is a key instigating event in ACC (Persson *et al*., 2009), suggesting that it is important to study the role of *MYB* in both fusion-negative and fusion-positive tumour samples. There is an urgent need to develop ACC models that are physiologically relevant, easy to maintain, and mimicking the main characteristics of the disease. Developing ACC cell lines that grow robustly *in vitro* while retaining key biomarkers over time, including *MYB* expression, has been challenging and has limited the availability of reliable ACC cell line models. Moreover, the dual myoepithelial/epithelial composition of ACC underlies its biological heterogeneity and the technical difficulties of ACC cell line establishment (Hantel *et al*., 2016).

It has been shown that fusion-positive and fusion-negative ACC samples exhibit similar gene expression profiles (Gao, R. *et al*., 2014). Likewise, gene expression profiles of MCF10A cells stably overexpressing *MYB* or different *MYB-NFIB* fusion variants were very similar and caused comparable biological changes (Andersson *et al*., 2020), suggesting that the overexpression of *MYB* is the main oncogenic player.

One major aim of this PhD study was to establish a new *in vitro* model that could more faithfully recapitulate the biological and gene expression profiles of ACC cells. We thought that inducible expression of *MYB* could establish an ACC-like state in glandular MCF10A breast cells, while at the same time offering a “normal” control in the uninduced condition with *MYB*-

OFF. The model was engineered by transducing MCF10A cells with the lentiviral vector pINDUCER21-MYB which contains the human *MYB* cDNA under the control of a DOX inducible promoter, allowing transient expression of the proto-oncogene. The combination of cellular and molecular properties of MCF10A, as well as the relatively ease in manipulating it in different assays and its wide adoption in biomedical research, made MCF10A a valid candidate to perform these studies. In particular, the glandular origin shared with ACC and the absent *MYB* expression in WT cells (Andersson *et al*., 2020; Imbalzano *et al*., 2009), provided the rationale for using MCF10A to build a new model of ACC. Indeed, it should be noted that a small fraction of triple negative breast cancers characterised by *MYB* gene rearrangements/ overexpression are classified as ACC (Zhang, Meilin *et al*., 2022). Therefore, the MM model could result potentially useful also in breast cancer setting or, taking into account its molecular characteristics, in other cancers harbouring *MYB* overexpression, e.g. leukaemia.

Basal levels of *MYB* in uninduced MM MYB cells (-DOX) condition were higher than in empty vector controls (MM EV ±DOX), highlighting leakiness of inducible systems, probably as consequence of the site of chromosomal integration (Garrick *et al*., 1998; Meyer-Ficca *et al*., 2004).

The biological relevance of the MM MYB cellular model was validated by Gene Ontology (GO) analysis. The most active biological process in MM MYB +DOX cells (*MYB*-ON) was cell cycle, followed by DNA replication, chromosome segregation, negative regulation of apoptotic processes, DNA repair, cell adhesion, and blood circulation. This result is consistent with recently reported data, including the multi-omics analysis performed on MCF10A in which master transcription factors, counting *MYB*, were activated after exposure to six ligands (EGF, HGF, OSM, IFNG, TGFB, and BMP2) known to stimulate different disease-associated signalling pathways of clinical relevance, such as MAPK, JAK/STAT, WNT, TGFB, and activation of genes related to the cell cycle progression, including the kinases *AURKA*, *CDK1*, *PLK1*, and *BUB1* (Gross *et al*., 2022). Gross and colleagues also identified a suite of enriched REACTOME pathways comparable to the one depicted in **Figure 3. 7**, including G1/S specific

transcription, unwinding of DNA, and processes linked to DNA damage induced by stress or activation of G2/M or DNA damage checkpoint associated kinases (Gross *et al*., 2022). The importance of *MYB* in the regulation of the cell-cycle has been also highlighted in the study published by Andersson and colleagues in which they established that knockdown of *MYB-NFIB* via *MYB* siRNAs leads to G1 arrest, reduced cell proliferation, and strong reduction of cells residing in the G2/M phase, thus underlying the impact of *MYB* in cell cycle progression of primary ACC cells (Andersson *et al*., 2017).

There are no available RNA-seq data in repositories online that we could use to establish a more detailed comparison. Therefore, we had to use ACC microarray datasets and compared them with our mRNA whole-transcriptome high-throughput sequencing on MM cells, facing the limitations that this comparison may imply. In fact, microarrays profile only a cluster of predefined transcripts/genes, suggesting that comparison with RNA-seq data is not ideal. However, this study may pave the way to future investigations which can take these variables into account.

The analysis of four publicly available ACC datasets, of which three microarray studies extracted from GEO repository database and one RNA-seq analysis generated by us, showed similar enrichment in biological processes. These datasets were also used to extract an ACC oncogenic signature from transcriptional data that could yield valuable insights on the biology of the tumour and that was used to validate MM MYB as a faithful *in vitro* model of ACC. Indeed, GSEA revealed that MM MYB +DOX (*MYB*-ON) showed a significant enrichment index, confirming the hypothesis that this cell line could be used with confidence as a model that recapitulates the ACC transcriptional landscape. Interestingly, MM MYB +DOX cells gradually lost *MYB* expression after serial passaging, similarly to the ACCX11 cell line (**Supplementary Figure 1**), a limitation already reported in Queimado *et al.* (1999) and Li *et al.* (2014), where ACC cells lost the *MYB-NFIB* fusion found in the primary tumours from which

they were derived, suggesting a secondary event interfering with stability of *MYB* levels in *in vitro* cultures (Li, J. *et al*., 2014; Queimado *et al*., 1999).

In conclusion, this chapter provides evidence the MM MYB model could be used as an avatar of ACC cells. The new model is easier to manipulate and cheaper to maintain than PDXs and PDX-derived cell lines. MCF10A cells and pINDUCER21-MYB are commercially available, therefore increasing the chances that other investigators could use the system to advance ACC research and improve patient's outcome.

Chapter IV

MYB transcriptionally controls the expression of *BUB1* in immortalised and transformed human glandular epithelial cells

4.1 Introduction

Although *MYB* activation is a hallmark of ACC (Persson *et al*., 2012), it is still unclear what the consequences of its activation are and the molecular factors with which it may cooperate in the carcinogenesis of ACC. Given its role in cell cycle, proliferation, and in transformation of haematopoietic cells, therapeutic targeting of MYB has been investigated in several studies (Pham *et al*., 2019; Ramaswamy *et al*., 2018; Uttarkar *et al*., 2016; Walf-Vorderwülbecke *et al*., 2018; Yusenko *et al*., 2020). For example, the Gonda laboratory reported how its suppression by using either antisense oligonucleotides or RNA interference inhibited proliferation of oestrogen receptor positive (ER+), but not ER negative (ER-), breast cancer cells, reflecting the link between MYB and the oestrogen signalling (Drabsch *et al*., 2007). Another study highlighted the efficacy of monensin, a novel polyether ionophore MYB inhibitor, in suppressing cell viability and inducing apoptosis in two different MYB-driven cancers, AML and ACC (Yusenko *et al*., 2020). Other therapeutic strategies targeting MYB involve peptidomimetic blockade (Ramaswamy *et al*., 2018) or cancer vaccine (Pham *et al*., 2019), used for the treatment of AML, CRC, and ACC, respectively. Despite promising results in experimental models (references as above), there have been only few clinical trials with MYB-targeting molecules. To date, according to the publicly available list of clinical trials, only a few reached phase II, suggesting that direct targeting of MYB may be difficult in clinical settings. A major complication is that *MYB* is a key gene in mammalian haematopoiesis (Westin *et al*., 1982). Thus, the essential role of MYB in important physiological processes, together with the lack of stable tumour lines and mouse models, have hindered drug development for the treatment of *MYB*-driven solid tumours, such as ACC.

The identification of *MYB*-downstream genes to be used as therapeutic targets could be a reasonable strategy to avoid the potential haematological toxicity of anti-MYB therapies. Thus, researchers have focused their attention on signalling pathways downstream of *MYB* in multiple cancers. The laboratory of Scott Ness used the breast cancer cell line MCF-7 to identify MYB target genes using chromatin immunoprecipitation coupled with genome promoter tiling microarray analysis and found MYB associated with over 10.000 promoters (Quintana *et al*., 2011). Using this strategy, the team identified several already known MYB targets, including cell cycle genes and transcription factors, such as *CCNB1*, *MYC*, and *CXCR4* but also novel MYB-regulated genes, such us *JUN*, *KLF4*, *NANOG*, and *SND1* (Quintana *et al*., 2011). A selection of *MYB* target genes identified in different published studies can be found in **Supplementary Table 1**. Interestingly, some of the *MYB* target genes encode for protein kinases (De Dominici *et al*., 2018; Ferrao *et al*., 1997; Ku *et al*., 1993). Among these, *ATR* was significantly upregulated in normal breast glandular cells overexpressing *MYB* (or *MYB-NFIB* fusion) as well as in ACC samples and PDXs (Andersson *et al*., 2020). Microarray analysis of ACC cells overexpressing *MYB* identified genes already known as MYB targets (i.e. *BIRC3*, *CDC2*, and *CXCR4*) together with new candidates, including *BUB1*, *CENPE*, *CENPF*, *EXO1*, *NDC80*, and *TTK* (Andersson *et al*., 2020). Based on these results and the possibility of using kinases as drug targets, the mitotic checkpoint BUB1 was selected as an interesting candidate for ACC therapy. In this chapter, the relationship between MYB and BUB1 was investigated to uncover molecular and functional aspects of this interaction.

4.2 Results

In this chapter, PDX-derived ACCX11 cells were used to quantify *BUB1* expression after knockdown of *MYB-NIFB* and for ChIP-seq analysis. ACCX11 cells were provided by Professor Göran Stenman, Sahlgrenska Cancer Center (University of Gothenburg, Sweden), in collaboration with the Adenoid Cystic Carcinoma Research Foundation (ACCRF, MA, USA), and XenoSTART (S. Antonio, Texas, USA). Immunohistochemistry (IHC) analysis was performed by Prof Rossano Lattanzio and Prof Gianluca Sala from in Chieti-Pescara University, Italy.

4.2.1 Analysis of *MYB* and *BUB1* expressions in publicly available ACC datasets

To validate the hypothesis that *BUB1* is a downstream effector of *MYB* in ACC, we analysed gene expression profiles from publicly available datasets. We used the microarray datasets from Andersson, Chowbina, and Gao, along with the RNA-seq data generated in this study. Details about the datasets are summarised in **Table 3. 3** (from **Chapter III**).

RNA-seq revealed that *BUB1* was upregulated in MM MYB cells upon addition of DOX and in ACCX11 samples compared to the NSG (**Figure 4. 1**). Increased expression of *BUB1* in MM MYB cells was confirmed by qPCR (**Figure 4. 2**).

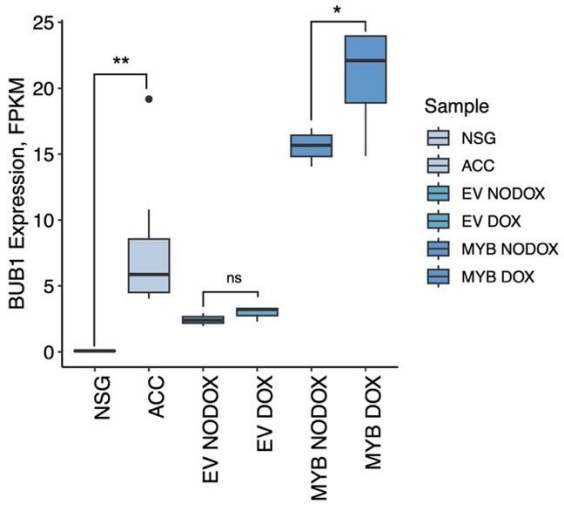

Figure 4. 1 | *BUB1* expression levels in ACC samples and MM cells. Boxplot showing *BUB1* expression in ACCX11 cells (ACC) compared to NSG. After addition of DOX, MM MYB cells showed increased expression of *BUB1* compared to the uninduced (NODOX) samples. No statistically significance was observed between EV samples with or without DOX. Expression values are reported in FPKM. p value ≤ 0.05 (*), 0.001(**); ns, not significant.

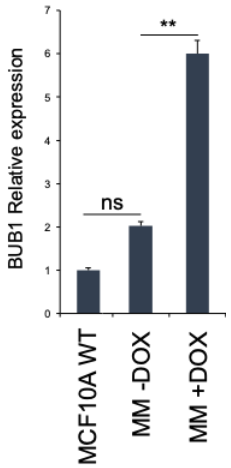

Figure 4. 2 | *BUB1* expression in induced or uninduced MM MYB cells. *BUB1* expression levels were quantified by RT-qPCR in MM MYB cells in the presence or absence of DOX. Gene expression was compared to naïve MCF10A cells (WT) used as control. p value ≤ 0.001 (**); ns, not significant.

MYB and *BUB1* expression levels in the combined datasets were increased in ACC samples compared to the NSG controls (**Figure 4. 3**). Moreover, Pearson correlation was used to assess whether *MYB* and *BUB1* were co-expressed in ACC. We found a significant linear relationship between the expression levels of *MYB* and *BUB1*, as indicated by a Pearson correlation value of 0.46 and a p value of 0.0063 (**Figure 4. 4**).

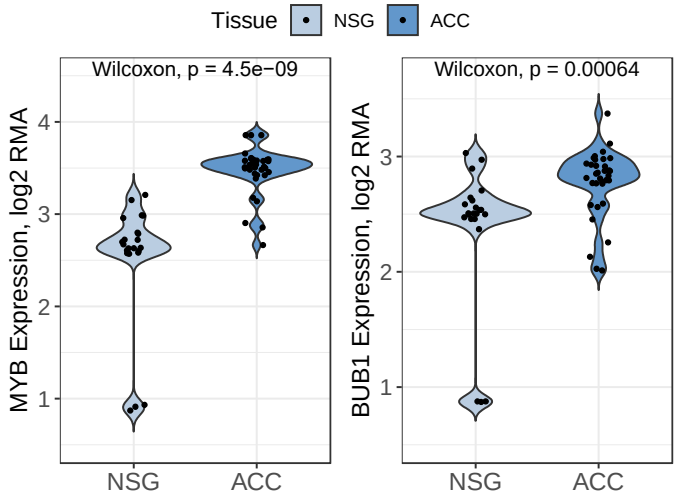

Figure 4. 3 | *MYB* and *BUB1* expression profile in ACC datasets. Violin plots showing *MYB* (left) and *BUB1* (right) expression; ACC samples were compared to NSG controls. Data were normalised and merged prior the plotting. Statistical analysis (Wilcoxon test) is shown at the top of the graphs. RMA, Robust Multi-Array Average.

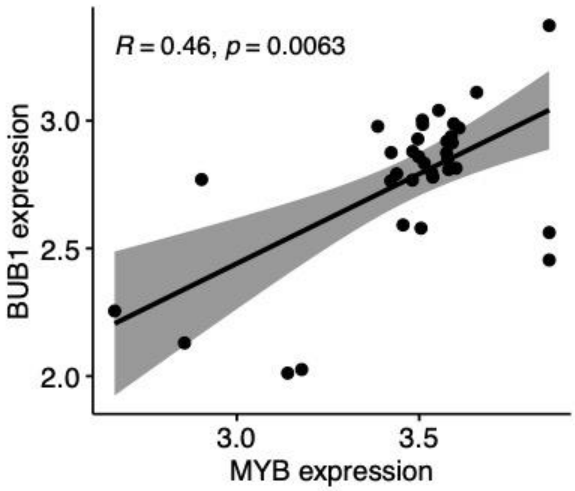

Figure 4. 4 | Pearson correlation analysis. Linear correlation profile of *MYB* and *BUB1* extrapolated from publicly available datasets showing the statistical relationship between the two variables. The grey area represents the correlation confidence interval (CI). R, Pearson correlation coefficient; p, p value.

To investigate whether *BUB1* is a direct downstream target of *MYB*, we analysed a microarray gene expression dataset in which *MYB-NFIB* was downregulated by RNA interference in ACC (Andersson *et al*., 2017). Treatment with two independent siRNAs targeting *MYB-NFIB* resulted in the downregulation of *MYB*, together with a concomitant decrease in *BUB1* expression level compared to the scramble siRNA control (**Figure 4. 5 A**). We have validated these results independently by using the same siRNA in the patient-derived ACC cell line ACCX11. RT-qPCR demonstrated that *BUB1* expression significantly declined after siRNA-mediated knockdown of *MYB-NFIB in vitro* (**Figure 4. 5 B**).

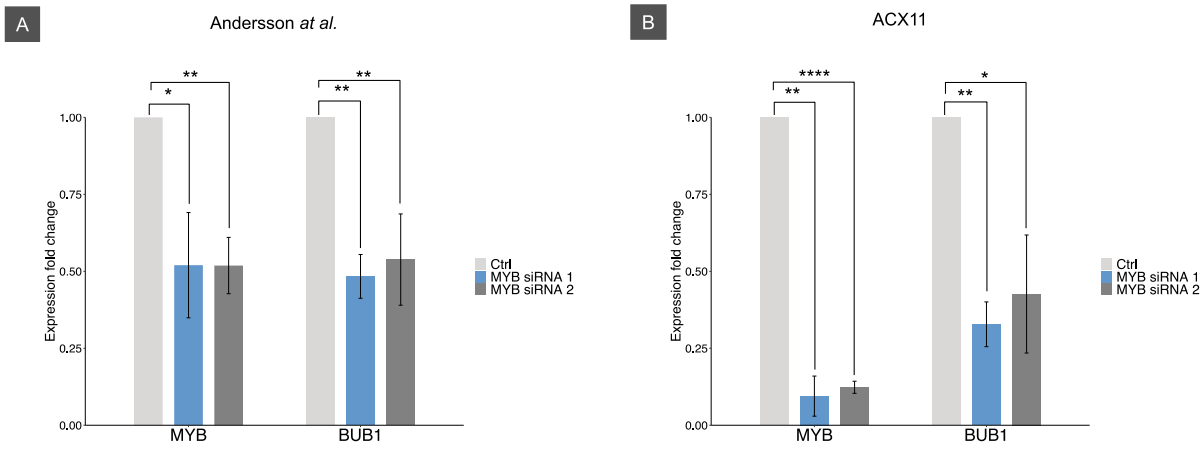

Figure 4. 5 | *MYB* and *BUB1* expression after *MYB-NFIB* knockdown by siRNAs. (**A**) Bar plots showing the expression fold changes of *MYB* and *BUB1* genes in ACC cells treated with two independent siRNAs, compared to the scramble control in GSE76094 microarray dataset and (**B**) after RT-qPCR in ACCX11 cultured cells.

4.2.2 BUB1 protein expression in ACC samples

To verify if BUB1 protein is expressed in ACC samples, the collaborating Chieti laboratory carried out immunohistochemical staining of BUB1 in 11 Tissue Microarray (TMA) samples, from a collection of XenoSTART Patient-Derived Xenograft (XPDX) models. 9 ACC samples were positive (82%), while 2 (18%, not shown) were negative for staining of BUB1 (**Figure 4. 6 A**). BUB1 protein was localised in the nucleus in five of the samples, whereas in the remaining samples three presented cytoplasmic and one diffuse staining (**Figure 4. 6 B**). In comparison, BUB1 was found to be localised in the cytoplasm of ACCX1 cells (**Figure 4. 6 A**).

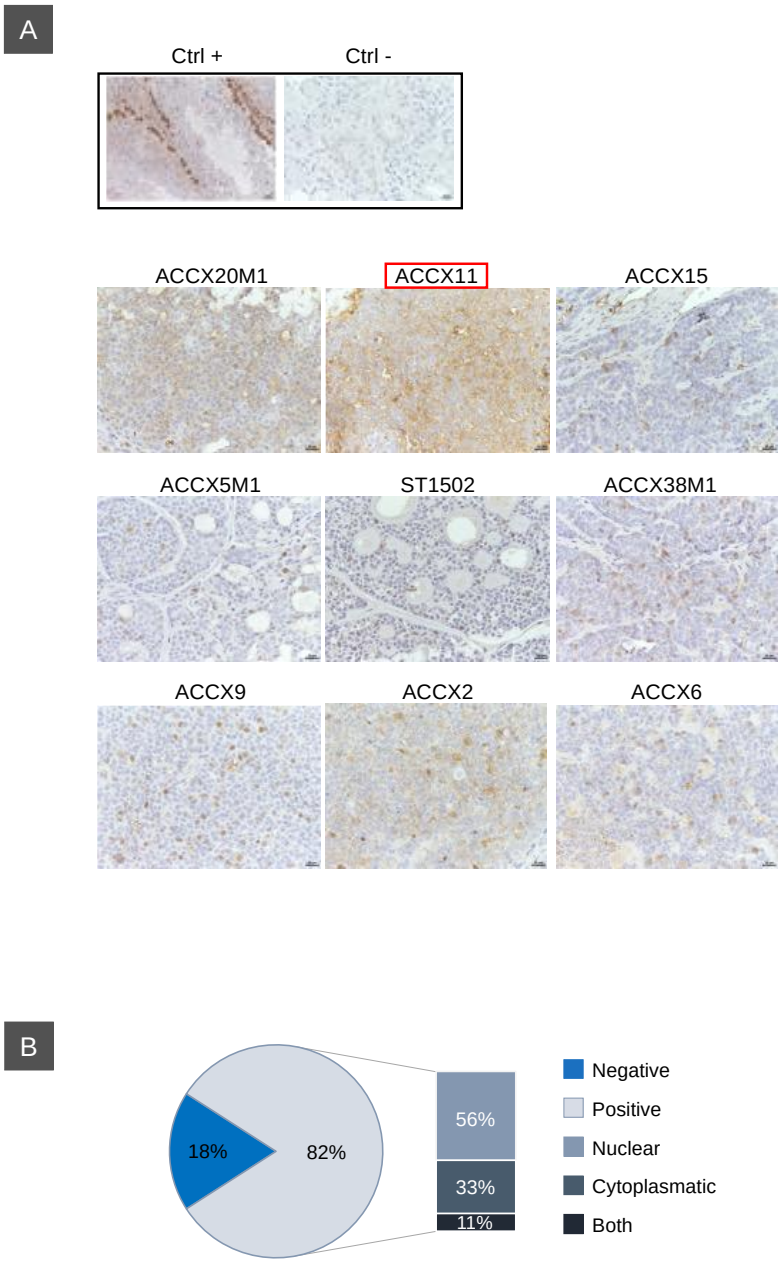

Figure 4. 6 | IHC analysis of ACC samples. (**A**) ACC TMAs samples were stained with a BUB1 specific antibody. Mouse testis tissue was used as positive control (Ctrl +) and normal parotid gland as negative control (Ctrl -). (**B**) Schematic representation of the number of ACC samples (express in percentage) classified according to the localisation of BUB1 protein. The red box highlights ACCX11. The assay was performed by Prof Gianluca Sala and Prof Rossano Lattanzio from G. D'Annunzio Chieti-Pescara University, Italy. Samples were provided by Adenoma Cystic Carcinoma Research Foundation (AACRF; Needham, MA, USA), in collaboration with the research organisation XenoSTART (S. Antonio, Texas, USA).

4.2.3 MYB transactivates the *BUB1* promoter *via* canonical MYB binding sequences

We hypothesised that MYB might transcriptionally activate the *BUB1* gene. Manual inspection of the *BUB1* 5' flanking region revealed several iterations of the G/TAACNG MYB consensus sequence in both DNA strands. Furthermore, using Cistrome Data Browser (Cistrome DB) (MYB ID: 50569, Cistrome DB) online tools, we confirmed that there were Chromatin IP (ChIP) MYB peaks overlapping with the putative MYB binding sequences in Jurkat leukaemia cells which constitutively express high levels of *MYB* (**Figure 4. 7**).

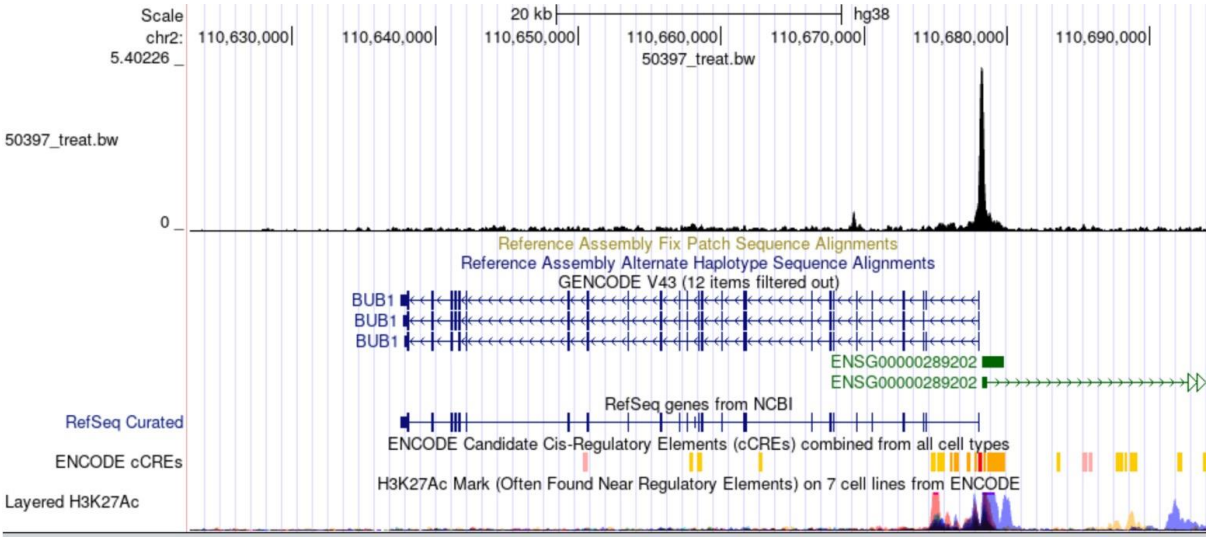

Figure 4. 7 | MYB binding peaks in the *BUB1* promoter. Cistrome DB analysis showing MYB binds the *BUB1* promoter around position 110 680 000. The MYB peak overlaps with H3K27 acetylation marks, indicating a transcriptionally active region.

To assess whether MYB could directly transactivate *BUB1* in gland cells, MCF10A cells were co-transfected with the wild type *BUB1* promoter region cloned in the pGL3 Firefly basic vector

(pGL3-BUB1 WT), and a pLXSN vector expressing MYB (pLXSN-MYB) (Sala *et al*., 1995), as described in the materials and methods section (**2.4 Luciferase assay**). Cells were also co-transfected with a plasmid encoding pRenilla luciferase to control for transfection efficiency. 36h after transfections, cells were lysed, and luminescence activity was quantified. There was a fourfold increase in luciferase activity in the presence of the pLXSN-MYB vector, compared to the empty vector control (pLXSN-EV) (**Figure 4. 8**) suggesting that the *BUB1* promoter was transactivated by MYB. To demonstrate that the effect was caused by direct interaction of MYB with the *BUB1* promoter, we used a *BUB1* promoter reporter plasmid (pGL3-BUB1 Mut) in which all the canonical MBSs were mutated, as described in the methods (**2.4 Luciferase assay**). As expected, mutation of the MYB-binding sites completely abolished MYB transactivation, confirming the specificity of the interaction (**Figure 4. 8**).

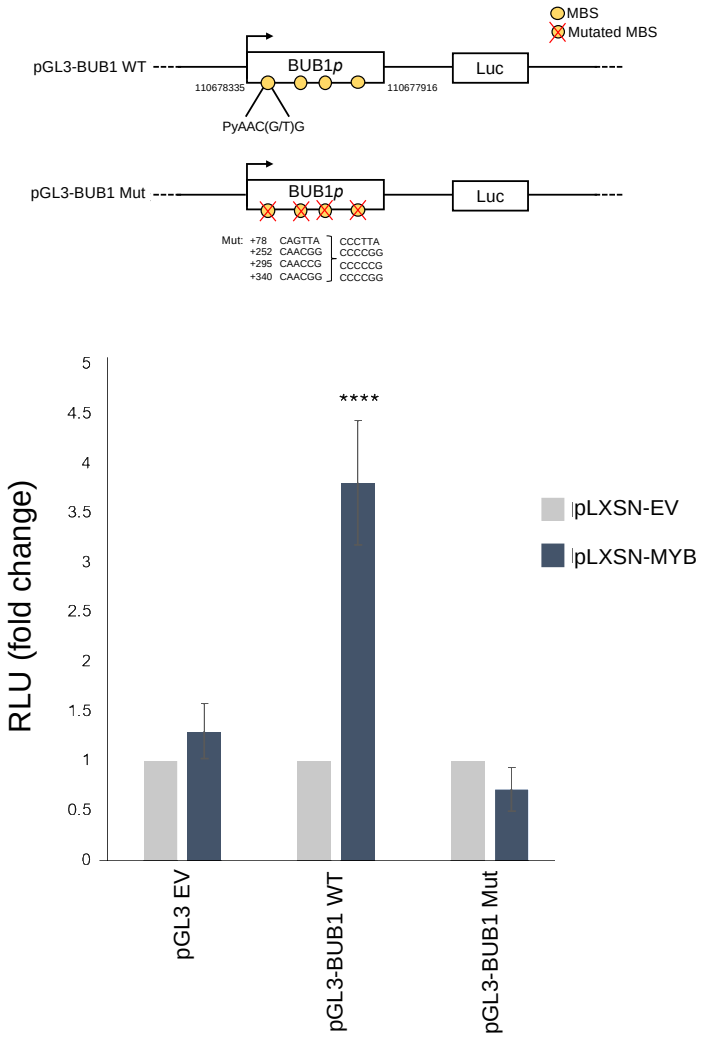

Figure 4. 8 | Dual-luciferase assay on MCF10A cells. MCF10A cells were co-transfected with luciferase reporter plasmids containing the *BUB1* promoter in the wild-type (pGL3-BUB1 WT) or MBSs-mutant (pGL3-BUB1 Mut) conformation and *MYB*-expression vector (pLXSN-MYB) or control vector (pLXSN-EV). pGL3 empty vector (pGL3 EV) was used as further control. A schematic representation of the constructs, the putative MBSs and the mutations introduced are shown on the top of the panel. RLU, relative light unit.

4.2.4 ChIP-seq analysis demonstrates that MYB directly binds the *BUB1* promoter in ACC cells *in vivo*

To investigate whether endogenous MYB binds the *BUB1* gene in ACC cells, we examined genome-wide MYB occupancy patterns in ACCX11 cells using ChIP-seq. Peaks were called with a p value cut-off of < 0.01 by using the Model-based Analysis of ChIP-Seq data (MACS) (Zhang, Yong *et al*., 2008). We identified the presence of peaks in the *BUB1* promoter region, located at – 0.84 Kb and – 0.177 Kb from the transcription start site (TSS) of the gene **Figure 4. 9**), similarly to what was observed from data in Cistrome DB for leukaemia cells (**Figure 4. 7**). Interestingly, we found other peaks that overlapped two enhancers in intragenic position (located at 110.662.587- 110.662.901 and 110.659.601- 110.659.800) (**Figure 4. 9**). The analysis on the three replicates can be found in **Supplementary Figure 2**. Locations of promoters and enhancers regulatory regions of *BUB1* are depicted in **Supplementary Figure 3**.

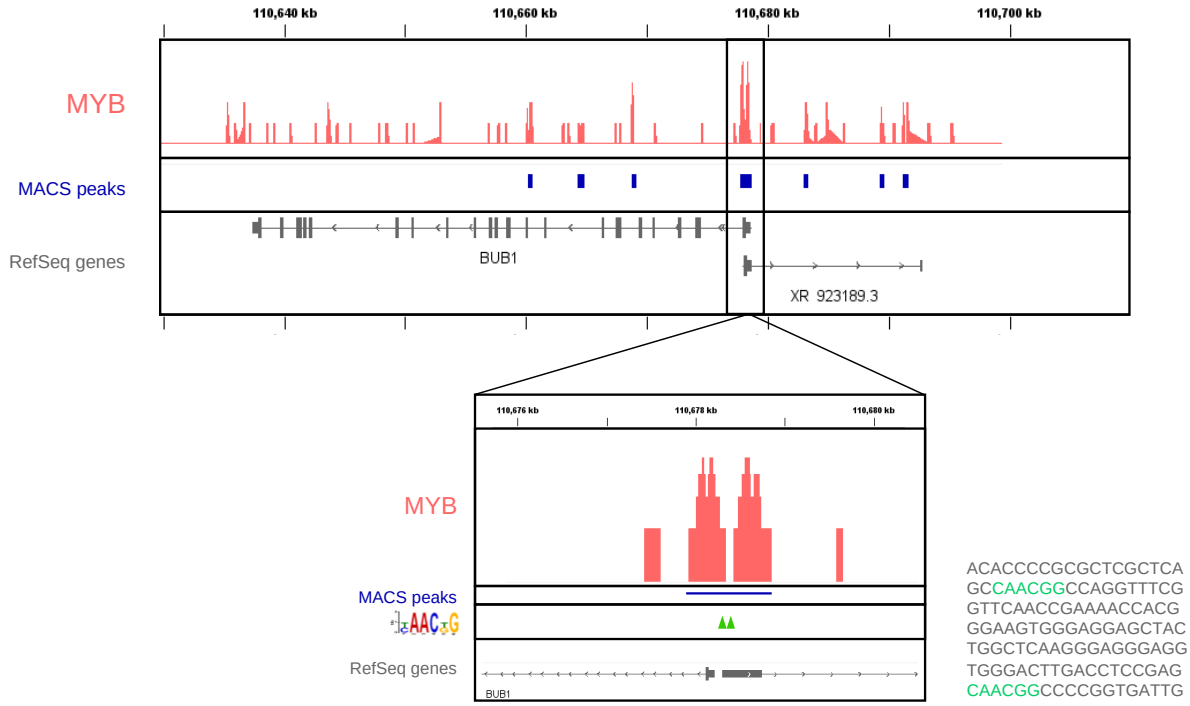

Figure 4. 9 | MYB binds *BUB1* promoter in ACCX11 cells *in vivo*. ChIP-seq analysis showing the localisation of MYB peaks (depicted in red) according to the reference sequence of the gene (RefSeq genes). The blue boxes under each peak indicate regions significantly enriched by the MYB binding as defined by the peak caller output of $p < 0.01$, analysed with MACS algorithm. MYB-binding peaks around the transcription start site (TSS) of *BUB1* are highlighted in the zoomed box. The green arrows indicate the position of MYB canonical binding site in the sequence. Portion of the gene sequence is shown on the right of the box and the canonical MBSs are highlighted in green.

4.3 Discussion

MYB plays an important role in the control of cell proliferation, apoptosis, and differentiation, and is highly expressed in immature proliferating cells, while its expression decreases as differentiation progresses (Kastan *et al*., 1989; Oh & Reddy, 1999; Ramsay, Robert G. & Gonda, 2008). *MYB* dysregulation has been reported in different cancers, including AML, non-Hodgkin lymphoma, CRC, and breast cancer (Li, Y. *et al*., 2016; Okada, M. *et al*., 1990; Thompson *et al*., 1997; Torelli *et al*., 1987). In addition to its physiological role in the haematopoietic system (Westin *et al*., 1982), *MYB* has also been shown to be expressed in mouse submandibular glands at embryonic day E14.5 (Visel *et al*., 2004), suggesting an involvement of *MYB* in salivary gland development.

Due to the potential role of *MYB* in the promotion of several human malignancies, MYB has been targeted with different molecules in preclinical cancer studies (Cicirò & Sala, 2021). Although direct targeting of key oncogenes is a logical approach, drugging transcription factors is notoriously difficult (Bushweller, 2019). This mainly stems from challenges associated with disorderly structures, lack of binding pockets and in difficulties in targeting the protein–DNA or protein–protein interfaces, (Arkin *et al*., 2014). Moreover, inhibition of tissue specific transcription factors such as MYB could block critical signalling pathways, generating severe side effects, potentially incompatible with life (Ramsay, Robert G. & Gonda, 2008).

ACC research has been seriously hampered by a limited knowledge of the biology and transcriptional landscape of ACC, the mechanisms leading to carcinogenesis and progression, as well as lack of relevant *in vitro* and *in vivo* models to test new therapeutic approaches (Persson *et al*., 2012). To gain insights into the molecular consequences of constitutive, high-

level expression of *MYB*, different groups have identified MYB target genes using high-throughput methodologies, such as chip-on-chip, microarray, and RNA-sequencing. For example, Andersson and colleagues performed microarray analysis on MCF10A cells transduced with retroviruses encoding *MYB* or *MYB-NFIB* fusion (Andersson *et al*., 2020). In this study, the MYB-activated genes showed significant overlap with previously published gene expression profiles of ACC samples (Andersson *et al*., 2017; Andersson *et al*., 2020). Biological pathways associated with the overexpressed genes included key players of the cell cycle, such as cyclins, centromere proteins, and checkpoint kinases, such as ATR and BUB1 (Andersson *et al*., 2020). Due to the importance of BUB1 as mitotic checkpoint, the interest in its role in cancer is increasing (Jiang, N. *et al*., 2021; Li, M. *et al*., 2022; Li, X. *et al*., 2020).

We detected immunoreactivity of BUB1 in the nucleus and/or cytoplasm of several ACC cell lines (**Figure 4. 6**). This finding contrasted with the knowledge of BUB1 as protein involved in cell cycle, and therefore its intracellular localization is postulated to be the nucleus. However, a number of studies have reported cytoplasmic immunolocalisation of other mitotic checkpoint kinases in cancer cells, such as BUB1B in breast and colon carcinomas, MAD2 in colon and gastric cancers (Li, G. & Zhang, 2004; Shin *et al*., 2003; Tanaka *et al*., 2001; Yuan *et al*., 2006). Although little is known about the association between BUB1 localisation and its function in malignant cells, distinct roles of aberrant BUB1 has been revealed, including its involvement in CIN, and the ability to negatively regulate p53-mediated early cell death (Gao, F. *et al*., 2009; Warren *et al*., 2002; Williams, G. L. *et al*., 2007). Hence, BUB1 may be implicated in other biological functions in addition to the mitotic checkpoint and may have important roles in proliferation and maintenance of cancers, suggesting the need of further investigation.

In this chapter, we studied the relationship between *MYB* and *BUB1*. Analyses of ACC gene expression datasets confirmed co-expression of *MYB* and *BUB1* in tumour samples, suggesting that *BUB1* expression may be controlled by *MYB* in this cancer. To assess whether MYB regulates *BUB1*, we performed a siRNA-mediated knockdown of *MYB* in an ACC cell

line. This caused a significant decrease in *BUB1* expression, validating the hypothesis that *BUB1* is downstream of *MYB*. Moreover, luciferase reporter assays confirmed that MYB binds to and activates the *BUB1* promoter when ectopically expressed in MCF10A cells. Data from Cistrome DB, a collection of ChIP sequencing and chromatin accessibility studies, indicates that MYB can bind to the *BUB1* promoter *in vivo* in leukaemia cells (Mansour *et al*., 2014). We confirmed these results also in our cultured ACC cells. Genome-wide maps of MYB chromatin occupancy in ACCX11 cells were generated using ChIP-seq and *BUB1* emerged as a direct MYB target. The main peaks were located in proximity of the TSS of *BUB1*, in agreement with the general knowledge of TFs preference to bind upstream regulatory elements of genes in the proximal promoter and modulate their expression (Vinson *et al*., 2011). Markedly, intragenic portions of *BUB1* were enriched in MYB motifs and called peaks overlapped them. A more accurate analysis uncovered that these portions corresponded to enhancer regions, close to loci of open chromatin, suggesting a possible regulation by MYB that may or may not cooperate with the MYB-mediated transactivation (**Figure 4. 9**).

Thorough investigation of the ChIP-seq data was beyond the scope of this project, therefore we limited the inspection to the main MYB target genes, such as *BCL2*, *CDC2l*, *KIT*, *CD34*, to further confirm the trustworthiness of this analysis and compared it to the results of Drier and colleagues (2016) (Drier *et al*., 2016).

In summary, given the difficulties in drugging MYB, the identification of the BUB1 kinase downstream of MYB might lead to the development of more effective therapeutic options for patients. Indeed, kinases are more amenable to pharmacological targeting than transcription factors, due to a stable structure and the presence of molecular pockets that can be used to develop small molecule inhibitors.

Chapter V

Inhibiting BUB1 activity with the small molecule inhibitor BAY1816032

5.1 Introduction

Due to their crucial role in cell signalling, kinases have emerged as potential therapeutic targets in pharmacology research (Wu *et al*., 2015). Kinases mediate a broad range of cellular processes such as apoptosis, differentiation, and proliferation (Adams, 2001). More than 530 human kinases have been identified and they are the second most targeted group in clinical therapies, following the G-protein-coupled receptor (Bhullar *et al*., 2018). This is mainly due to the degree of similarity that kinases share in their 3D structures, giving the possibility to design kinase inhibitors that perturb the ATP-binding site of the proteins (Knighton *et al*., 1991; Wu *et al*., 2015). So far, there are 72 FDA-approved therapeutic agents that target about two dozen different protein kinases (Roskoski Jr, 2022). Deregulation of kinases leads to a variety of pathophysiological changes that may culminate in cancer cell proliferation and tumour progression (Bhullar *et al*., 2018).

Pioneering studies on the role of kinases in pathological conditions have revealed that targeting these proteins is also promising in cancer (Huang, Min *et al*., 2014; Ma & Adjei, 2009; Sun & Bernards, 2014). In particular, kinases involved in the mitotic spindle checkpoint have been proposed to be excellent cancer therapeutic targets (Kaestner *et al*., 2011). The mitotic kinase BUB1 has been associated with the development of solid cancers, including papillary renal cell carcinoma, gastric cancer, osteosarcoma, and pancreatic ductal adenocarcinoma (Gao, Z., Zhang, Duan, Yan, Fan, Fang, & Liu, 2019; Piao *et al*., 2019; Shigeishi *et al*., 2001). BUB1 is part of the BUB and mitotic arrest-deficient (MAD) families of proteins that play a crucial role in the organisation of the spindle checkpoint, preserving correct ploidy during mitosis (Bernard *et al*., 1998).

Targeting BUB1 has been shown to be a promising strategy in osteosarcoma patients, where inhibition of the kinase markedly suppressed cell proliferation, migration, invasion, and induced apoptosis. It has been reported that *BUB1* promotes bladder cancer by phosphorylating STAT3, activating a JAK/STAT-mediated cascade, and leading to cancer proliferation and progression (Grivennikov *et al*., 2009). Pharmacological targeting of BUB1 in bladder cancer cells suppressed tumour progression *in vivo* (Jiang, N. *et al*., 2021). Dysregulation of *BUB1* was also observed in paediatric glioblastoma (Morales *et al*., 2013). Combinatorial treatment with temozolomide (TMZ, a standard chemotherapeutic drug used in glioblastoma treatment) and siRNAs against *BUB1* and its partner in mitotic checkpoint spindle assembly *BUBR1*, reduced proliferation and colony formation of glioblastoma cells with increased formation of micronuclei, accompanied by cell cycle arrest and apoptosis (Morales *et al*., 2013). Dysregulation of the cell cycle is one of the hallmarks of cancer (Hanahan & Weinberg, 2000), making cell cycle arrest a primary mechanism of action of chemotherapeutic drugs, such as taxanes and alkaloids. On the other hand, inactivation of cell cycle checkpoints leads tumour cells to proceed into cell division, causing lethal accumulation of DNA damage and aneuploidy. Thus, targeting cell cycle checkpoints is emerging as a successful strategy in cancer treatment (Dominguez-Brauer *et al*., 2015; Siemeister *et al*., 2019).

Following the analysis of the relationship between MYB and BUB1 in **Chapter IV**, in this chapter we investigate whether inhibition of BUB1 could be a promising therapeutic strategy for MYB-dependent cancers, such as ACC.

5.2 Results

ACCX11 cells were provided by Professor Göran Stenman, Sahlgrenska Cancer Center (University of Gothenburg, Sweden), in collaboration with the Adenoid Cystic Carcinoma Research Foundation (ACCRF, MA, USA), and XenoSTART (S. Antonio, Texas, USA). Three-dimensional (3D) ACC spheroids and *in vivo* experiments were performed by the Adenoid Cystic Carcinoma Research Foundation (ACCRF, MA, USA) in collaboration with the biotech companies Kiyatec (Greeneville, SC) and XenoSTART (S. Antonio, Texas, USA).

5.2.1 Pharmacological inhibition of BUB1 in ACC cell models

To evaluate the impact of BUB1 inhibition in *MYB*-related cancers, we treated MM MYB cells, MCF10A cells containing an inducible *MYB* transgene discussed in the previous chapter (**Chapter IV**), with BAY1816032, a selective inhibitor of the catalytic activity of the kinase BUB1 (Siemeister *et al*., 2017). In the presence of the inducer DOX, escalating concentrations of the drug caused loss of viability, with an IC_{50} of 4.0 μM, whereas in the absence of doxycycline-induced *MYB* the drug had almost no effect (**Figure 5. 1 A**). To rule out non-specific interactions between DOX and the BAY inhibitor, we repeated the dose response experiment with MCF10A cells transduced with the empty control virus (MM EV). As expected, no significant reduction in cell viability was detected in the presence of increasing concentrations of BAY1816032, with or without DOX treatment, demonstrating that the effect of the small molecule inhibitor is genuinely *MYB*-dependent, (**Figure 5. 1 B**).

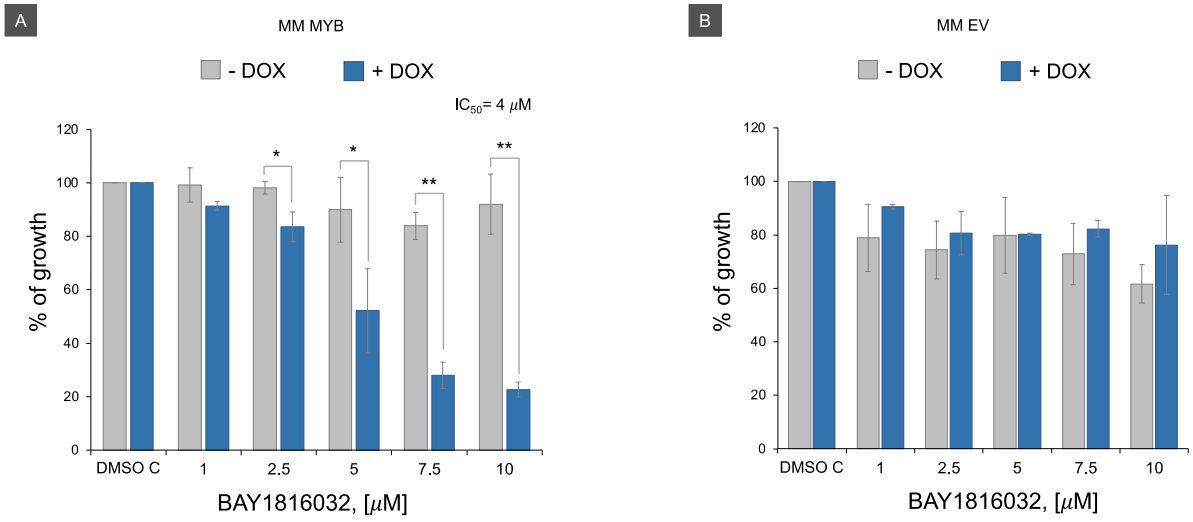

Figure 5. 1 | Drugging BUB1 causes inhibition of MCF10A cells in a *MYB*-dependent manner. (**A**) Induced (+DOX) or non-induced (-DOX) MM MYB cells were cultured in the presence of different concentrations of the BUB1 inhibitor BAY1816032. Cells were harvested 72 h after plating and percentages of cell growth compared to the vehicle (DMSO) control were calculated implementing the MTT assay. (**B**) The experiment was repeated as in (**A**), except that the cells used were the empty vector infected MCF10A (MM EV). Error bars indicate standard errors. p value ≤ 0.05 (*), 0.001(**); ns, not significant.

To validate BUB1 inhibition as a therapeutic strategy in ACC, we treated PDX-derived ACCX11 cells with BAY1816032 for 72 h. Pharmacological inhibition of BUB1 led to decreased cell viability in a dose-dependent fashion, with an IC_{50} of 2.95 μM. Interestingly, the treatment had no significant effect on naïve MCF10A, used as a glandular *MYB*-negative control cell line (**Figure 5. 2**). To assess whether the kinase inhibitor was inducing tumour cell apoptosis, we performed a caspase activation assay. ACCX11 cells were treated with increasing concentration of BAY1816032 for 48 h after which they were harvested, and the caspase activity was quantified. A concentration of the drug of 2 µM was sufficient to produce a significant increase of luminogenic Caspase 3/7 substrate signal, supporting the hypothesis that the BAY inhibitor induces programmed cell death in ACCX11 cells (**Figure 5. 3**).

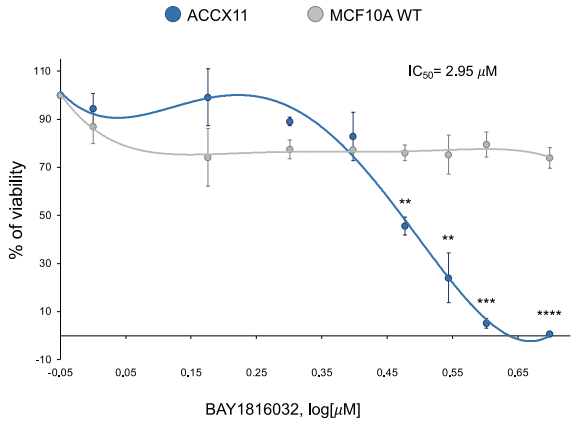

Figure 5. 2 | ACCX11 cells viability in the presence of BAY1816032. Cells were exposed to escalating concentrations of BAY1816032. MCF10A cells (grey line) were used as normal cell control. Error bars indicate standard errors. p value ≤ 0.001 (**), 0.00001 (****).

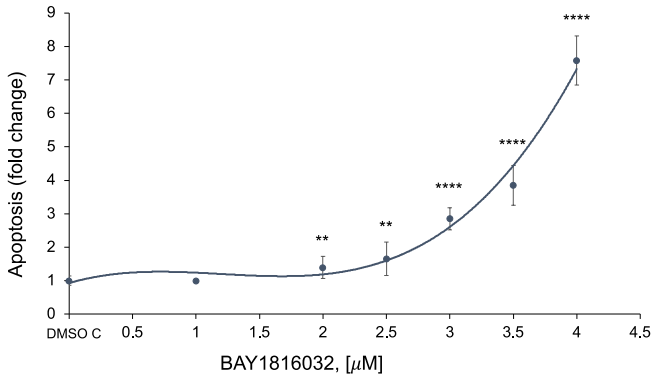

Figure 5. 3 | Inhibition of BUB1 induces ACC cells apoptosis. ACCX11 cells were treated with BAY18169032 and 48 h later caspase 3/7 activity was quantified by luminescence. DMSO was used as negative control. Errors bars indicate standard errors. p value ≤ 0.001 (**), 0.00001 (****).

Changes in cell viability were also assessed in multicellular tumour spheroid (MCTS). 3D models of ACCX11 cells were established by the Adenoid Cystic Carcinoma Research Foundation (ACCRF, MA, USA) in collaboration with Kiyatec (Greeneville, SC) and were used

to assess the effects of BAY1816032. After 96 h of incubation with the drug, the viability of 3D spheroids was quantified. Consistent with the results obtained with 2D cultures (**Figure 5. 2**), the viability of ACCX11 spheroids decreased as the drug concentration increased, with a calculated IC_{50} of 1.24 µM (**Figure 5. 4**). Data was normalised on DMSO vehicle control. Overall, BUB1 inhibitions caused strong reduction in cell viability in both 2D and 3D cultured cells. Treatment with high doses of BAY1816032 disrupted the spherical shape of the cultures, compared to the 3D structure of the cells treated with a low dose of BAY1816032 (**Figure 5. 5**).

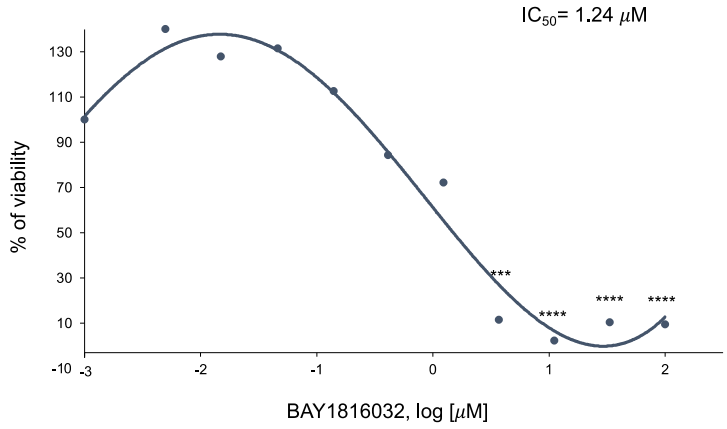

Figure 5. 4 | Viability assay in 3D spheroid cultured ACCX11. Analysis of Cell-Titer Glo assay in ACCX11 cells cultured as 3D multicellular tumour spheroid (MCTS) after treatment with increasing doses of BAY1816032. p value ≤ 0.00001 (****). This experiment was performed by the Adenoid Cystic Carcinoma Research Foundation (ACCRF, MA, USA), and XenoSTART (S. Antonio, Texas, USA) in collaboration with Kiyatec company (Greeneville, SC).

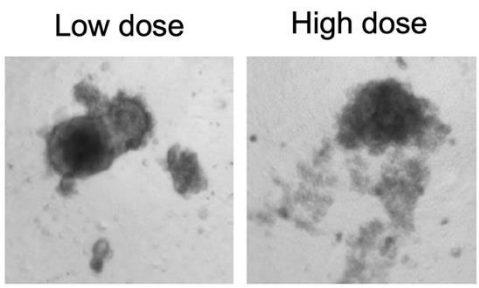

Figure 5. 5 | Morphology of ACCX11 spheroids in the presence of different concentrations of BAY1816032after 10-day culturing. Both images refer to spheroids after treatment with a low dose (<10 μM, left) and high dose (>10 μM, right) of the BAY16018232 compound after been cultured for 10 days. The inhibition of BUB1 causes the disruption of the 3D spherical structure indicating a strong effect on the morphology of glandular structures. This experiment was performed by the Adenoid Cystic Carcinoma Research Foundation (ACCRF, MA, USA), and XenoSTART (S. Antonio, Texas, USA) in collaboration with Kiyatec company (Greeneville, SC).

5.2.2 Effect of BAY1816032 *in vivo*

We used BAY1816032 in an ACC PDX mouse model to evaluate its efficacy *in vivo*. ACCX11 tumour specimens were implanted into the flanks of NSG immunodeficient mice and let grow until palpable. Mice were then randomised into drug (20mg/kg of BAY1816032) and control groups, which were monitored until tumours had reached the predetermined study endpoint volume-wise. The study was conducted by XenoSTART. At the end of the experiment, mice receiving the BAY1816032 treatment did not show benefit in comparison with the control group. The drug was safe, since no weight changes were detected in BAY1816032 treated mice compared to the control group. Data regarding the experiment cannot be disclosed at this stage due to confidentiality policy.

5.3 Discussion

BUB1 is important for correct chromosome segregation and genomic stability. It exerts this function by coordinating centromere recruitment of shugoshin proteins (SGO1 and SGO2), which are essential for the protection of centromeric cohesin from premature degradation. It also aids in the localisation of the chromosome passenger complex (CPC), consisting of inner centromere protein (INCENP), survivin, borealin, and Aurora kinase B (AURKB), to the centromeres (Kawashima *et al*., 2010; Wang, Fangwei *et al*., 2011). Thus, inhibition of BUB1 impairs the resolution of microtubule–kinetochore attachment errors, resulting in an unsustainable degree of chromosome alignment defects (Siemeister *et al*., 2019). Increased expression of BUB1 has been associated with several cancers, where it promotes a pro-tumourigenic phenotype (Gao, Z. *et al*., 2019; Piao *et al*., 2019; Shigeishi *et al*., 2001).
Previous studies have indicated that small molecule inhibitors of BUB1, such as BAY320 or BAY524, can inhibit the kinase catalytic activity in biological settings (Baron *et al*., 2016; Faesen *et al*., 2017). However, these drugs showed limited pharmacokinetic properties making them unsuitable for *in vivo* investigations (Baron *et al*., 2016; Faesen *et al*., 2017). On the other hand, Siemeister and colleagues (2017) were able to develop a new inhibitor, called BAY1816032, orally available, relatively non-toxic and with favourable pharmacokinetic characteristics (Siemeister *et al*., 2017).

Having established that BUB1 is a kinase activated downstream of MYB in the previous chapter, we wanted to investigate whether inhibiting BUB1 could have an impact against cancer cells with high levels of MYB. Pharmacological blockade of BUB1 caused an inhibition of cell growth in MM MYB +DOX cells, but not in MM MYB -DOX cells, suggesting that

hyperactivation of the *MYB* oncogene sensitises cells to the BUB1 inhibitor. We conclude that, in principle, BAY1816032 could be used for therapy of *MYB*-dependent cancers, such as ACC. Dose-response assays with the BAY inhibitor showed reduced viability and increased apoptosis of ACCX11 cells (both in 2D or 3D systems), suggesting a potential for clinical application in this rare cancer. Although BAY1816032 worked *in vitro*, it did not show any significant benefit in an ACC model *in vivo*. Previous *in vivo* studies, in which the BAY inhibitor was used for the treatment of other solid malignancies, displayed similar results, suggesting that BAY1816032 might not be effective in cancer models when used as a single drug (Siemeister *et al*., 2019). Notably, nude mice injected with triple negative breast cancer cells SUM-149 showed significant tumour growth reduction when treated with BAY1816032 in combination with paclitaxel. Similarly, single agent treatment with BAY1816032 or the PARP inhibitor olaparib showed little or no efficacy against the triple negative cancer cell line MDA-MB-436, whereas the combinatorial treatment significantly slowed tumour growth (Siemeister *et al*., 2019). Therefore, inhibition of BUB1 *per se* might not be sufficient to trigger a considerable antitumour response but can prompt antiproliferative effects in a synergistic or additive way when combined with other small molecule inhibitors or chemotherapeutic drugs.

Chapter VI

General discussion

6.1 ACC complexity and the unmet need of models

ACC is a rare malignancy of glandular origin characterised by a slow but relentlessly progressive course, often accompanied by resistance to therapy and ultimately death (Frierson & Moskaluk, 2013). Development of more effective targeted therapies can benefit from a better knowledge of the molecular and genetic alterations that are unique to the neoplasm (Al-Lazikani *et al*., 2012; Ledford, 2016). However, the lack of reliable ACC models has hindered the understanding of the biology of the disease.

The main molecular feature of ACC is the upregulation of *MYB*, often accompanied by the presence of the t(6;9) translocation and the production of the fusion transcript *MYB-NFIB* in around half of the cases (Persson *et al*., 2009). In fact, almost the totality of ACC cases shows upregulation of *MYB* regardless of the fusion status, suggesting that *MYB* may have a stronger role in pathogenesis than *NFIB*, of which the effective involvement in cancer development and progression has not been fully elucidated yet.

In this Thesis, three aspects of ACC were addressed: (1) the generation of an *in vitro* model to capture the role of *MYB*, (2) the validation of *BUB1* as a target of *MYB*, (3) the potential use of BUB1 inhibition as a therapeutic strategy.

To address our first aim and investigate the role of *MYB*, we engineered the human epithelial breast glandular cell line MCF10A with a lentiviral vector carrying a *MYB* inducible system under the control of the antibiotic doxycycline (DOX) (MM MYB ±DOX). The switchable system allowed us to perform functional experiment and provide new insight in the transcriptional activation of *MYB* in glandular tissue.

ACC tumour complexity is emphasised by its biphasic feature, implying co-proliferation of epithelial and mesenchymal elements (Xu *et al*., 2017).

Choosing the optimal cell line as tumour model depends on a variety of factors, including specific genomic and morphological characteristics, as well as practical issues such as cellular growth and culturing conditions. We reasoned that the widely used immortalised yet non-tumourigenic mammary glandular epithelial cell line MCF10A, came to the aid of our purpose, thanks to its glandular composition and absent expression of *MYB* in parental cells that may serve as negative reference (Andersson *et al*., 2020; Imbalzano *et al*., 2009).
However, despite MCF10A being a good cell line to exploit in this context, the non-transformed nature of MCF10A cells makes them incapable of forming xenografts in immunocompromised mice, setting the limitation of working on this model only for *in vitro* studies (Dawson *et al*., 1996; Lourenco *et al*., 2019).

Importantly, the MM MYB model reflected clinical features of ACC tumours. We performed a comprehensive comparison of differentially expressed genes between MM cells with or without *MYB* overexpression in order to establish the biological relevance of the "MYB-ON" system through Gene Ontology (GO) analysis. Cell cycle, DNA replication, chromosome segregation, and DNA repair pathways were the top activated biological processes. Activation of cell cycle and DNA replication-related events suggests an increased potential for proliferation, in accordance with what was observed in the MCF10A retroviral system engineered to overexpress *MYB* in our laboratory (Andersson *et al*., 2020). Interestingly, top activated pathways in +DOX condition were comparable with the ones observed in ACCX11 cells (**Figure 3. 7** and **Figure 3. 10**). However, although RNA-seq allows dissection of gene expression at high resolution, we performed the analysis on the only cell line available for this PhD study. Hence, to interrogate the transcriptional significance of MM MYB +DOX cells, we compared these cells to every ACC microarray dataset derived from public domain resources, revealing similarities to the ones already discussed. Therefore, the transcriptional identity of our MM MYB cells overexpressing *MYB* (MM MYB +DOX) was akin to the ones extrapolated from the datasets and from the RNA-seq, strengthening the reliability of the engineered *in vitro* model for future works.

Previous research has established that *MYB* expression alone is sufficient for increasing proliferative activity of human epithelial glandular cells (Andersson *et al*., 2020), suggesting that ACC transformation might solely depend on *MYB* activation. Nevertheless, due to the immortalised nature of the MCF10A line, it was not possible for us to determine the true transformative capacity of *MYB* alone in the MM MYB model. The tumour mutation burden (TMB) of ACC is lower than the most common types of solid tumours, and this low-rate matches ACC indolent clinical behaviour, but raises questions on other additional mutations essential for ACC pathogenesis (Frierson & Moskaluk, 2013; Ho, Allen S. *et al*., 2013; Stephens *et al*., 2013; Stransky *et al*., 2011). Two independent studies have previously addressed the need of recurrent mutations in ACC through exome sequencing; however, no candidates that might cooperate with activated MYB protein were identified (Ho, Allen S. *et al*., 2013; Stephens *et al*., 2013), raising the question of whether mutations in regulatory regions or non-coding RNAs could play an additive role. Molecularly, overexpression of the oncogene *MYB* is the main alteration of ACC; however, a fraction of ACCs with physiological expression of *MYB* has been reported, suggesting that there is a possibility of secondary events supporting the tumourigenesis of human glands (Brill *et al*., 2011; Park, Susan *et al*., 2020). Based on these results, ACC might fall in the category of cancers characterised by “oncogene addiction”, as they show dependency on a master oncoprotein to maintain the malignant phenotype. Weinstein and Joe (2006) proposed the oncogene addiction phenomenon as a consequence of the multistage carcinogenic process, reasoning that the protein encoded by these oncogenes have a variety of roles in regulatory networks (Weinstein & Joe, 2006; Weinstein & Joe, 2008). Future studies using the MM MYB model could explore the contribution of candidate mutations based on patient studies to determine whether the cooperative action with MYB could affect the phenotype.

One of the challenges associated with the strenuous efforts to develop ACC models is the scarcity of ACC patients. To further complicate the development of stable ACC cell lines, it has been shown that cultured cells are incapable of preserving ACC histological and (cyto)genetic

characteristics after prolonged passages *in vitro* (Jiang, Y. *et al*., 2019). PDXs have been reported reassuring results in cellular maintenance, however, *in vivo* growth of tumour cells is time-consuming, expensive, and tumour engraftment capacity is not always fulfilled (Cho *et al*., 2016).

Unfortunately, the MM MYB +DOX system failed to retain *MYB* expression after several passages, which is also a feature observed in ACCX11 cells and experienced by other research groups working with primary ACC cells (**Supplementary Figure 1**) (Li, J. *et al*., 2014; Queimado *et al*., 1999). The reasons behind the loss of expression are not elucidated yet, forcing short-term *in vitro* studies on ACC and exposing researchers to the need to constantly repeat the *in vitro-in vivo* cycles also dramatically increase the time-requirement, and the risk of straying from the original characteristics of the patients' cells' morphology and/or molecular profile. However, MM MYB +DOX provided a novel reliable and cut-price alternative, easy to reproduce, rendering the development an ACC-like profile more accessible.

6.2 Systemic therapies and new approaches: is BUB1 a valid target in ACC?

There is currently no chemotherapy recognised to be effective in the treatment of patients with ACC. Several drugs have been investigated for the treatment of ACC, including 5-FU, gemcitabine, epirubicin, vinorelbine, cisplatin, and paclitaxel (Airoldi *et al*., 2001; Dick Haan *et al*., 1992; Gilbert *et al*., 2006; Tannock & Sutherland, 1980; Van Herpen *et al*., 2008; Vermorken *et al*., 1993). Due to the rarity of the cancer, the number of patients involved in the trials has been scarce, rendering the interpretation of the efficacy of the different compounds unreliable. However, although limited, results from clinical studies still advocate the possibility of using a specific translational therapy on ACC (**Table 1. 3**).

Of note, phase II clinical trials involving gemcitabine, paclitaxel, or vinorelbine as single agents displayed minimum or no objective response in patients (0/21, 0/14, and 2/13, respectively) (Airoldi *et al*., 2001; Gilbert *et al*., 2006; Van Herpen *et al*., 2008), corroborating the lack of efficacy of these drugs that we observed in ACCX11 cells *in vitro* (**Supplementary Figure 4**).

Identification of *MYB* molecular aberration in tumours and the profound dependency of ACC cells on MYB has been a major breakthrough in ACC research. Although it is reasonable to think that *MYB* is the Achilles heel of this cancer and therapies against MYB may restore its physiological activity and re-establish a non-neoplastic condition, MYB has been traditionally considered impossible to target pharmacologically (Bushweller, 2019). Despite the broad therapeutic promise of modulators of DNA-binding transcription factors (Bushweller, 2019; Lambert *et al*., 2018), including MYB (Uttarkar *et al*., 2015; Uttarkar *et al*., 2016; Uttarkar *et al*., 2017; Walf-Vorderwülbecke *et al*., 2018; Yusenko *et al*., 2020), there are major roadblocks associated to the potential imbalanced activity consequent to the inhibition of such master

regulators involved in human homeostasis (Kim, Daniel Jong-Woong, 2021). To avoid potential lethal effect of targeting MYB, investigating new potential *MYB*-related genes is essential. To this aim, we focused our attention on the kinase BUB1, previously uncovered by microarray analysis as one of the MYB-associated effectors in the MCF10A cells overexpressing *MYB and MYB-NFIB* (Andersson *et al*., 2020).

To our knowledge, this is the first study revealing a direct axis linking *MYB* and *BUB1* and demonstrating that the kinase could be used as a therapeutic target in the context of ACC. We showed that ectopic expression of MYB directly transactivated *BUB1* by binding its promoter region, similarly to what recently obtained by Cheng and colleagues (2022) in prostate cancer (Chen, L. *et al*., 2022).

To establish the biological importance of BUB1 in glandular cells, we treated cells with BAY1816032, a selective inhibitor of the kinetic activity of BUB1. While *in vitro* model displayed sensitivity to the treatment, tumour-bearing mice models did not affect the tumour proliferative capacity. We experienced the weakness of the *in vitro* systems and how *in vivo* experiments may lead to different observations and results, due to the complexity of an entire living organism (Graudejus *et al*., 2018). Because of the favourable pharmacokinetic profile and tolerability of BAY1816032, this compound is prone to be combined with other compounds for both *in vitro* and *in vivo* investigations. To this regard, it has been shown that the same compound used as single agent in murine models harbouring breast cancer cells did not exhibit any antiproliferative effect; however, combination of BAY1816032 with paclitaxel or olaparib significantly affected tumour volume growth (Siemeister *et al*., 2019). Interestingly, paclitaxel or olaparib alone were ineffective against cancer cells proliferation, strengthening the idea of the need for a combinatorial treatment to reduce and delay tumour outgrowth (Siemeister *et al*., 2019). Notably, the combination of BAY1816032 with cisplatin, irinotecan, 5-FU, or gemcitabine was antagonistic, revealing a heterogeneous spectrum of effectiveness (Siemeister *et al*., 2019). By exploring the public clinicogenomic cancer dataset The Cancer Genome Atlas (TCGA) at pan-cancer level, we observed that *BUB1* expression influences the

efficacy of standard therapeutic drugs in different tumour types (**Supplementary Figure 5**); therefore, expression of *BUB1* may be used as a biomarker to predict efficacy of commonly used chemotherapeutic drugs.

From the TCGA dataset, we also discovered a significant increase of *BUB1* expression in many solid cancers, relative to normal tissue controls (**Supplementary Figure 6 A-B**), suggesting that *BUB1* may have a growth promoting role in a vast array of malignancies. Interestingly, most of the cancers analysed showed significant correlation between *BUB1* and *MYB* levels (**Supplementary Figure 7**), suggesting that transcriptional activation of *BUB1* operated by MYB could be occurring not only in ACC but also in most human cancers. The new knowledge regarding BUB1 and MYB in different cancers (and in particular in ACC), may provide fertile ground to further analyse the mechanism of action by which *MYB* overexpressing cells are sensitise towards BUB1 inhibitors. Future works may take into consideration the idea of exploiting BUB1 as therapeutic target in combination with standard, approved, chemotherapeutic drugs with the main aim of proving how BUB1 can affect cancer cell response and improve the course of the disease. Additional studies can provide insight on BUB1 role in ACC patients stratification, allowing a better care pathway, with the goal of making them a personalised targeted therapy to ameliorate patient's quality of life.

In conclusion, in this PhD study, we have demonstrated that BUB1 is a *bona fide* MYB target gene in ACC. Since drugging MYB is not currently feasible in the clinical setting, pharmaceutical targeting of MYB-regulated kinases, such as BUB1, hold promise to become an excellent therapeutic strategy for cancer patients.

Supplementary data

Supplementary Table 1 | Partial list of reported MYB-target genes.

GENE	PROTEIN	STUDY
ADA	Adenosine deaminase	(Berge *et al*., 2007; Ess *et al*., 1995)
ATR	Ataxia telangiectasia Rad3-related protein	(Andersson *et al*., 2020)
BCL2	B-cell lymphoma 2	(Peng *et al*., 2007; Salomoni *et al*., 1997)
BIRC5	Survivin	(Zhou *et al*., 2011)
CAR1	Carbonic anhydrase 1	(Ess *et al*., 1995)
CCNB1	Cyclin B1	(Nakata *et al*., 2007; Quintana *et al*., 2011)
CCNE1	Cyclin E1	(Cheasley *et al*., 2015; Nakata *et al*., 2007)
CD4	Cluster of differentiation 4	(Allen III *et al*., 2001)
CDK1/CDC2	Cyclin-dependent kinase 1/Cell division cycle protein 2	(Ku *et al*., 1993)
CDK6	Cyclin-dependent kinase 6	(De Dominici *et al*., 2018)
CXCR4	C-X-C chemokine receptor type 4	(Liu, F. *et al*., 2006)
ELA2	Neutrophil elastase 2	(Lausen *et al*., 2006; Oelgeschläger, Michael *et al*., 1996)

GATA3	GATA-3	(Maurice *et al*., 2007)
IGF1R	Insulin-like growth factor 1 receptor	(Andersson *et al*., 2017; Calvo *et al*., 2017)
KIT	(c-)KIT/ Cluster of differentiation 117	(Hogg *et al*., 1997; Ratajczak *et al*., 1998)
H2AFZ	H2A histone Z	(Hooper *et al*., 2008)
MAT2A	Methionine adenyl-transferase II, alpha	(Yang, H. *et al*., 2001; ZENG *et al*., 2001)
MIM1	Mitochondrial import protein 1	(Dudek, Henryk *et al*., 1992)
MYC	c-Myc	(Berge *et al*., 2007; Cogswell *et al*., 1993; Nakagoshi *et al*., 1992)
PTCRA	Pre-T cell antigen receptor alpha	(Reizis & Leder, 2001)
RAG2	Recombination activating gene 2	(Kishi *et al*., 2002; Wang, Qian-Fei *et al*., 2000)
TAL1	T-cell acute lymphocytic leukaemia protein 1	(Mansour *et al*., 2014)
TCRD	TCR delta chain	(Carabana *et al*., 2005)
VEGF	Vascular endothelial growth factor	(Lutwyche *et al*., 2006)

Supplementary Table 2 | TCGA dataset samples and sites.

ABBREVIATION	CANCER	SITE
A(D)CC	Adrenocortical carcinoma	Adrenal gland
BLCA	Bladder urothelial carcinoma	Bladder
BRCA	Breast invasive carcinoma	Breast
CESC	Cervical squamous cell carcinoma and endocervical adenocarcinoma	Cervix
CHOL	Choloangiocarcinoma	Bile duct
COAD	Colon adenocarcinoma	Colon
DLBC	Lymphoid Neoplasm Diffuse Large B-cell Lymphoma	B-cells
ESCA	Esophageal carcinoma	Esophagus
GBM	Glioblastoma multiforme	Brain
HNSC	Head and neck squamous cell carcinoma	Head and neck
KICH	Kidney chromophobe	Kidney
KIRC	Kidney renal clear cell carcinoma	Kidney
KIRP	Kidney renal papillary cell carcinoma	Kindey
LGG	Lower grade glioma	Brain
LIHC	Liver hepatocellular carcinoma	Liver
LUAD	Lung adenocarcinoma	Liver
LUSC	Lung squamous cell carcinoma	Liver
MESO	Mesothelioma	Mesothelium
OV	Ovarian serous cystadenocarcinoma	Ovary
PAAD	Pancreatic adenocarcinoma	Pancreas

PCPG	Pheochromocytoma and paraganglioma	Adrenal gland
PRAD	Prostate adenocarcinoma	Prostate
READ	Rectum adenocarcinoma	Colon
SARC	Sarcoma	Bones and soft tissue
SKCM	Skin cutaneous melanoma	Skin
STAD	Stomach adenocarcinoma	Stomach
TGCT	Testicular germ cell tumors	Testis
THCA	Thyroid carcinoma	Thyroid
THYM	Thymoma	Thymus
UCEC	Uterine corpus endometrial carcinoma	Uterus
UCS	Uterine carcinosarcoma	Uterus
UVM	Uveal melanoma	Eye

Supplementary Table 3 | Top 100 differentially expressed genes upregulated in MM MYB +DOX compared to MM MYB -DOX. *MYB* is highlighted. P ADJ, p adjusted (False Discovery rate (FDR)). Genes were filtered for FDR ≤ 0.05 and ordinated for decreasing log2 fold change.

GENE	LOG2 FOLD CHANGE	P VALUE	P ADJ	REGULATION	CONFIDENCE
CTAGE11P	6.675642847	5.22E-06	0.002800431	Up	****
ZNF853	6.410443454	0.001432516	0.098129989	Up	***
CCDC106	6.067215545	0.000377394	0.050928571	Up	***
TRIM71	5.996050886	0.020803358	0.371823705	Up	*
MYB	**5.986535181**	**2.86E-23**	**1.19E-19**	**Up**	****
SLC47A1	5.781880685	0.001417644	0.097882132	Up	***
LINC02593	5.529741686	0.007719102	0.237708674	Up	**
ELOVL2	5.129485237	0.03915181	0.481512281	Up	*
MX2	5.073960295	0.000393078	0.051886692	Up	***
CEMIP	5.025941018	1.48E-09	3.52E-06	Up	****
KIF5C	4.73539775	0.000356536	0.049439698	Up	***
HOXC10	4.72867763	0.008683086	0.251280958	Up	**
COLGALT2	4.713896324	0.010951298	0.281972928	Up	**
COL25A1	4.708926104	0.010170097	0.272546991	Up	**
A2M	4.474935233	9.21E-05	0.02129109	Up	****
PLA2G4E	4.292626418	7.87E-06	0.00396987	Up	****
RPP25	3.986368489	6.14E-06	0.003191778	Up	****
CXCL10	3.906721424	0.005641915	0.20735399	Up	**
UNC5C	3.812518999	4.69E-05	0.013693829	Up	****
HPCAL4	3.69355132	0.001384562	0.097591869	Up	***

MOXD1	3.685040822	0.003549423	0.1640622	Up	**
KLF17	3.619690081	0.000261569	0.042257356	Up	***
USP44	3.603019627	0.011440222	0.283703857	Up	**
ADAM22	3.564277915	0.007802307	0.238658816	Up	**
RNF150	3.547264877	2.87E-09	5.40E-06	Up	****
EYA2	3.512991771	0.004650061	0.188730537	Up	**
LAMA4	3.500906437	0.006844364	0.227839164	Up	**
GSDMA	3.483889686	3.79E-25	3.15E-21	Up	****
RSPH10B2	3.409278835	0.002534915	0.134334338	Up	**
UAP1L1	3.364325566	0.029431639	0.426604938	Up	*
PPP1R14A	3.339390922	0.009092813	0.256191988	Up	**
PARVB	3.308504024	0.001306578	0.095097309	Up	***
WNT11	3.272198426	0.01266999	0.296524102	Up	**
LHX6	3.182183968	0.001865032	0.114396946	Up	***
GBP4	3.159097973	0.000486111	0.058442564	Up	***
RARB	3.150180491	0.03517418	0.463052498	Up	*
ALPK2	3.114080461	0.012530814	0.294094151	Up	**
CDK15	3.10107992	8.53E-05	0.020288119	Up	****
DMC1	2.994194557	0.03134051	0.440626128	Up	*
MPO	2.99384431	0.002957881	0.148250418	Up	**
TMEM121	2.962951478	0.000628344	0.066514791	Up	***
ADAMTS17	2.900689224	0.019729045	0.364278641	Up	**
GAREM2	2.823241225	0.008722359	0.251542559	Up	**
ZYG11A	2.817458185	0.047393966	0.520208175	Up	*

PAX6	2.806297107	0.008918558	0.2545537	Up	**
WNT5B	2.790193763	0.000951904	0.083366722	Up	***
ITGA7	2.734841717	0.033892768	0.454367897	Up	*
CHST4	2.71445823	1.82E-05	0.007400665	Up	****
DERL3	2.70868822	0.057887567	0.554458726	Up	*
PELI2	2.700900582	0.054101509	0.541931072	Up	*
BHLHE41	2.684089018	9.58E-05	0.021847095	Up	****
ADAMTS3	2.641856749	0.036047458	0.466793539	Up	*
NR2F1	2.636706432	0.004321824	0.182809044	Up	**
GFI1	2.62588098	0.033924786	0.454367897	Up	*
LINC01085	2.551086547	0.006528446	0.225707042	Up	**
MESP1	2.551002082	0.018594887	0.359789436	Up	**
HOXA11-AS	2.45537599	0.028925518	0.423106088	Up	*
PPM1E	2.443430734	0.020718386	0.371046935	Up	*
SOWAHA	2.441724985	0.030539166	0.435506208	Up	*
SCARF2	2.407888684	0.016621335	0.340776338	Up	**
GPAT3	2.399288399	0.000349612	0.04888691	Up	***
HOXB6	2.394571055	0.027389289	0.413399836	Up	*
HOXC4	2.38625159	0.021418528	0.376486557	Up	*
APBB1	2.372686506	0.003740517	0.169532276	Up	**
IFFO1	2.355662545	0.004257052	0.181380907	Up	**
HOXA11	2.297480342	0.004196634	0.179979367	Up	**
JCAD	2.280166351	0.001890575	0.114396946	Up	***
ARHGEF10	2.249619579	0.013758026	0.311261385	Up	**

NRIP3	2.242579999	0.049377583	0.52804819	Up	*
RFLNB	2.239689698	0.000775979	0.07426947	Up	***
PI4KAP1	2.201997293	0.024535985	0.396002703	Up	*
LARGE2	2.153288687	0.045910166	0.514381356	Up	*
ADAM23	2.148932207	0.001867019	0.114396946	Up	***
SHISA2	2.144452608	0.05295493	0.5390341	Up	*
NR6A1	2.131416619	0.004364057	0.183743367	Up	**
ADRA2C	2.128054023	0.032036783	0.443773294	Up	*
NRARP	2.093025552	0.003149764	0.153542638	Up	**
CHDH	2.090124601	0.011669544	0.286402961	Up	**
DNM1	2.066722262	0.028595552	0.421526	Up	*
GATA2	2.049283127	0.050465218	0.534526558	Up	*
CCDC74B	2.033671355	0.01967006	0.363677548	Up	**
REEP2	2.030753094	0.011073932	0.281972928	Up	**
VSIG10L	2.022994078	0.019153647	0.362178045	Up	**
PCOLCE2	1.976888824	0.001153366	0.090957389	Up	***
CAND2	1.976425042	0.026342178	0.405185498	Up	*
JAM3	1.961213806	0.017144638	0.346767228	Up	**
CXCL11	1.932784427	0.024390187	0.39546139	Up	*
CDHR3	1.921425077	0.019108876	0.362178045	Up	**
MPP2	1.915885348	0.034066595	0.454585523	Up	*
DSCAM	1.907552498	1.78E-05	0.007400665	Up	****
FLNC	1.902639427	0.027929984	0.417061956	Up	*
NTN1	1.876972359	0.008138052	0.242248999	Up	**

Supplementary Table 4 | Top 100 differentially expressed genes in upregulated ACC cells from Andersson database. *MYB* is highlighted. Genes were filtered for FDR ≤ 0.05 and ordinated for decreasing log2 fold change.

GENE	LOG2 FOLD CHANGE	P VALUE	P ADJ	REGULATION	CONFIDENCE
HORMAD1	0.89213783	1.93E-10	1.47E-08	Up	****
MYB	**0.84697945**	**9.22E-13**	**3.24E-10**	**Up**	****
GABRP	0.75193462	1.98E-12	5.68E-10	Up	****
HAPLN1	0.74981242	4.79E-07	5.96E-06	Up	****
ABCA13	0.7164187	2.58E-10	1.87E-08	Up	****
BMPR1B	0.70720871	6.44E-16	2.31E-12	Up	****
PDZK1P1	0.69794737	4.56E-05	0.00025582	Up	****
PDZK1	0.69794737	4.56E-05	0.00025582	Up	****
ART3	0.6681816	5.02E-07	6.18E-06	Up	****
NETO2	0.66548999	1.96E-08	4.81E-07	Up	****
ZNF730	0.66093781	2.17E-12	6.01E-10	Up	****
RN7SKP240	0.65611984	1.40E-11	2.31E-09	Up	****
PRAME	0.65202058	1.86E-14	1.83E-11	Up	****
FABP7	0.64089862	1.36E-14	1.58E-11	Up	****
ELAVL2	0.63904645	5.90E-11	6.28E-09	Up	****
TBX22	0.63743853	1.72E-11	2.71E-09	Up	****
ANLN	0.63258511	1.15E-14	1.46E-11	Up	****
RNA5SP101	0.62033523	4.54E-09	1.53E-07	Up	****
RNU6-302P	0.60245845	1.05E-09	5.40E-08	Up	****

RNU6-446P	0.59408654	3.02E-10	2.06E-08	Up	****
OR2L8	0.58621485	5.68E-07	6.86E-06	Up	****
ZNF726	0.57899202	6.11E-12	1.39E-09	Up	****
CDK1	0.57675683	9.97E-10	5.21E-08	Up	****
VTCN1	0.57362768	6.75E-15	9.06E-12	Up	****
BRIP1	0.57051645	5.93E-12	1.36E-09	Up	****
FNDC1	0.56992441	2.79E-09	1.07E-07	Up	****
OR2L2	0.56835149	1.87E-07	2.80E-06	Up	****
OR2AK2	0.56558098	2.98E-07	4.06E-06	Up	****
DTL	0.55866954	4.71E-10	2.88E-08	Up	****
HELLS	0.54835335	9.36E-14	6.45E-11	Up	****
SNORA72	0.54674306	3.66E-06	3.10E-05	Up	****
LINC01667	0.5370638	2.22E-05	0.00014083	Up	****
VCAN	0.52995838	2.67E-12	6.99E-10	Up	****
KIF11	0.5194619	1.23E-10	1.03E-08	Up	****
OR2L5	0.51700674	2.59E-06	2.31E-05	Up	****
SHC4	0.51061181	3.67E-09	1.32E-07	Up	****
DLX5	0.50523046	3.03E-06	2.64E-05	Up	****
SYCP2	0.50348588	1.17E-10	9.86E-09	Up	****
CCNB2	0.49988228	8.20E-11	7.75E-09	Up	****
XRCC2	0.49680259	4.27E-11	5.07E-09	Up	****
TOP2A	0.49585189	5.34E-11	5.92E-09	Up	****
CENPF	0.49573719	3.26E-10	2.14E-08	Up	****
TTK	0.49382075	2.08E-08	4.99E-07	Up	****

RNA5SP157	0.48560484	5.93E-08	1.14E-06	Up	****
CENPK	0.48510544	2.07E-09	8.67E-08	Up	****
RNU6-637P	0.48018087	0.00019502	0.00088035	Up	***
NUSAP1	0.47659492	2.86E-10	1.99E-08	Up	****
CENPU	0.47229991	1.09E-11	1.98E-09	Up	****
KRT15	0.46765698	3.89E-06	3.26E-05	Up	****
ZNF300	0.46615317	1.32E-12	4.16E-10	Up	****
RAPGEF4	0.4658005	1.94E-07	2.88E-06	Up	****
RNU6-674P	0.46506125	1.07E-09	5.46E-08	Up	****
DUXAP10	0.46337824	4.99E-12	1.17E-09	Up	****
PTH2R	0.46190645	0.00250718	0.00761351	Up	**
PRLR	0.45807086	2.11E-08	5.04E-07	Up	****
ADGRV1	0.45402419	0.00011583	0.00056598	Up	****
PCLAF	0.45280212	1.60E-08	4.18E-07	Up	****
RPS24	0.45279077	2.85E-06	2.50E-05	Up	****
OBP2B	0.45119868	1.26E-07	2.04E-06	Up	****
GUCY1A1	0.4493344	3.83E-09	1.35E-07	Up	****
GINS1	0.44704048	2.47E-12	6.56E-10	Up	****
RASGRP1	0.44686369	7.16E-08	1.31E-06	Up	****
SLC12A1	0.44374509	2.22E-05	0.00014062	Up	****
EZH2	0.44263498	3.53E-15	5.37E-12	Up	****
NLN	0.44243006	1.38E-12	4.28E-10	Up	****
BUB1B	0.44168495	7.53E-11	7.30E-09	Up	****
RNU6-1003P	0.43816692	1.20E-07	1.96E-06	Up	****

KIF14	0.43764569	9.48E-09	2.77E-07	Up	****
LINC02487	0.437522	0.00030225	0.00127228	Up	***
POLE2	0.43697368	1.18E-10	9.92E-09	Up	****
HEY2	0.43622312	1.39E-06	1.39E-05	Up	****
TDRD12	0.4347428	0.0093138	0.02283094	Up	**
MELK	0.43345808	3.12E-10	2.09E-08	Up	****
TPX2	0.43237384	1.95E-09	8.32E-08	Up	****
EDIL3	0.43192282	1.32E-07	2.12E-06	Up	****
DKK1	0.4247637	0.00015132	0.0007096	Up	***
GLYATL2	0.42030902	0.00032704	0.00135892	Up	***
ZNF286A	0.41968677	2.77E-13	1.36E-10	Up	****
ZNF286B	0.41968677	2.77E-13	1.36E-10	Up	****
ZNF286A-TBC1D26	0.41968677	2.77E-13	1.36E-10	Up	****
KNL1	0.41857955	3.54E-09	1.29E-07	Up	****
RN7SL73P	0.4182692	0.0003982	0.0015985	Up	***
RPL24P8	0.4182692	0.0003982	0.0015985	Up	***
RPL24	0.4182692	0.0003982	0.0015985	Up	***
SKA3	0.41786658	2.05E-08	4.95E-07	Up	****
SERPINE2	0.41756123	9.19E-06	6.73E-05	Up	****
SHCBP1	0.41625138	9.42E-08	1.63E-06	Up	****
RNA5SP346	0.41565498	0.00098562	0.00343766	Up	***
AADAT	0.41543912	1.98E-08	4.85E-07	Up	****
ASPN	0.41516045	0.00250235	0.00760156	Up	**
TMSB15B	0.41471215	2.97E-09	1.12E-07	Up	****

PLK4	0.41459754	9.70E-11	8.58E-09	Up	****
VIT	0.41412027	6.17E-05	0.00033199	Up	****
CKS2	0.41198799	8.04E-09	2.41E-07	Up	****
CENPI	0.41082475	1.68E-09	7.64E-08	Up	****
DIAPH3	0.41072892	2.92E-10	2.01E-08	Up	****
MKI67	0.41004835	3.48E-09	1.27E-07	Up	****
PARPBP	0.40977352	1.97E-09	8.35E-08	Up	****
FAM111B	0.40871178	2.17E-08	5.19E-07	Up	****
ST3GAL4	0.40743091	6.66E-11	6.66E-09	Up	****

Supplementary Table 5 | Top 100 differentially expressed genes in upregulated ACC cells from Chowbina database. *MYB* is highlighted. Genes were filtered for FDR ≤ 0.05 and ordinated for decreasing log2 fold change.

GENE	LOG2 FOLD CHANGE	P VALUE	P ADJ	REGULATION	CONFIDENCE
EN1	6.04059354	3.01E-12	1.64E-09	Up	****
FABP7	5.92613776	1.67E-08	2.45E-06	Up	****
IGF2	5.61381622	5.07E-05	0.00104071	Up	****
MYB	**5.41311003**	**4.60E-05**	**0.00096597**	**Up**	****
FNDC1	5.09886147	1.55E-09	3.42E-07	Up	****
VCAN	4.99819954	5.66E-06	0.00021992	Up	****
IGFBP2	4.99606766	4.53E-06	0.00018731	Up	****
RRM2	4.94537289	4.96E-08	5.99E-06	Up	****
COL27A1	4.82953275	1.07E-07	1.09E-05	Up	****
NUSAP1	4.7867362	3.55E-08	4.66E-06	Up	****
HAPLN1	4.68972911	0.00633487	0.03772405	Up	**
GABRP	4.60316414	2.25E-07	1.98E-05	Up	****
VTCN1	4.59027596	5.43E-08	6.39E-06	Up	****
SOX11	4.49325499	0.00909669	0.04911993	Up	**
PCLAF	4.43466531	7.11E-08	8.11E-06	Up	****
HORMAD1	4.30752547	1.03E-06	6.20E-05	Up	****
LAMB1	4.2180471	1.77E-08	2.59E-06	Up	****
CKS2	4.13922976	5.54E-09	9.42E-07	Up	****
TTYH1	4.13722216	0.00010515	0.00180266	Up	****
DTL	4.11459974	7.75E-07	5.08E-05	Up	****

TOP2A	4.10106158	6.28E-07	4.38E-05	Up	****
ASPM	4.08522542	7.57E-07	4.99E-05	Up	****
PNMA8A	4.07222369	5.47E-05	0.00110669	Up	****
CDCA7	4.03277266	2.18E-08	3.07E-06	Up	****
PRAME	4.01045853	7.86E-08	8.74E-06	Up	****
PBK	3.98652301	4.04E-06	0.00016974	Up	****
NRCAM	3.96362984	1.43E-08	2.15E-06	Up	****
EZH2	3.9308591	6.53E-07	4.53E-05	Up	****
ART3	3.93005526	1.35E-05	0.00041026	Up	****
SOX4	3.88032844	3.42E-08	4.52E-06	Up	****
BASP1	3.81780376	2.33E-08	3.26E-06	Up	****
CENPU	3.80269213	1.73E-06	8.72E-05	Up	****
KIF11	3.80062968	1.15E-07	1.16E-05	Up	****
LGR6	3.77654375	0.0004709	0.00553466	Up	***
SERPINE2	3.77151196	1.49E-05	0.00044003	Up	****
DLGAP5	3.77014347	4.09E-06	0.00017135	Up	****
TTK	3.74170154	7.35E-06	0.00026533	Up	****
COL11A1	3.73140278	0.00161422	0.0137943	Up	***
COL9A2	3.7159813	1.23E-05	0.00038586	Up	****
MIR483	3.70854505	0.00321259	0.02294151	Up	**
INS-IGF2	3.70854505	0.00321259	0.02294151	Up	**
MFAP2	3.70441833	0.00046845	0.00550882	Up	***
GINS1	3.70114619	2.15E-06	0.00010252	Up	****
CDC7	3.69875565	0.00017337	0.00264558	Up	***

PRC1	3.6680321	2.45E-07	2.12E-05	Up	****
KIF20A	3.66601867	1.15E-06	6.68E-05	Up	****
NETO2	3.66061385	0.00390977	0.02646169	Up	**
MELK	3.63689514	1.26E-07	1.23E-05	Up	****
NPNT	3.62746331	0.00245824	0.01893654	Up	**
BUB1B	3.60805284	2.88E-06	0.00012872	Up	****
SLC35F3	3.6008696	0.00011951	0.00197506	Up	****
ANLN	3.5831178	3.10E-07	2.58E-05	Up	****
E2F7	3.56483462	1.07E-06	6.39E-05	Up	****
ZWINT	3.56046338	7.41E-07	4.94E-05	Up	****
TMSB15A	3.54688019	6.53E-05	0.00128037	Up	****
LINC01139	3.52653143	0.00259024	0.01969497	Up	**
DLX2	3.50356647	0.00828964	0.04585868	Up	**
CENPK	3.49927126	0.00020931	0.00305425	Up	***
HMMR	3.47450946	3.39E-07	2.77E-05	Up	****
WDFY2	3.46571814	1.97E-06	9.56E-05	Up	****
FAM83D	3.45542458	5.38E-06	0.00021319	Up	****
ZNF300	3.44476881	7.90E-08	8.74E-06	Up	****
PCDHB10	3.42607489	2.46E-05	0.00062702	Up	****
EFHD1	3.39496915	1.87E-10	6.34E-08	Up	****
OBP2B	3.37606868	0.00011448	0.001907	Up	****
CDK1	3.37282853	5.89E-06	0.00022538	Up	****
MTHFD1L	3.29704266	1.27E-06	7.06E-05	Up	****
MIR100HG	3.29660651	0.00025216	0.00349687	Up	***

CDC20	3.25868422	1.46E-05	0.00043311	Up	****
TP53	3.24665758	7.83E-10	1.97E-07	Up	****
MOK	3.22153185	3.26E-05	0.00075569	Up	****
ZNF367	3.20270786	1.13E-06	6.62E-05	Up	****
NDC80	3.18599734	3.98E-05	0.00086219	Up	****
RAD51AP1	3.18087398	2.37E-06	0.00010933	Up	****
BAMBI	3.15996619	2.83E-05	0.00067893	Up	****
SPARC	3.15974268	1.94E-06	9.48E-05	Up	****
UBE2SP1	3.13970659	8.33E-08	9.04E-06	Up	****
UBE2S	3.13970659	8.33E-08	9.04E-06	Up	****
UBE2SP2	3.13970659	8.33E-08	9.04E-06	Up	****
PDE9A	3.1360691	5.64E-09	9.48E-07	Up	****
CCNB1	3.13129911	1.80E-05	0.00050555	Up	****
ZNF727	3.11555949	0.00018039	0.0027339	Up	***
MIA	3.11325772	7.30E-05	0.0013835	Up	****
MIA-RAB4B	3.11325772	7.30E-05	0.0013835	Up	****
PRELP	3.10945043	0.00425019	0.0281494	Up	**
MLC1	3.10885397	0.0056868	0.03477257	Up	**
HELLS	3.09247353	1.03E-05	0.00034	Up	****
COLEC12	3.08856344	0.00133036	0.01203568	Up	***
TPX2	3.08716842	1.19E-05	0.00037688	Up	****
IGDCC4	3.084614	0.00067735	0.00719583	Up	***
RACGAP1	3.05240595	8.79E-06	0.00030475	Up	****
RFLNA	3.05082202	0.00051716	0.00592726	Up	***

NEK2	3.04867288	0.0001136	0.00189501	Up	****
NUDT11	3.04350644	6.95E-07	4.75E-05	Up	****
TMEFF1	3.03636107	0.0025554	0.01949024	Up	**
MSANTD3-TMEFF1	3.03636107	0.0025554	0.01949024	Up	**
MARCKSL1	3.00481511	0.00052726	0.00602292	Up	***
SOX8	3.00059656	0.00221801	0.01752689	Up	**
KRT5	2.99681887	3.42E-09	6.24E-07	Up	****
SHC4	2.98719611	0.00604698	0.03641304	Up	**

Supplementary Table 6 | Top 100 differentially expressed genes in upregulated ACC cells from Gao database. *MYB* is highlighted. Genes were filtered for FDR ≤ 0.05 and ordinated for decreasing log2 fold change.

GENE	LOG2 FOLD CHANGE	P VALUE	P ADJ	REGULATION	CONFIDENCE
ART3	0.67935827	2.43E-13	8.86E-10	Up	****
MYB	**0.63042863**	**1.19E-09**	**2.83E-07**	**Up**	****
SHC4	0.60767572	4.55E-11	2.76E-08	Up	****
RN7SKP240	0.59132741	2.50E-15	2.64E-11	Up	****
RNPS1	0.55532933	4.70E-05	0.00054425	Up	****
FABP7	0.55436947	1.30E-11	1.22E-08	Up	****
PDZK1P1	0.54900041	1.29E-06	3.88E-05	Up	****
PDZK1	0.54900041	1.29E-06	3.88E-05	Up	****
TBX22	0.5462117	2.14E-09	4.63E-07	Up	****
RNU6-853P	0.54614575	8.84E-08	6.38E-06	Up	****
HORMAD1	0.53812108	3.40E-05	0.00042964	Up	****
RNU6-637P	0.53247878	1.56E-06	4.36E-05	Up	****
KAT7	0.52131329	7.87E-05	0.0007973	Up	****
VCAN	0.51390686	1.55E-12	2.83E-09	Up	****
RNU6-540P	0.5090587	3.66E-07	1.66E-05	Up	****
ABCA13	0.50776709	2.79E-06	6.74E-05	Up	****
PRAME	0.49965249	4.25E-10	1.35E-07	Up	****
HAPLN1	0.49907447	4.26E-06	9.23E-05	Up	****
RNU6-446P	0.49622005	1.17E-07	7.62E-06	Up	****
ELAVL2	0.48450786	9.35E-08	6.44E-06	Up	****

FNDC1	0.48069652	4.97E-11	2.82E-08	Up	****
RNA5SP101	0.47667856	2.66E-09	5.44E-07	Up	****
PCDHB4	0.4647641	6.83E-07	2.58E-05	Up	****
RNU6-674P	0.46395115	1.33E-07	8.46E-06	Up	****
IL17RB	0.46309928	2.57E-10	9.47E-08	Up	****
BMPR1B	0.46307375	7.33E-10	2.08E-07	Up	****
DNAH14	0.46090218	1.57E-07	9.42E-06	Up	****
VTCN1	0.45335164	3.19E-07	1.51E-05	Up	****
ITGA9	0.44355078	1.89E-14	1.20E-10	Up	****
RNU6-433P	0.44026722	4.56E-07	1.94E-05	Up	****
ZNF730	0.43935682	3.97E-11	2.59E-08	Up	****
RNU6-831P	0.43746892	6.55E-08	5.20E-06	Up	****
NETO2	0.43454259	5.33E-07	2.17E-05	Up	****
CCDC144CP	0.43192957	4.40E-09	7.00E-07	Up	****
CCDC144A	0.43192957	4.40E-09	7.00E-07	Up	****
CCDC144B	0.43192957	4.40E-09	7.00E-07	Up	****
GABRP	0.42908634	1.04E-07	7.03E-06	Up	****
DUXAP8	0.42856773	3.11E-15	2.64E-11	Up	****
SEMA6D	0.42765534	2.95E-11	2.15E-08	Up	****
SYCP2	0.42746006	1.87E-06	5.00E-05	Up	****
PCDHB3	0.42333659	1.71E-05	0.00025659	Up	****
AADAT	0.42220992	7.07E-10	2.02E-07	Up	****
DUXAP10	0.41587303	3.09E-15	2.64E-11	Up	****
PLCL1	0.40891366	4.16E-09	6.89E-07	Up	****

RNU6-302P	0.40548902	7.85E-08	5.80E-06	Up	****
RNU6-944P	0.40371664	7.82E-06	0.00014146	Up	****
LRRN1	0.40298417	2.91E-05	0.00038193	Up	****
NTRK3	0.40120395	2.67E-10	9.47E-08	Up	****
OR5P2	0.39910974	4.50E-06	9.60E-05	Up	****
EDIL3	0.39852538	1.57E-05	0.00023988	Up	****
SNORA72	0.38930299	1.11E-05	0.00018553	Up	****
LINC00665	0.38822186	1.61E-11	1.32E-08	Up	****
LINC01535	0.38822186	1.61E-11	1.32E-08	Up	****
LAMB1	0.38680502	2.10E-10	8.50E-08	Up	****
HEY2	0.38652217	1.17E-08	1.45E-06	Up	****
PXDN	0.38592589	3.53E-09	6.25E-07	Up	****
RNU6-1078P	0.38569979	4.14E-05	0.00049757	Up	****
PCDHB10	0.38296335	1.15E-08	1.43E-06	Up	****
SCRG1	0.38249044	4.75E-06	9.99E-05	Up	****
OR2L8	0.38194593	3.01E-05	0.00039231	Up	****
ZNF711	0.38185062	2.01E-11	1.56E-08	Up	****
RNU6-1052P	0.38137616	3.59E-06	8.05E-05	Up	****
ST8SIA6	0.38050068	5.95E-05	0.00064706	Up	****
OBP2B	0.37934072	4.42E-09	7.00E-07	Up	****
RNU6-1079P	0.37765373	1.44E-08	1.67E-06	Up	****
EFHD1	0.37444045	8.86E-13	1.74E-09	Up	****
MFGE8	0.37383908	4.49E-12	7.16E-09	Up	****
MMP16	0.37267307	1.75E-07	1.02E-05	Up	****

RASGRP1	0.37199506	6.29E-07	2.42E-05	Up	****
NID1	0.36872384	3.11E-08	2.97E-06	Up	****
ZNF726	0.36701721	4.75E-08	4.18E-06	Up	****
BAMBI	0.36282955	1.14E-07	7.51E-06	Up	****
COL9A1	0.36266435	1.94E-06	5.13E-05	Up	****
EIF3D	0.3626212	7.16E-06	0.00013305	Up	****
CBX3	0.36237291	2.16E-07	1.18E-05	Up	****
VIT	0.35917076	2.69E-07	1.35E-05	Up	****
CEP170	0.35889924	2.71E-06	6.60E-05	Up	****
ANKRD36	0.35699288	1.54E-07	9.36E-06	Up	****
SEPTIN4	0.35515236	6.34E-10	1.84E-07	Up	****
NRCAM	0.35339438	1.27E-06	3.82E-05	Up	****
GUCY1A1	0.35163716	1.46E-07	9.05E-06	Up	****
MYEF2	0.35115042	7.92E-09	1.08E-06	Up	****
PRLR	0.35001727	2.77E-06	6.71E-05	Up	****
RNU6-747P	0.34965688	1.18E-06	3.63E-05	Up	****
RNU6-1217P	0.34965688	1.18E-06	3.63E-05	Up	****
RNU6-355P	0.34965688	1.18E-06	3.63E-05	Up	****
RNU6-177P	0.34965688	1.18E-06	3.63E-05	Up	****
RNU6-447P	0.34965688	1.18E-06	3.63E-05	Up	****
RNU6-860P	0.34965688	1.18E-06	3.63E-05	Up	****
RNU6-241P	0.34965688	1.18E-06	3.63E-05	Up	****
LINC01002	0.34965688	1.18E-06	3.63E-05	Up	****
RNU6-1319P	0.34965688	1.18E-06	3.63E-05	Up	****

RNU6-1118P	0.34965688	1.18E-06	3.63E-05	Up	****
RNU6-1199P	0.34965688	1.18E-06	3.63E-05	Up	****
RNU6-1076P	0.34965688	1.18E-06	3.63E-05	Up	****
RNU6-1100P	0.34965688	1.18E-06	3.63E-05	Up	****
RNU6-785P	0.34965688	1.18E-06	3.63E-05	Up	****
RNU6-791P	0.34965688	1.18E-06	3.63E-05	Up	****
RNU6-705P	0.34965688	1.18E-06	3.63E-05	Up	****
RNU6-1054P	0.34965688	1.18E-06	3.63E-05	Up	****

Supplementary Table 7 | ACC gene patient signature. List of the 156 genes extrapolated from the intersection of the upregulated genes from the publicly available datasets analysed (Andersson, Chowbina, Gao) and the RNA-seq produced in this study (Cicirò).

ACC GENE SIGNATURE					
PNMA8A	SHC4	ZWILCH	KIF14	NCAPG2	BZW2
TMEFF1	GGH	ATIC	GINS1	C1GALT1C1L	MTHFD2
ARNT2	TFAP2A	SCRG1	WDR12	MCM3	BICD1
CHODL	HEY2	GABRP	PRELP	ARL9	TOP2A
TTK	CENPU	WDFY2	MYH10	OLFM2	ANKRD50
OBP2B	CENPK	HAPLN3	AADAT	EFNA3	BCL2
VCAN	CENPE	TM4SF1	ZBED4	ZNF286B	CHEK1
AGPAT5	WDHD1	FAT1	NUDT11	ZNF286A	RASGRP1
C4orf46	GART	BUB1B	SLC25A15	CCND1	TRAM1L1
STK26	CHML	FAM216A	BUB1	SGO2	SLC35F3
PCDHB10	CCDC138	PGAP1	BAMBI	RFC3	PLK4
CDC7	NOTCH1	KPNA2	ZNF260	COL11A1	APBB2
RPP40	TPST1	BMPR1B	ZNF257	VIT	RAD51AP1
SOX4	PRAME	SCHIP1	MLC1	ZNF681	TRPS1
NETO2	SERPINH1	FAM178B	TP53	ST3GAL4	APBA2
E2F7	FLVCR1	EZH2	ZNF239	CTTNBP2NL	SDC2
E2F3	DDIAS	TTYH1	PUS7	ABI2	SELENOI
DTL	DIPK1C	SPARC	ART3	PCDHB3	DAPK1
SKA3	ZFP37	WEE1	NCAPG	PCDHB2	ZNF300
FABP7	SERPINE2	TUSC3	KNTC1	POLR1B	MOK

PLXDC2	FNDC1	AFAP1	PLSCR3	EFHD1	FANCI
SPPL3	UBE2T	PRKDC	CDC25B	MYB	NCKAP5
BRCA2	LAMB1	ANLN	ARHGEF9	GUCY1B1	MTHFD1L
NUF2	TEX14	KIF23	LIMK2	CHD1L	CDC42EP3
VTCN1	POLE2	EN1	EPHX4	KIAA0895	RPGRIP1L
ZNF492	HORMAD1	KIF15	GLMN	GUCY1A1	MIA

Supplementary Table 8 | List of enriched genes from Gene Set Enrichment Analysis (GSEA). Core enriched genes in MM MYB +DOX cells against ACC patient signature. *MYB* is highlighted.

GENE	RANK METRIC SCORE	RUNNING ES
MYB	**1.734**	**0.0174**
RFC3	1.389	0.0302
PLK4	1.331	0.0441
NCAPG	1.284	0.0577
C4orf46	1.274	0.0716
RAD51AP1	1.272	0.0857
NUF2	1.219	0.0979
BUB1	1.201	0.1108
UBE2T	1.200	0.1242
TTK	1.186	0.1370
DDIAS	1.170	0.1498
WDHD1	1.165	0.1626
SKA3	1.157	0.1754
HELLS	1.139	0.1873
CENPE	1.117	0.1991

CDC7	1.112	0.2113
GUCY1B1	1.101	0.2231
SGO2	1.096	0.2352
ZNF286B	1.094	0.2474
POLE2	1.093	0.2595
GINS1	1.073	0.2706
FANCI	1.061	0.2818
MTHFD2	1.061	0.2936
TPST1	1.036	0.3038
KIF15	1.033	0.3150
GLMN	1.030	0.3264
BCL2	1.026	0.3376
KNTC1	1.022	0.3485
CCDC138	1.017	0.3597
SLC25A15	1.013	0.3708
CHODL	0.995	0.3807
WEE1	0.976	0.3905
CENPU	0.975	0.4013
KPNA2	0.961	0.4108
AADAT	0.950	0.4207

BUB1B	0.949	0.4312
CENPK	0.899	0.4364
ANLN	0.886	0.4449
FAM216A	0.884	0.4547
SLC35F3	0.849	0.4588
DTL	0.835	0.4666
ZWILCH	0.830	0.4745
NCAPG2	0.822	0.4827
ARNT2	0.817	0.4911
KIAA0895	0.807	0.4987
RPGRIP1L	0.802	0.5073
KIF23	0.800	0.5159
EZH2	0.780	0.5219
OLFM2	0.772	0.5293
RPP40	0.762	0.5362
MTHFD1L	0.755	0.5435
SCHIP1	0.751	0.5513
MOK	0.721	0.5525
KIF14	0.704	0.5568
BRCA2	0.691	0.5611

STK26	0.688	0.5681
ZNF239	0.686	0.5755
BAMBI	0.656	0.5756
PNMA8A	0.648	0.5810
MCM3	0.636	0.5846
MYH10	0.622	0.5876
CHEK1	0.601	0.5876
HEY2	0.590	0.5907
APBA2	0.589	0.5970
TOP2A	0.581	0.6013
E2F7	0.581	0.6076
GUCY1A1	0.577	0.6121
PRAME	0.575	0.6162
EFHD1	0.574	0.6225
NUDT11	0.571	0.6268
AFAP1	0.568	0.6310
SDC2	0.566	0.6361
ABI2	0.555	0.6361
ZNF492	0.546	0.6372
ARL9	0.546	0.6427

RASGRP1	0.529	0.6373
FLVCR1	0.527	0.6420
NETO2	0.522	0.6459
AGPAT5	0.494	0.6385
PCDHB3	0.490	0.6377
PLSCR3	0.475	0.6372
SHC4	0.470	0.6398
HAPLN3	0.453	0.6376
ATIC	0.445	0.6393
WDFY2	0.441	0.6422
WDR12	0.439	0.6463
SOX4	0.435	0.6493

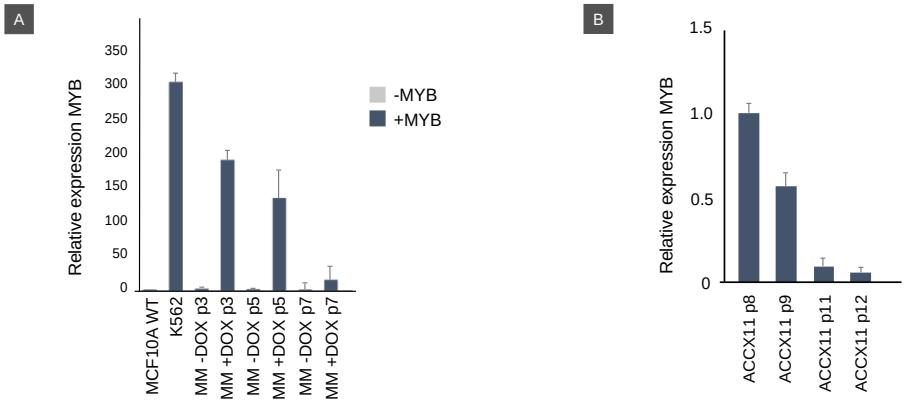

Supplementary Figure 1 | qPCR analysis on cells at different culturing passages.

(**A**) Graphs showing *MYB* expression levels in MCF10A cells transduced with pINDUCER21-MYB vector (MM) in presence or absence of DOX or (**B**) in ACCX11 cells. MCF10A was used as negative control, while K562 was used as positive control for *MYB* overexpression. p followed by a number indicates the different passages of the cell culture. For MM cells the p0 counts as the moment of the transduction, for ACCX11 cells the passage counting starts at the moment of the first *in vitro* seeding after being expanded in xenograft. Experiment was performed in triplicates. ACCX11 cells were provided by Professor Göran Stenman, Sahlgrenska Cancer Center (University of Gothenburg, Sweden), in collaboration with the Adenoid Cystic Carcinoma Research Foundation (ACCRF, MA, USA), and XenoSTART (S. Antonio, Texas, USA).

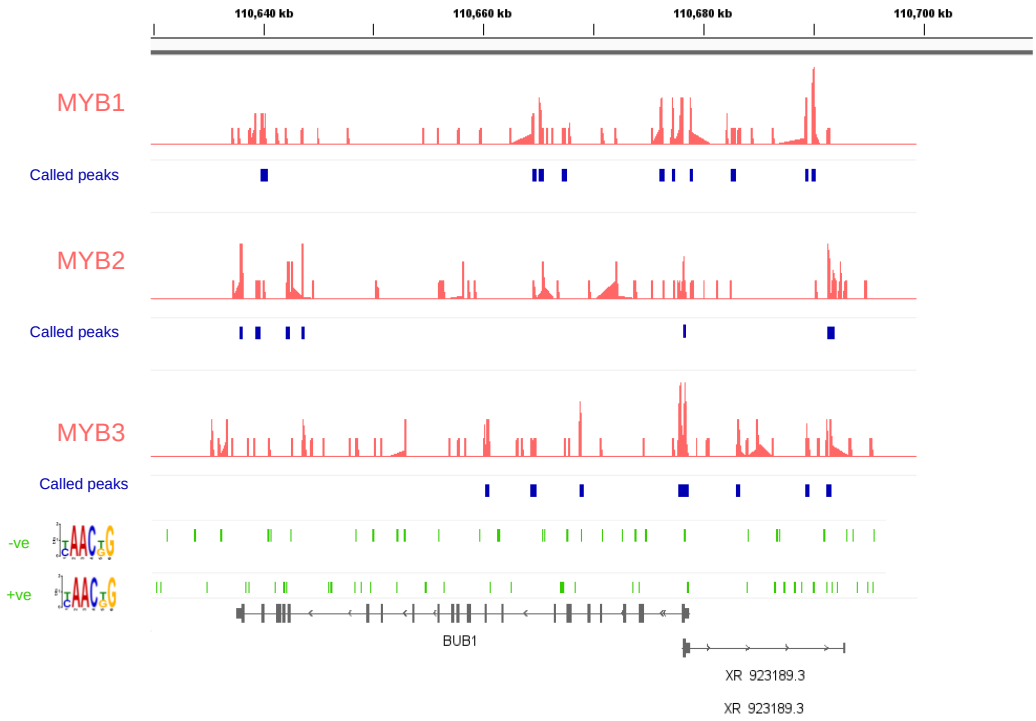

Supplementary Figure 2 | Visualization of labelling peaks using ChIP-seq read mapping data. ChIP enriched sequences found in the three replicates in *BUB1* region (chromosome 2). Overall, peaks were called when found in 2 out of 3 samples at overlapping regions. In green the position of the MYB canonical motif (sequence on the left) in the negative and positive strand (-ve and +ve, respectively).

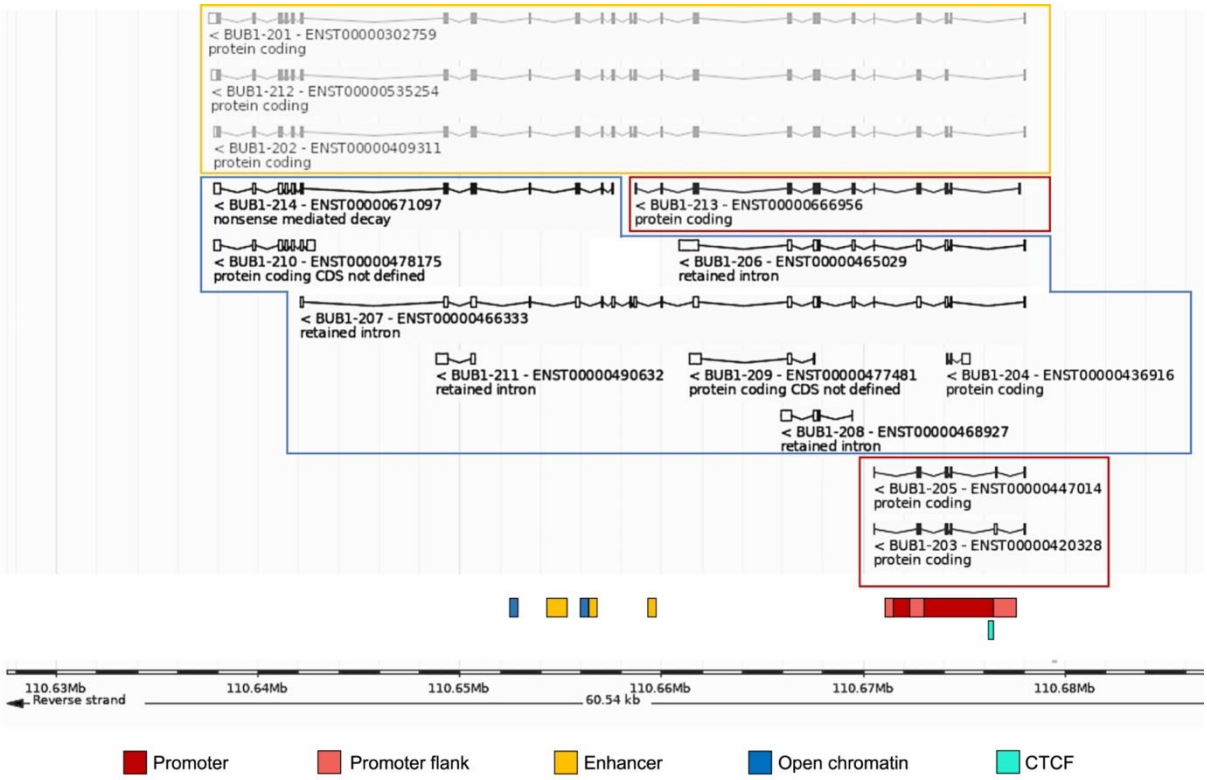

Supplementary Figure 3 | *BUB1* comprehensive set from GENCODE 43. Representation of *BUB1* transcripts and regulatory builds, including regions of promoter and enhancers. Figure as to be interpreted from right to left, as the reverse strand is shown. Colours of boxes indicate protein coding in red and yellow, with transcripts from Ensembl and Ensembl/Havana merged, respectively; in blue processed transcripts of non-protein coding. The figure was adapted from Ensembl; access number of the gene: 169679.

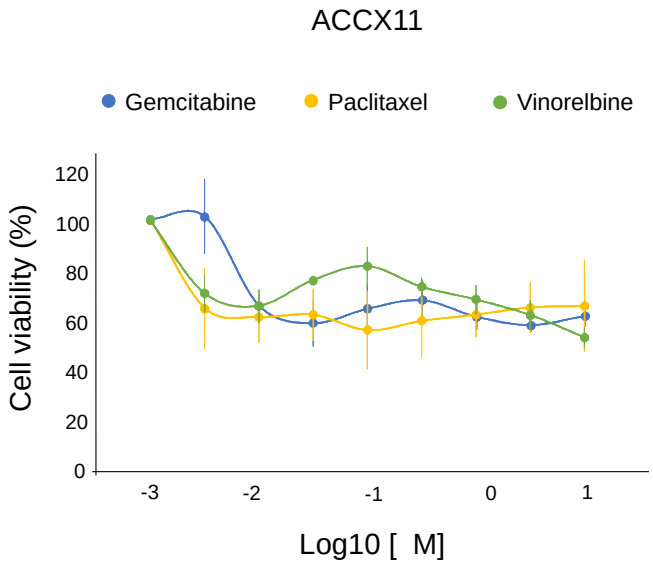

Supplementary Figure 4 | Treatment of ACCX11 cells with standard therapeutic drugs. Graph showing the percentage of cell viability of cultured ACCX11 cells after pharmacological treatment of increasing doses of three standard chemotherapeutic drugs: gemcitabine, paclitaxel, and vinorelbine. The drugs were selected due to test the efficacy of drugs exerting different mechanisms of action. Gemcitabine interferes with DNA synthesis, paclitaxel stabilises the microtubule, and vinorelbine inhibits microtubule assembly. Experiment was performed in triplicates. ACCX11 cells were provided by Professor Göran Stenman, Sahlgrenska Cancer Center (University of Gothenburg, Sweden), in collaboration with the Adenoid Cystic Carcinoma Research Foundation (ACCRF, MA, USA), and XenoSTART (S. Antonio, Texas, USA).

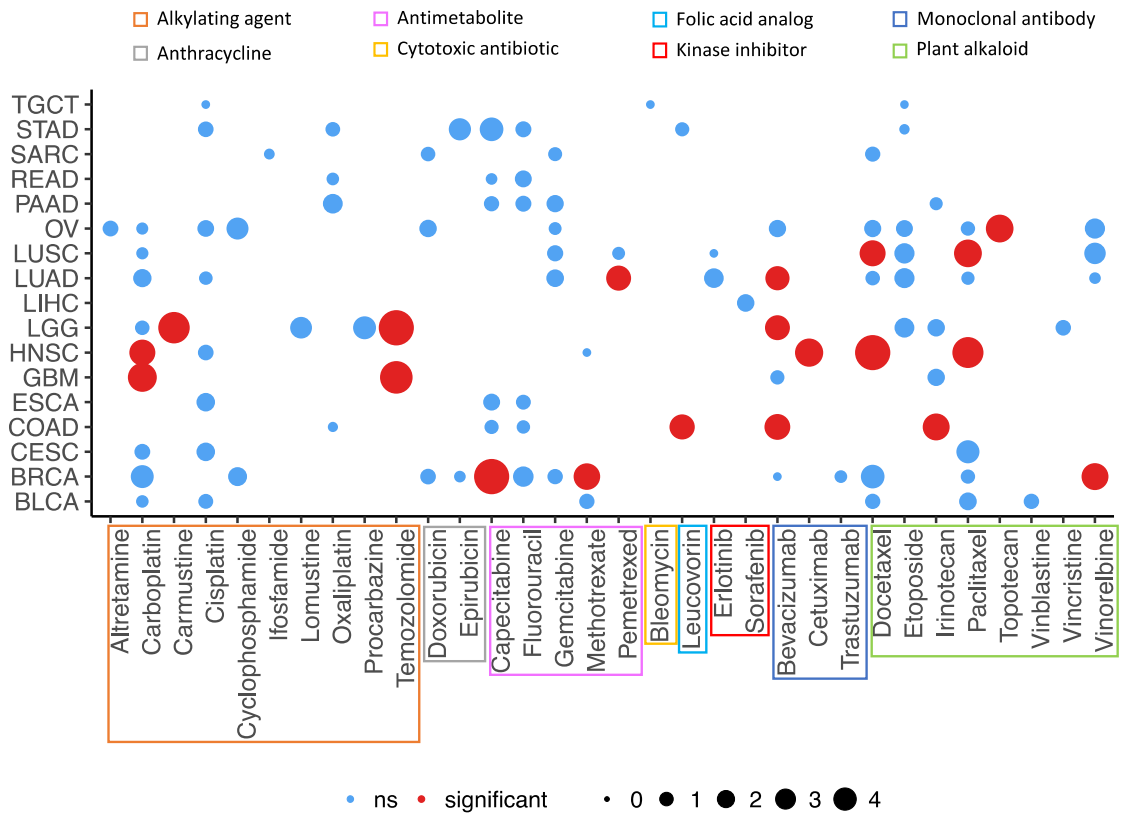

Supplementary Figure 5 | Analysis of sensitivity of different cancers to approved standard chemotherapies according to *BUB1* expression. Bubble plot showing the sensitivity to standard chemotherapeutic drugs, grouped by classes, according to *BUB1* overexpression. Colours indicate a significant correlation between high levels of *BUB1* and sensitivity (i.e. efficacy) to drugs; red colour indicates a significant relationship, blue a non-significant one. Size of the bubbles represents the strength of the relationship. Strong relationship means that patients harbouring *BUB1* overexpression are likely to benefit from the therapy. ns, not significant.

A

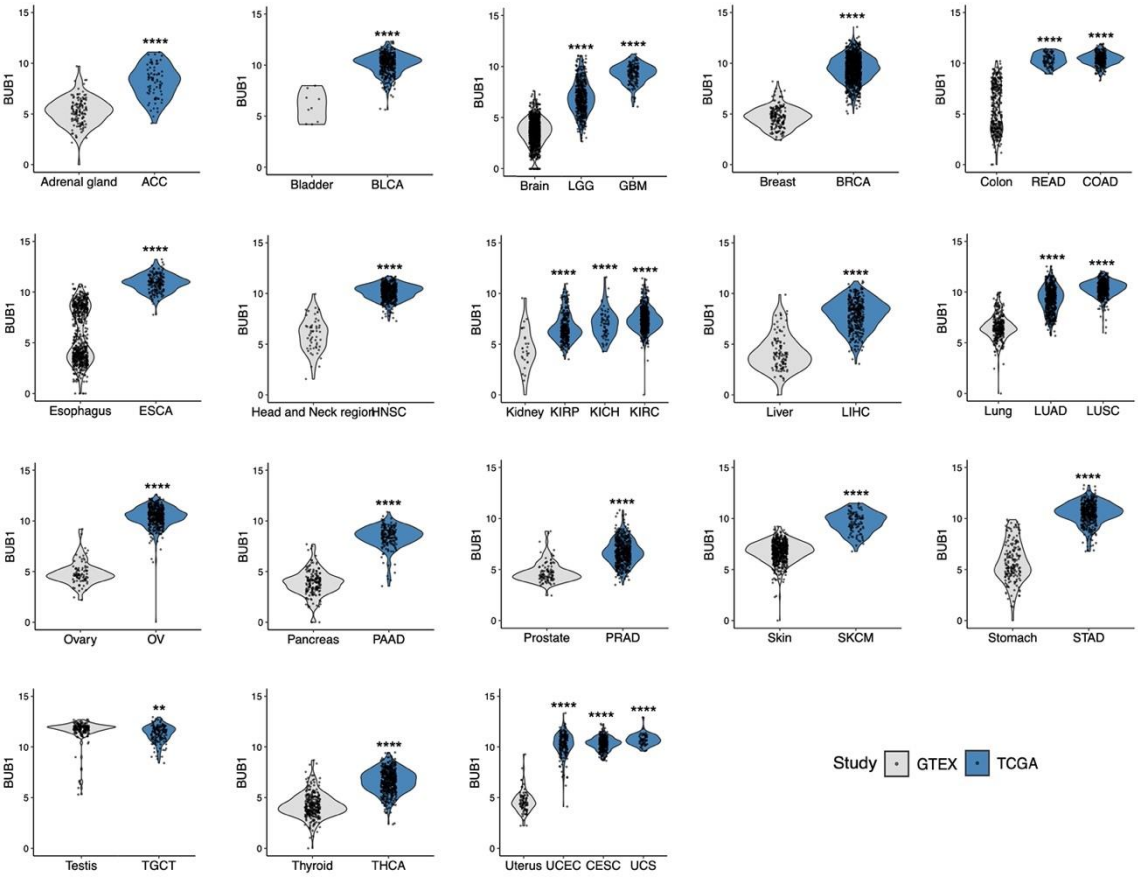
BUB1
Adrenal gland
ACC
Bladder
BLCA
Brain
LGG
GBM
Breast
BRCA
Colon
READ
COAD
Esophagus
ESCA
Head and Neck region
HNSC
Kidney
KIRP
KICH
KIRC
Liver
LIHC
Lung
LUAD
LUSC
Ovary
OV
Pancreas
PAAD
Prostate
PRAD
Skin
SKCM
Stomach
STAD
Testis
TGCT
Thyroid
THCA
Uterus
UCEC
CESC
UCS
Study
GTEX
TCGA

[Continued]

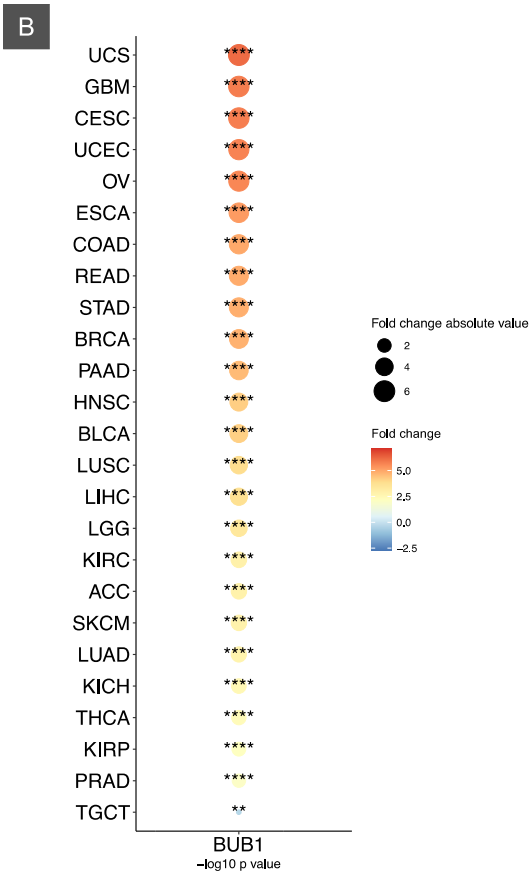

Supplementary Figure 6 | *In silico* analysis of *BUB1* expression change in tumours sample from TCGA cohort compared to corresponding healthy tissues from GTEx. (**A**) Grid showing violin plots of matching tumours and normal tissues for each anatomical site in which *BUB1* resulted significantly overexpressed. Mean expression of *BUB1* was compared between the normal GTEx cohort (grey) and tumour TCGA cohort (blue). (**B**) Graph showing the fold change of *BUB1* expression and its statistical significance in different tumours compared to their corresponding healthy tissues. Fold change strength is represented by intensity-scaled colours, red colour indicates positive fold change, meaning upregulation of the gene, whereases the blue colour indicates negative fold change, meaning downregulation of expression. The size of the points shows the absolute value of the fold change. Statistical significance was determined by Wilcoxon test. Expression values in (**A**) are defined as log2(norm_count+1); in (**B**) showed as –log10(pvalue).

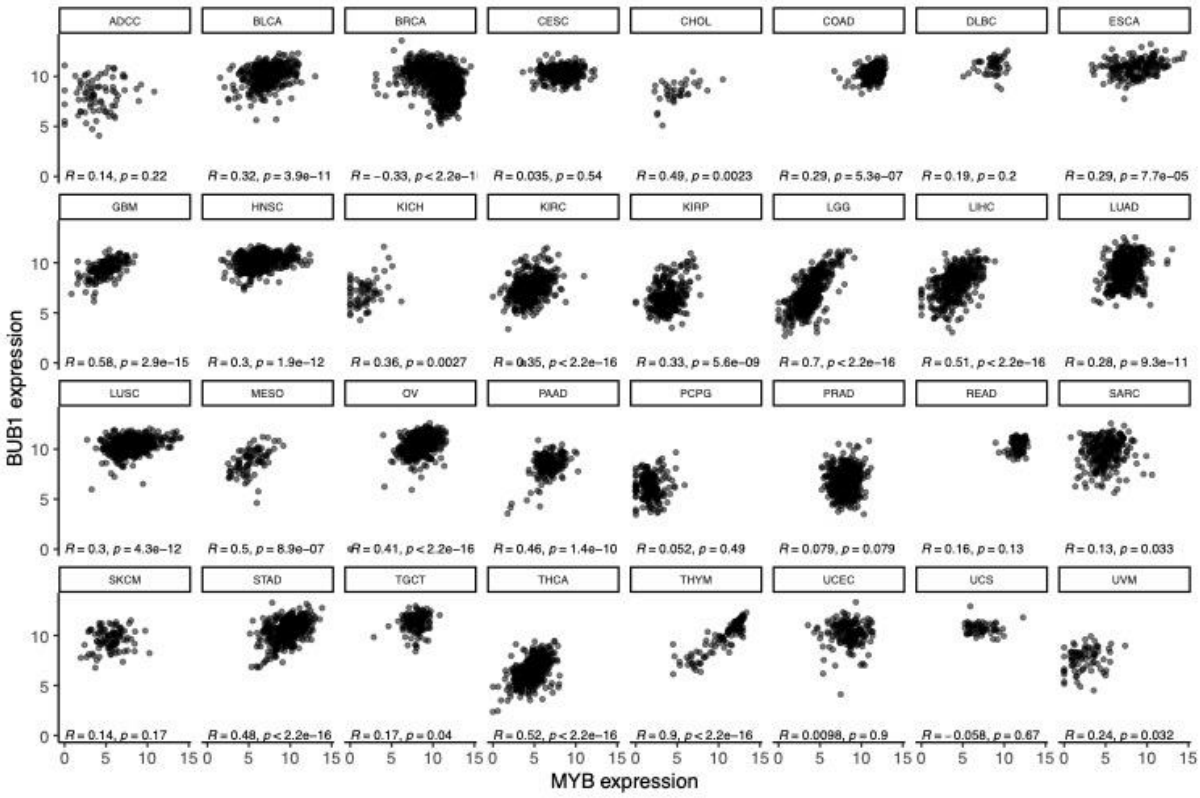

Supplementary Figure 7 | Correlation between *MYB* and *BUB1* expressions. Linear correlation profile of MYB and BUB1 extrapolated from the TCGA dataset showing the statistical relationship between the two variables at pan-cancer level. A R value higher than ±0.3 indicates a significant positive or negative correlation, respectively. R, Pearson correlation coefficient; p, p value.

Bibliography

Adenoid Cystic Carcinoma: Stages, Cancer.Net; Conquer Cancer, the ASCO foundation (2021). Available at https://www.cancer.net/cancer-types/adenoid-cystic-carcinoma/stages.

Adams, J. A. (2001). Kinetic and catalytic mechanisms of protein kinases. *Chemical Reviews, 101*(8), 2271-2290.

Agulnik, M., Cohen, E. W., Cohen, R. B., Chen, E. X., Vokes, E. E., Hotte, S. J., Winquist, E., Laurie, S., Hayes, D. N., & Dancey, J. E. (2007). Phase II study of lapatinib in recurrent or metastatic epidermal growth factor receptor and/or erbB2 expressing adenoid cystic carcinoma and non–adenoid cystic carcinoma malignant tumors of the salivary glands. *Journal of Clinical Oncology, 25*(25), 3978-3984.

Airoldi, M., Pedani, F., Succo, G., Gabriele, A. M., Ragona, R., Marchionatti, S., & Bumma, C. (2001). Phase II randomized trial comparing vinorelbine versus vinorelbine plus cisplatin in patients with recurrent salivary gland malignancies. *Cancer, 91*(3), 541-547.

Al-Lazikani, B., Banerji, U., & Workman, P. (2012). Combinatorial drug therapy for cancer in the post-genomic era. *Nature Biotechnology, 30*(7), 679-692.

Allen III, R. D., Kim, H. K., Sarafova, S. D., & Siu, G. (2001). Negative regulation of CD4 gene expression by a HES-1–c-Myb complex. *Molecular and Cellular Biology, 21*(9), 3071-3082.

Almeida, L. O., Guimarães, D. M., Martins, M. D., Martins, M. A., Warner, K. A., Nör, J. E., Castilho, R. M., & Squarize, C. H. (2017). Unlocking the chromatin of adenoid cystic carcinomas using HDAC inhibitors sensitize cancer stem cells to cisplatin and induces tumor senescence. *Stem Cell Research, 21*, 94-105.

American Joint Committee on Cancer AJCC. Major Salivary Glands. In: AJCC Cancer Staging Manual. 8th ed. New York, NY: Springer; 2017:95.

Amit, M., Binenbaum, Y., Sharma, K., Ramer, N., Ramer, I., Agbetoba, A., Glick, J., Yang, X., Lei, D., & Bjørndal, K. (2015). Incidence of cervical lymph node metastasis and its association with outcomes in patients with adenoid cystic carcinoma. An international collaborative study. *Head & Neck, 37*(7), 1032-1037.

Amit, M., Binenbaum, Y., Trejo–Leider, L., Sharma, K., Ramer, N., Ramer, I., Agbetoba, A., Miles, B., Yang, X., & Lei, D. (2015). International collaborative validation of intraneural invasion as a prognostic marker in adenoid cystic carcinoma of the head and neck. *Head & Neck, 37*(7), 1038-1045.

Andersson, M. K., Afshari, M. K., Andrén, Y., Wick, M. J., & Stenman, G. (2017). Targeting the oncogenic transcriptional regulator MYB in adenoid cystic carcinoma by inhibition of IGF1R/AKT signaling. *JNCI: Journal of the National Cancer Institute, 109*(9), djx017.

Andersson, M. K., Mangiapane, G., Nevado, P. T., Tsakaneli, A., Carlsson, T., Corda, G., Nieddu, V., Abrahamian, C., Chayka, O., & Rai, L. (2020). ATR is a MYB regulated gene and potential therapeutic target in adenoid cystic carcinoma. *Oncogenesis, 9*(1), 1-10.

Arkin, M. R., Tang, Y., & Wells, J. A. (2014). Small-molecule inhibitors of protein-protein interactions: progressing toward the reality. *Chemistry & Biology, 21*(9), 1102-1114.

Aziz, N., Wu, J., Dubendorff, J. W., Lipsick, J. S., Sturgill, T. W., & Bender, T. P. (1993). c-Myb and v-Myb are differentially phosphorylated by p42mapk in vitro. *Oncogene, 8*(8), 2259-2265.

Aziz, N., Miglarese, M. R., Hendrickson, R. C., Shabanowitz, J., Sturgill, T. W., Hunt, D. F., & Bender, T. P. (1995). Modulation of c-Myb-induced transcription activation by a phosphorylation site near the negative regulatory domain. *Proceedings of the National Academy of Sciences, 92*(14), 6429-6433.

Balamucki, C. J., Amdur, R. J., Werning, J. W., Vaysberg, M., Morris, C. G., Kirwan, J. M., & Mendenhall, W. M. (2012). Adenoid cystic carcinoma of the head and neck. *American Journal of Otolaryngology, 33*(5), 510-518.

Bandopadhayay, P., Ramkissoon, L. A., Jain, P., Bergthold, G., Wala, J., Zeid, R., Schumacher, S. E., Urbanski, L., O'Rourke, R., & Gibson, W. J. (2016). MYB-QKI rearrangements in angiocentric glioma drive tumorigenicity through a tripartite mechanism. *Nature Genetics, 48*(3), 273-282.

Barnum, K. J., & O'Connell, M. J. (2014). Cell cycle regulation by checkpoints. *Cell Cycle Control: Mechanisms and Protocols,* , 29-40.

Baron, A. P., Von Schubert, C., Cubizolles, F., Siemeister, G., Hitchcock, M., Mengel, A., Schröder, J., Fernandez-Montalvan, A., von Nussbaum, F., & Mumberg, D. (2016). Probing the catalytic functions of Bub1 kinase using the small molecule inhibitors BAY-320 and BAY-524. *Elife, 5*, e12187.

Bartůněk, P., Kralova, J., Blendinger, G., Dvořák, M., & Zenke, M. (2003). GATA-1 and c-myb crosstalk during red blood cell differentiation through GATA-1 binding sites in the c-myb promoter. *Oncogene, 22*(13), 1927-1935.

Batsakis, J. G. (1979). *Tumors of the head and neck: clinical and pathological considerations*. Williams & Wilkins.

Belani, C. P., Eisenberger, M. A., & Gray, W. C. (1988). Preliminary experience with chemotherapy in advanced salivary gland neoplasms. *Medical and Pediatric Oncology, 16*(3), 197-202.

Belloni, E., Shing, D., Tapinassi, C., Viale, A., Mancuso, P., Malazzi, O., Gerbino, E., Dall'Olio, V., Egurbide, I., & Odero, M. D. (2011). In vivo expression of an aberrant MYB-GATA1 fusion induces leukemia in the presence of GATA1 reduced levels. *Leukemia, 25*(4), 733-736.

Bender, T. P., Kremer, C. S., Kraus, M., Buch, T., & Rajewsky, K. (2004). Critical functions for c-Myb at three checkpoints during thymocyte development. *Nature Immunology, 5*(7), 721-729.

Berge, T., Matre, V., Brendeford, E. M., Sæther, T., Lüscher, B., & Gabrielsen, O. S. (2007). Revisiting a selection of target genes for the hematopoietic transcription factor c-Myb using chromatin immunoprecipitation and c-Myb knockdown. *Blood Cells, Molecules, and Diseases, 39*(3), 278-286.

Bernard, P., Hardwick, K., & Javerzat, J. (1998). Fission yeast bub1 is a mitotic centromere protein essential for the spindle checkpoint and the preservation of correct ploidy through mitosis. *The Journal of Cell Biology, 143*(7), 1775-1787.

Bhattasali, O., Holliday, E., Kies, M. S., Hanna, E. Y., Garden, A. S., Rosenthal, D. I., Morrison, W. H., Gunn, G. B., Fuller, C. D., & Zhu, X. R. (2016). Definitive proton radiation therapy and concurrent cisplatin for unresectable head and neck adenoid cystic carcinoma: a series of 9 cases and a critical review of the literature. *Head & Neck, 38*(S1), E1472-E1480.

Bhullar, K. S., Lagarón, N. O., McGowan, E. M., Parmar, I., Jha, A., Hubbard, B. P., & Rupasinghe, H. P. (2018). Kinase-targeted cancer therapies: progress, challenges and future directions. *Molecular Cancer, 17*(1), 1-20.

Bianchi, E., Zini, R., Salati, S., Tenedini, E., Norfo, R., Tagliafico, E., Manfredini, R., & Ferrari, S. (2010). c-myb supports erythropoiesis through the transactivation of KLF1 and LMO2 expression. *Blood, the Journal of the American Society of Hematology, 116*(22), e99-e110.

Bie, L., Zhao, G., Cheng, P., Rondeau, G., Porwollik, S., Ju, Y., Xia, X., & McClelland, M. (2011). The accuracy of survival time prediction for patients with glioma is improved by measuring mitotic spindle checkpoint gene expression. *PloS One, 6*(10), e25631.

Biedenkapp, H., Borgmeyer, U., Sippel, A. E., & Klempnauer, K. (1988). Viral myb oncogene encodes a sequence-specific DNA-binding activity. *Nature, 335*(6193), 835-837.

Bies, J., Markus, J., & Wolff, L. (2002). Covalent attachment of the SUMO-1 protein to the negative regulatory domain of the c-Myb transcription factor modifies its stability and transactivation capacity. *Journal of Biological Chemistry, 277*(11), 8999-9009.

Bies, J., & Wolff, L. (1997). Oncogenic activation of c-Myb by carboxyl-terminal truncation leads to decreased proteolysis by the ubiquitin-26S proteasome pathway. *Oncogene, 14*(2), 203-212.

Billroth, T. (1859). Beobachtungen über geschwülste der speicheldrüsen. *Archiv Für Pathologische Anatomie Und Physiologie Und Für Klinische Medicin, 17*(5), 357-375.

Biswas, K. D., Saha, J., Sen, I., Biswas, G., Sinha, R., Saha, D., & Dutta, S. (2014). Unusual presentations of adenoid cystic carcinoma in extra-salivary gland subsites in head and neck region: a case series. *Indian Journal of Otolaryngology and Head & Neck Surgery, 66*, 286-290.

Bjørndal, K., Krogdahl, A., Therkildsen, M. H., Charabi, B., Kristensen, C. A., Andersen, E., Schytte, S., Primdahl, H., Johansen, J., Pedersen, H. B., Andersen, L. J., & Godballe, C. (2015). Salivary adenoid cystic carcinoma in Denmark 1990–2005: Outcome and independent prognostic factors including the benefit of radiotherapy. Results of the Danish Head and Neck Cancer Group (DAHANCA). *Oral Oncology, 51*(12), 1138-1142. 10.1016/j.oraloncology.2015.10.002

Bolanos-Garcia, V. M., Kiyomitsu, T., D'Arcy, S., Chirgadze, D. Y., Grossmann, J. G., Matak-Vinkovic, D., Venkitaraman, A. R., Yanagida, M., Robinson, C. V., & Blundell, T. L. (2009). The crystal structure of the N-terminal region of BUB1 provides insight into the mechanism of BUB1 recruitment to kinetochores. *Structure, 17*(1), 105-116.

Bologna-Molina, R., Mosqueda-Taylor, A., Molina-Frechero, N., Mori-Estevez, A. D., & Sánchez-Acuña, G. (2013). Comparison of the value of PCNA and Ki-67 as markers of cell proliferation in ameloblastic tumor. *Medicina Oral, Patologia Oral Y Cirugia Bucal, 18*(2), e174.

Boyle, T. A. C., St. Laurent, S., Semus, S., & Joseph, N. (2020). Epidemiology of Adenoid Cystic Carcinoma in the United States. *Journal of Clinical Oncology*, *38*(15), e13600.

Brayer, K. J., Frerich, C. A., Kang, H., & Ness, S. A. (2016). Recurrent Fusions in MYB and MYBL1 Define a Common, Transcription Factor–Driven Oncogenic Pathway in Salivary Gland Adenoid Cystic CarcinomaMYB and MYBL1 Fusions in Adenoid Cystic Carcinoma. *Cancer Discovery, 6*(2), 176-187.

Brill, L. B., Kanner, W. A., Fehr, A., Andrén, Y., Moskaluk, C. A., Löning, T., Stenman, G., & Frierson, H. F. (2011). Analysis of MYB expression and MYB-NFIB gene fusions in adenoid cystic carcinoma and other salivary neoplasms. *Modern Pathology, 24*(9), 1169-1176.

Broderick, P., Dobbins, S. E., Chubb, D., Kinnersley, B., Dunlop, M. G., Tomlinson, I., & Houlston, R. S. (2017). Validation of recently proposed colorectal cancer susceptibility gene variants in an analysis of families and patients—a systematic review. *Gastroenterology, 152*(1), 75-77. e4.

Brufsky, A. M., & Dickler, M. N. (2018). Estrogen receptor-positive breast cancer: exploiting signaling pathways implicated in endocrine resistance. *The Oncologist, 23*(5), 528-539.

Burke, C. J., Thomas, R. H., & Howlett, D. (2011). Imaging the major salivary glands. *British Journal of Oral and Maxillofacial Surgery, 49*(4), 261-269.

Bushweller, J. H. (2019). Targeting transcription factors in cancer—from undruggable to reality. *Nature Reviews Cancer, 19*(11), 611-624.

Cahill, D. P., Lengauer, C., Yu, J., Riggins, G. J., Willson, J. K., Markowitz, S. D., Kinzler, K. W., & Vogelstein, B. (1998). Mutations of mitotic checkpoint genes in human cancers. *Nature, 392*(6673), 300-303.

Calvo, E., Soria, J., Ma, W. W., Wang, T., Bahleda, R., Tolcher, A. W., Gernhardt, D., O'Connell, J., Millham, R., & Giri, N. (2017). A Phase I Clinical Trial and Independent Patient-Derived Xenograft Study of Combined Targeted Treatment with Dacomitinib and Figitumumab in Advanced Solid TumorsDacomitinib plus Figitumumab in Advanced Solid Tumors. *Clinical Cancer Research, 23*(5), 1177-1185.

Cantù, G. (2021a). Adenoid cystic carcinoma. An indolent but aggressive tumour. Part A: from aetiopathogenesis to diagnosis. *Acta Otorhinolaryngologica Italica, 41*(3), 206.

Cantù, G. (2021b). Adenoid cystic carcinoma. An indolent but aggressive tumour. Part B: treatment and prognosis. *Acta Otorhinolaryngologica Italica, 41*(4), 296.

Cantu, G., Solero, C. L., Riccio, S., Colombo, S., Pompilio, M., Aboh, I. V., Formillo, P., & Arana, G. H. (2010). Surgery for malignant maxillary tumors involving the middle cranial fossa. *Skull Base, 20*(02), 55.

Carabana, J., Ortigoza, E., & Krangel, M. S. (2005). Regulation of the murine Dδ2 promoter by upstream stimulatory factor 1, Runx1, and c-Myb. *The Journal of Immunology, 174*(7), 4144-4152.

Carroll, D. K., Carroll, J. S., Leong, C., Cheng, F., Brown, M., Mills, A. A., Brugge, J. S., & Ellisen, L. W. (2006). p63 regulates an adhesion programme and cell survival in epithelial cells. *Nature Cell Biology, 8*(6), 551-561.

Cerda, T., Sun, X. S., Vignot, S., Marcy, P., Baujat, B., Baglin, A., Ali, A. M., Testelin, S., Reyt, E., Janot, F., & Thariat, J. (2014). A rationale for chemoradiation (vs radiotherapy) in salivary gland cancers? On behalf of the REFCOR (French rare head and neck cancer network). *Critical Reviews in Oncology/Hematology, 91*(2), 142-158. 10.1016/j.critrevonc.2014.02.002

Chae, Y. K., Chung, S. Y., Davis, A. A., Carneiro, B. A., Chandra, S., Kaplan, J., Kalyan, A., & Giles, F. J. (2015). Adenoid cystic carcinoma: current therapy and potential therapeutic advances based on genomic profiling. *Oncotarget, 6*(35), 37117.

Chahal, M., Pleasance, E., Grewal, J., Zhao, E., Ng, T., Chapman, E., Jones, M. R., Shen, Y., Mungall, K. L., & Bonakdar, M. (2018). Personalized oncogenomic analysis of metastatic adenoid cystic carcinoma: using whole-genome sequencing to inform clinical decision-making. *Molecular Case Studies, 4*(2), a002626.

Chau, N. G., Hotte, S. J., Chen, E. X., Chin, S. F., Turner, S., Wang, L., & Siu, L. L. (2012). A phase II study of sunitinib in recurrent and/or metastatic adenoid cystic carcinoma (ACC) of the salivary glands: current progress and challenges in evaluating molecularly targeted agents in ACC. *Annals of Oncology, 23*(6), 1562-1570.

Cheasley, D., Pereira, L., Sampurno, S., Sieber, O., Jorissen, R., Xu, H., Germann, M., Yuqian, Y., Ramsay, R. G., & Malaterre, J. (2015). Defective Myb Function Ablates Cyclin E1 Expression and Perturbs Intestinal CarcinogenesisMyb Regulates Cyclin E1 in Colorectal Cancer. *Molecular Cancer Research, 13*(8), 1185-1196.

Chen, C., Choudhury, S., Wangsa, D., Lescott, C. J., Wilkins, D. J., Sripadhan, P., Liu, X., Wangsa, D., Ried, T., & Moskaluk, C. (2017). A multiplex preclinical model for adenoid cystic carcinoma of the salivary gland identifies regorafenib as a potential therapeutic drug. *Scientific Reports, 7*(1), 1-15.

Chen, J., Gnepp, D. R., & Bedrossian, C. W. (1988). Adenoid cystic carcinoma of the salivary glands: an immunohistochemical analysis. *Oral Surgery, Oral Medicine, Oral Pathology, 65*(3), 316-326.

Chen, L., Song, Y., Hou, T., Li, X., Cheng, L., Li, Y., & Xing, Y. (2022). Circ_0004087 interaction with SND1 promotes docetaxel resistance in prostate cancer by boosting the mitosis error correction mechanism. *Journal of Experimental & Clinical Cancer Research, 41*(1), 1-18.

Chen, Q., Zhang, M., Pan, X., Yuan, X., Zhou, L., Yan, L., Zeng, L., Xu, J., Yang, B., & Zhang, L. (2021). Bub1 and CENP-U redundantly recruit Plk1 to stabilize kinetochore-microtubule attachments and ensure accurate chromosome segregation. *Cell Reports, 36*(12), 109740.

Cheng, J., Saku, T., Okabe, H., & Furthmayr, H. (1992). Basement membranes in adenoid cystic carcinoma an immunohistochemical study. *Cancer, 69*(11), 2631-2640.

Cho, S., Kang, W., Han, J. Y., Min, S., Kang, J., Lee, A., Kwon, J. Y., Lee, C., & Park, H. (2016). An integrative approach to precision cancer medicine using patient-derived xenografts. *Molecules and Cells, 39*(2), 77.

Choi, Y., Kim, S., Yoon, D. H., Kim, J. Y., Lee, S., & Cho, K. (2013). Clinical characteristics and prognostic factors of adenoid cystic carcinoma of the head and neck. *The Laryngoscope, 123*(6), 1430-1438.

Chummun, S., McLean, N. R., Kelly, C. G., Dawes, P., Fellows, S., Meikle, D., & Soames, J. V. (2001). Adenoid cystic carcinoma of the head and neck. *British Journal of Plastic Surgery, 54*(6), 476-480.

Ciccolallo, L., Licitra, L., Cantú, G., Gatta, G., & EUROCARE Working Group. (2009). Survival from salivary glands adenoid cystic carcinoma in European populations. *Oral Oncology, 45*(8), 669-674.

Cicirò, Y., & Sala, A. (2021). MYB oncoproteins: emerging players and potential therapeutic targets in human cancer. *Oncogenesis, 10*(2), 1-15.

Clappier, E., Cuccuini, W., Kalota, A., Crinquette, A., Cayuela, J., Dik, W. A., Langerak, A. W., Montpellier, B., Nadel, B., Walrafen, P., Delattre, O., Aurias, A., Leblanc, T., Dombret, H., Gewirtz, A. M., Baruchel, A., Sigaux, F., & Soulier, J. (2007). The C-MYB locus is involved in chromosomal translocation and genomic duplications in human T-cell acute leukemia (T-ALL), the translocation defining a new T-ALL subtype in very young children. *Blood, 110*(4), 1251-1261. 10.1182/blood-2006-12-064683

Coca-Pelaz, A., Rodrigo, J. P., Bradley, P. J., Vander Poorten, V., Triantafyllou, A., Hunt, J. L., Strojan, P., Rinaldo, A., Haigentz, M., Takes, R. P., Mondin, V., Teymoortash, A., Thompson, L. D. R., & Ferlito, A. (2015). Adenoid cystic carcinoma of the head and neck – An update. *Oral Oncology, 51*(7), 652-661. 10.1016/j.oraloncology.2015.04.005

Cogswell, J. P., Cogswell, P. C., Kuehl, W. M., Cuddihy, A. M., Bender, T. M., Engelke, U., Marcu, K. B., & Ting, J. P. (1993). Mechanism of c-myc regulation by c-Myb in different cell lineages. *Molecular and Cellular Biology, 13*(5), 2858-2869.

Conley, J., & Dingman, D. L. (1974). Adenoid cystic carcinoma in the head and neck (cylindroma). *Archives of Otolaryngology, 100*(2), 81-90.

Corradini, F., Cesi, V., Bartella, V., Pani, E., Bussolari, R., Candini, O., & Calabretta, B. (2005). Enhanced proliferative potential of hematopoietic cells expressing degradation-resistant c-Myb mutants. *Journal of Biological Chemistry, 280*(34), 30254-30262.

Creagan, E. T., Woods, J. E., Rubin, J., & Schaid, D. J. (1988). Cisplatin-based chemotherapy for neoplasms arising from salivary glands and contiguous structures in the head and neck. *Cancer, 62*(11), 2313-2319.

Cures, A., House, C., Kanei-Ishii, C., Kemp, B., & Ramsay, R. G. (2001). Constitutive c-Myb amino-terminal phosphorylation and DNA binding activity uncoupled during entry and passage through the cell cycle. *Oncogene, 20*(14), 1784-1792.

Dahse, R., Driemel, O., Schwarz, S., Kromeyer-Hauschild, K., Berndt, A., & Kosmehl, H. (2009). KRAS status and epidermal growth factor receptor expression as determinants for anti-EGFR therapies in salivary gland carcinomas. *Oral Oncology, 45*(9), 826-829.

Dai, P., Akimaru, H., Tanaka, Y., Hou, D., Yasukawa, T., Kanei-Ishii, C., Takahashi, T., & Ishii, S. (1996). CBP as a transcriptional coactivator of c-Myb. *Genes & Development, 10*(5), 528-540.

Dang, T. T., Esparza, M. A., Maine, E. A., Westcott, J. M., & Pearson, G. W. (2015). ΔNp63α Promotes Breast Cancer Cell Motility through the Selective Activation of Components of the Epithelial-to-Mesenchymal Transition ProgramΔNp63α Controls Breast Cancer Cell Motility. *Cancer Research, 75*(18), 3925-3935.

D'Arcy, S., Davies, O. R., Blundell, T. L., & Bolanos-Garcia, V. M. (2010). Defining the molecular basis of BubR1 kinetochore interactions and APC/C-CDC20 inhibition. *Journal of Biological Chemistry, 285*(19), 14764-14776.

Dawson, P. J., Wolman, S. R., Tait, L., Heppner, G. H., & Miller, F. R. (1996). MCF10AT: a model for the evolution of cancer from proliferative breast disease. *The American Journal of Pathology, 148*(1), 313.

De Dominici, M., Porazzi, P., Soliera, A. R., Mariani, S. A., Addya, S., Fortina, P., Peterson, L. F., Spinelli, O., Rambaldi, A., & Martinelli, G. (2018). Targeting CDK6 and BCL2 exploits the “MYB addiction” of Ph acute lymphoblastic leukemia. *Cancer Research, 78*(4), 1097-1109.

de Sousa, L. G., Jovanovic, K., & Ferrarotto, R. (2022). Metastatic Adenoid Cystic Carcinoma: Genomic Landscape and Emerging Treatments. *Current Treatment Options in Oncology, 23*(8), 1135-1150.

de Voer, R. M., Geurts van Kessel, A., Weren, R. D. A., Ligtenberg, M. J. L., Smeets, D., Fu, L., Vreede, L., Kamping, E. J., Verwiel, E. T. P., Hahn, M., Ariaans, M., Spruijt, L., van Essen, T., Houge, G., Schackert, H. K., Sheng, J. Q., Venselaar, H., van Ravenswaaij–Arts, C. M. A., van Krieken, J. H. J. M., . . . Kuiper, R. P. (2013). Germline Mutations in the Spindle Assembly Checkpoint Genes BUB1 and BUB3 Are Risk Factors for Colorectal Cancer. *Gastroenterology, 145*(3), 544-547. 10.1053/j.gastro.2013.06.001

Derynck, R., & Zhang, Y. E. (2003). Smad-dependent and Smad-independent pathways in TGF-β family signalling. *Nature, 425*(6958), 577-584.

Dick Haan, L. D., De Mulder, P. H., Vermorken, J. B., Schornagel, J. H., Vermey, A., & Verweij, J. (1992). Cisplatin-based chemotherapy in advanced adenoid cystic carcinoma of the head and neck. *Head & Neck, 14*(4), 273-277.

Dillon, P. M., Moskaluk, C., Fracasso, P. M., Petroni, G. R., & Thomas, C. Y. (2013). Phase II Study of Dovitinib (TKI258) in Patients with Progressive Metastatic Adenoid Cystic Carcinoma.*Clinical Cancer Research*, *23(15)*, 4138-4145*,*

Dituri, F., Mancarella, S., Cigliano, A., & Giannelli, G. (2019). TGF-β as multifaceted orchestrator in HCC progression: signaling, EMT, immune microenvironment, and novel therapeutic perspectives. Paper presented at the *Seminars in Liver Disease, 39*(01) 53.

Djursby, M., Madsen, M. B., Frederiksen, J. H., Berchtold, L. A., Therkildsen, C., Willemoe, G. L., Hasselby, J. P., Wikman, F., Okkels, H., & Skytte, A. (2020). New pathogenic germline variants in very early onset and familial colorectal cancer patients. *Frontiers in Genetics, 11*, 566266.

Dodd, R. L., & Slevin, N. J. (2006). Salivary gland adenoid cystic carcinoma: a review of chemotherapy and molecular therapies. *Oral Oncology, 42*(8), 759-769.

Dominguez-Brauer, C., Thu, K. L., Mason, J. M., Blaser, H., Bray, M. R., & Mak, T. W. (2015). Targeting mitosis in cancer: emerging strategies. *Molecular Cell, 60*(4), 524-536.

Drabsch, Y., Hugo, H., Zhang, R., Dowhan, D. H., Miao, Y. R., Gewirtz, A. M., Barry, S. C., Ramsay, R. G., & Gonda, T. J. (2007). Mechanism of and requirement for estrogen-regulated MYB expression in estrogen-receptor-positive breast cancer cells. *Proceedings of the National Academy of Sciences, 104*(34), 13762-13767.

Dreyfuss, A. I., Clark, J. R., Fallon, B. G., Posner, M. R., Norris Jr, C. M., & Miller, D. (1987). Cyclophosphamide, doxorubicin, and cisplatin combination chemotherapy for advanced carcinomas of salivary gland origin. *Cancer, 60*(12), 2869-2872.

Drier, Y., Cotton, M. J., Williamson, K. E., Gillespie, S. M., Ryan, R. J., Kluk, M. J., Carey, C. D., Rodig, S. J., Sholl, L. M., & Afrogheh, A. H. (2016). An oncogenic MYB feedback loop drives alternate cell fates in adenoid cystic carcinoma. *Nature Genetics, 48*(3), 265-272.

Dubendorff, J. W., Whittaker, L. J., Eltman, J. T., & Lipsick, J. S. (1992). Carboxy-terminal elements of c-Myb negatively regulate transcriptional activation in cis and in trans. *Genes & Development, 6*(12b), 2524-2535.

Dudek, H., & Reddy, E. P. (1989). Identification of two translational products for c-myb. *Oncogene, 4*(9), 1061-1066.

Dudek, H., Tantravahi, R. V., Rao, V. N., Reddy, E. S., & Reddy, E. P. (1992). Myb and Ets proteins cooperate in transcriptional activation of the mim-1 promoter. *Proceedings of the National Academy of Sciences, 89*(4), 1291-1295.

Eggesbø, H. B. (2012). Imaging of sinonasal tumours. *Cancer Imaging,* , 136.

El-Naggar, A. K. (2017). *WHO classification of head and neck tumours*. International Agency.

Ellington, C. L., Goodman, M., Kono, S. A., Grist, W., Wadsworth, T., Chen, A. Y., Owonikoko, T., Ramalingam, S., Shin, D. M., & Khuri, F. R. (2012). Adenoid cystic carcinoma of the head and neck: incidence and survival trends based on 1973-2007 surveillance, epidemiology, and end results data. *Cancer, 118*(18), 4444-4451.

Elowe, S., & Bolanos-Garcia, V. M. (2022). The spindle checkpoint proteins BUB1 and BUBR1: (SLiM)ming down to the basics. *Trends in Biochemical Sciences, 47*(4), 352-366. 10.1016/j.tibs.2022.01.004

El-Rifai, W., Rutherford, S., Knuutila, S., Frierson, H. F., & Moskaluk, C. A. (2001). Novel DNA Copy Number Losses in Chromosome 12g12-q13 in Adenoid Cystic Carcinoma. *Neoplasia, 3*(3), 173-178. 10.1038/sj.neo.7900158

Ess, K. C., Whitaker, T. L., Cost, G. J., Witte, D. P., Hutton, J. J., & Aronow, B. J. (1995). A central role for a single c-Myb binding site in a thymic locus control region. *Molecular and Cellular Biology, 15*(10), 5707-5715.

Estey, E. H. (2018). Acute myeloid leukemia: 2019 update on risk-stratification and management. *American Journal of Hematology, 93*(10), 1267-1291.

Faesen, A. C., Thanasoula, M., Maffini, S., Breit, C., Müller, F., Van Gerwen, S., Bange, T., & Musacchio, A. (2017). Basis of catalytic assembly of the mitotic checkpoint complex. *Nature, 542*(7642), 498-502.

Fang, Y., Peng, Z., Wang, Y., Gao, K., Liu, Y., Fan, R., Zhang, H., Xie, Z., & Jiang, W. (2022). Current opinions on diagnosis and treatment of adenoid cystic carcinoma. *Oral Oncology, 130*, 105945. 10.1016/j.oraloncology.2022.105945

Feeney, L., Hapuarachi, B., Adderley, H., Rack, S., Morgan, D., Walker, R., Rauch, R., Herz, E., Kaye, J., Harrington, K., & Metcalf, R. (2022). Clinical disease course and survival outcomes following disease recurrence in adenoid cystic carcinoma with and without NOTCH signaling pathway activation. *Oral Oncology, 133*, 106028. 10.1016/j.oraloncology.2022.106028

Ferlito, A., Rinaldo, A., Altavilla, G., & Doglioni, C. (1997). Basaloid squamous cell carcinoma of the larynx and hypopharynx. *Annals of Otology, Rhinology & Laryngology, 106*(12), 1024-1035.

Ferrao, P., Gonda, T. J., & Ashman, L. K. (1997). Expression of constitutively activated human c-Kit in Myb transformed early myeloid cells leads to factor independence, histiocytic differentiation, and tumorigenicity. *Blood, the Journal of the American Society of Hematology, 90*(11), 4539-4552.

Ferrarotto, R., Mitani, Y., Diao, L., Guijarro, I., Wang, J., Zweidler-McKay, P., Bell, D., William Jr, W. N., Glisson, B. S., & Wick, M. J. (2017). Activating NOTCH1 mutations define a distinct subgroup of patients with adenoid cystic carcinoma who have poor prognosis, propensity to bone and liver metastasis, and potential responsiveness to Notch1 inhibitors. *Journal of Clinical Oncology, 35*(3), 352.

Ferrarotto, R., Mitani, Y., McGrail, D. J., Li, K., Karpinets, T. V., Bell, D., Frank, S. J., Song, X., Kupferman, M. E., & Liu, B. (2021). Proteogenomic analysis of salivary adenoid cystic carcinomas defines molecular subtypes and identifies therapeutic targets. *Clinical Cancer Research, 27*(3), 852-864.

Finetti, P., Cervera, N., Charafe-Jauffret, E., Chabannon, C., Charpin, C., Chaffanet, M., Jacquemier, J., Viens, P., Birnbaum, D., & Bertucci, F. (2008). Sixteen–kinase gene expression identifies luminal breast cancers with poor prognosis. *Cancer Research, 68*(3), 767-776.

Foos, G., Natour, S., & Klempnauer, K. H. (1993). TATA-box dependent trans-activation of the human HSP70 promoter by Myb proteins. *Oncogene, 8*(7), 1775-1782.

Fordice, J., Kershaw, C., El-Naggar, A., & Goepfert, H. (1999). Adenoid cystic carcinoma of the head and neck: predictors of morbidity and mortality. *Archives of Otolaryngology–Head & Neck Surgery, 125*(2), 149-152.

Frankish, A., Diekhans, M., Ferreira, A., Johnson, R., Jungreis, I., Loveland, J., Mudge, J. M., Sisu, C., Wright, J., & Armstrong, J. (2019). GENCODE reference annotation for the human and mouse genomes. *Nucleic Acids Research, 47*(D1), D766-D773.

Freier, K., Flechtenmacher, C., Walch, A., Devens, F., Mühling, J., Lichter, P., Joos, S., & Hofele, C. (2005). Differential KIT expression in histological subtypes of adenoid cystic carcinoma (ACC) of the salivary gland. *Oral Oncology, 41*(9), 934-939. 10.1016/j.oraloncology.2005.05.005

Freier, K., Flechtenmacher, C., Walch, A., Ohl, S., Devens, F., Burke, B., Hassfeld, S., Lichter, P., Joos, S., & Hofele, C. (2005). Copy number gains on 22q13 in adenoid cystic carcinoma of the salivary gland revealed by comparative genomic hybridization and tissue microarray analysis. *Cancer Genetics and Cytogenetics, 159*(1), 89-95. 10.1016/j.cancergencyto.2004.09.007

Frerich, C. A., Sedam, H. N., Kang, H., Mitani, Y., El-Naggar, A. K., & Ness, S. A. (2019). N-terminal truncated Myb with new transcriptional activity produced through use of an alternative MYB promoter in salivary gland adenoid cystic carcinoma. *Cancers, 12*(1), 45.

Frierson Jr, H. F., El-Naggar, A. K., Welsh, J. B., Sapinoso, L. M., Su, A. I., Cheng, J., Saku, T., Moskaluk, C. A., & Hampton, G. M. (2002). Large scale molecular analysis identifies genes with altered expression in salivary adenoid cystic carcinoma. *The American Journal of Pathology, 161*(4), 1315-1323.

Frierson, H. F., & Moskaluk, C. A. (2013). Mutation signature of adenoid cystic carcinoma: evidence for transcriptional and epigenetic reprogramming. *The Journal of Clinical Investigation, 123*(7)

Fujii, K., Murase, T., Beppu, S., Saida, K., Takino, H., Masaki, A., Ijichi, K., Kusafuka, K., Iida, Y., & Onitsuka, T. (2017). MYB, MYBL 1, MYBL 2 and NFIB gene alterations and MYC overexpression in salivary gland adenoid cystic carcinoma. *Histopathology, 71*(5), 823-834.

Funasaka, Y., Boulton, T., Cobb, M., Yarden, Y., Fan, B., Lyman, S. D., Williams, D. E., Anderson, D. M., Zakut, R., & Mishima, Y. (1992). c-Kit-kinase induces a cascade of protein tyrosine phosphorylation in normal human melanocytes in response to mast cell growth factor and stimulates mitogen-activated protein kinase but is down-regulated in melanomas. *Molecular Biology of the Cell, 3*(2), 197-209.

Fushimi, C., Tada, Y., Takahashi, H., Nagao, T., Ojiri, H., Masubuchi, T., Matsuki, T., Miura, K., Kawakita, D., & Hirai, H. (2018). A prospective phase II study of combined androgen blockade in patients with androgen receptor-positive metastatic or locally advanced unresectable salivary gland carcinoma. *Annals of Oncology, 29*(4), 979-984.

Ganly, I., Amit, M., Kou, L., Palmer, F. L., Migliacci, J., Katabi, N., Yu, C., Kattan, M. W., Binenbaum, Y., & Sharma, K. (2015). Nomograms for predicting survival and recurrence in patients with adenoid cystic carcinoma. An international collaborative study. *European Journal of Cancer, 51*(18), 2768-2776.

Gao, F., Ponte, J. F., Papageorgis, P., Levy, M., Ozturk, S., Lambert, A. W., Thiagalingam, A., Abdolmaleky, H. M., Sullivan, B. A., & Thiagalingam, S. (2009). hBub1 negatively regulates p53 mediated early cell death upon mitotic checkpoint activation. *Cancer Biology & Therapy, 8*(7), 636-644.

Gao, R., Cao, C., Zhang, M., Lopez, M., Yan, Y., Chen, Z., Mitani, Y., Zhang, L., Zajac-Kaye, M., & Liu, B. (2014). A unifying gene signature for adenoid cystic cancer identifies parallel MYB-dependent and MYB-independent therapeutic targets. *Oncotarget, 5*(24), 12528.

Gao, Y., Zhang, W., Liu, C., & Li, G. (2019). miR-200 affects tamoxifen resistance in breast cancer cells through regulation of MYB. *Scientific Reports, 9*(1), 18844.

Gao, Z., Zhang, D., Duan, Y., Yan, L., Fan, Y., Fang, Z., & Liu, Z. (2019). A five-gene signature predicts overall survival of patients with papillary renal cell carcinoma. *PLoS One, 14*(3), e0211491.

Garrick, D., Fiering, S., Martin, D. I., & Whitelaw, E. (1998). Repeat-induced gene silencing in mammals. *Nature Genetics, 18*(1), 56-59.

Gencturk, M., Ozturk, K., Caicedo-Granados, E., Li, F., & Cayci, Z. (2019). Application of diffusion-weighted MR imaging with ADC measurement for distinguishing between the histopathological types of sinonasal neoplasms. *Clinical Imaging, 55*, 76-82.

George, O. L., & Ness, S. A. (2014). Situational awareness: regulation of the myb transcription factor in differentiation, the cell cycle and oncogenesis. *Cancers, 6*(4), 2049-2071.

Geurts, J. M., Schoenmakers, E. F., RoÈijer, E., AstroÈm, A., Stenman, G., & van de Ven, W. J. (1998). Identification of NFIB as recurrent translocation partner gene of HMGIC in pleomorphic adenomas. *Oncogene, 16*(7), 865-872.

Gewirtz, A. M., & Calabretta, B. (1988). A c-myb antisense oligodeoxynucleotide inhibits normal human hematopoiesis in vitro. *Science, 242*(4883), 1303-1306.

Ghabach, B., Anderson, W. F., Curtis, R. E., Huycke, M. M., Lavigne, J. A., & Dores, G. M. (2010). Adenoid cystic carcinoma of the breast in the United States (1977 to 2006): a population-based cohort study. *Breast Cancer Research, 12*, 1-9.

Gilbert, J., Li, Y., Pinto, H. A., Jennings, T., Kies, M. S., Silverman, P., & Forastiere, A. A. (2006). Phase II trial of taxol in salivary gland malignancies (E1394): a trial of the Eastern Cooperative Oncology Group. *Head & Neck: Journal for the Sciences and Specialties of the Head and Neck, 28*(3), 197-204.

Giles, K. M., Kalinowski, F. C., Candy, P. A., Epis, M. R., Zhang, P. M., Redfern, A. D., Stuart, L. M., Goodall, G. J., & Leedman, P. J. (2013). Axl Mediates Acquired Resistance of Head and Neck Cancer Cells to the Epidermal Growth Factor Receptor Inhibitor ErlotinibAxl Promotes Erlotinib Resistance in Head and Neck Cancer. *Molecular Cancer Therapeutics, 12*(11), 2541-2558.

Gillespie, M. B., Albergotti, W. G., & Eisele, D. W. (2012). Recurrent salivary gland cancer. *Current Treatment Options in Oncology, 13*, 58-70.

Glinsky, G. V., Berezovska, O., & Glinskii, A. B. (2005). Microarray analysis identifies a death-from-cancer signature predicting therapy failure in patients with multiple types of cancer. *The Journal of Clinical Investigation, 115*(6), 1503-1521.

Goldhirsch, A., Winer, E. P., Coates, A. S., Gelber, R. D., Piccart-Gebhart, M., Thürlimann, B., Senn, H., Albain, K. S., André, F., & Bergh, J. (2013). Personalizing the treatment of women with early breast cancer: highlights of the St Gallen International Expert Consensus on the Primary Therapy of Early Breast Cancer 2013. *Annals of Oncology, 24*(9), 2206-2223.

Gonda, T. J., Buckmaster, C., & Ramsay, R. G. (1989). Activation of c-myb by carboxy-terminal truncation: relationship to transformation of murine haemopoietic cells in vitro. *The EMBO Journal, 8*(6), 1777-1783.

Gonda, T. J., & Metcalf, D. (1984). Expression of myb, myc and fos proto-oncogenes during the differentiation of a murine myeloid leukaemia. *Nature, 310*(5974), 249-251.

Grabsch, H., Takeno, S., Parsons, W. J., Pomjanski, N., Boecking, A., Gabbert, H. E., & Mueller, W. (2003). Overexpression of the mitotic checkpoint genes BUB1, BUBR1, and BUB3 in gastric cancer—association with tumour cell proliferation. *The Journal of Pathology: A Journal of the Pathological Society of Great Britain and Ireland, 200*(1), 16-22.

Graudejus, O., Ponce Wong, R. D., Varghese, N., Wagner, S., & Morrison, B. (2018). Bridging the gap between in vivo and in vitro research: Reproducing in vitro the mechanical and electrical environment of cells in vivo. *Frontiers in Cellular Neuroscience, 12*

Greenman, C., Stephens, P., Smith, R., Dalgliesh, G. L., Hunter, C., Bignell, G., Davies, H., Teague, J., Butler, A., & Stevens, C. (2007). Patterns of somatic mutation in human cancer genomes. *Nature, 446*(7132), 153-158.

Grivennikov, S., Karin, E., Terzic, J., Mucida, D., Yu, G., Vallabhapurapu, S., Scheller, J., Rose-John, S., Cheroutre, H., & Eckmann, L. (2009). IL-6 and Stat3 are required for survival of intestinal epithelial cells and development of colitis-associated cancer. *Cancer Cell, 15*(2), 103-113.

Gross, S. M., Dane, M. A., Smith, R. L., Devlin, K. L., McLean, I. C., Derrick, D. S., Mills, C. E., Subramanian, K., London, A. B., & Torre, D. (2022). A multi-omic analysis of MCF10A cells provides a resource for integrative assessment of ligand-mediated molecular and phenotypic responses. *Communications Biology, 5*(1), 1-20.

Gründer, A., Qian, F., Ebel, T. T., Mincheva, A., Lichter, P., Kruse, U., & Sippel, A. E. (2003). Genomic organization, splice products and mouse chromosomal localization of genes for transcription factor Nuclear Factor One. *Gene, 304*, 171-181.

Han, J. Y., Han, Y. K., Park, G., Kim, S. D., & Geun Lee, C. (2015). Bub1 is required for maintaining cancer stem cells in breast cancer cell lines. *Scientific Reports, 5*(1), 1-10.

Hanahan, D., & Weinberg, R. A. (2000). The hallmarks of cancer. *Cell, 100*(1), 57-70.

Hantel, C., Shapiro, I., Poli, G., Chiapponi, C., Bidlingmaier, M., Reincke, M., Luconi, M., Jung, S., & Beuschlein, F. (2016). Targeting heterogeneity of adrenocortical carcinoma: Evaluation and extension of preclinical tumor models to improve clinical translation. *Oncotarget, 7*(48), 79292.

Haruki, N., Saito, H., Harano, T., Nomoto, S., Takahashi, T., Osada, H., Fujii, Y., & Takahashi, T. (2001). Molecular analysis of the mitotic checkpoint genes BUB1, BUBR1 and BUB3 in human lung cancers. *Cancer Letters, 162*(2), 201-205. 10.1016/S0304-3835(00)00675-3.

Head and Neck Cancer, guidelines. ASCO American Society of clinical oncology. Available at https://old-prod.asco.org/practice-patients/guidelines/head-and-neck-cancer.

Heinrich, M. C., Corless, C. L., Demetri, G. D., Blanke, C. D., Von Mehren, M., Joensuu, H., McGreevey, L. S., Chen, C., Van den Abbeele, A. D., & Druker, B. J. (2003). Kinase mutations and imatinib response in patients with metastatic gastrointestinal stromal tumor. *Journal of Clinical Oncology, 21*(23), 4342-4349.

Hellquist, H. B., Sundelin, K., Di Bacco, A., Tytor, M., Manzotti, M., & Viale, G. (1997). Tumour growth fraction and apoptosis in salivary gland acinic cell carcinomas. Prognostic implications of Ki-67 and bcl-2 expression and of in situ end labelling (TUNEL). *The Journal of Pathology: A Journal of the Pathological Society of Great Britain and Ireland, 181*(3), 323-329.

Hernando, E., Orlow, I., Liberal, V., Nohales, G., Benezra, R., & Cordon-Cardo, C. (2001). Molecular analyses of the mitotic checkpoint components hsMAD2, hBUB1 and hBUB3 in human cancer. *International Journal of Cancer, 95*(4), 223-227.

Hess, J. L., Bittner, C. B., Zeisig, D. T., Bach, C., Fuchs, U., Borkhardt, A., Frampton, J., & Slany, R. K. (2006). c-Myb is an essential downstream target for homeobox-mediated transformation of hematopoietic cells. *Blood, 108*(1), 297-304.

Hitre, E., Budai, B., Takacsi-Nagy, Z., Rubovszky, G., Toth, E., Remenar, E., Polgár, C., & Láng, I. (2013). Cetuximab and platinum-based chemoradio-or chemotherapy of patients with epidermal growth factor receptor expressing adenoid cystic carcinoma: a phase II trial. *British Journal of Cancer, 109*(5), 1117-1122.

Ho, A. L., Sherman, E. J., Fury, M. G., Baxi, S. S., Haque, S., Sima, C. S., Antonescu, C. R., Katabi, N., & Pfister, D. G. (2014). Phase II Study of Axitinib in Patients with Progressive, Recurrent/Metastatic Adenoid Cystic Carcinoma*. Journal of Clinical Oncology*. *32(15)*, 6093.

Ho, A. S., Kannan, K., Roy, D. M., Morris, L. G., Ganly, I., Katabi, N., Ramaswami, D., Walsh, L. A., Eng, S., & Huse, J. T. (2013). The mutational landscape of adenoid cystic carcinoma. *Nature Genetics, 45*(7), 791-798.

Ho, A. S., Ochoa, A., Jayakumaran, G., Zehir, A., Mayor, C. V., Tepe, J., Makarov, V., Dalin, M. G., He, J., & Bailey, M. (2019). Genetic hallmarks of recurrent/metastatic adenoid cystic carcinoma. *The Journal of Clinical Investigation, 129*(10), 4276-4289.

Hogg, A., Schirm, S., Nakagoshi, H., Bartley, P., Ishii, S., Bishop, J. M., & Gonda, T. J. (1997). Inactivation of a c-Myb/estrogen receptor fusion protein in transformed primary cells leads to granulocyte/macrophage differentiation and down regulation of c-kit but not c-myc or cdc2. *Oncogene, 15*(24), 2885-2898.

Holst, V. A., Marshall, C. E., Moskaluk, C. A., & Frierson Jr, H. F. (1999). KIT protein expression and analysis of c-kit gene mutation in adenoid cystic carcinoma. *Modern Pathology: An Official Journal of the United States and Canadian Academy of Pathology, Inc, 12*(10), 956-960.

Hooper, J., Maurice, D., Argent-Katwala, M. J., & Weston, K. (2008). Myb proteins regulate expression of histone variant H2A. Z during thymocyte development. *Immunology, 123*(2), 282-289.

Hotte, S. J., Winquist, E. W., Lamont, E., MacKenzie, M., Vokes, E., Chen, E. X., Brown, S., Pond, G. R., Murgo, A., & Siu, L. L. (2005). Imatinib mesylate in patients with adenoid cystic cancers of the salivary glands expressing c-kit: a Princess Margaret Hospital phase II consortium study. *Journal of Clinical Oncology, 23*(3), 585-590.

Hoyt, M. A., Totis, L., & Roberts, B. T. (1991). S. cerevisiae genes required for cell cycle arrest in response to loss of microtubule function. *Cell, 66*(3), 507-517.

Huang, E., Nocka, K., Beier, D. R., Chu, T., Buck, J., Lahm, H., Wellner, D., Leder, P., & Besmer, P. (1990). The hematopoietic growth factor KL is encoded by the SI locus and is the ligand of the c-kit receptor, the gene product of the W locus. *Cell, 63*(1), 225-233.

Huang, M., Shen, A., Ding, J., & Geng, M. (2014). Molecularly targeted cancer therapy: some lessons from the past decade. *Trends in Pharmacological Sciences, 35*(1), 41-50.

Huang, M., Ma, D., Sun, K., Yu, G., Guo, C., & Gao, F. (1997). Factors influencing survival rate in adenoid cystic carcinoma of the salivary glands. *International Journal of Oral and Maxillofacial Surgery, 26*(6), 435-439.

Huber, P. E., Debus, J., Latz, D., Zierhut, D., Bischof, M., Wannenmacher, M., & Engenhart-Cabillic, R. (2001). Radiotherapy for advanced adenoid cystic carcinoma: neutrons, photons or mixed beam? *Radiotherapy and Oncology, 59*(2), 161-167.

Hugo, H., Cures, A., Suraweera, N., Drabsch, Y., Purcell, D., Mantamadiotis, T., Phillips, W., Dobrovic, A., Zupi, G., & Gonda, T. J. (2006). Mutations in the MYB intron I regulatory sequence increase transcription in colon cancers. *Genes, Chromosomes and Cancer, 45*(12), 1143-1154.

Husain, Q., Kanumuri, V. V., Svider, P. F., Radvansky, B. M., Boghani, Z., Liu, J. K., & Eloy, J. A. (2013). Sinonasal adenoid cystic carcinoma: systematic review of survival and treatment strategies. *Otolaryngology--Head and Neck Surgery, 148*(1), 29-39.

Ichimura, K., Mungall, A. J., Fiegler, H., Pearson, D. M., Dunham, I., Carter, N. P., & Collins, V. P. (2006). Small regions of overlapping deletions on 6q26 in human astrocytic tumours identified using chromosome 6 tile path array-CGH. *Oncogene, 25*(8), 1261-1271.

Imbalzano, K. M., Tatarkova, I., Imbalzano, A. N., & Nickerson, J. A. (2009). Increasingly transformed MCF-10A cells have a progressively tumor-like phenotype in three-dimensional basement membrane culture. *Cancer Cell International, 9*(1), 1-11.

Ishida, E., Ogawa, T., Rokugo, M., Ishikawa, T., Wakamori, S., Ohkoshi, A., Usubuchi, H., Higashi, K., Ishii, R., & Nakanome, A. (2020). Management of adenoid cystic carcinoma of the head and neck: a single-institute study with over 25-year follow-up. *Head & Face Medicine, 16*, 1-9.

Izquierdo, M. A., Van Der Valk, P., Van Ark-otte, J., Rubio, G., Germa-Lluch, J. R., Ueda, R., Scheper, R. J., Takahashi, T., & Giaccone, G. (1995). Differential expression of the c-kit proto-oncogene in germ cell tumours. *The Journal of Pathology, 177*(3), 253-258.

Jakob, J. A., Kies, M. S., Glisson, B. S., Kupferman, M. E., Liu, D. D., Lee, J. J., El-Naggar, A. K., Gonzalez–Angulo, A. M., & Blumenschein Jr, G. R. (2015). Phase II study of gefitinib in patients with advanced salivary gland cancers. *Head & Neck, 37*(5), 644-649.

Jaso, J., & Malhotra, R. (2011). Adenoid cystic carcinoma. *Archives of Pathology & Laboratory Medicine, 135*(4), 511-515.

Jiang, N., Liao, Y., Wang, M., Wang, Y., Wang, K., Guo, J., Wu, P., Zhong, B., Guo, T., & Wu, C. (2021). BUB1 drives the occurrence and development of bladder cancer by mediating the STAT3 signaling pathway. *Journal of Experimental & Clinical Cancer Research, 40*(1), 1-17.

Jiang, Y., Gao, R., Cao, C., Forbes, L., Li, J., Freeberg, S., Fredenburg, K. M., Justice, J. M., Silver, N. L., & Wu, L. (2019). MYB-activated models for testing therapeutic agents in adenoid cystic carcinoma. *Oral Oncology, 98*, 147-155.

Jones, A. S., Hamilton, J. W., Rowley, H., Husband, D., & Helliwell, T. R. (1997). Adenoid cystic carcinoma of the head and neck. *Clinical Otolaryngology & Allied Sciences, 22*(5), 434-443.

Ju, W., Zhao, T., Liu, Y., Tan, Y., Dong, M., Sun, Q., Wang, L., Li, J., & Zhong, L. (2019). Computed tomographic features of adenoid cystic carcinoma in the palate. *Cancer Imaging, 19*, 1-9.

Kaestner, P., Aigner, A., & Bastians, H. (2011). Therapeutic targeting of the mitotic spindle checkpoint through nanoparticle-mediated siRNA delivery inhibits tumor growth in vivo. *Cancer Letters, 304*(2), 128-136.

Kanei-Ishii, C., Yasukawa, T., Morimoto, R. I., & Ishii, S. (1994). c-Myb-induced trans-activation mediated by heat shock elements without sequence-specific DNA binding of c-Myb. *Journal of Biological Chemistry, 269*(22), 15768-15775.

Kang, J., Yang, M., Li, B., Qi, W., Zhang, C., Shokat, K. M., Tomchick, D. R., Machius, M., & Yu, H. (2008). Structure and substrate recruitment of the human spindle checkpoint kinase Bub1. *Molecular Cell, 32*(3), 394-405.

Kasper, L. H., Boussouar, F., Ney, P. A., Jackson, C. W., Rehg, J., Van Deursen, J. M., & Brindle, P. K. (2002). A transcription-factor-binding surface of coactivator p300 is required for haematopoiesis. *Nature, 419*(6908), 738-743.

Kastan, M. B., Slamon, D. J., & Civin, C. I. (1989). Expression of protooncogene c-myb in normal human hematopoietic cells.

Kawashima, S. A., Yamagishi, Y., Honda, T., Ishiguro, K., & Watanabe, Y. (2010). Phosphorylation of H2A by Bub1 prevents chromosomal instability through localizing shugoshin. *Science, 327*(5962), 172-177.

Khan, A. J., DiGiovanna, M. P., Ross, D. A., Sasaki, C. T., Carter, D., Son, Y. H., & Haffty, B. G. (2001). Adenoid cystic carcinoma: a retrospective clinical review. *International Journal of Cancer, 96*(3), 149-158.

Kim, D., Pertea, G., Trapnell, C., Pimentel, H., Kelley, R., & Salzberg, S. L. (2013). TopHat2: accurate alignment of transcriptomes in the presence of insertions, deletions and gene fusions. *Genome Biology, 14*(4), 1-13.

Kim, D. J. (2021). Transcription Factors as Direct Mediators of Homeostasis and Defense, Yale Graduate *School of Arts and Sciences Dissertations. 258.*

Kim, M., Kim, J. S., Roh, J., Lee, J. H., Cho, K., Choi, S., Nam, S. Y., & Kim, S. Y. (2013). Utility of 18 F-FDG PET/CT for detecting neck metastasis in patients with salivary gland carcinomas: preoperative planning for necessity and extent of neck dissection. *Annals of Surgical Oncology, 20*, 899-905.

Kim, T., & Gartner, A. (2021). Bub1 kinase in the regulation of mitosis. *Animal Cells and Systems, 25*(1), 1-10.

Kishi, H., Jin, Z., Wei, X., Nagata, T., Matsuda, T., Saito, S., & Muraguchi, A. (2002). Cooperative binding of c-Myb and Pax-5 activates the RAG-2 promoter in immature B cells. *Blood, the Journal of the American Society of Hematology, 99*(2), 576-583.

Klebig, C., Korinth, D., & Meraldi, P. (2009). Bub1 regulates chromosome segregation in a kinetochore-independent manner. *Journal of Cell Biology, 185*(5), 841-858.

Knighton, D. R., Zheng, J., Ten Eyck, L. F., Ashford, V. A., Xuong, N., Taylor, S. S., & Sowadski, J. M. (1991). Crystal structure of the catalytic subunit of cyclic adenosine monophosphate-dependent protein kinase. *Science, 253*(5018), 407-414.

Kokemueller, H., Eckardt, A., Brachvogel, P., & Hausamen, J. (2004). Adenoid cystic carcinoma of the head and neck—a 20 years experience. *International Journal of Oral and Maxillofacial Surgery, 33*(1), 25-31.

Kopan, R., & Ilagan, M. X. G. (2009). The canonical Notch signaling pathway: unfolding the activation mechanism. *Cell, 137*(2), 216-233.

Kops, G. J., Weaver, B. A., & Cleveland, D. W. (2005). On the road to cancer: aneuploidy and the mitotic checkpoint. *Nature Reviews Cancer, 5*(10), 773-785.

Korpal, M., Lee, E. S., Hu, G., & Kang, Y. (2008). The miR-200 family inhibits epithelial-mesenchymal transition and cancer cell migration by direct targeting of E-cadherin transcriptional repressors ZEB1 and ZEB2. *Journal of Biological Chemistry, 283*(22), 14910-14914.

Ku, D., Wen, S., Engelhard, A., Nicolaides, N. C., Lipson, K. E., Marino, T. A., & Calabretta, B. (1993). c-myb transactivates cdc2 expression via Myb binding sites in the 5'-flanking region of the human cdc2 gene. *Journal of Biological Chemistry, 268*(3), 2255-2259.

Lahortiga, I., De Keersmaecker, K., Van Vlierberghe, P., Graux, C., Cauwelier, B., Lambert, F., Mentens, N., Beverloo, H. B., Pieters, R., & Speleman, F. (2007). Duplication of the MYB oncogene in T cell acute lymphoblastic leukemia. *Nature Genetics, 39*(5), 593-595.

Lambert, M., Jambon, S., Depauw, S., & David-Cordonnier, M. (2018). Targeting transcription factors for cancer treatment. *Molecules, 23*(6), 1479.

Langmead, B., & Salzberg, S. L. (2012). Fast gapped-read alignment with Bowtie 2. *Nature Methods, 9*(4), 357-359.

Laurie, S. A., Ho, A. L., Fury, M. G., Sherman, E., & Pfister, D. G. (2011). Systemic therapy in the management of metastatic or locally recurrent adenoid cystic carcinoma of the salivary glands: a systematic review. *The Lancet Oncology, 12*(8), 815-824.

Lausen, J., Liu, S., Fliegauf, M., Lübbert, M., & Werner, M. H. (2006). ELA2 is regulated by hematopoietic transcription factors, but not repressed by AML1-ETO. *Oncogene, 25*(9), 1349-1357.

Ledford, H. (2016). Cocktails for cancer with a measure of immunotherapy. *Nature, 532*(7598), 162-164.

Lee, A., Givi, B., Osborn, V. W., Schwartz, D., & Schreiber, D. (2017). Patterns of care and survival of adjuvant radiation for major salivary adenoid cystic carcinoma. *The Laryngoscope, 127*(9), 2057-2062.

Lee, H., Lazor, J. W., Assadsangabi, R., & Shah, J. (2019). An imager's guide to perineural tumor spread in head and neck cancers: Radiologic footprints on 18F-FDG PET, with CT and MRI correlates. *Journal of Nuclear Medicine, 60*(3), 304-311.

Lee, H., Trainer, A. H., Friedman, L. S., Thistlethwaite, F. C., Evans, M. J., Ponder, B. A. J., & Venkitaraman, A. R. (1999). Mitotic Checkpoint Inactivation Fosters Transformation in Cells Lacking the Breast Cancer Susceptibility Gene, Brca2. *Molecular Cell, 4*(1), 1-10. 10.1016/S1097-2765(00)80182-3

Lee, Y., Wong, K. T., King, A. D., & Ahuja, A. T. (2008). Imaging of salivary gland tumours. *European Journal of Radiology, 66*(3), 419-436.

Leontiou, I., London, N., May, K. M., Ma, Y., Grzesiak, L., Medina-Pritchard, B., Amin, P., Jeyaprakash, A. A., Biggins, S., & Hardwick, K. G. (2019). The Bub1-TPR domain interacts directly with Mad3 to generate robust spindle checkpoint arrest. *Current Biology, 29*(14), 2407-2414. e7.

Li, G., & Zhang, H. (2004). Mad2 and p27 expression profiles in colorectal cancer and its clinical significance. *World Journal of Gastroenterology: WJG, 10*(21), 3218.

Li, H., Handsaker, B., Wysoker, A., Fennell, T., Ruan, J., Homer, N., Marth, G., Abecasis, G., Durbin, R., & 1000 Genome Project Data Processing Subgroup. (2009). The sequence alignment/map format and SAMtools. *Bioinformatics, 25*(16), 2078-2079.

Li, J., Perlaky, L., Rao, P., Weber, R. S., & El-Naggar, A. K. (2014). Development and characterization of salivary adenoid cystic carcinoma cell line. *Oral Oncology, 50*(10), 991-999.

Li, M., Chen, F., Clifton, N., Sullivan, D. M., Dalton, W. S., Gabrilovich, D. I., & Nefedova, Y. (2010). Combined inhibition of Notch signaling and Bcl-2/Bcl-xL results in synergistic antimyeloma effect. *Molecular Cancer Therapeutics, 9*(12), 3200-3209.

Li, M., Duan, X., Xiao, Y., Yuan, M., Zhao, Z., Cui, X., Wu, D., & Shi, J. (2022). BUB1 is identified as a potential therapeutic target for pancreatic cancer treatment. *Frontiers in Public Health,* , 1503.

Li, N., Xu, L., Zhao, H., El-Naggar, A. K., & Sturgis, E. M. (2012). A comparison of the demographics, clinical features, and survival of patients with adenoid cystic carcinoma of major and minor salivary glands versus less common sites within the Surveillance, Epidemiology, and End Results registry. *Cancer, 118*(16), 3945-3953.

Li, P., Yuan, H., Kuang, X., Zhang, T., & Ma, L. (2022). Network module function enrichment analysis of lung squamous cell carcinoma and lung adenocarcinoma. *Medicine, 101*(47), e31798.

Li, R., & Murray, A. W. (1991). Feedback control of mitosis in budding yeast. *Cell, 66*(3), 519-531.

Li, X., He, J., Yu, M., Zhang, W., & Sun, J. (2020). BUB1 gene is highly expressed in gastric cancer: analysis based on Oncomine database and bioinformatics. *Nan Fang Yi Ke Da Xue Xue Bao= Journal of Southern Medical University, 40*(5), 683-692.

Li, Y., Jin, K., van Pelt, G. W., van Dam, H., Yu, X., Mesker, W. E., Ten Dijke, P., Zhou, F., & Zhang, L. (2016). c-Myb Enhances Breast Cancer Invasion and Metastasis through the Wnt/β-Catenin/Axin2 Pathwayc-Myb Potentiates Wnt Signaling in Breast Cancer. *Cancer Research, 76*(11), 3364-3375.

Licitra, L., Cavina, R., Grandi, C., Di Palma, S., Guzzo, M., Demicheli, R., & Molinari, R. (1996). Cisplatin, doxorubicin and cyclophosphamide in advanced salivary gland carcinoma. *Annals of Oncology, 7*(6), 640-642.

Licitra, L., Marchini, S., Spinazzè, S., Rossi, A., Rocca, A., Grandi, C., & Molinari, R. (1991). Cisplatin in advanced salivary gland carcinoma. A phase II study of 25 patients. *Cancer, 68*(9), 1874-1877.

Lieu, Y. K., & Reddy, E. P. (2009). Conditional c-myb knockout in adult hematopoietic stem cells leads to loss of self-renewal due to impaired proliferation and accelerated differentiation. *Proceedings of the National Academy of Sciences, 106*(51), 21689-21694.

Lin, G., Chai, J., Yuan, S., Mai, C., Cai, L., Murphy, R. W., Zhou, W., & Luo, J. (2016). VennPainter: a tool for the comparison and identification of candidate genes based on Venn diagrams. *PloS One, 11*(4), e0154315.

Lindsley, K. L., Cho, P., Stelzer, K. J., Koh, W. J., Austin-Seymour, M., Russell, K. J., Laramore, G. E., & Griffin, T. W. (1996). Clinical trials of neutron radiotherapy in the United States. *Bulletin Du Cancer/Radiothérapie, 83*, 78s-86s.

Lipsick, J. S., & Baluda, M. A. (1986). The myb oncogene. *Gene Amplification and Analysis, 4*, 73-98.

Lipsick, J. S., & Wang, D. (1999). Transformation by v-Myb. *Oncogene, 18*(19), 3047-3055.

Liu, F., Lei, W., O'Rourke, J. P., & Ness, S. A. (2006). Oncogenic mutations cause dramatic, qualitative changes in the transcriptional activity of c-Myb. *Oncogene, 25*(5), 795-805.

Liu, J., Shao, C., Tan, M. L., Mu, D., Ferris, R. L., & Ha, P. K. (2012). Molecular biology of adenoid cystic carcinoma. *Head & Neck, 34*(11), 1665-1677.

Lloyd, S., James, B. Y., Wilson, L. D., & Decker, R. H. (2011). Determinants and patterns of survival in adenoid cystic carcinoma of the head and neck, including an analysis of adjuvant radiation therapy. *American Journal of Clinical Oncology, 34*(1), 76-81.

Locati, L. D., Bossi, P., Perrone, F., Potepan, P., Crippa, F., Mariani, L., Casieri, P., Orsenigo, M., Losa, M., & Bergamini, C. (2009). Cetuximab in recurrent and/or metastatic salivary gland carcinomas: a phase II study. *Oral Oncology, 45*(7), 574-578.

Locati, L. D., Perrone, F., Losa, M., Mela, M., Casieri, P., Orsenigo, M., Cortelazzi, B., Negri, T., Tamborini, E., & Quattrone, P. (2009). Treatment relevant target immunophenotyping of 139 salivary gland carcinomas (SGCs). *Oral Oncology, 45*(11), 986-990.

Lorenzo, P. I., Brendeford, E. M., Gilfillan, S., Gavrilov, A. A., Leedsak, M., Razin, S. V., Eskeland, R., Sæther, T., & Gabrielsen, O. S. (2011). Identification of c-Myb target genes in K562 cells reveals a role for c-Myb as a master regulator. *Genes & Cancer, 2*(8), 805-817.

Lourenco, C., Kalkat, M., Houlahan, K. E., De Melo, J., Longo, J., Done, S. J., Boutros, P. C., & Penn, L. Z. (2019). Modelling the MYC-driven normal-to-tumour switch in breast cancer. *Disease Models & Mechanisms, 12*(7), dmm038083.

Love, M. I., Huber, W., & Anders, S. (2014). Moderated estimation of fold change and dispersion for RNA-seq data with DESeq2. *Genome Biology, 15*(12), 1-21.

Lüscher, B., Christenson, E., Litchfield, D. W., Krebs, E. G., & Eisenman, R. N. (1990). Myb DNA binding inhibited by phosphorylation at a site deleted during oncogenic activation. *Nature, 344*(6266), 517-522.

Lutwyche, J. K., Keough, R. A., Hunter, J., Coles, L. S., & Gonda, T. J. (2006). DNA binding-independent transcriptional activation of the vascular endothelial growth factor gene (VEGF) by the Myb oncoprotein. *Biochemical and Biophysical Research Communications, 344*(4), 1300-1307.

Ma, W. W., & Adjei, A. A. (2009). Novel agents on the horizon for cancer therapy. *CA: A Cancer Journal for Clinicians, 59*(2), 111-137.

Macarenco, R. S., Uphoff, T. S., Gilmer, H. F., Jenkins, R. B., Thibodeau, S. N., Lewis, J. E., Molina, J. R., Yang, P., & Aubry, M. (2008). Salivary gland-type lung carcinomas: an EGFR immunohistochemical, molecular genetic, and mutational analysis study. *Modern Pathology, 21*(9), 1168-1175.

Madden, S. K., de Araujo, A. D., Gerhardt, M., Fairlie, D. P., & Mason, J. M. (2021). Taking the Myc out of cancer: toward therapeutic strategies to directly inhibit c-Myc. *Molecular Cancer, 20*(1), 1-18.

Mahmood, U., Koshy, M., Goloubeva, O., & Suntharalingam, M. (2011). Adjuvant radiation therapy for high-grade and/or locally advanced major salivary gland tumors. *Archives of Otolaryngology–Head & Neck Surgery, 137*(10), 1025-1030.

Malaterre, J., Carpinelli, M., Ernst, M., Alexander, W., Cooke, M., Sutton, S., Dworkin, S., Heath, J. K., Frampton, J., & McArthur, G. (2007). c-Myb is required for progenitor cell homeostasis in colonic crypts. *Proceedings of the National Academy of Sciences, 104*(10), 3829-3834.

Mandelbaum, J., Shestopalov, I. A., Henderson, R. E., Chau, N. G., Knoechel, B., Wick, M. J., & Zon, L. I. (2018). Zebrafish blastomere screen identifies retinoic acid suppression of MYB in adenoid cystic carcinoma. *Journal of Experimental Medicine, 215*(10), 2673-2685.

Mansour, M. R., Abraham, B. J., Anders, L., Berezovskaya, A., Gutierrez, A., Durbin, A. D., Etchin, J., Lawton, L., Sallan, S. E., & Silverman, L. B. (2014). An oncogenic super-enhancer formed through somatic mutation of a noncoding intergenic element. *Science, 346*(6215), 1373-1377.

Marceau, A. H., Brison, C. M., Nerli, S., Arsenault, H. E., McShan, A. C., Chen, E., Lee, H., Benanti, J. A., Sgourakis, N. G., & Rubin, S. M. (2019). An order-to-disorder structural switch activates the FoxM1 transcription factor. *Elife, 8*, e46131.

Marchio, C., Weigelt, B., & Reis-Filho, J. S. (2010). Adenoid cystic carcinomas of the breast and salivary glands (or 'The strange case of Dr Jekyll and Mr Hyde'of exocrine gland carcinomas). *Journal of Clinical Pathology, 63*(3), 220-228.

Matsuzaki, H., Hara, M., Yanagi, Y., Asaumi, J., Katase, N., Unetsubo, T., Hisatomi, M., Konouchi, H., Takenobu, T., & Nagatsuka, H. (2012). Magnetic resonance imaging (MRI) and dynamic MRI evaluation of extranodal non-Hodgkin lymphoma in oral and maxillofacial regions. *Oral Surgery, Oral Medicine, Oral Pathology and Oral Radiology, 113*(1), 126-133.

Matsuzaki, H., Yanagi, Y., Hara, M., Katase, N., Hisatomi, M., Unetsubo, T., Konouchi, H., Takenobu, T., Nagatsuka, H., & Asaumi, J. (2012). Diagnostic value of dynamic contrast-enhanced MRI for submucosal palatal tumors. *European Journal of Radiology, 81*(11), 3306-3312.

Mattox, D. E., Von Hoff, D. D., & Balcerzak, S. P. (1990). Southwest Oncology Group study of mitoxantrone for treatment of patients with advanced adenoid cystic carcinoma of the head and neck. *Investigational New Drugs, 8*, 105-107.

Maurice, D., Hooper, J., Lang, G., & Weston, K. (2007). c-Myb regulates lineage choice in developing thymocytes via its target gene Gata3. *The EMBO Journal, 26*(15), 3629-3640.

McIntyre, J. B., Ko, J. J., Siever, J., Chan, A. M., Simpson, R. H., Hao, D., & Lau, H. Y. (2019). MYB-NFIB gene fusions identified in archival adenoid cystic carcinoma tissue employing NanoString analysis: an exploratory study. *Diagnostic Pathology, 14*, 1-11.

Meyer, C., Schneider, B., Jakob, S., Strehl, S., Attarbaschi, A., Schnittger, S., Schoch, C., Jansen, M., van Dongen, J., & Den Boer, M. L. (2006). The MLL recombinome of acute leukemias. *Leukemia, 20*(5), 777-784.

Meyer-Ficca, M. L., Meyer, R. G., Kaiser, H., Brack, A. R., Kandolf, R., & Küpper, J. (2004). Comparative analysis of inducible expression systems in transient transfection studies. *Analytical Biochemistry, 334*(1), 9-19.

Millar, B. M., Kerba, M., Youngson, B., Lockwood, G. A., & Liu, F. (2004). The potential role of breast conservation surgery and adjuvant breast radiation for adenoid cystic carcinoma of the breast. *Breast Cancer Research and Treatment, 87*, 225-232.

Miller, E. D., Blakaj, D. M., Swanson, B. J., Xiao, W., Gillison, M. L., Wei, L., Bhatt, A. D., Diavolitsis, V. M., Wobb, J. L., & Kang, S. Y. (2017). Sinonasal adenoid cystic carcinoma: treatment outcomes and association with human papillomavirus. *Head & Neck, 39*(7), 1405-1411.

Miller, L. E., Au, V., Mokhtari, T. E., Goss, D., Faden, D. L., & Varvares, M. A. (2022). A contemporary review of molecular therapeutic targets for adenoid cystic carcinoma. *Cancers, 14*(4), 992.

Mink, S., Kerber, U., & Klempnauer, K. (1996). Interaction of C/EBPbeta and v-Myb is required for synergistic activation of the mim-1 gene. *Molecular and Cellular Biology, 16*(4), 1316-1325.

Mitani, Y., Liu, B., Rao, P. H., Borra, V. J., Zafereo, M., Weber, R. S., Kies, M., Lozano, G., Futreal, P. A., & Caulin, C. (2016). Novel MYBL1 Gene Rearrangements with Recurrent MYBL1–NFIB Fusions in Salivary Adenoid Cystic Carcinomas Lacking t (6; 9) TranslocationsMYBL1–NFIB Fusions in Adenoid Cystic Carcinoma. *Clinical Cancer Research, 22*(3), 725-733.

Mitani, Y., Rao, P. H., Futreal, P. A., Roberts, D. B., Stephens, P. J., Zhao, Y., Zhang, L., Mitani, M., Weber, R. S., & Lippman, S. M. (2011). Novel Chromosomal Rearrangements and Break Points at the t (6; 9) in Salivary Adenoid Cystic Carcinoma: Association with MYB–NFIB Chimeric Fusion, MYB Expression, and Clinical OutcomeAlterations Related to t (6; 9) in Adenoid Cystic Carcinoma. *Clinical Cancer Research, 17*(22), 7003-7014.

Mitra, P., Yang, R., Sutton, J., Ramsay, R. G., & Gonda, T. J. (2016). CDK9 inhibitors selectively target estrogen receptor-positive breast cancer cells through combined inhibition of MYB and MCL-1 expression. *Oncotarget, 7*(8), 9069-9083.

Molina, J. R., Aubry, M. C., Lewis, J. E., Wampfler, J. A., Williams, B. A., Midthun, D. E., Yang, P., & Cassivi, S. D. (2007). Primary salivary gland-type lung cancer: spectrum of clinical presentation, histopathologic and prognostic factors. *Cancer: Interdisciplinary International Journal of the American Cancer Society, 110*(10), 2253-2259.

Morales, A. G., Pezuk, J. A., Brassesco, M. S., de Oliveira, J. C., de Paula Queiroz, R. G., Machado, H. R., Carlotti, C. G., Neder, L., de Oliveira, H. F., & Scrideli, C. A. (2013). BUB1 and BUBR1 inhibition decreases proliferation and colony formation, and enhances radiation sensitivity in pediatric glioblastoma cells. *Child's Nervous System, 29*(12), 2241-2248.

Morita, N., Murase, T., Ueda, K., Nagao, T., Kusafuka, K., Nakaguro, M., Urano, M., Taguchi, K., Yamamoto, H., & Kano, S. (2021). Pathological evaluation of tumor grade for salivary adenoid cystic carcinoma: A proposal of an objective grading system. *Cancer Science, 112*(3), 1184-1195.

Morse, E., Fujiwara, R. J., Judson, B., Prasad, M. L., & Mehra, S. (2019). Positive surgical margins in parotid malignancies: institutional variation and survival association. *The Laryngoscope, 129*(1), 129-137.

Moskaluk, C. A. (2013). Adenoid cystic carcinoma: clinical and molecular features. *Head and Neck Pathology, 7*, 17-22.

Moskaluk, C. A., Baras, A. S., Mancuso, S. A., Fan, H., Davidson, R. J., Dirks, D. C., Golden, W. L., & Frierson, H. F. (2011). Development and characterization of xenograft model systems for adenoid cystic carcinoma. *Laboratory Investigation, 91*(10), 1480-1490.

Mu, X., Li, Y., He, L., Guan, H., Wang, J., Wei, Z., He, Y., Liu, Z., Li, R., & Peng, X. (2021). Prognostic nomogram for adenoid cystic carcinoma in different anatomic sites. *Head & Neck, 43*(1), 48-59.

Mucenski, M. L., McLain, K., Kier, A. B., Swerdlow, S. H., Schreiner, C. M., Miller, T. A., Pietryga, D. W., Scott Jr, W. J., & Potter, S. S. (1991). A functional c-myb gene is required for normal murine fetal hepatic hematopoiesis. *Cell, 65*(4), 677-689.

Mulholland, P. J., Fiegler, H., Mazzanti, C., Gorman, P., Sasieni, P., Adams, J., Jones, T. A., Babbage, J. W., Vatcheva, R., & Ichimura, K. (2006). Genomic profiling identifies discrete deletions associated with translocations in glioblastoma multiforme. *Cell Cycle, 5*(7), 783-791.

Mur, P., De Voer, R. M., Olivera-Salguero, R., Rodríguez-Perales, S., Pons, T., Setién, F., Aiza, G., Valdés-Mas, R., Bertini, A., & Pineda, M. (2018). Germline mutations in the spindle assembly checkpoint genes BUB1 and BUB3 are infrequent in familial colorectal cancer and polyposis. *Molecular Cancer, 17*(1), 1-6.

Myrie, K. A., Percy, M. J., Azim, J. N., Neeley, C. K., & Petty, E. M. (2000). Mutation and expression analysis of human BUB1 and BUB1B in aneuploid breast cancer cell lines. *Cancer Letters, 152*(2), 193-199. 10.1016/S0304-3835(00)00340-2

Nagel, S., Kaufmann, M., Scherr, M., Drexler, H. G., & MacLeod, R. A. (2005). Activation of HLXB9 by juxtaposition with MYB via formation of t (6; 7)(q23; q36) in an AML-M4 cell line (GDM-1). *Genes, Chromosomes and Cancer, 42*(2), 170-178.

Nakagawa, T., Kollmeyer, T. M., Morlan, B. W., Anderson, S. K., Bergstralh, E. J., Davis, B. J., Asmann, Y. W., Klee, G. G., Ballman, K. V., & Jenkins, R. B. (2008). A tissue biomarker panel predicting systemic progression after PSA recurrence post-definitive prostate cancer therapy. *PloS One, 3*(5), e2318.

Nakagoshi, H., Kanei-Ishii, C., Sawazaki, T., Mizuguchi, G., & Ishii, S. (1992). Transcriptional activation of the c-myc gene by the c-myb and B-myb gene products. *Oncogene, 7*(6), 1233-1240.

Nakata, Y., Shetzline, S., Sakashita, C., Kalota, A., Rallapalli, R., Rudnick, S. I., Zhang, Y., Emerson, S. G., & Gewirtz, A. M. (2007). c-Myb contributes to G2/M cell cycle transition in human hematopoietic cells by direct regulation of cyclin B1 expression. *Molecular and Cellular Biology, 27*(6), 2048-2058.

Nascimento, A. G., Amaral, A. L. P., Prado, L. A. F., Kligerman, J., & Silveira, T. R. P. (1986). Adenoid cystic carcinoma of salivary glands. A study of 61 cases with clinicopathologic correlation. *Cancer, 57*(2), 312-319.

Naylor, E., Sarkar, P., Perlis, C. S., Giri, D., Gnepp, D. R., & Robinson-Bostom, L. (2008). Primary cutaneous adenoid cystic carcinoma. *Journal of the American Academy of Dermatology, 58*(4), 636-641.

NCCN clinical practice guidelines in oncology, Head and Neck Cancers (2019). Available at http://www.nccn.org.

Ning, Y., He, W., Bian, D., Xie, D., & Jiang, G. (2019). Tracheo–bronchial adenoid cystic carcinoma: A retrospective study. *Asia-Pacific Journal of Clinical Oncology, 15*(4), 244-249.

Nocka, K., Majumder, S., Chabot, B., Ray, P., Cervone, M., Bernstein, A., & Besmer, P. (1989). Expression of c-kit gene products in known cellular targets of W mutations in normal and

W mutant mice--evidence for an impaired c-kit kinase in mutant mice. *Genes & Development, 3*(6), 816-826.

Nomura, N., Takahashi, M., Matsui, M., Ishii, S., Date, T., Sasamoto, S., & Ishizaki, R. (1988). Isolation of human cDNA clones of myb-related genes, A-myb and B-myb. *Nucleic Acids Research, 16*(23), 11075-11089.

Nordgård, S., Franzén, G., Boysen, M., & Halvorsen, T. B. (1997). Ki-67 as a prognostic marker in adenoid cystic carcinoma assessed with the monoclonal antibody MIB1 in paraffin sections. *The Laryngoscope, 107*(4), 531-536.

Nordkvist, A., Mark, J., Gustafsson, H., Bang, G., & Stenman, G. (1994). Non-random chromosome rearrangements in adenoid cystic carcinoma of the salivary glands. *Genes, Chromosomes and Cancer, 10*(2), 115-121.

North, J. P., McCalmont, T. H., Fehr, A., van Zante, A., Stenman, G., & LeBoit, P. E. (2015). Detection of MYB alterations and other immunohistochemical markers in primary cutaneous adenoid cystic carcinoma. *The American Journal of Surgical Pathology, 39*(10), 1347-1356.

Nyati, S., Schinske-Sebolt, K., Pitchiaya, S., Chekhovskiy, K., Chator, A., Chaudhry, N., Dosch, J., Van Dort, M. E., Varambally, S., & Kumar-Sinha, C. (2015). The kinase activity of the Ser/Thr kinase BUB1 promotes TGF-β signaling. *Science Signaling, 8*(358), ra1.

O'Brien, C. A., Kreso, A., & Dick, J. E. (2009). Cancer stem cells in solid tumors: an overview. Paper presented at the *Seminars in Radiation Oncology, , 19*(2) 71-77.

Ochel, H., Gademann, G., Röcken, C., & Wördehoff, H. (2005). Effects of imatinib mesylate on adenoid cystic carcinomas. *Anticancer Research, 25*(5), 3659-3664.

OelgeschlaÈger, M., Kowenz-Leutz, E., Schreek, S., Leutz, A., & LuÈscher, B. (2001). Tumorigenic N-terminal deletions of c-Myb modulate DNA binding, transactivation, and cooperativity with C/EBP. *Oncogene, 20*(50), 7420-7424.

Oelgeschläger, M., Janknecht, R., Krieg, J., Schreek, S., & Lüscher, B. (1996). Interaction of the co-activator CBP with Myb proteins: effects on Myb-specific transactivation and on the cooperativity with NF-M. *The EMBO Journal, 15*(11), 2771-2780.

Oelgeschläger, M., Nuchprayoon, I., Lüscher, B., & Friedman, A. D. (1996). C/EBP, c-Myb, and PU. 1 cooperate to regulate the neutrophil elastase promoter. *Molecular and Cellular Biology, 16*(9), 4717-4725.

Ogata, K., Hojo, H., Aimoto, S., Nakai, T., Nakamura, H., Sarai, A., Ishii, S., & Nishimura, Y. (1992). Solution structure of a DNA-binding unit of Myb: a helix-turn-helix-related motif with conserved tryptophans forming a hydrophobic core. *Proceedings of the National Academy of Sciences, 89*(14), 6428-6432.

Oh, I., & Reddy, E. P. (1999). The myb gene family in cell growth, differentiation and apoptosis. *Oncogene, 18*(19), 3017-3033.

Ohshima, K., Haraoka, S., Yoshioka, S., Hamasaki, M., Fujiki, T., Suzumiya, J., Kawasaki, C., Kanda, M., & Kikuchi, M. (2000). Mutation analysis of mitotic checkpoint genes (hBUB1

and hBUBR1) and microsatellite instability in adult T-cell leukemia/lymphoma. *Cancer Letters, 158*(2), 141-150.

Okada, M., Tada, M., Kanda, N., Masuda, M., Mizoguchi, H., Kazuma, M., Wada, E., Kubota, K., & Nomura, Y. (1990). c-myb gene analysis in T-cell malignancies with del (6q). *Cancer Genetics and Cytogenetics, 48*(2), 229-236.

Okada, T., Kamada, T., Tsuji, H., Mizoe, J., Baba, M., Kato, S., Yamada, S., Sugahara, S., Yasuda, S., & Yamamoto, N. (2010). Carbon ion radiotherapy: clinical experiences at National Institute of Radiological Science (NIRS). *Journal of Radiation Research, 51*(4), 355-364.

Oplatek, A., Ozer, E., Agrawal, A., Bapna, S., & Schuller, D. E. (2010). Patterns of recurrence and survival of head and neck adenoid cystic carcinoma after definitive resection. *The Laryngoscope, 120*(1), 65-70.

O'Rourke, J. P., & Ness, S. A. (2008). Alternative RNA splicing produces multiple forms of c-Myb with unique transcriptional activities. *Molecular and Cellular Biology, 28*(6), 2091-2101.

Panaccione, A., Zhang, Y., Ryan, M., Moskaluk, C. A., Anderson, K. S., Yarbrough, W. G., & Ivanov, S. V. (2017). MYB fusions and CD markers as tools for authentication and purification of cancer stem cells from salivary adenoid cystic carcinoma. *Stem Cell Research, 21*, 160-166.

Park, S., Gaur, A. B., Lengyel, E., & Peter, M. E. (2008). The miR-200 family determines the epithelial phenotype of cancer cells by targeting the E-cadherin repressors ZEB1 and ZEB2. *Genes & Development, 22*(7), 894-907.

Park, S., Vora, M., van Zante, A., Humtsoe, J., Kim, H., Yom, S., Agarwal, S., & Ha, P. (2020). Clinicopathologic implications of Myb and Beta-catenin expression in adenoid cystic carcinoma. *Journal of Otolaryngology-Head & Neck Surgery, 49*, 1-8.

Parker, D., Rivera, M., Zor, T., Henrion-Caude, A., Radhakrishnan, I., Kumar, A., Shapiro, L. H., Wright, P. E., Montminy, M., & Brindle, P. K. (1999). Role of secondary structure in discrimination between constitutive and inducible activators. *Molecular and Cellular Biology, 19*(8), 5601-5607.

Patel, K. J., Pambuccian, S. E., Ondrey, F. G., Adams, G. L., & Gaffney, P. M. (2006). Genes associated with early development, apoptosis and cell cycle regulation define a gene expression profile of adenoid cystic carcinoma. *Oral Oncology, 42*(10), 994-1004.

Peng, S., Lalani, S., Leavenworth, J. W., Ho, I., & Pauza, M. E. (2007). c-Maf interacts with c-Myb to down-regulate Bcl-2 expression and increase apoptosis in peripheral CD4 cells. *European Journal of Immunology, 37*(10), 2868-2880.

Penner, C. R., Folpe, A. L., & Budnick, S. D. (2002). C-kit expression distinguishes salivary gland adenoid cystic carcinoma from polymorphous low-grade adenocarcinoma. *Modern Pathology, 15*(7), 687-691.

Perera, D., Tilston, V., Hopwood, J. A., Barchi, M., Boot-Handford, R. P., & Taylor, S. S. (2007). Bub1 maintains centromeric cohesion by activation of the spindle checkpoint. *Developmental Cell, 13*(4), 566-579.

Pérez-Losada, J., Sánchez-Martın, M., Rodrıguez-Garcıa, A., Sánchez, M. L., Orfao, A., Flores, T., & Sánchez-Garcıa, I. (2002). Zinc-finger transcription factor Slug contributes to the function of the stem cell factor c-kit signaling pathway. *Blood, the Journal of the American Society of Hematology, 100*(4), 1274-1286.

Persson, M., Andersson, M. K., Mitani, Y., Brandwein-Weber, M. S., Frierson Jr, H. F., Moskaluk, C., Fonseca, I., Ferrarotto, R., Boecker, W., & Loening, T. (2022). Rearrangements, Expression, and Clinical Significance of MYB and MYBL1 in Adenoid Cystic Carcinoma: A Multi-Institutional Study. *Cancers, 14*(15), 3691.

Persson, M., Andrén, Y., Mark, J., Horlings, H. M., Persson, F., & Stenman, G. (2009). Recurrent fusion of MYB and NFIB transcription factor genes in carcinomas of the breast and head and neck. *Proceedings of the National Academy of Sciences, 106*(44), 18740-18744.

Persson, M., Andrén, Y., Moskaluk, C. A., Frierson Jr, H. F., Cooke, S. L., Futreal, P. A., Kling, T., Nelander, S., Nordkvist, A., & Persson, F. (2012). Clinically significant copy number alterations and complex rearrangements of MYB and NFIB in head and neck adenoid cystic carcinoma. *Genes, Chromosomes and Cancer, 51*(8), 805-817.

Perzin, K. H., Gullane, P., & Clairmont, A. C. (1978). Adenoid cystic carcinomas arising in salivary glands. A correlation of histologic features and clinical course. *Cancer, 42*(1), 265-282.

Pesenti, M. E., Weir, J. R., & Musacchio, A. (2016). Progress in the structural and functional characterization of kinetochores. *Current Opinion in Structural Biology, 37*, 152-163.

Pfeffer, M. R., Talmi, Y., Catane, R., Symon, Z., Yosepovitch, A., & Levitt, M. (2007). A phase II study of Imatinib for advanced adenoid cystic carcinoma of head and neck salivary glands. *Oral Oncology, 43*(1), 33-36.

Pham, T., Pereira, L., Roth, S., Galletta, L., Link, E., Akhurst, T., Solomon, B., Michael, M., Darcy, P., & Sampurno, S. (2019). First-in-human phase I clinical trial of a combined immune modulatory approach using TetMYB vaccine and Anti-PD-1 antibody in patients with advanced solid cancer including colorectal or adenoid cystic carcinoma: The MYPHISMO study protocol (NCT03287427). *Contemporary Clinical Trials Communications, 16*, 100409.

Piao, J., Zhu, L., Sun, J., Li, N., Dong, B., Yang, Y., & Chen, L. (2019). High expression of CDK1 and BUB1 predicts poor prognosis of pancreatic ductal adenocarcinoma. *Gene, 701*, 15-22.

Pilkinton, M., Sandoval, R., Song, J., Ness, S. A., & Colamonici, O. R. (2007). Mip/LIN-9 regulates the expression of B-Myb and the induction of cyclin A, cyclin B, and CDK1. *Journal of Biological Chemistry, 282*(1), 168-175.

Pinto, E., Chen, X., Rodriguez-Galindo, C., Zhang, J., Ribeiro, R., & Zambetti, G. (2016). Whole-genome sequencing identifies genetic alterations in pediatric adrenocortical tumors. *Horm.Res.Paediatr, 86*(1)

Poorten, V. V., Hunt, J., Bradley, P. J., Haigentz Jr, M., Rinaldo, A., Mendenhall, W. M., Suarez, C., Silver, C., Takes, R. P., & Ferlito, A. (2014). Recent trends in the management of minor salivary gland carcinoma. *Head & Neck, 36*(3), 444-455.

Putri, G. H., Anders, S., Pyl, P. T., Pimanda, J. E., & Zanini, F. (2022). Analysing high-throughput sequencing data in Python with HTSeq 2.0. *Bioinformatics, 38*(10), 2943-2945.

Queimado, L., Lopes, C., Du, F., Martins, C., Fonseca, I., Bowcock, A. M., Soares, J., & Lovett, M. (1999). In vitro transformation of cell lines from human salivary gland tumors. *International Journal of Cancer, 81*(5), 793-798.

Quelen, C., Lippert, E., Struski, S., Demur, C., Soler, G., Prade, N., Delabesse, E., Broccardo, C., Dastugue, N., & Mahon, F. (2011). Identification of a transforming MYB-GATA1 fusion gene in acute basophilic leukemia: a new entity in male infants. *Blood, the Journal of the American Society of Hematology, 117*(21), 5719-5722.

Quintana, A. M., Liu, F., O'Rourke, J. P., & Ness, S. A. (2011). Identification and regulation of c-Myb target genes in MCF-7 cells. *BMC Cancer, 11*(1), 1-12.

Ramaswamy, K., Forbes, L., Minuesa, G., Gindin, T., Brown, F., Kharas, M. G., Krivtsov, A. V., Armstrong, S. A., Still, E., & De Stanchina, E. (2018). Peptidomimetic blockade of MYB in acute myeloid leukemia. *Nature Communications, 9*(1), 1-13.

Ramkissoon, L. A., Horowitz, P. M., Craig, J. M., Ramkissoon, S. H., Rich, B. E., Schumacher, S. E., McKenna, A., Lawrence, M. S., Bergthold, G., & Brastianos, P. K. (2013). Genomic analysis of diffuse pediatric low-grade gliomas identifies recurrent oncogenic truncating rearrangements in the transcription factor MYBL1. *Proceedings of the National Academy of Sciences, 110*(20), 8188-8193.

Ramsay, R. G., Thompson, M. A., Hayman, J. A., Reid, G., Gonda, T. J., & Whitehead, R. H. (1992). Myb expression is higher in malignant human colonic carcinoma and premalignant adenomatous polyps than in normal mucosa. *Cell Growth and Differentiation, 3*, 723.

Ramsay, R. G. (2005). c-Myb a stem-progenitor cell regulator in multiple tissue compartments. *Growth Factors, 23*(4), 253-261.

Ramsay, R. G., & Gonda, T. J. (2008). MYB function in normal and cancer cells. *Nature Reviews Cancer, 8*(7), 523-534.

Ramsay, R. G., Morrice, N., Van Eeden, P., Kanagasundaram, V., Nomura, T., De Blaquiere, J., Ishii, S., & Wettenhall, R. (1995). Regulation of c-Myb through protein phosphorylation and leucine zipper interactions. *Oncogene, 11*(10), 2113-2120.

Rao, P. H., Roberts, D., Zhao, Y., Bell, D., Harris, C. P., Weber, R. S., & El-Naggar, A. K. (2008). Deletion of 1p32-p36 is the most frequent genetic change and poor prognostic marker in adenoid cystic carcinoma of the salivary glands. *Clinical Cancer Research, 14*(16), 5181-5187.

Ratajczak, M. Z., Perrotti, D., Melotti, P., Powzaniuk, M., Calabretta, B., Onodera, K., Kregenow, D. A., Machalinski, B., & Gewirtz, A. M. (1998). Myb and ets proteins are candidate regulators of c-kit expression in human hematopoietic cells. *Blood, the Journal of the American Society of Hematology, 91*(6), 1934-1946.

Reizis, B., & Leder, P. (2001). The upstream enhancer is necessary and sufficient for the expression of the pre-T cell receptor α gene in immature T lymphocytes. *The Journal of Experimental Medicine, 194*(7), 979-990.

Response evaluation criteria in solid tumors (RECIST 1.1), European Organisation for Research and Treatment of Cancer (EORTC), National Cancer Institute (NCI) (2000). Available at https://recist.eortc.org/recist-1-1-2/.

Rettig, E. M., Talbot Jr, C. C., Sausen, M., Jones, S., Bishop, J. A., Wood, L. D., Tokheim, C., Niknafs, N., Karchin, R., & Fertig, E. J. (2016). Whole-genome sequencing of salivary gland adenoid cystic carcinoma. *Cancer Prevention Research, 9*(4), 265-274.

Ricke, R. M., Jeganathan, K. B., Malureanu, L., Harrison, A. M., & Van Deursen, J. M. (2012). Bub1 kinase activity drives error correction and mitotic checkpoint control but not tumor suppression. *Journal of Cell Biology, 199*(6), 931-949.

Ricke, R. M., Jeganathan, K. B., & van Deursen, J. M. (2011). Bub1 overexpression induces aneuploidy and tumor formation through Aurora B kinase hyperactivation. *Journal of Cell Biology, 193*(6), 1049-1064.

Robin Charles, & Joseph A. Laboulbene. (1853). Trois productions morbides. *Compte Rendu De La Société De Biologie, 5*(185-196)

Roden, A. C., Greipp, P. T., Knutson, D. L., Kloft-Nelson, S. M., Jenkins, S. M., Marks, R. S., Aubry, M. C., & García, J. J. (2015). Histopathologic and cytogenetic features of pulmonary adenoid cystic carcinoma. *Journal of Thoracic Oncology, 10*(11), 1570-1575.

Roh, J., Ryu, C. H., Choi, S., Kim, J. S., Lee, J. H., Cho, K., Nam, S. Y., & Kim, S. Y. (2007). Clinical utility of 18F-FDG PET for patients with salivary gland malignancies. *Journal of Nuclear Medicine, 48*(2), 240-246.

Romani, C., Lorini, L., Bozzola, A., Bignotti, E., Tomasoni, M., Ardighieri, L., Bugatti, M., Battocchio, S., Ravaggi, A., & Tomasini, D. (2023). Functional profiles of curatively treated adenoid cystic carcinoma unveil prognostic features and potentially targetable pathways. *Scientific Reports, 13*(1), 1809.

Roskoski Jr, R. (2022). Properties of FDA-approved Small Molecule Protein Kinase Inhibitors: A 2023 Update. *Pharmacological Research,* , 106552.

Roussel, M., Saule, S., Lagrou, C., Rommens, C., Beug, H., Graf, T., & Stehelin, D. (1979). Three new types of viral oncogene of cellular origin specific for haematopoietic cell transformation. *Nature, 281*(5731), 452-455.

Ru, H. Y., Chen, R. L., Lu, W. C., & Chen, J. H. (2002). hBUB1 defects in leukemia and lymphoma cells. *Oncogene, 21*(30), 4673-4679.

Safdieh, J., Givi, B., Osborn, V., Lederman, A., Schwartz, D., & Schreiber, D. (2017). Impact of adjuvant radiotherapy for malignant salivary gland tumors. *Otolaryngology–Head and Neck Surgery, 157*(6), 988-994.

Sakakibara-Konishi, J., Ikezawa, Y., Oizumi, S., Kikuchi, J., Kikuchi, E., Mizugaki, H., Kinoshita, I., Dosaka-Akita, H., & Nishimura, M. (2017). Combined antitumor effect of γ-

secretase inhibitor and ABT-737 in Notch-expressing non-small cell lung cancer. *International Journal of Clinical Oncology, 22*, 257-268.

Sakura, H., Kanei-Ishii, C., Nagase, T., Nakagoshi, H., Gonda, T. J., & Ishii, S. (1989). Delineation of three functional domains of the transcriptional activator encoded by the c-myb protooncogene. *Proceedings of the National Academy of Sciences, 86*(15), 5758-5762.

Sala, A., Bellon, T., Melotti, P., Peschle, C., & Calabretta, B. (1995). Inhibition of erythro-myeloid differentiation by constitutive expression of a DNA binding-deficient c-myb mutant: implication for c-myb function.

Salomoni, P., Perrotti, D., Martinez, R., Franceschi, C., & Calabretta, B. (1997). Resistance to apoptosis in CTLL-2 cells constitutively expressing c-Myb is associated with induction of BCL-2 expression and Myb-dependent regulation of bcl-2 promoter activity. *Proceedings of the National Academy of Sciences, 94*(7), 3296-3301.

Sandberg, M. L., Sutton, S. E., Pletcher, M. T., Wiltshire, T., Tarantino, L. M., Hogenesch, J. B., & Cooke, M. P. (2005). c-Myb and p300 regulate hematopoietic stem cell proliferation and differentiation. *Developmental Cell, 8*(2), 153-166.

Sano, Y., & Ishii, S. (2001). Increased affinity of c-Myb for CREB-binding protein (CBP) after CBP-induced acetylation. *Journal of Biological Chemistry, 276*(5), 3674-3682.

Sarlomo-Rikala, M., Kovatich, A. J., Barusevicius, A., & Miettinen, M. (1998). CD117: a sensitive marker for gastrointestinal stromal tumors that is more specific than CD34. *Modern Pathology: An Official Journal of the United States and Canadian Academy of Pathology, Inc, 11*(8), 728-734.

Sato, M., Sekido, Y., Horio, Y., Takahashi, M., Saito, H., Minna, J. D., Shimokata, K., & Hasegawa, Y. (2000). Infrequent mutation of the hBUB1 and hBUBR1 genes in human lung cancer. *Japanese Journal of Cancer Research, 91*(5), 504-509.

Schliekelman, M., Cowley, D. O., O'Quinn, R., Oliver, T. G., Lu, L., Salmon, E. D., & Van Dyke, T. (2009). Impaired Bub1 function in vivo compromises tension-dependent checkpoint function leading to aneuploidy and tumorigenesis. *Cancer Research, 69*(1), 45-54.

Schmidt, R. L., Hall, B. J., & Layfield, L. J. (2011). A systematic review and meta-analysis of the diagnostic accuracy of ultrasound-guided core needle biopsy for salivary gland lesions. *American Journal of Clinical Pathology, 136*(4), 516-526.

Schmidt, R. L., Hall, B. J., Wilson, A. R., & Layfield, L. J. (2011). A systematic review and meta-analysis of the diagnostic accuracy of fine-needle aspiration cytology for parotid gland lesions. *American Journal of Clinical Pathology, 136*(1), 45-59.

Schmidt, R. L., Hunt, J. P., Hall, B. J., Wilson, A. R., & Layfield, L. J. (2011). A systematic review and meta-analysis of the diagnostic accuracy of frozen section for parotid gland lesions. *American Journal of Clinical Pathology, 136*(5), 729-738.

Schramm, V. L., Srodes, C., & Myers, E. N. (1981). Cisplatin therapy for adenoid cystic carcinoma. *Archives of Otolaryngology, 107*(12), 739-741.

Séveno, C., Loussouarn, D., Bréchet, S., Campone, M., Juin, P., & Barillé-Nion, S. (2012). γ-Secretase inhibition promotes cell death, Noxa upregulation, and sensitization to BH3 mimetic ABT-737 in human breast cancer cells. *Breast Cancer Research, 14*, 1-15.

Shaikh, A. H., MOHAMMAD, T., & QURESHI, N. R. (2014). HISTOPATHOLOGICAL PATTERNS OF ORAL SQUAMOUS CELL CARCINOMA. *Pakistan Oral & Dental Journal, 34*(3)

Shapiro, L. H. (1995). Myb and Ets proteins cooperate to transactivate an early myeloid gene. *Journal of Biological Chemistry, 270*(15), 8763-8771.

Sheiness, D., & Gardinier, M. (1984). Expression of a proto-oncogene (proto-myb) in hemopoietic tissues of mice. *Molecular and Cellular Biology, 4*(7), 1206-1212.

Shen-Ong, G. L. (1987). Alternative internal splicing in c-myb RNAs occurs commonly in normal and tumor cells. *The EMBO Journal, 6*(13), 4035-4039.

Shen, C., Xu, T., Huang, C., Hu, C., & He, S. (2012). Treatment outcomes and prognostic features in adenoid cystic carcinoma originated from the head and neck. *Oral Oncology, 48*(5), 445-449.

Sherr, C. J. (1996). Cancer cell cycles. *Science, 274*(5293), 1672-1677.

Shichiri, M., Yoshinaga, K., Hisatomi, H., Sugihara, K., & Hirata, Y. (2002). Genetic and epigenetic inactivation of mitotic checkpoint genes hBUB1 and hBUBR1 and their relationship to survival. *Cancer Research, 62*(1), 13-17.

Shigeishi, H., Oue, N., Kuniyasu, H., Wakikawa, A., Yokozaki, H., Ishikawa, T., & Yasui, W. (2001). Expression of Bub1 gene correlates with tumor proliferating activity in human gastric carcinomas. *Pathobiology, 69*(1), 24-29.

Shigeishi, H., Yokozaki, H., Kuniyasu, H., Nakagawa, H., Ishikawa, T., Tahara, E., & Yasui, W. (2001). No mutations of the Bub1 gene in human gastric carcinomas. *Oncology Reports, 8*(4), 791-794.

Shigeishi, H., Yoneda, S., Taki, M., Nobumori, T., Ohta, K., Higashikawa, K., Yasui, W., & Kamata, N. (2006). Correlation of human Bub1 expression with tumor-proliferating activity in salivary gland tumors. *Oncology Reports, 15*(4), 933-938.

Shikatani, E. A., Chandy, M., Besla, R., Li, C. C., Momen, A., El-Mounayri, O., Robbins, C. S., & Husain, M. (2016). c-Myb regulates proliferation and differentiation of adventitial Sca1 vascular smooth muscle cell progenitors by transactivation of myocardin. *Arteriosclerosis, Thrombosis, and Vascular Biology, 36*(7), 1367-1376.

Shin, H., Baek, K., Jeon, A., Park, M., Lee, S., Kang, C., Lee, H., Yoo, S., Chung, D., & Sung, Y. (2003). Dual roles of human BubR1, a mitotic checkpoint kinase, in the monitoring of chromosomal instability. *Cancer Cell, 4*(6), 483-497.

Siemeister, G., Mengel, A., Bone, W., Schröder, J., Zitzmann-Kolbe, S., Briem, H., Fernández-Montalván, A. E., Holton, S., Mönning, U., & Ahsen, O. v. (2017). BAY 1816032, a novel BUB1 kinase inhibitor with potent antitumor activity. *Cancer Research, 77*(13_Supplement), 287.

Siemeister, G., Mengel, A., Fernández-Montalván, A. E., Bone, W., Schröder, J., Zitzmann-Kolbe, S., Briem, H., Prechtl, S., Holton, S. J., & Mönning, U. (2019). Inhibition of BUB1 Kinase by BAY 1816032 Sensitizes Tumor Cells toward Taxanes, ATR, and PARP Inhibitors In Vitro and In VivoAntitumor Activity of the BUB1 Kinase Inhibitor BAY 1816032. *Clinical Cancer Research, 25*(4), 1404-1414.

Sood, S., McGurk, M., & Vaz, F. (2016). Management of salivary gland tumours: United Kingdom national multidisciplinary guidelines. *The Journal of Laryngology & Otology, 130*(S2), S142-S149.

Spiro, R. H., Huvos, A. G., & Strong, E. W. (1974). Adenoid cystic carcinoma of salivary origin: a clinicopathologic study of 242 cases. *The American Journal of Surgery, 128*(4), 512-520.

Spiro, R. H., Huvos, A. G., & Strong, E. W. (1979). Adenoid cystic carcinoma: factors influencing survival. *American Journal of Surgery, 138*(4), 579-583.

Sramko, M., Markus, J., Kabát, J., Wolff, L., & Bies, J. (2006). Stress-induced inactivation of the c-Myb transcription factor through conjugation of SUMO-2/3 proteins. *Journal of Biological Chemistry, 281*(52), 40065-40075.

Stenman, G., Andersson, M. K., & Andrén, Y. (2010). New tricks from an old oncogene: gene fusion and copy number alterations of MYB in human cancer. *Cell Cycle, 9*(15), 3058-3067.

Stephens, P. J., Davies, H. R., Mitani, Y., Van Loo, P., Shlien, A., Tarpey, P. S., Papaemmanuil, E., Cheverton, A., Bignell, G. R., & Butler, A. P. (2013). Whole exome sequencing of adenoid cystic carcinoma. *The Journal of Clinical Investigation, 123*(7), 2965-2968.

Stodulski, D., Mikaszewski, B., Majewska, H., Wiśniewski, P., & Stankiewicz, C. (2017). Close surgical margin after conservative parotidectomy in early stage low-/intermediate-grade parotid carcinoma: outcome of watch and wait policy. *Oral Oncology, 68*, 1-4.

Stransky, N., Egloff, A. M., Tward, A. D., Kostic, A. D., Cibulskis, K., Sivachenko, A., Kryukov, G. V., Lawrence, M. S., Sougnez, C., & McKenna, A. (2011). The mutational landscape of head and neck squamous cell carcinoma. *Science, 333*(6046), 1157-1160.

Sun, C., & Bernards, R. (2014). Feedback and redundancy in receptor tyrosine kinase signaling: relevance to cancer therapies. *Trends in Biochemical Sciences, 39*(10), 465-474.

Surveillance, Epidemiology and End Results (SEER), National Cancer Institute (NCI). Available at http://seer.cancer.gov/.

Suzuki, H., & Forrest, A. R. (2009). van NE. *Daub CO, Balwierz PJ, Irvine KM, Lassmann T, Ravasi T, Hasegawa Y, De Hoon MJ, Katayama S, Schroder K, Carninci P, Tomaru Y, Kanamori-Katayama M, Kubosaki A, Akalin A, Ando Y, Arner E, Asada M Et al,* , 553-562.

Szanto, P. A., Luna, M. A., Tortoledo, M. E., & White, R. A. (1984). Histologic grading of adenoid cystic carcinoma of the salivary glands. *Cancer, 54*(6), 1062-1069.

Takahashi, T., Haruki, N., Nomoto, S., Masuda, A., Saji, S., Osada, H., & Takahashi, T. (1999). Identification of frequent impairment of the mitotic checkpoint and molecular analysis of

the mitotic checkpoint genes, hsMAD2 and p55CDC, in human lung cancers. *Oncogene, 18*(30), 4295-4300.

Takahashi, T., Suwabe, N., Dai, P., Yamamoto, M., Ishii, S., & Nakano, T. (2000). Inhibitory interaction of c-Myb and GATA-1 via transcriptional co-activator CBP. *Oncogene, 19*(1), 134-140.

Tanaka, K., Nishioka, J., Kato, K., Nakamura, A., Mouri, T., Miki, C., Kusunoki, M., & Nobori, T. (2001). Mitotic checkpoint protein hsMAD2 as a marker predicting liver metastasis of human gastric cancers. *Japanese Journal of Cancer Research, 92*(9), 952-958.

Tang, Y., Liang, X., Zheng, M., Zhu, Z., Zhu, G., Yang, J., & Chen, Y. (2010). Expression of c-kit and Slug correlates with invasion and metastasis of salivary adenoid cystic carcinoma. *Oral Oncology, 46*(4), 311-316.

Tang, Z., Shu, H., Oncel, D., Chen, S., & Yu, H. (2004). Phosphorylation of Cdc20 by Bub1 provides a catalytic mechanism for APC/C inhibition by the spindle checkpoint. *Molecular Cell, 16*(3), 387-397.

Taniguchi, H., Yamada, T., Wang, R., Tanimura, K., Adachi, Y., Nishiyama, A., Tanimoto, A., Takeuchi, S., Araujo, L. H., & Boroni, M. (2019). AXL confers intrinsic resistance to osimertinib and advances the emergence of tolerant cells. *Nature Communications, 10*(1), 259.

Tannock, I. F., & Sutherland, D. J. (1980). Chemotherapy for adenocystic carcinoma. *Cancer, 46*(3), 452-454.

TNM Classification of Malignant Tumours. UICC (update 2023). Available at https://www.uicc.org/.

Terhaard, C. H., Lubsen, H., Rasch, C. R., Levendag, P. C., Kaanders, H. H., Tjho-Heslinga, R. E., van Den Ende, P. L., Burlage, F., Head, D., & Neck Oncology Cooperative Group. (2005). The role of radiotherapy in the treatment of malignant salivary gland tumors. *International Journal of Radiation Oncology* Biology* Physics, 61*(1), 103-111.

Thoeny, H. C. (2007). Imaging of salivary gland tumours. *Cancer Imaging, 7*(1), 52.

Thomas, M. D., Kremer, C. S., Ravichandran, K. S., Rajewsky, K., & Bender, T. P. (2005). c-Myb is critical for B cell development and maintenance of follicular B cells. *Immunity, 23*(3), 275-286.

Thompson, M. A., Flegg, R., Westin, E. H., & Ramsay, R. G. (1997). Microsatellite deletions in the c-myb transcriptional attenuator region associated with over-expression in colon tumour cell lines. *Oncogene, 14*(14), 1715-1723.

Thompson, M. A., & Ramsay, R. G. (1995). Myb: an old oncoprotein with new roles. *Bioessays, 17*(4), 341-350.

Thomson, D. J., Silva, P., Denton, K., Bonington, S., Mak, S. K., Swindell, R., Homer, J., Sykes, A. J., Lee, L. W., & Yap, B. K. (2015). Phase II trial of sorafenib in advanced salivary adenoid cystic carcinoma of the head and neck. *Head & Neck, 37*(2), 182-187.

Tilston, V., Taylor, S. S., & Perera, D. (2009). Inactivating the spindle checkpoint kinase Bub1 during embryonic development results in a global shutdown of proliferation. *BMC Research Notes, 2*, 1-7.

Togashi, Y., Dobashi, A., Sakata, S., Sato, Y., Baba, S., Seto, A., Mitani, H., Kawabata, K., & Takeuchi, K. (2018). MYB and MYBL1 in adenoid cystic carcinoma: diversity in the mode of genomic rearrangement and transcripts. *Modern Pathology, 31*(6), 934-946.

Toida, M., Balázs, M., Mori, T., Ishimaru, J., Ichihara, H., Fujitsuka, H., Hyodo, I., Yokoyama, K., Tatematsu, N., & Ádány, R. (2001). Analysis of genetic alterations in salivary gland tumors by comparative genomic hybridization. *Cancer Genetics and Cytogenetics, 127*(1), 34-37. 10.1016/S0165-4608(00)00410-6

Tomita, A., Towatari, M., Tsuzuki, S., Hayakawa, F., Kosugi, H., Tamai, K., Miyazaki, T., Kinoshita, T., & Saito, H. (2000). c-Myb acetylation at the carboxyl-terminal conserved domain by transcriptional co-activator p300. *Oncogene, 19*(3), 444-451.

Torelli, G., Venturelli, D., Coló, A., Zanni, C., Selleri, L., Moretti, L., Calabretta, B., & Torelli, U. (1987). Expression of c-myb protooncogene and other cell cycle-related genes in normal and neoplastic human colonic mucosa. *Cancer Research, 47*(20), 5266-5269.

Tsang, W., Chan, J., Lee, K. C., Leung, A., & Fu, Y. T. (1991). Basaloid-squamous carcinoma of the upper aerodigestive tract and so-called adenoid cystic carcinoma of the oesophagus: the same tumour type? *Histopathology, 19*(1), 35-46.

Uttarkar, S., Dukare, S., Bopp, B., Goblirsch, M., Jose, J., & Klempnauer, K. (2015). Naphthol AS-E phosphate inhibits the activity of the transcription factor Myb by blocking the interaction with the KIX domain of the coactivator p300. *Molecular Cancer Therapeutics, 14*(6), 1276-1285.

Uttarkar, S., Frampton, J., & Klempnauer, K. (2017). Targeting the transcription factor Myb by small-molecule inhibitors. *Experimental Hematology, 47*, 31-35. https://doi.org/10.1016/j.exphem.2016.12.003

Uttarkar, S., Piontek, T., Dukare, S., Schomburg, C., Schlenke, P., Berdel, W. E., Müller-Tidow, C., Schmidt, T. J., & Klempnauer, K. (2016). Small-molecule disruption of the Myb/p300 cooperation targets acute myeloid leukemia cells. *Molecular Cancer Therapeutics, 15*(12), 2905-2915.

Van Herpen, C., Locati, L. D., Buter, J., Thomas, J., Bogaerts, J., Lacombe, D., de Mulder, P., Awada, A., Licitra, L., & Bernier, J. (2008). Phase II study on gemcitabine in recurrent and/or metastatic adenoid cystic carcinoma of the head and neck (EORTC 24982). *European Journal of Cancer, 44*(17), 2542-2545.

van Weert, S., van der Waal, I., Witte, B. I., René Leemans, C., & Bloemena, E. (2015). Histopathological grading of adenoid cystic carcinoma of the head and neck: Analysis of currently used grading systems and proposal for a simplified grading scheme. *Oral Oncology, 51*(1), 71-76. 10.1016/j.oraloncology.2014.10.007

Vander Poorten, V. L., Balm, A. J., Hilgers, F. J., Tan, I. B., Loftus-Coll, B. M., Keus, R. B., van Leeuwen, F. E., & Hart, A. A. (1999). The development of a prognostic score for patients with parotid carcinoma. *Cancer: Interdisciplinary International Journal of the American Cancer Society, 85*(9), 2057-2067.

Vegiopoulos, A., García, P., Emambokus, N., & Frampton, J. (2006). Coordination of erythropoiesis by the transcription factor c-Myb. *Blood, 107*(12), 4703-4710.

Vékony, H., Ylstra, B., Wilting, S. M., Meijer, G. A., Van de Wiel, M. A., Leemans, C. R., van der Waal, I., & Bloemena, E. (2007). DNA copy number gains at loci of growth factors and their receptors in salivary gland adenoid cystic carcinoma. *Clinical Cancer Research, 13*(11), 3133-3139.

Vered, M., Braunstein, E., & Buchner, A. (2002). Immunohistochemical study of epidermal growth factor receptor in adenoid cystic carcinoma of salivary gland origin. *Head & Neck: Journal for the Sciences and Specialties of the Head and Neck, 24*(7), 632-636.

Vermorken, J. B., Verweij, J., De Mulder, P., Cognetti, F., Clavel, M., Rodenhuis, S., Kirkpatrick, A., & Snow, G. B. (1993). Epirubicin in patients with advanced or recurrent adenoid cystic carcinoma of the head and neck: a phase II study of the EORTC Head and Neck Cancer Cooperative Group. *Annals of Oncology, 4*(9), 785-788.

Verweij, J., De Mulder, P., De Graeff, A., Vermorken, J. B., Wildier, J., Kerger, J., Schornagel, J., Cognetti, F., Kirkpatrick, A., & Sahmoud, T. (1996). Phase II study on mitoxantrone in adenoid cystic carcinomas of the head and neck. *Annals of Oncology, 7*(8), 867-869.

Vinson, C., Chatterjee, R., & Fitzgerald, P. (2011). Transcription factor binding sites and other features in human and Drosophila proximal promoters. *A Handbook of Transcription Factors,* , 205-222.

Vischioni, B., Dhanireddy, B., Severo, C., Bonora, M., Ronchi, S., Vitolo, V., Fiore, M. R., D'Ippolito, E., Petrucci, R., & Barcellini, A. (2020). Reirradiation of salivary gland tumors with carbon ion radiotherapy at CNAO. *Radiotherapy and Oncology, 145*, 172-177.

Visel, A., Thaller, C., & Eichele, G. (2004). GenePaint. org: an atlas of gene expression patterns in the mouse embryo. *Nucleic Acids Research, 32*(suppl_1), D552-D556.

von Holstein, S. L., Fehr, A., Persson, M., Therkildsen, M. H., Prause, J. U., Heegaard, S., & Stenman, G. (2013). Adenoid cystic carcinoma of the lacrimal gland: MYB gene activation, genomic imbalances, and clinical characteristics. *Ophthalmology, 120*(10), 2130-2138.

Vuong, D., Simpson, P. T., Green, B., Cummings, M. C., & Lakhani, S. R. (2014). Molecular classification of breast cancer. *Virchows Archiv, 465*, 1-14.

Wagner, V. P., Bingle, C. D., & Bingle, L. (2022). MYB-NFIB fusion transcript in adenoid cystic carcinoma: Current state of knowledge and future directions. *Critical Reviews in Oncology/Hematology, 176*, 103745. 10.1016/j.critrevonc.2022.103745

Walf-Vorderwülbecke, V., Pearce, K., Brooks, T., Hubank, M., Van Den Heuvel-Eibrink, M. M., Zwaan, C. M., Adams, S., Edwards, D., Bartram, J., & Samarasinghe, S. (2018). Targeting acute myeloid leukemia by drug-induced c-MYB degradation. *Leukemia, 32*(4), 882-889.

Wang, D. M., Sevcikova, S., Wen, H., Roberts, S., & Lipsick, J. S. (2007). v-Myb represses the transcription of Ets-2. *Oncogene, 26*(8), 1238-1244.

Wang, F., Ulyanova, N. P., van der Waal, M. S., Patnaik, D., Lens, S. M., & Higgins, J. M. (2011). A positive feedback loop involving Haspin and Aurora B promotes CPC accumulation at centromeres in mitosis. *Current Biology, 21*(12), 1061-1069.

Wang, F., Sha, Y., Zhao, M., Wan, H., Zhang, F., Cheng, Y., & Tang, W. (2017). High-resolution diffusion-weighted imaging improves the diagnostic accuracy of dynamic contrast-enhanced sinonasal magnetic resonance imaging. *Journal of Computer Assisted Tomography, 41*(2), 199-205.

Wang, L., Yang, X., An, N., & Liu, J. (2020). Bioinformatics analysis of BUB1 expression and gene regulation network in lung adenocarcinoma. *Translational Cancer Research, 9*(8), 4820.

Wang, Q., Lauring, J., & Schlissel, M. S. (2000). c-Myb binds to a sequence in the proximal region of the RAG-2 promoter and is essential for promoter activity in T-lineage cells. *Molecular and Cellular Biology, 20*(24), 9203-9211.

Wang, R., Yu, H., & Deng, C. (2004). A requirement for breast-cancer-associated gene 1 (BRCA1) in the spindle checkpoint. *Proceedings of the National Academy of Sciences, 101*(49), 17108-17113.

Wang, X., Angelis, N., & Thein, S. L. (2018). MYB – A regulatory factor in hematopoiesis. *Gene, 665*, 6-17. https://doi.org/10.1016/j.gene.2018.04.065

Wang, Y., Ma, S., Wang, W., Huang, C., Zhao, Z., Liu, B., Zhang, W., Zhao, Y., Zhang, L., & Sun, Z. (2014). Inhibition of survivin reduces HIF-1α, TGF-β1 and TFE3 in salivary adenoid cystic carcinoma. *PloS One, 9*(12), e114051.

Wang, Z., Katsaros, D., Shen, Y., Fu, Y., Canuto, E. M., Benedetto, C., Lu, L., Chu, W., Risch, H. A., & Yu, H. (2015). Biological and clinical significance of MAD2L1 and BUB1, genes frequently appearing in expression signatures for breast cancer prognosis. *PloS One, 10*(8), e0136246.

Ward, A., Balwierz, A., Zhang, J. D., Küblbeck, M., Pawitan, Y., Hielscher, T., Wiemann, S., & Sahin, Ö. (2013). Re-expression of microRNA-375 reverses both tamoxifen resistance and accompanying EMT-like properties in breast cancer. *Oncogene, 32*(9), 1173-1182.

Warner, K. A., Oklejas, A. E., Pearson, A. T., Zhang, Z., Wu, W., Divi, V., Rodriguez-Ramirez, C., Castilho, R. M., Polverini, P. J., & Nör, J. E. (2018). UM-HACC-2A: MYB-NFIB fusion-positive human adenoid cystic carcinoma cell line. *Oral Oncology, 87*, 21-28.

Warren, C. D., Brady, D. M., Johnston, R. C., Hanna, J. S., Hardwick, K. G., & Spencer, F. A. (2002). Distinct chromosome segregation roles for spindle checkpoint proteins. *Molecular Biology of the Cell, 13*(9), 3029-3041.

Weinstein, I. B., Begemann, M., Zhou, P., Han, E. K., Sgambato, A., Doki, Y., Arber, N., Ciaparrone, M., & Yamamoto, H. (1997). Disorders in cell circuitry associated with multistage carcinogenesis: exploitable targets for cancer prevention and therapy. *Clinical Cancer Research: An Official Journal of the American Association for Cancer Research, 3*(12), 2696-2702.

Weinstein, I. B., & Joe, A. (2008). Oncogene addiction. *Cancer Research, 68*(9), 3077-3080.

Weinstein, I. B., & Joe, A. K. (2006). Mechanisms of disease: oncogene addiction—a rationale for molecular targeting in cancer therapy. *Nature Clinical Practice Oncology, 3*(8), 448-457.

West, R. B., Kong, C., Clarke, N., Gilks, T., Lipsick, J., Cao, H., Kwok, S., Montgomery, K. D., Varma, S., & Le, Q. (2011). MYB expression and translocation in adenoid cystic carcinomas and other salivary gland tumors with clinicopathologic correlation. *The American Journal of Surgical Pathology, 35*(1), 92.

Westin, E. H., Gallo, R. C., Arya, S. K., Eva, A., Souza, L. M., Baluda, M. A., Aaronson, S. A., & Wong-Staal, F. (1982). Differential expression of the amv gene in human hematopoietic cells. *Proceedings of the National Academy of Sciences, 79*(7), 2194-2198.

Wijeratne, T. U., Guiley, K. Z., Lee, H., Müller, G. A., & Rubin, S. M. (2022). Cyclin-dependent kinase-mediated phosphorylation and the negative regulatory domain of transcription factor B-Myb modulate its DNA binding. *Journal of Biological Chemistry, 298*(9), 102319. 10.1016/j.jbc.2022.102319

Williams, B. B., Wall, M., Miao, R. Y., .Williams, B., Bertoncello, I., Kershaw, M. H., Mantamadiotis, T., Haber, M., Norris, M. D., & Gautam, A. (2008). Induction of T cell-mediated immunity using a c-Myb DNA vaccine in a mouse model of colon cancer. *Cancer Immunology, Immunotherapy, 57*, 1635-1645.

Williams, G. L., Roberts, T. M., & Gjoerup, O. V. (2007). Bub1: escapades in a cellular world. *Cell Cycle, 6*(14), 1699-1704.

Woida, F. M., & Ribeiro-Silva, A. (2007). Adenoid cystic carcinoma of the Bartholin gland: an overview. *Archives of Pathology & Laboratory Medicine, 131*(5), 796-798.

Wong, S. J., Cohen, E. E., Karrison, T., Hayes, D. N., Kies, M. S., Cullen, K. J., Tanvetyanon, T., Argiris, A., Takebe, N., & Lim, D. (2013). A Phase II Study of Dasatanib (BMS 354825) in Recurrent Or Metastatic Ckit-Expressing Adenoid Cystic (ACC) and Non-ACC Malignant Salivary Glands Tumors (MSGT). *Head and Neck Cancer, 27(2)*, 318–323.

Woo, C. H., Sopchak, L., & Lipsick, J. S. (1998). Overexpression of an alternatively spliced form of c-Myb results in increases in transactivation and transforms avian myelomonoblasts. *Journal of Virology, 72*(8), 6813-6821.

Wrana, J. L., Attisano, L., Wieser, R., Ventura, F., & Massagué, J. (1994). Mechanism of activation of the TGF-β receptor. *Nature, 370*(6488), 341-347.

Wu, P., Nielsen, T. E., & Clausen, M. H. (2015). FDA-approved small-molecule kinase inhibitors. *Trends in Pharmacological Sciences, 36*(7), 422-439.

Xiao, C. C., Zhan, K. Y., White-Gilbertson, S. J., & Day, T. A. (2016). Predictors of nodal metastasis in parotid malignancies: a national cancer data base study of 22,653 patients. *Otolaryngology--Head and Neck Surgery, 154*(1), 121-130.

Xing, D., Bakhsh, S., Melnyk, N., Isacson, C., Ho, J., Huntsman, D. G., Gilks, C. B., Ronnett, B. M., & Horlings, H. M. (2017). Frequent NFIB-associated gene rearrangement in adenoid cystic carcinoma of the vulva. *International Journal of Gynecological Pathology, 36*(3), 289-293.

Xu, B., Drill, E., Ho, A., Ho, A., Dunn, L., Pireto-Granada, C. N., Chan, T., Ganly, I., Ghossein, R., & Katabi, N. (2017). Predictors of outcome in adenoid cystic carcinoma of salivary glands: a clinicopathologic study with correlation between MYB fusion and protein expression. *The American Journal of Surgical Pathology, 41*(10), 1422.

Yamaguchi, K., Okami, K., Hibi, K., Wehage, S. L., Jen, J., & Sidransky, D. (1999). Mutation analysis of hBUB1 in aneuploid HNSCC and lung cancer cell lines. *Cancer Letters, 139*(2), 183-187. 10.1016/S0304-3835(99)00035-X

Yang, G., Fu, H., Zhang, J., Lu, X., Yu, F., Jin, L., Bai, L., Huang, B., Shen, L., & Feng, Y. (2010). RNA-binding protein quaking, a critical regulator of colon epithelial differentiation and a suppressor of colon cancer. *Gastroenterology, 138*(1), 231-240. e5.

Yang, H., Huang, Z., Wang, J., & Lu, S. C. (2001). The role of c-Myb and Sp1 in the up-regulation of methionine adenosyltransferase 2A gene expression in human hepatocellular carcinoma. *The FASEB Journal, 15*(9), 1507-1516.

Yang, R., Nanayakkara, D., Kalimutho, M., Mitra, P., Khanna, K. K., Dray, E., & Gonda, T. J. (2019). MYB regulates the DNA damage response and components of the homology-directed repair pathway in human estrogen receptor-positive breast cancer cells. *Oncogene, 38*(26), 5239-5249.

Yuan, B., Xu, Y., Woo, J., Wang, Y., Bae, Y. K., Yoon, D., Wersto, R. P., Tully, E., Wilsbach, K., & Gabrielson, E. (2006). Increased expression of mitotic checkpoint genes in breast cancer cells with chromosomal instability. *Clinical Cancer Research, 12*(2), 405-410.

Yusenko, M. V., Trentmann, A., Andersson, M. K., Ghani, L. A., Jakobs, A., Paz, M. A., Mikesch, J., von Kries, J. P., Stenman, G., & Klempnauer, K. (2020). Monensin, a novel potent MYB inhibitor, suppresses proliferation of acute myeloid leukemia and adenoid cystic carcinoma cells. *Cancer Letters, 479*, 61-70.

ZENG, Z., YANG, H., HUANG, Z., CHEN, C., WANG, J., & LU, S. C. (2001). The role of c-Myb in the up-regulation of methionine adenosyltransferase 2A expression in activated Jurkat cells. *Biochemical Journal, 353*(1), 163-168.

Zenga, J., Parikh, A. S., Emerick, K. S., Lin, D. T., Faquin, W. C., & Deschler, D. G. (2018). Close margins and adjuvant radiotherapy in acinic cell carcinoma of the parotid gland. *JAMA Otolaryngology–Head & Neck Surgery, 144*(11), 1011-1016.

Zenga, J., Yu, Z., Parikh, A., Chen, J. X., Lin, D. T., Emerick, K. S., Faquin, W. C., Varvares, M. A., & Deschler, D. G. (2019). Mucoepidermoid carcinoma of the parotid: very close margins and adjuvant radiotherapy. *Orl, 81*(1), 55-62.

Zhang, C., Xia, R., Han, J., Wang, B., Tian, W., Zhong, L., Tian, Z., Wang, L., Hu, Y., & Li, J. (2013). Adenoid cystic carcinoma of the head and neck: clinicopathologic analysis of 218 cases in a Chinese population. *Oral Surgery, Oral Medicine, Oral Pathology and Oral Radiology, 115*(3), 368-375.

Zhang, G., Kruse, T., López-Méndez, B., Sylvestersen, K. B., Garvanska, D. H., Schopper, S., Nielsen, M. L., & Nilsson, J. (2017). Bub1 positions Mad1 close to KNL1 MELT repeats to promote checkpoint signalling. *Nature Communications, 8*(1), 15822.

Zhang, M., Liu, Y., Yang, H., Jin, F., & Zheng, A. (2022). Breast adenoid cystic carcinoma: a report of seven cases and literature review. *BMC Surgery, 22*(1), 1-7.

Zhang, Y., Liu, T., Meyer, C. A., Eeckhoute, J., Johnson, D. S., Bernstein, B. E., Nusbaum, C., Myers, R. M., Brown, M., & Li, W. (2008). Model-based analysis of ChIP-Seq (MACS). *Genome Biology, 9*(9), 1-9.

Zhang, Y., Song, C., Wang, L., Jiang, H., Zhai, Y., Wang, Y., Fang, J., & Zhang, G. (2022). Zombies Never Die: The Double Life Bub1 Lives in Mitosis. *Frontiers in Cell and Developmental Biology, 10*

Zhang, Z., Lee, J. C., Lin, L., Olivas, V., Au, V., LaFramboise, T., Abdel-Rahman, M., Wang, X., Levine, A. D., & Rho, J. K. (2012). Activation of the AXL kinase causes resistance to EGFR-targeted therapy in lung cancer. *Nature Genetics, 44*(8), 852-860.

Zhao, L., Glazov, E. A., Pattabiraman, D. R., Al-Owaidi, F., Zhang, P., Brown, M. A., Leo, P. J., & Gonda, T. J. (2011). Integrated genome-wide chromatin occupancy and expression analyses identify key myeloid pro-differentiation transcription factors repressed by Myb. *Nucleic Acids Research, 39*(11), 4664-4679.

Zhou, F., Zhang, L., van Laar, T., van Dam, H., & Ten Dijke, P. (2011). GSK3β inactivation induces apoptosis of leukemia cells by repressing the function of c-Myb. *Molecular Biology of the Cell, 22*(18), 3533-3540.

Zhu, L., Pan, Y., Chen, X., & Hou, P. (2020). BUB1 promotes proliferation of liver cancer cells by activating SMAD2 phosphorylation. *Oncology Letters, 19*(5), 3506-3512.

Zich, J., & Hardwick, K. G. (2010). Getting down to the phosphorylated 'nuts and bolts' of spindle checkpoint signalling. *Trends in Biochemical Sciences, 35*(1), 18-27.

Zvrko, E., & Golubović, M. (2009). Laryngeal adenoid cystic carcinoma. *ACTA Otorhinolaryngologica Italica, 29*(5), 279.